

Geologie

**Provenance of Late Palaeozoic sediments
in the southern Patagonian Andes:
age estimates, sources, and depositional setting**

Inaugural-Dissertation
zur Erlangung des Doktorgrades
der Naturwissenschaften im Fachbereich Geowissenschaften
der Mathematisch-Naturwissenschaftlichen Fakultät
der Westfälischen Wilhelms-Universität Münster

vorgelegt von
Carita Augustsson
aus Norra Sandby (Schweden)

- 2003 -

Augustsson, C., 2003: Provenance of Late Palaeozoic sediments in the southern Patagonian Andes: age estimates, sources, and depositional setting, Dissertation, Westfälische Wilhelms-Universität Münster, Germany, 94 pp.

Correspondence:

Carita Augustsson
Geologisch-Paläontologisches Institut und Museum
Westfälische Wilhelms-Universität
Corrensstraße 24
48 149 Münster
Germany

E-mail: augustss@uni-muenster.de

Tel. +49-251-83 339 97

Fax: +49-251-83 339 33

Dekan: Hans Kerp
Erster Gutachter: Heinrich Bahlburg
Zweiter Gutachter: Klaus Mezger
Tag der mündlichen Prüfung: 27.01.2004.
Tag der Promotion: 30.01.2004.

Table of contents

Abstract	5
1. Introduction	7
1.1. Geological setting	7
1.2. Aims	12
1.3. Age	13
2. Sample descriptions	16
3. Petrography	17
3.1. Light framework mineral content	17
3.1.1. Light framework mineral content: methods	17
3.1.2. Light framework mineral content: results and implications	17
3.2. Cathodoluminescence of quartz	17
3.2.1. Cathodoluminescence of quartz: methods	21
3.2.2. Cathodoluminescence of quartz: results	22
3.2.3. Cathodoluminescence of quartz: new data evaluation method	22
3.2.4. Cathodoluminescence of quartz: implications	27
3.3. Heavy minerals	28
3.3.1. Heavy minerals: methods	29
3.3.2. Heavy minerals: content	29
3.3.3. Heavy minerals: chemical composition of tourmaline	33
3.4. Petrography: discussion	37
4. Whole-rock chemistry	39
4.1. Whole-rock major and trace element chemistry	39
4.1.1. Whole-rock major and trace element chemistry: methods	39
4.1.2. Whole-rock major and trace element chemistry: results and chemical weathering	39
4.1.3. Whole-rock major and trace element chemistry: implications	45
4.2. Sm-Nd and Rb-Sr isotopes	50
4.2.1. Sm-Nd and Rb-Sr isotopes: methods	50
4.2.2. Sm-Nd isotopes: results and implications	51
4.2.3. Rb-Sr isotopes: results and implications	52
4.3. Whole-rock chemistry: discussion	54
5. Zircon U-Pb ages and Hf isotopes	57
5.1. U-Pb ages	57
5.1.1. U-Pb ages: methods	57
5.1.2. U-Pb ages: results	58
5.1.3. U-Pb ages: implications	68
5.2. Hf isotopes	70
5.2.1. Hf isotopes: methods	71

5.2.2. Hf isotopes: results and implications	72
5.3. Zircon U-Pb and Hf isotope signatures: discussion	74
5.3.1. The Early to Late Carboniferous	74
5.3.2. The Early Permian	80
6. Final remarks	81
6.1. Conclusions	82
Acknowledgements	84
References	84

Abstract

In the southern Patagonian Andes of Chile and Argentina the Late Palaeozoic basement of the Andes is mainly composed of metasediments. SHRIMP U-Pb ages of detrital zircons from turbiditic rocks of the Cochrane unit, which belongs to the Eastern Andean Metamorphic Complex in Chile, constrain the maximum depositional age to Devonian to Early Carboniferous for this unit. SHRIMP U-Pb ages further restrict deposition of the Bahía de la Lancha Formation in Argentina to late Early Carboniferous times. The main sediment sources of the Cochrane unit and the Bahía de la Lancha Formation were generally dominated by felsic rocks, as revealed by the whole-rock chemistry ($\text{Th/Sc} = 0.6\text{-}1.9$). The sedimentary detritus is dominated by recycled metasedimentary and metamorphic material, as revealed by cathodoluminescence of quartz, chemistry of tourmaline and zoning of zircon. The source material was of continental origin and had been recycled within the crust before becoming part of the studied turbidite deposits as indicated by whole-rock Sr and Nd isotope signatures and U-Pb ages of detrital zircons ($^{87}\text{Sr}/^{86}\text{Sr}(T = 250 \text{ Ma}) = 0.709\text{-}0.718$; $\epsilon_{\text{Nd}}(T = 320\text{-}350 \text{ Ma}) = -8 \text{ to } -2$; $\text{Nd } T_{\text{DM}}^* = 1170\text{-}1540 \text{ Ma}$; *ca.* 90 % of the zircons have U-Pb ages of < 1500 Ma, with a dominance in the interval 350-700 Ma). As indicated by the U-Pb ages and Hf isotope signatures of single zircons, the original main source areas for the detrital grains encompassed present extra-Andean Patagonia, as well as the Argentinean Sierra de la Ventana slightly north of Patagonia. Furthermore, southern Africa, East Antarctica and the Falkland Plateau, which formed an area in the interior of Gondwana, were probably important original source areas for the sediments. The part of the Eastern Andean Metamorphic Complex that crops out on the shoreline of Fiordo Peel (*ca.* 50°45'S) in the southern Chilean archipelago has a Late Carboniferous - Early Permian maximum depositional age, as deduced from the SHRIMP U-Pb dating. Magmatic source material dominates the sediments, as revealed by the abundance of zircons with magmatic zoning. The primary sources were mainly felsic and had a continental setting ($\text{Th/Sc} = 0.8\text{-}1.1$; $^{87}\text{Sr}/^{86}\text{Sr}(T = 250 \text{ Ma}) = 0.705\text{-}0.710$; $\epsilon_{\text{Nd}}(T=280) = -5 \text{ to } -4$; $\text{Nd } T_{\text{DM}}^* = 1270\text{-}1320 \text{ Ma}$; > 40 % of the zircons have U-Pb ages between 290 and 330 Ma). The sediments most likely had short transportation paths. With the data above, this study supports an onset of subduction at the Late Palaeozoic Pacific margin of Gondwana (present coordinates) in Late Carboniferous times.

□Andes, Argentina, cathodoluminescence, Chile, detrital zircons, geochemistry, Gondwana, heavy minerals, Hf, Palaeozoic, Patagonia, provenance, quartz, Rb-Sr, SHRIMP, Sm-Nd, tourmaline, turbidites, U-Pb.

Kurzfassung

In den Südpatagonischen Anden in Chile und Argentinien besteht das Spätpaläozoische Grundgebirge der Anden hauptsächlich aus Metasedimenten. SHRIMP-U-Pb-Datierungen von detritischen Zirkonen aus Turbiditablagerungen der „Cochrane unit“, welche dem chilenischen „Eastern Andean Metamorphic Complex“ angehört, weisen auf ein maximales devonisch-frühkarbonisches Ablagerungsalter hin. Die Bahía de la Lancha Formation wird in das späte Frühkarbon gestellt. Im Allgemeinen sind die Quellgesteine der Sedimente felsisch, wie an der Gesamtgesteinschemie ($\text{Th}/\text{Sc} = 0,6-1,9$) gezeigt werden kann. Katodolumineszenz von Quarzkörnern, Turmalin-Chemismus und die Zonierungen der Zirkone deuten darauf hin, dass der Detritus dieser geologischen Einheiten hauptsächlich aus wiederaufbereitetem und recyceltem, metasedimentärem und metamorphem Material bestand. Das Quellmaterial war kontinental und wurde in der Kruste vor der Ablagerung der untersuchten Sedimente recycelt. Dies deutet sich in Sr- und Nd-Isotopie der Gesamtgesteinsanalysen ebenso an wie in den U-Pb Altern detritischer Zirkone ($^{87}\text{Sr}/^{86}\text{Sr}(T = 250 \text{ Ma}) = 0,709-0,718$; $\epsilon_{\text{Nd}}(T = 320-350 \text{ Ma}) = -8 \text{ to } -2$; $\text{Nd } T_{\text{DM}}^* = 1170-1540 \text{ Ma}$; ca. 90 % der Zirkone haben U-Pb-Alter jünger als 1500 Ma mit einer Dominanz im Intervall 350-700 Ma). U-Pb-Datierungen und Hf-Isotopie von Einzelzirkonen lässt vermuten, dass die ursprünglichen Hauptquellen in Patagonien östlich der Anden sowie in der Sierra de la Ventana in Argentinien etwas nördlich Patagoniens zu finden sind. Auch der südliche Teil Afrikas, die Ostantarktis und das Falklandplateau, welche ein zusammenhängendes Gebiet innerhalb Gondwanas bildeten, waren wahrscheinlich wichtige ursprüngliche Liefergebiete. Der aufgeschlossene Teil des „Eastern Andean Metamorphic Complex“ an der Küste von Fiordo Peel (ca. $50^{\circ}45'\text{S}$) im Archipel Südchiles hat ein spätkarbonisch-frühpermisches maximales Ablagerungsalter. Die Zirkonzonierung zeigt, dass in den Sedimenten überwiegend magmatisches Material vorliegt. Die primäre Quellen waren hauptsächlich felsische mit kontinentalem Ursprung ($\text{Th}/\text{Sc} = 0,8-1,1$; $^{87}\text{Sr}/^{86}\text{Sr}(T = 250 \text{ Ma}) = 0,705-0,710$; $\epsilon_{\text{Nd}}(T = 280 \text{ Ma}) = -5 \text{ to } -4$; $\text{Nd } T_{\text{DM}}^* = 1270-1320 \text{ Ma}$; > 40 % der Zirkone haben U-Pb-Alter zwischen 290 und 330 Ma). Höchstwahrscheinlich hatten die Sedimente kurze Transportwege. Mit Hilfe der obengenannten Daten stützt diese Studie einen Beginn von Subduktion am pazifischen Kontinentalrand des spätkarbonischen Gondwana (heutige Lage).

□Anden, Argentinien, Chile, detritische Zirkone, Geochemie, Gondwana, Hf, Kathodolumineszenz, Liefergebiet, Paläozoikum, Patagonien, Quarz, Rb-Sr, Schwerminerale, SHRIMP, Sm-Nd, Turmalin, Turbidite, U-Pb.

1. Introduction

Provenance analysis, the research field that uses compositional features of sediments to characterise their source rocks, can be used for the reconstruction of palaeo-environments. Source rock formation, weathering and erosional processes, transportation and deposition of sedimentary detritus, as well as post-depositional processes such as diagenesis and metamorphism, all affect the petrology and chemical composition of sedimentary rocks. However, a number of different and independent analysis methods can be used to reveal the source rocks of sediments. The information obtained from rocks and minerals can be used to reconstruct, *e. g.*, the tectonic setting of the depositional basin, and it can be an important key in studies of the plate tectonic evolution of continents. Such information is used in this provenance study of Late Palaeozoic turbidites from the southern Patagonian Andes.

In Patagonia, in the southernmost Chilean and Argentinean Andes, the basement of the Cenozoic mountain-range is mainly composed of sedimentary rocks of Late Palaeozoic to Early Mesozoic age (*e. g.*, Hervé *et al.*, 2000). Partly, it has been unclear if these sediments were deposited at an active or a passive continental margin. This study is a contribution to the understanding of the plate tectonic evolution of the Late Palaeozoic - Early Mesozoic southwest Pacific margin of Gondwana (present coordinates; see Section 1.2.).

1.1. Geological setting

A plate tectonic model with eastward pre-Andean subduction under Patagonia at the Pacific margin of Gondwana (present coordinates) was presented by Forsythe (1982) for Late Palaeozoic to Early Mesozoic times. Chilean Andean Patagonia and western Argentinean Patagonia (Fig. 1a) were suggested to be part of a fore-arc province. Time constraints allow the subduction underneath southern Patagonia to have started in the Late Carboniferous, as indicated by (mainly errorchron) whole-rock Rb-Sr ages of sedimentary rocks (*ca.* \leq 290 Ma; Hervé, 1988; Pankhurst *et al.*, 1992; Hervé *et al.*, 2000). Zircon fission-track ages support metamorphism in Early Permian times (\leq *ca.* 270 Ma; Thomson & Hervé, 2002). Before the Early Carboniferous and Permian, there is no recorded evidence of subduction in this region.

The oldest rocks in the southern Patagonian Andes have been dated with fossils as Lower to Middle Devonian (Fortey *et al.*, 1992). Based on faunal similarities and provincialism, Fortey *et al.* (1992) suggested that a marine platform extended from Chiloé (Fig. 1a), via southern Patagonia, to the Islas Malvinas (Falkland Islands), that were situated southeast of southern Africa (present coordinates) in the Late Palaeozoic. Based on the stable platform affinity of the fossil assemblage, Fortey *et al.* (1992) suggested that at least parts of the turbidite sequence of Chiloé were deposited at a passive margin. Thus, the onset of the South Patagonian Late Palaeozoic subduction is bracketed between Middle Devonian and Late Carboniferous - Permian times. Further north, the onset of subduction might have been earlier, as indicated by Devonian to Carboniferous K-Ar and whole-rock Rb-Sr ages of metamorphism at Pichilemu in Chile (*ca.* 34°30'S; Hervé *et al.*, 1974, 1984).

The Palaeozoic sedimentary rocks are the oldest exposed rocks in the Southern Andean Patagonia (southernmost Argentina and Chile) and constitute the basement of the southern Patagonian Andes. They are composed mainly of siliciclastic rocks dominated by turbidites, and minor limestone intercalations. Based on fossil evidence the ages of these rocks range from Devonian in the north to Permian and Triassic further south (Fig. 1a;

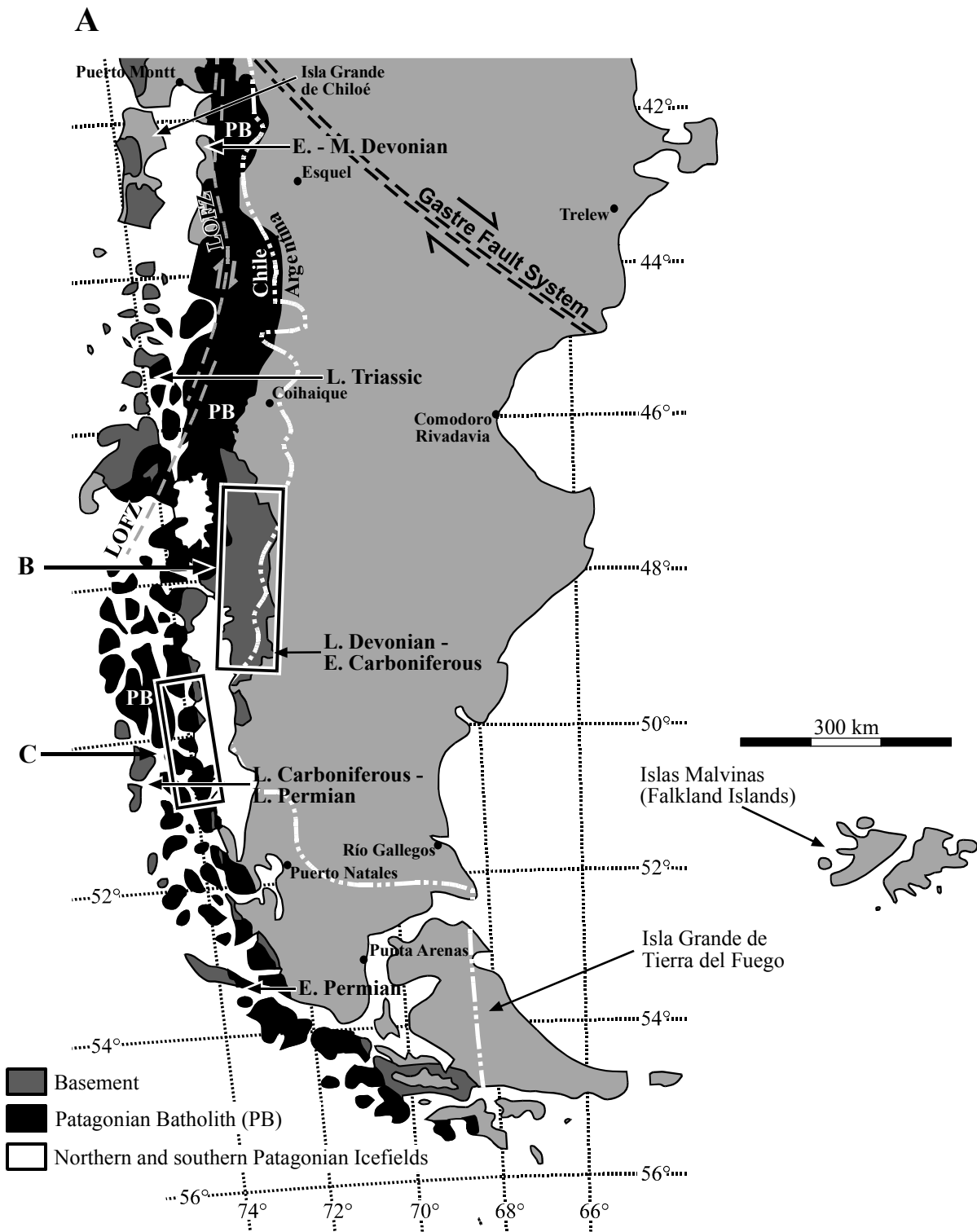
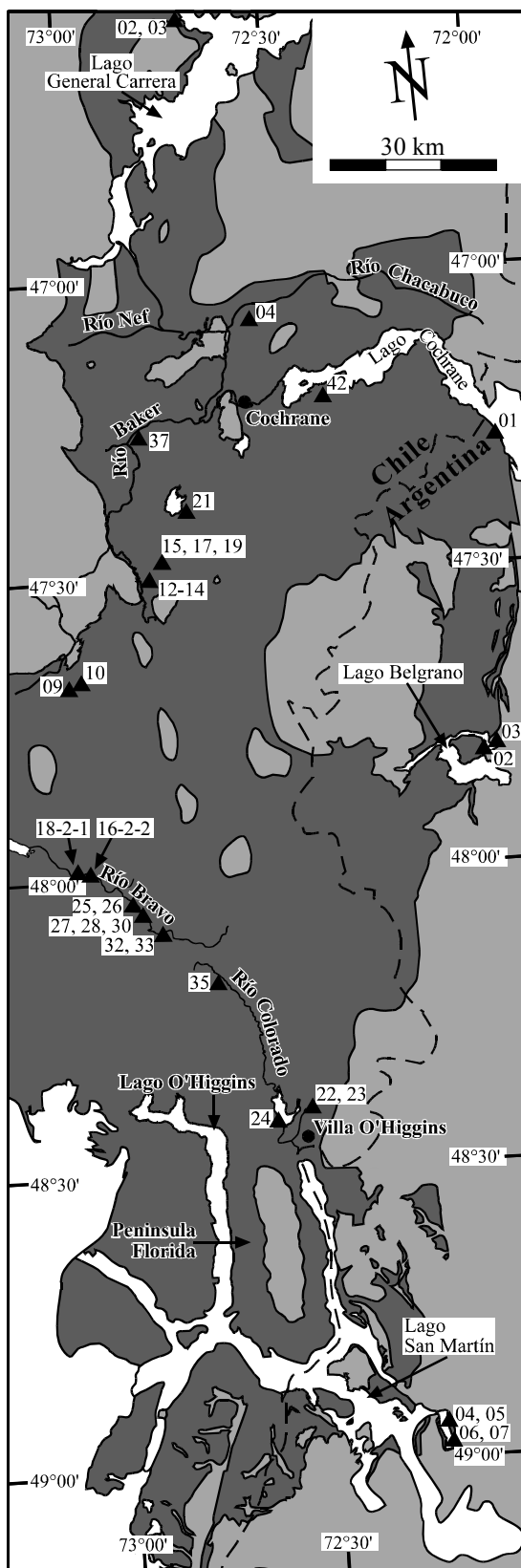


Fig. 1. (a) Southern Patagonia with age estimates of the Andean basement rocks determined from fossils. LOFZ = Liquiñe-Ofqui Fault Zone, PB = Patagonian Batholith. Map compiled after Escobar (1980) and Caminos & González (1996). For further references, see the main text. (b) Northern study area. The basement sediments belonging to the Eastern Andean Metamorphic Complex are situated in Chile, close to the Argentinean border. The Bahía de la Lancha Formation crops out in the area of Lago San Martín in Argentina and the Río Lácteo Formation crops out in the areas of Lago Belgrano and the Argentinean sector of Lago Cochrane (= Lago Pueyrredón in Argentina). Numbered triangles = sampling points. The Chilean and the Argentinean samples have the prefixes CA-00- and CA-01-, respectively. Map compiled after Lagally (1975), Nullo *et al.* (1978), Yoshida (1981) and Giacosa *et al.* (1999). (c) Southern study area. Numbered triangles = sampling points. Map modified after Escobar (1980).

B



C



- Basement
- Mesozoic - Cenozoic, post-basement
- Southern Patagonian Icefield

Riccardi, 1971; Ling *et al.*, 1985; Ling & Forsythe, 1987; Fortey *et al.*, 1992; Fang *et al.*, 1998). Estimates of maximum and minimum ages for the deposition, based on a combination of zircon U-Pb and fission track ages, indicate similar depositional ages as the fossil evidence does (Fig. 2; Thomson & Hervé, 2002). The sediments are interpreted as subduction complexes accreted to the margin of Gondwana in Late Palaeozoic to Early Mesozoic times (Forsythe, 1982), as indicated by whole-rock Rb-Sr ages (*ca.* 290-140 Ma; Hervé, 1988; Pankhurst *et al.*, 1992; Hervé *et al.*, 2000) and zircon fission track dating (270-209 Ma; Thomson & Hervé, 2002). The western part of the deposits was incorporated into an accretionary or front wedge, and the eastern part into its backstop. This process resulted in deformation and metamorphism of the basement rocks, ranging from sub-greenschist facies in the eastern part to blueschist facies in the western part (Hervé *et al.*, 1999; Willner *et al.*, 2000; Ramírez & Sassi, 2001). The sediments were further subject to large scale deformation and folding during the build-up of the Andes in Late Cretaceous to Cenozoic times (Ramos, 1989).

Traditionally, the metamorphic basement of *central* Chile is separated into a western and an eastern series (González-Bonorino & Aguirre, 1970; Aguirre *et al.*, 1972). They were suggested to be the high and low metamorphic part, respectively, of a paired metamorphic belt (Aguirre *et al.*, 1972). In the southern Chilean archipelago, a similar separation into a western high-grade belt with metamorphic grades up to blueschist facies and an eastern low-grade metamorphic belt of sub-greenschist to greenschist facies rocks can be made (*e. g.*, Hervé *et al.*, 2000; Olivares *et al.*, 2003). Recent publication (*e. g.*, Hervé *et al.*, 2000; Bandel & Quinzio-Sinn, 1999, and references therein) recognise the southern Chilean metamorphic basement as being of varying age and of different origin. The western part is interpreted to include oceanic accretionary complexes, whereas the eastern part has a continental origin. The rocks treated here belong to the low-grade eastern belt.

The eastern low-grade metamorphic belt crops out in Chile and Argentina. The mainland part along the Argentinean border in southern Chile south of *ca.* 46°S, as well as the archipelago part along the Chilean coastline down to *ca.* 52°S is known as the Eastern Andean Metamorphic Complex (Hervé, 1993; Fig. 2). In Argentina, the Río Lácteo and Bahía de la Lancha formations along the Chilean border are treated as its equivalents (*e. g.*, Hervé *et al.*, 2000). It has been unclear if these sediments were deposited at an active margin and directly incorporated into its accretionary or front wedge and its backstop, or if deposition took place at a passive margin with inclusion of the sediments into the wedge and its backstop at a later stage.

Lagally (1975) described two distinct successions for the mainland part of the Eastern Andean Metamorphic Complex. The Lago General Carrera unit, dominated by micaschists, greenschists and marbles, is situated in the area of Lago General Carrera, and the Cochrane unit, mainly composed of greywackes and shales, is situated south of Río Chacabuco and Río Nef (*ca.* 47°S; Fig. 1b). If the units are stratigraphically equivalent or not has not been clarified (Bell & Suárez, 2000, and references therein). The Cochrane unit extends down to Lago O'Higgins at 49°S. It is equivalent to the Bahía de la Lancha Formation, which crops out in Argentina in the area of Lago San Martín (= Lago O'Higgins in Chile; Fig. 1b; Riccardi, 1971). The Bahía de la Lancha Formation is dominated by alternating layers of arenites and shales. The Río Lácteo Formation crops out in the area of Lago Belgrano and

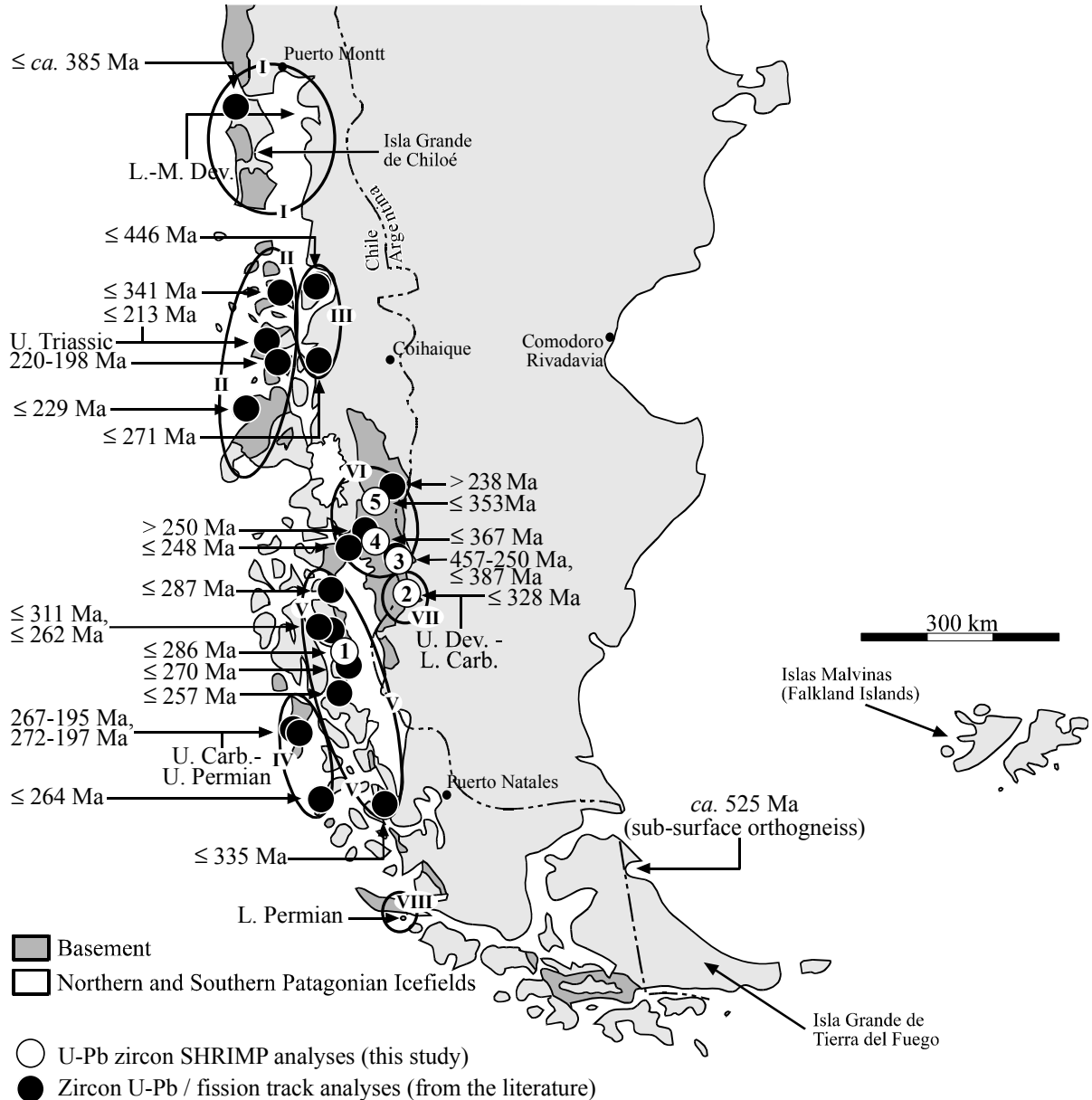


Fig. 2. Summary of published ages of the basement of the Patagonian Andes and ages of pre-depositional rocks in extra-Andean southern Chile and Argentina. 1-5 = SHRIMP U-Pb dating from this study. Sample localities: I = Chiloé, II = Chonos Metamorphic Complex, III = Main Range Metamorphic Complex, IV = Duque de York Metamorphic Complex, V = Southern Chilean archipelago (Eastern Andean Metamorphic Complex), VI = Cochrane unit (Eastern Andean Metamorphic Complex), VII = Bahía de la Lancha Formation, VIII = Estrecho de Magallanes. The U-Pb ages are based on the youngest concordant grain in each sample. For the U-Pb ages, their 1σ -errors were considered (except for the zircon at Chiloé), and 2σ -errors for the fission track ages. U-Pb and fission track ages of detrital zircons are from Duhart *et al.* (2001), Hervé & Fanning (2001), Thomson & Hervé (2002), Hervé *et al.* (2003a), and this study. Fossil dating are from Riccardi (1971), Ling *et al.* (1985), Ling & Forsythe (1987), Fortey *et al.* (1992), and Fang *et al.* (1998). U-Pb dating of orthogneisses are from Söllner *et al.* (2000), and Pankhurst *et al.* (2003b).

Lago Pueyrredón (= Lago Cochrane in Chile) further north on the Argentinean side (Fig. 1b). This Formation is in contact with the Chilean Cochrane unit. The Río Lácteo Formation is compositionally similar to the Cochrane unit with its dominance of greywackes and shales.

This study includes the Chilean Eastern Andean Metamorphic Complex, as well as the two Argentinean formations (*ca.* $46^{\circ}30' - 51^{\circ}00'S$; Fig. 1b-c). The studied rocks are interpreted as turbidite deposits, which have been subjected to low-grade metamorphism and

deformation. In the southern part of the mainland study area (Fig. 1b), single turbidite beds with typical sedimentary structures like grading and ripple cross-laminations are relatively well preserved, whereas to the north the rocks are more deformed and metamorphosed. The deposits are mostly thin-bedded sand dominated $T_{a-c/d}$ or base absent $T_{b-c/d}$ turbidites with medium sand as the largest observed grain size. Bedding planes are usually parallel and major channelling is absent. The deposits were possibly formed in lobe environments (*cf.* Mutti & Normark, 1987). Four stages of post-depositional deformation, associated with the Late Palaeozoic to Early Mesozoic easterly-directed subduction at the margin of Gondwana (present coordinates) and the build-up of the Andes in Cretaceous to Cenozoic times, have been determined for the Eastern Andean Metamorphic Complex (Bell & Suárez, 2000). The E-W shortening is less pronounced in the southern part of the mainland study area than in the northern part (Ramos, 1989). The metamorphic pressure during the Late Palaeozoic - Early Mesozoic metamorphic phase is estimated to have been intermediate (8 ± 4 kb; Ramírez *et al.*, 2001).

The outcrops of the Eastern part of the Eastern Andean Metamorphic Complex in the Chilean mainland and archipelago, as well as the Argentinean formations, are separated by the Mesozoic-Cenozoic Patagonian Batholith from basement outcrops further to the west in the Chilean archipelago (Fig. 1a). In the north, the Liquiñe-Ofqui Fault Zone, a NNE-SSW trending dextral shear zone, which has been active at least since the Oligocene, may have displaced the western part of the metamorphic basement of the Andes northward by 440-550 km from a former position closer to the Eastern Andean Metamorphic Complex (Fig. 1a; García *et al.*, 1988). Further, in Jurassic times the southern part of Patagonia might have undergone major displacement along the Gastre Fault System, a NW-SE trending dextral shear zone in northern Patagonia (Fig. 1a; Rapela & Pankhurst, 1992). Rapela & Pankhurst (1992) argue that a dextral displacement of 500 km is possible.

1.2. Aims

The aim of the presented study is to reconstruct the sedimentary and palaeogeographic development of the Late Palaeozoic to Early Mesozoic Pacific continental margin of Gondwana in southern Chile (present coordinates). Several different analytical techniques are combined in this study to elucidate source rock characteristics of the sediments of the Eastern Andean Metamorphic Complex, the Río Lácteo and Bahía de la Lancha formations and to obtain information about the sedimentary transportation paths and the tectonic setting in the present Patagonian Andes at the time of deposition. They include the analysis of the light minerals (including cathodoluminescence colour spectra of quartz grains) and the heavy mineral fraction (including chemistry of tourmaline grains). Furthermore, a set of whole-rock samples was analysed for its major and trace element chemistry and Sm-Nd and Rb-Sr isotope systematics. In addition, single detrital zircons from five samples were dated with the sensitive high-resolution ion micro-probe (SHRIMP) U-Pb method, and selected zircons were analysed for their Hf isotope signatures. The results from the cathodoluminescence (CL) study, as well as parts of the whole-rock element chemistry and Sm-Nd isotopes were published in Augustsson & Bahlburg (2003a, 2003b). The resulting information concerning depositional conditions, characteristics of the source rocks and depositional age indications are used as a contribution to the understanding of the plate tectonic evolution of the Late

Palaeozoic - Early Mesozoic south-west Pacific margin of Gondwana (present coordinates).

As mentioned above, the data presented in this thesis are obtained with four different petrographic techniques as well as three whole-rock chemistry, and two zircon analysis techniques. The results of these are discussed in three separate Sections (3.4., 4.3. & 5.3.). The main regional implications and interpretations are discussed in Sections 4.3. and 5.3.

1.3. Age

The Eastern Andean Metamorphic Complex and the Río Lácteo Formation are correlated with the Bahía de la Lancha Formation and have been assumed to be similar in age (Riccardi & Rolleri, 1980). No fossil evidence for the depositional age of the Eastern Andean Metamorphic Complex or the Río Lácteo Formation has been reported. In the Bahía de la Lancha Formation, Upper Devonian to Lower Carboniferous plant remains and tetrapod traces have been found (Riccardi, 1971; Fig. 2 & 3). However, estimates of maximum depositional ages from U-Pb dating of detrital zircons (Hervé *et al.*, 2003a; this study), and minimum depositional ages from zircon fission track dating (Thomson & Hervé, 2002), indicate a much more complex history of these geological units than earlier assumed. Published depositional ages for the basement sediments of the southern Patagonian Andes up to date are summarized in Figure 2. An attempt to reconstruct the chronology of the sediments in different geographical areas is presented in Figure 3. To a large degree, this is based on assumptions made from U-Pb zircon age spectra of sedimentary samples. Thus, large uncertainties remain.

A sediment sample of the Bahía de la Lancha Formation indicates deposition of this Formation not earlier than in the Early Carboniferous (this study; Fig. 3). This is in agreement with the Upper Devonian to Lower Carboniferous fossil ages of this Formation (Riccardi, 1971). However, one zircon U-Pb age from two different growth phases indicate that the Bahía de la Lancha Formation might be even younger (see Section 5.1.3.).

For the Río Lácteo Formation, no fossil ages have been reported. It has a Late Carboniferous to Permian minimum depositional age, as indicated from an intruding tonalite, which has a K-Ar age of 283 ± 10 Ma (Ramos, 1989; Fig. 3).

The Cochrane unit of the Eastern Andean Metamorphic Complex has been assumed to be equivalent to the Bahía de la Lancha and Río Lácteo formations (Riccardi & Rolleri, 1980). However, U-Pb and fission track data of the Cochrane unit (Thomson & Hervé, 2002; Hervé *et al.*, 2003a; this study) point to either a long continuous depositional time span for this unit, partly contemporaneous with metamorphism, or several periods of sedimentation, partly post-dating the deposition of the Bahía de la Lancha Formation (Fig. 3). This is also indicated by a basic dyke at Río Bravo (Fig. 1b), with a K-Ar intrusion age of 246 ± 9 Ma (Yoshida, 1981), which is similar to the maximum depositional age of a sediment further to the west (Fig. 2 & 3). An Early Carboniferous sedimentary phase is probable, most likely in the area of Lago O'Higgins / Lago San Martín, where the Early Carboniferous Bahía de la Lancha Formation crops out. However, detrital zircons of Permian age in a sediment from Fiordo Baker (Hervé *et al.*, 2003a; Fig. 2) indicate a much younger age of deposition for parts of the Cochrane unit. Therefore, the Cochrane unit is separated into two depositional phases in Figure 3. By the time of deposition of the younger, possibly Triassic, part, the older, possibly Carboniferous, part of the Cochrane unit had already undergone metamorphism

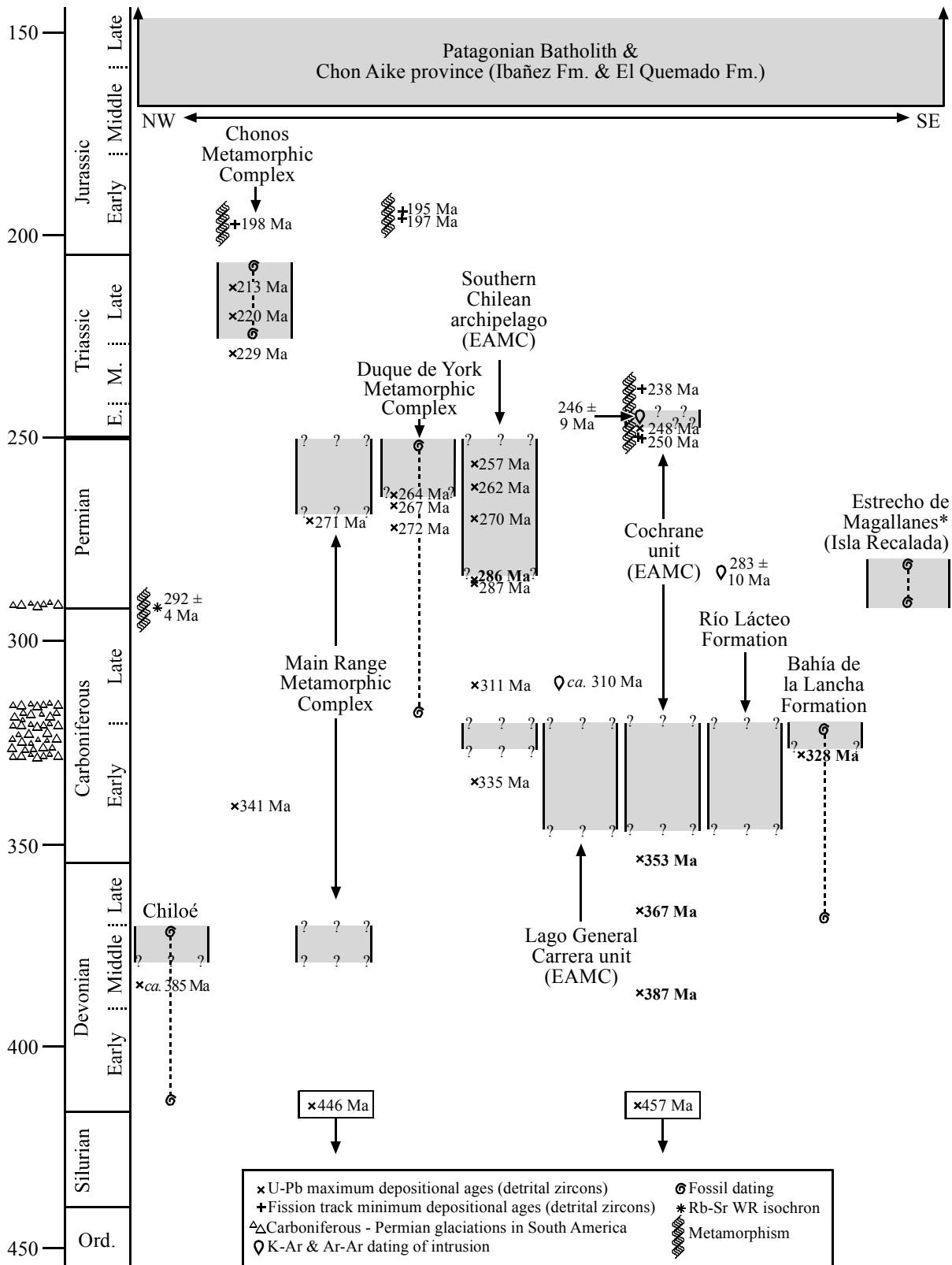


Fig. 3. Stratigraphy of the Late Palaeozoic - Early Mesozoic of the south Patagonian Andes (ca. 42-52°S). For location of the different metamorphic complexes and geographical areas, see Figures 1b and 2. Rb-Sr data: Pankhurst *et al.* (1992). K-Ar- & Ar-Ar data: Yoshida (1981); Ramos (1989); R. de la Cruz (pers. comm.). Estimates of glacial extensions from González (1990). For further references, see Figure 2. For the U-Pb ages, their 1σ-errors were considered (except for the zircon at Chiloé), and 2σ-errors for the fission track ages. The time scale was compiled by Remane (2000). EAMC = Eastern Andean Metamorphic Complex. *Hervé *et al.* (2003b) report that unpublished data indicates an Early Permian depositional age also for sediments on Isla Desolación north of Isla Recalada.

(Fig. 3).

An indication of the minimum age of the Lago General Carrera unit is given by K-Ar and Ar-Ar ages of a granite, intruding into the basement sediments. The dating gave ages of the granite of 307 ± 7 Ma and 311 ± 3 Ma (R. de la Cruz, pers. comm.; Fig. 3). This indicates deposition in the Carboniferous at the latest.

Similar to the Cochrane unit, the part of the Eastern Andean Metamorphic Complex cropping out in the southern Chilean archipelago might have several different depositional ages. The SHRIMP U-Pb data of several samples indicate Permian maximum depositional ages (Hervé *et al.*, 2003a; this study; Fig. 3). Deposition shortly after the growth of the youngest zircons would imply a depositional timespan throughout the Permian, or several shorter pulses of sedimentation. The presence of sediments with older youngest zircons (Hervé *et al.*, 2003a) makes it possible that parts of the Eastern Andean Metamorphic Complex in the southern Chilean archipelago have an older age (*cf.* Fig. 3).

The stratigraphy in Figure 3 points to the fact that the present nomenclature for the Eastern Andean Metamorphic Complex might be inappropriate. However, to avoid confusion while awaiting further investigations leading to a better understanding of the age relationships for these sediments, the present nomenclature is used throughout this thesis.

The existing indications of depositional ages of the Eastern Andean Metamorphic Complex, the Río Lácteo and the Bahía de la Lancha formations confirm that a large part, if not all, of these sediments are younger than the sediments at Chiloé, where a biostratigraphic age and a U-Pb age constrain the deposition to the Middle Devonian (Fortey *et al.*, 1992; Duhart *et al.*, 2001; Fig. 2 & 3). The Eastern Andean Metamorphic Complex might partly be coeval with the Duque de York Metamorphic Complex and sediments on Isla Recalada in the vicinity of the Strait of Magellan (Fig. 2 & 3). It might also be partly coeval with the Main Range Metamorphic Complex, although the age of these sediments is not well constrained (Hervé *et al.*, 2003a; Fig. 2 & 3). Furthermore, the Eastern Andean Metamorphic Complex is older than the Late Triassic sediments of the Chonos Metamorphic Complex (Fang *et al.*, 1998; Hervé & Fanning, 2001; Fig. 2 & 3).

The minimum depositional ages are stratigraphically constrained by the overlying volcanic Chon Aike province (Ibañez and El Quemado formations) of Jurassic to Early Cretaceous age (Pankhurst *et al.*, 1998a, and references therein), and the Patagonian Batholith, active from Middle Jurassic to Cenozoic times (Bruce *et al.*, 1991, and references therein; Pankhurst *et al.*, 1999). However, fission track data (Thomson & Hervé, 2002) indicate several metamorphic phases for the basement sediments in Permian to Early Jurassic times, predating both the Patagonian Batholith and the Chon Aike province. Further, a Late Carboniferous (292 ± 4 Ma) Rb-Sr whole-rock isochron from the metamorphosed basement sediments at Chiloé (Pankhurst *et al.*, 1992) indicates that the Late Palaeozoic subduction at the South Patagonian Pacific margin of Gondwana (present coordinates) might have been active already at that stage.

2. Sample descriptions

The majority of the sediment samples collected and finally analysed for this study are from the Cochrane unit. Additionally, the Lago General Carrera unit, the part of the Eastern Andean Metamorphic Complex cropping out in the southern Chilean archipelago, the Río Lácteo and Bahía de la Lancha formations were studied.

Most of the studied rocks are sandstones from medium to thick sediment beds (*ca.* 10-50 cm). They are usually grey greywackes and moderately sorted. Most of them are dominated by an apparent grain size of 50-300 μm . All of the analysed sandstones are dominated by subrounded quartz grains. Many of the sandstones show cleavage defined by mica-rich planes. In addition seven grey pelites and one breccia have been analysed.

Lago General Carrera unit. The greywacke of the Lago General Carrera unit (CA-00-03) is grey and has a dominant grain size of 50-150 μm . The rock is cut by thin (≤ 1 mm wide) quartz veins. The pelite CA-00-02 is very finely laminated and shows crenulation cleavage defined by mica planes. These samples were collected *ca.* 100 m apart from each other.

Cochrane unit. The greywackes CA-00-09, -13, -15, -17, -23, -26, -28 and -30 of the Cochrane unit have dominant grain sizes of 50/100-150/300 μm . CA-00-12, -21, -35 and -42 are greywackes dominated by grains 20/50-250 μm large and a finer grained quartz matrix. CA-00-21 and CA-00-35 are cut by thin (≤ 1 mm wide) quartz veins. CA-00-10 is a greywacke relatively rich in secondary biotite and is dominated by quartz grains 50-150 μm large. CA-00-04 is a greywacke dominated by grains *ca.* 100 μm large. It shows crenulation cleavage defined by mica planes. CA-00-37 is the coarsest of the greywackes with a dominant grain size of 100-700 μm . The matrix is dominated by quartz. CA-00-32 and CA-00-33 are greywackes that represent the coarse grained parts of two completely sampled 10-15 cm thick base absent $T_{b-d/e}$ turbidites. They grade from planar sandstone into ripple cross lamination, followed by symmetrical ripples and parallel lamination, underlaying several cm of mudstone. The coarsest grain size is *ca.* 500 μm for CA-00-32 and *ca.* 300 μm for CA-00-33.

The pelites CA-00-19 and -27 are thinly laminated. CA-00-27 shows interlayering of mm-thick laminae of coarser grained asymmetric ripples and cleavage defined by mica planes. Also pelite CA-00-14 shows cleavage along mica planes. CA-00-25 is a pelite with crenulation cleavage and cross-cutting thin (< 1 mm wide) veins containing secondary pyrite.

The grey breccia CA-00-24 derives from a 2-3 dm thick breccia layer. It contains sedimentary rock fragments up to > 10 mm in size.

Río Lácteo Formation. The greywackes of the Río Lácteo Formation (CA-01-02, -03) are grey and have dominant grain sizes of 50-100 μm . They are cut by quartz veins. CA-01-02 is weakly laminated. The pelite CA-01-01 show mica planes with crenulation cleavage.

Bahía de la Lancha Formation. The sandstones of the Río Lácteo Formation (CA-01-04 to -07) are grey and have dominant grain sizes of 100/150-300 μm . The base of the sandstone layer of CA-01-05 shows load cast.

Southern Chilean archipelago. The greywackes of the southern sampling area in the southern Chilean archipelago (FA-01, -02 and -11) are grey and have dominant grain sizes of 50/100-100/350 μm . FA-01 and FA-11 are rich in secondary biotite. FA-10 is a fine-laminated pelite. The greywackes of the northern sampling area in the southern Chilean archipelago (FF-01, -04 and -06) are grey and dominated by grains 50-150 μm in size. FF-04 is rich in secondary biotite.

3. Petrography

The light and heavy mineral compositions of sediments are widely used as provenance proxies (*e. g.*, Marsaglia & Ingersoll, 1992; Nechaev & Isphording, 1993; von Eynatten & Gaupp, 1999; Wozazek & Krawinkel, 2002). Especially the analysis of the light mineral framework composition, can be rather unproductive compared to the analytical effort needed (von Eynatten *et al.*, 2003). Nevertheless, the framework petrography gives the first important indications of the nature of the sediment and should therefore not be underrated. Here, the study of the light and heavy mineral compositions are combined with the cathodoluminescence characteristics of single detrital quartz grains and the analysis of the major element composition of single detrital tourmaline grains.

3.1. Light framework mineral content

3.1.1. Light framework mineral content: methods

One arenite and 20 greywacke samples with minor post-depositional metamorphic and deformational overprints were selected for the petrographic study. The $\geq 63 \mu\text{m}$ grain-size population of 19 of these samples were point-counted with the Gazzi-Dickinson method (Dickinson, 1970) to determine their framework petrographic composition (Tab. 1). 340-940 light mineral grains, with a total of *ca.* 1000 points, were counted in each sample.

3.1.2. Light framework mineral content: results and implications

The greywackes from the Eastern Andean Metamorphic Complex and the Río Lácteo Formation have matrix contents of 40-60 %, whereas the sediments from the Bahía de la Lancha Formation have < 28 % matrix (Tab. 1). The clasts are dominated by angular to subrounded quartz and to a minor degree plagioclase grains (Tab. 1, Fig. 4). Lithic fragments are rare and they are totally dominated by sedimentary rock fragments. The rock fragments of one breccia from close to Villa O'Higgins (CA-00-24; Fig. 1b), and with clasts up to several cm in size, are all of sedimentary origin. In the greywackes, there are signs of alteration of feldspars to clay minerals, and secondary precipitation of calcite as veinlets and cement in the matrix. Heavy minerals are sparse and often dominated by zircons (Tab. 1).

The tectonic setting of the depositional basin can be deduced by the framework petrography with the aid of the ternary diagram of Dickinson & Suczek (1979; Fig. 4), provided that matrix contents are < 25 %. Most of the samples in this study have matrix contents above this value. It is most likely that the matrix contents were lower prior to alteration (*cf.* Galloway, 1974). Recalculation down to 25 %, assuming that the matrix originates from labile rock fragments and feldspars (*cf.* Dickinson, 1970), reveals a possible original framework composition with a lower quartz fraction than the present one (Fig. 4). Due to the observed alteration, the framework petrography is not satisfactory as provenance indicator for the studied sediments.

3.2. Cathodoluminescence of quartz¹

Mature sediments dominated by quartz grains usually have been modified considerably from source area to depositional basin. With a lack of provenance-characteristic rock fragments,

¹The results in Section 3.2 are published in Augustsson & Bahlburg (2003b).

Table 1. *Petrography*

	Cochrane unit											
	CA-00 -09-S	CA-00 -13-S	CA-00 -15-S	CA-00 -17-S	CA-00 -23-S	CA-00 -26-S	CA-00 -28-S	CA-00 -30-S	CA-00 -32-S	CA-00 -32A-S ¹	CA-00 -32B-S ¹	CA-00 -33A-S ¹
Quartz	365	355	469	386	452	295	479	422		550	507	406
Feldspar	34	71	189	97	84	59	72	78		53	59	47
Lithic fragments*	2	-	3	2	-	-	1	4		1	-	-
Quartz (%)	91.0	83.3	71.0	79.6	84.3	83.3	86.8	83.7		91.1	89.6	89.6
Feldspar (%)	8.5	16.7	28.6	20.0	15.7	16.7	13.0	15.5		8.8	10.4	10.4
Lithic fragments (%)	0.5	-	0.5	0.4	-	-	0.2	0.8		0.2	-	-
Matrix (%)	58.7	55.7	32.1	48.8	45.6	63.7	43.9	48.1		36.4	41.3	52.4
Zircon	12		4	44	21			65	10			
Tourmaline	13		2	7	8			22	11			
Rutile	4		1	22	17			48	13			
Anatase / brookite	-		-	5	-			11	-			
Garnet	-		-	-	2			-	192¶			
Titanite†	-		88	-	73			-	-			
Epidote‡	55		59	-	-			-	-			
Allanite	7		5	-	-			-	3			
Apatite	10		8	5	9			11	8			
Chromite	-		-	-	1			-	2			
Undefined	1		1	18	1			1	-			
Others§	-		1	-	-			-	-			
Sum	102		169	101	132			158	239			
ZTR (%)	28.7		4.1	72.3	34.8			85.4	14.2			
Pumpellyite	-		-	-	-			-	-			
Chlorite	-		4	11	6			37	7			
Biotite	10		-	-	-			-	1			
Muscovite	2		2	1	1			-	-			
TiO ₂ -leucoxen	3		-	88	-			22	23			
Opaque	377		31	131	63			146	7			

	Cochrane unit			Río Lácteo Formation	Bahía de la Lancha Formation			Southern Chilean Archipelago			
	CA-00 -33B-S ¹	CA-00 -37-S	CA-00 -42-S	CA-01 -03-S	CA-01 -04-S	CA-01 -05-S	CA-01 -06-S	CA-01 -07-S	FF -01-S	FA -01-S	FA -02-S
Quartz	400	332		374	539	653	584	758	461	386	285
Feldspar	22	120		25	146	125	149	180	37	80	55
Lithic fragments*	-	14		-	4	-	2	-	5	8	6
Quartz (%)	94.8	71.2		93.7	78.2	83.9	79.5	80.8	91.7	81.4	82.4
Feldspar (%)	5.2	25.8		6.3	21.2	16.1	20.3	19.2	7.4	16.9	15.9
Lithic fragments (%)	-	3.0		-	0.6	-	0.3	-	1.0	1.7	1.7
Matrix (%)	56.9	41.4		56.9	27.5	16.6	23.6	4.5	49.2	41.1	64.4
Zircon			6		34	4	25	3			9
Tourmaline			1		20	11	16	1			-
Rutile			8		21	18	38	7			-
Anatase / brookite			-		3	-	-	-			-
Garnet			1		-	17¶	-	46¶			3¶
Titanite†			50		-	-	-	-			-
Epidote‡			53		-	-	-	-			-
Allanite			1		-	-	-	-			1
Apatite			4		16	16	15	2			6
Chromite			-		1	2	2	-			-
Undefined			2		1	-	-	1			1
Others§			-		4	6	2	-			1
Sum			126		100	74	98	60		21	
ZTR (%)			11.9		75.0	44.6	80.6	18.3		42.9	
Pumpellyite			-		-	-	1	-			-
Chlorite			1		31	5	18	3		40	
Biotite			-		2	-	-	-		334	
Muscovite			-		1	-	-	2		2	
TiO ₂ -leucoxen			-		80	28	32	10		-	
Opaque			6		194	179	280	160		322	

- = not detected. *Solely of sedimentary origin. †Includes leucoxen with CaTiSiO₃-composition. ‡Includes zoisite and clinozoisite.

§Kyanite, staurolite, chloritoid, wollastonite, monazite and scheelite. ||Includes 11 grains of an unidentified Zn-rich mineral and three grains of an unidentified Ca- & Ce-rich mineral. ¶Close to almandine composition, single analysis from CA-01-07:

Fe_{1.97}Mg_{0.84}Ca_{0.14}Mn_{0.04}Al_{2.01}Si_{3.00}O₁₂. ¹A- & B-samples from the same turbidite beds. A-samples are coarser-grained than B-samples.

the framework petrography of quartz-rich sandstones is not always reliable as a provenance indicator. However, along with other techniques the cathodoluminescence (CL) characteristics of quartz can be used as provenance indicators (*e. g.*, Götze & Zimmerle, 2000). The CL characteristics depend on variations in temperature, pressure and chemical

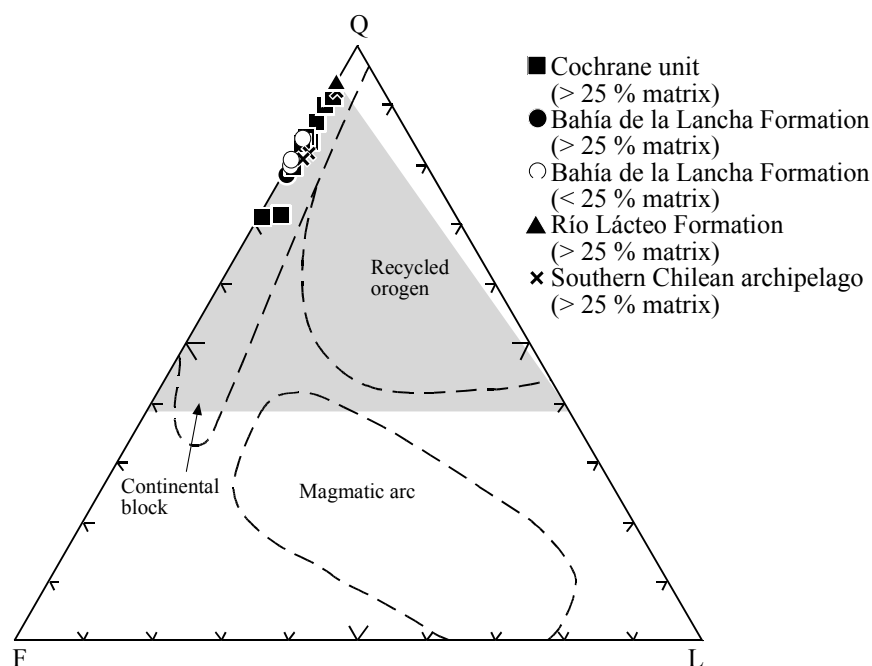


Fig. 4. Framework petrography. Discriminating fields after Dickinson & Suczek (1979). Q = total quartz, F = feldspar, L = lithic fragments. Recalculation of the matrix contents down to 25 % gives possible original compositions for all sediments in the grey field.

environment during quartz crystal growth and later events (*e. g.*, Zinkernagel, 1978; Matter & Ramseyer, 1985). Thus, the CL signal of single quartz grains can be used as indicators for the source rocks. This assumes that the CL properties of the single quartz grains in the analysed sediments were achieved in the sedimentary source area and have remained unchanged since then.

CL spectra are usually dominated by two emission bands. One is in the blue wavelength interval at 460-490 nm, and the other in the red interval at 610-640 nm (Fig. 5). They are caused by intrinsic lattice defects and nonbridging oxygen hole centers, respectively (Götze *et al.*, 2001, and references therein). The trough between the emission bands will be positioned at different wavelengths in response to differences in the peak positions, and the width, height and symmetry of the peaks.

The CL colour of quartz and its implications for provenance studies have been treated by several authors (*e. g.*, Zinkernagel, 1978; Götze *et al.*, 2001). The most important quartz types are presented below.

(1) Crystallisation at high temperatures and fast cooling generates red or bright blue luminescing quartz. This usually appears in volcanic rocks, or in rocks affected by contact metamorphism. The CL spectrum of red luminescing quartz is dominated by a high peak in the red wavelength interval, and it has a lower peak in the blue range (from now on called red peak or red emission band, and blue peak or blue emission band, respectively). The trough between the emission bands is deep. Spectra of quartz with a bright blue CL colour are dominated by a high blue peak. The red peak is much less pronounced, with the result that the trough between the peaks appears to be situated at longer wavelengths than for red luminescing quartz (Fig. 5). An intermediate variant, with violet CL colours, occurs when the peaks are approximately of the same height.

(2) With lower crystallisation temperatures and slower cooling, the CL signal of

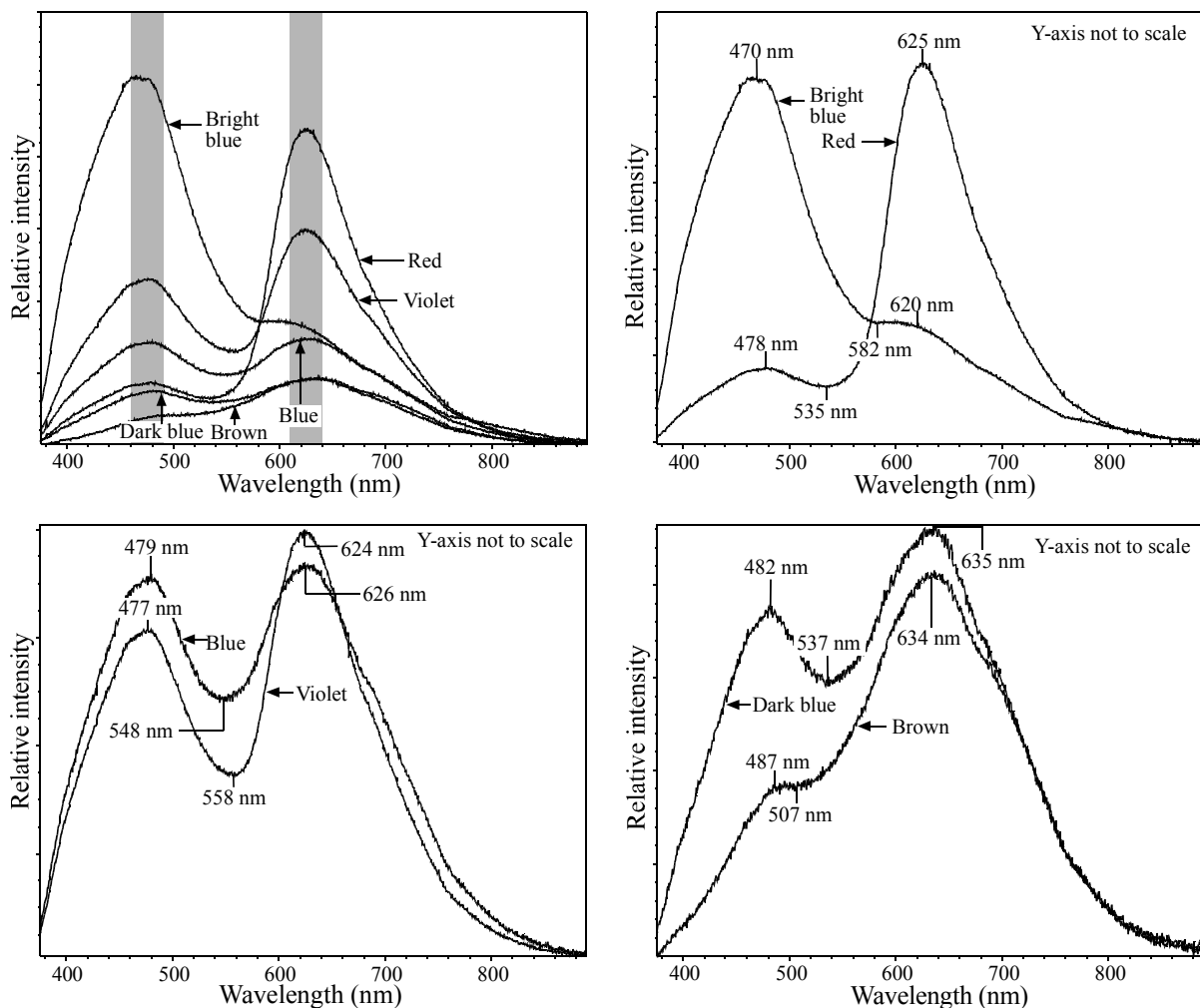


Fig. 5. Typical spectra for different CL colours of quartz. All spectra are from sample CA-00-30 and measured with the same machine settings. Grey fields = areas for the mains peaks.

quartz is less intense and the grains usually appear dark blue. This type is common in plutonic rocks, due to their slower cooling rates compared to volcanic rocks. In the corresponding spectrum, the red peak is higher than the blue one. The emission bands are not as high, and the trough not as deep, as for quartz of volcanic origin. As a consequence of the peak characteristics, the trough is situated at shorter wavelengths than for bright blue luminescing quartz (Fig. 5).

(3) According to Zinkernagel (1978), diagenetically grown quartz, and quartz that crystallises below *ca.* 300°C, is non-luminescent. Thus, the CL spectrum should lack emission bands. However, others (*e. g.*, Ramseyer *et al.*, 1988; Neuser *et al.*, 1989) have observed different CL colours for authigenic quartz from weak blue through green to red-brown. These colours are often short-lived, and turn into a dark brown shade after seconds, or a few minutes, of electron bombardment.

(4) Regional metamorphism can alter the original CL signal. This usually results in a brown appearance of the quartz grains. The corresponding spectrum is dominated by the red peak and has a much less pronounced blue peak. The emission bands are situated at slightly longer wavelengths, and the trough at shorter wavelengths, than for blue or red luminescing quartz (Fig. 5). For quartz affected by a high metamorphic grade, the original CL colour may change into a blue shade. Boggs *et al.* (2002) compared the red, green and blue colour intensities in photographs of quartz of different origin, and noted that the colour intensities of

metamorphic quartz can be similar to those of plutonic and volcanic origin.

In provenance studies dealing with the CL colours of quartz, commonly only optical observations of the CL colours are performed. However, optical recognition of colours is always subjective and can differ markedly from one observer to another. Excitation conditions also affect the brightness of the observed colours. In an attempt to overcome these problems, in this study the CL spectra of individual quartz grains were compared; the apparent positions of the blue and the red peaks and their relative heights were evaluated and used as provenance indicators for sediments.

3.2.1. Cathodoluminescence of quartz: methods

Samples from the Cochrane unit and the Bahía de la Lancha Formation with low calcite contents and with CL colours in quartz typically unaffected by post-depositional metamorphism were chosen for the CL study. Post-depositional metamorphism has affected the CL characteristics of individual quartz grains in some samples from the study area, and incorporation of such samples in the CL study would overestimate the population of quartz grains with metamorphic sources. Furthermore, calcite is a strongly luminescing mineral, with its main CL peak in the red wavelength range, close to the position for the red CL peaks of quartz. It can therefore affect the much weaker CL signal of quartz, if not dissolved prior to CL analysis. The above criteria are fulfilled for three of the greywacke samples from the Cochrane unit (CA-00-28, -30 and -35) and all four samples from the Argentinean Bahía de la Lancha Formation (CA-01-04, -05, -06 and -07). CL spectra were measured for randomly selected quartz grains of the $\geq 130 \mu\text{m}$ size population in these samples. Sample CA-00-35 from the Chilean Eastern Andean Metamorphic Complex is a special case. It is affected by post-depositional metamorphism and has not been point-counted, but could be used for the CL study, since the CL characteristics of the $\geq 130 \mu\text{m}$ quartz grain population were not affected. In this sample, 18 quartz grains were analysed. 32-87 grains were selected in each of the other six samples; the amount of grains analysed in each sample being dependent on the availability of grains $\geq 130 \mu\text{m}$ large.

The CL investigations were carried out with polished thin sections coated with carbon. A hot-cathode luminescence microscope (HC-1LM) coupled with a water-cooled ANDOR OE-CCD detector was used. The spot diameter was $40 \mu\text{m}$. The system was operated at 13 kV with a sample current of $5 \mu\text{A}$. The spectra were measured at temperatures between -70° and -64°C . Wavelength calibrations were made with Hg and Ar lamps. Spectral lines with wavelengths between 375 and 890 nm, and a resolution of $\leq 1.04 \text{ nm}$ (*cf.* Kaus, 2002), were recorded. All spectra are background-corrected and had measuring times of $100 \cdot 1.063 \text{ s}$, *i. e.*, totally 106.3 s.

In this study, the distribution of quartz grains with different CL properties was used as a guide to the source rocks for the studied sediments. However, caution must be employed in the interpretation. Long exposures to CL light can affect the CL colour and the detected signal (*e. g.*, Neuser *et al.*, 1996; Götze & Zimmerle, 2000). The alteration of CL colours and spectra is not only dependent on the exposure times but is also a function of excitation conditions. With the chosen settings and measuring times the CL signal from the quartz grains is sufficiently high to be unaffected by small variations in the background signal. Small changes in the spectra were observed during measurement. The blue peak decreased slightly, whereas

the red emission band increased slightly. These changes were, however, small and not considered to affect the larger spectral variations between quartz of different origin.

3.2.2. Cathodoluminescence of quartz: results

The CL study reveals red to blue and brown luminescing quartz grains. Optically, 49 % of the grains in all studied samples were classified as brown quartz, 27 % as dark blue, 16 % as blue (neither bright blue nor dark blue), < 1% as bright blue, 5 % as violet and 2 % as red (Fig. 6a). To overcome the subjective perception of colours, CL spectra from single quartz grains were classified into different spectral types based on the scheme of Zinkernagel (1978), who presented typical spectra for the most common CL colours of quartz. Typical spectra for each CL colour class are presented in Figure 5. This classification shows that 35 % of the quartz grains have CL spectra typical of brown luminescing quartz, 26 % of dark blue, 21 % of blue, 8 % of bright blue, 5% of violet and 5 % typical of red luminescing quartz. This is a notable difference compared to the results based on optically identified CL colours (Fig. 6a).

3.2.3. Cathodoluminescence of quartz: new data evaluation method

The classification of single CL spectra can be tedious. To avoid classification of seemingly similar spectra into different colour categories, a thorough comparison between individual spectra must be undertaken. A less time consuming alternative is to compare the peak positions, and their relative heights. The two main CL peaks for quartz in the blue and the red wavelength intervals, respectively, show slightly different positions for quartz with different

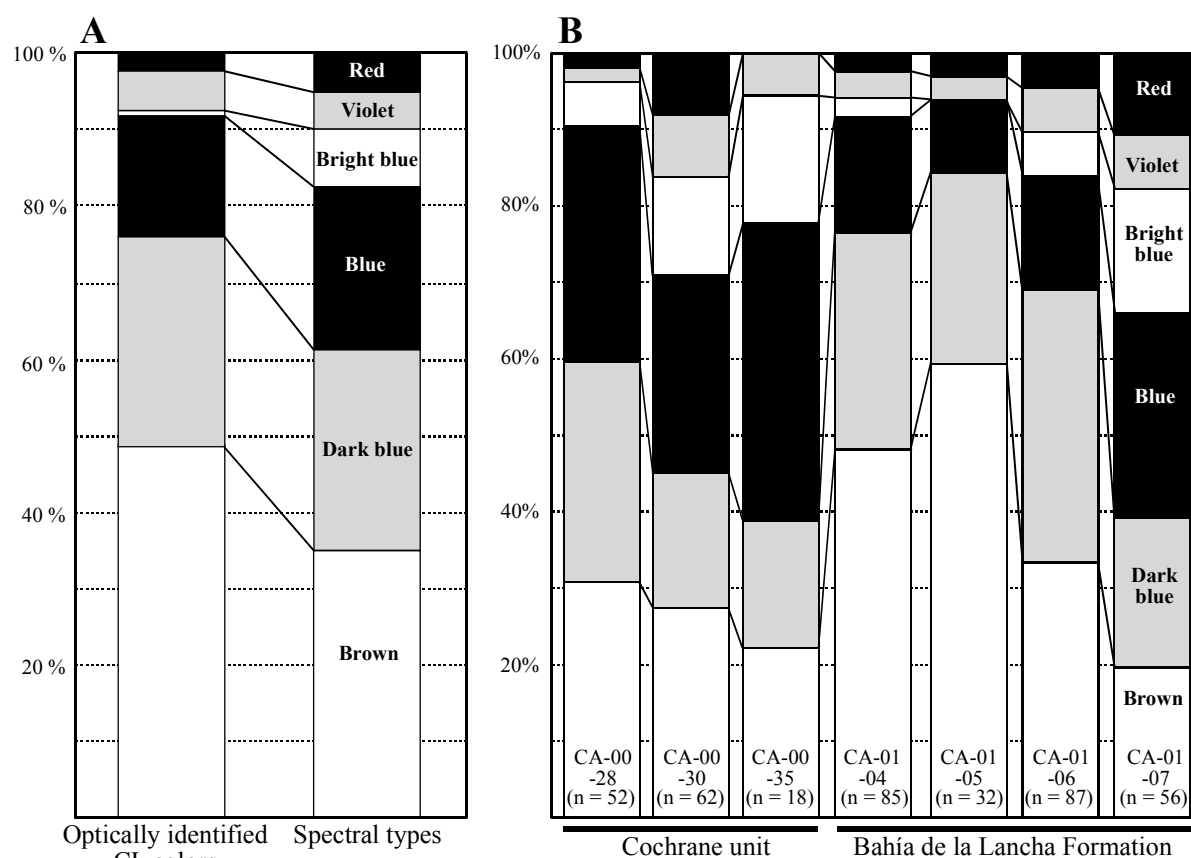


Fig. 6. (a) Comparison between the optical CL classification of quartz and the classification based on the CL spectral types for the total quartz grain population. (b) Results from the spectral identification for the individual samples.

CL colours. In response to differences in peak heights and peak widths, the trough between the peaks changes in position (*cf.* Fig. 5). Quartz that has cooled slowly from relatively low temperatures and quartz affected by regional metamorphism (dark blue and brown luminescing quartz, respectively) show longer wavelengths for the two main peaks than quartz with fast cooling from crystallisation at high temperatures (particularly bright blue luminescing quartz). The troughs in spectra typical for bright blue luminescing quartz are positioned at longer wavelengths than in spectra from dark blue or brown luminescing quartz. This is caused by the dominance of the blue peak. A comparison of the peak positions and the trough position has been made in the wavelength diagram of Figure 7. There, the measured quartz grains are sorted after their optically identified CL colours. As a result of the subjective perception of colours, large overlaps occur for different CL colours.

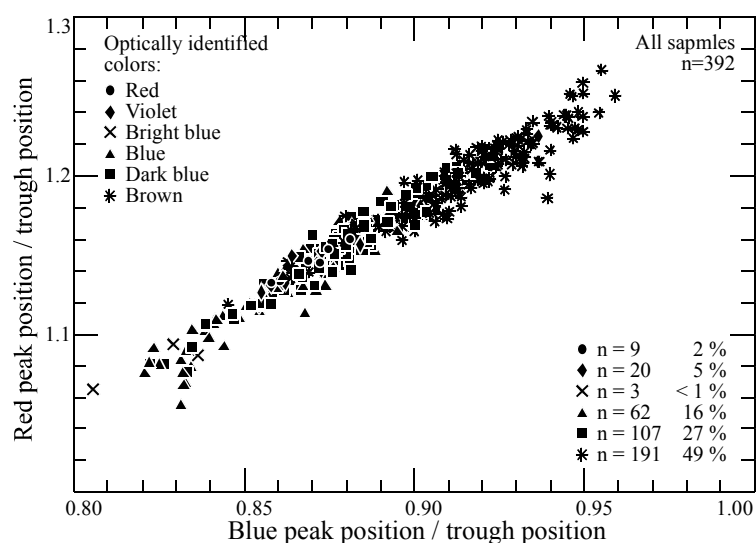


Fig. 7. Comparison of the wavelength positions of the two main peaks to the trough position for the total quartz grain population. The symbols indicate optically detected colours.

Comparison of the peak and trough positions sorted according to spectral types, instead of optically identified colours, leads to a more objective view of the “real” CL colour of the quartz grains. In Figure 8, where the quartz grains are sorted after spectral types, only minor overlap occurs for spectra typical of bright blue, blue, dark blue and brown luminescing quartz grains. The diagram gives an overview of the most common spectral types of quartz grains, and consequently a broad indication of the conditions for the last event affecting the CL properties of the quartz grains. A linear correlation is apparent from bright blue, through blue and dark blue to brown luminescing quartz. This is marked with an arrow in Figure 8a. Since the trough position depends on the peak properties, this trend is expected. However, with the present sample population such a correlation could not be confirmed for spectra typical for red and violet luminescing quartz. Further, the blue peak is often composed of two closely spaced emission bands, which is most obvious for blue luminescing quartz (*cf.* Fig. 5). The additional emission band, at longer wavelengths, might be the result of incorporation of trace amounts of Al in the quartz lattice (Götze *et al.*, 2001, and references therein). For the present sample population, the complexity of the blue peak does not seem to have an effect on the separation into different spectral types, based on the positions of the main peaks.

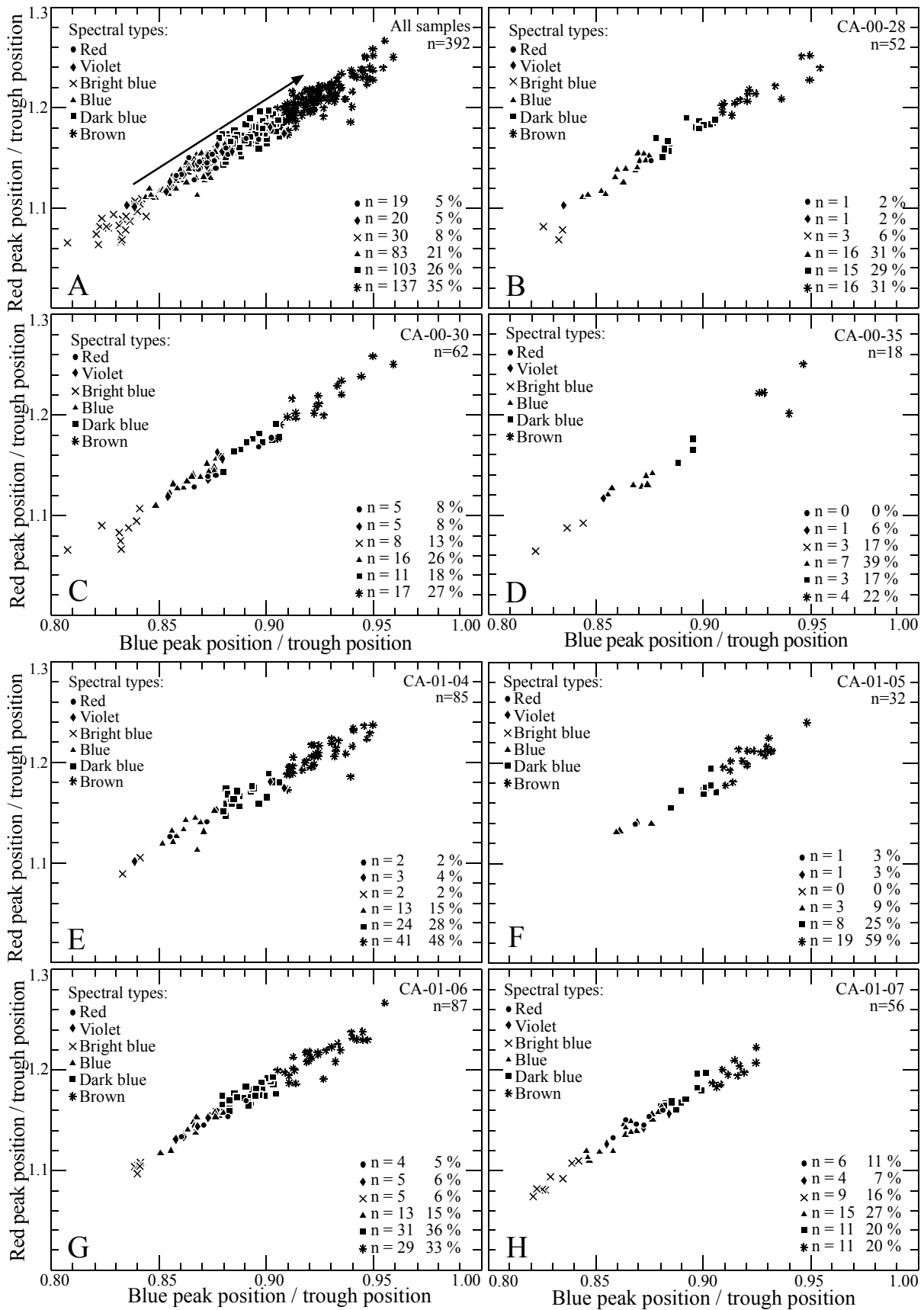


Fig. 8. Comparison of the wavelength positions of the two main peaks to the trough position, sorted by spectral types. (a) The 392 randomly selected quartz grains from all seven samples. The arrow shows the trend from blue luminescing quartz grains affected by events at high temperatures towards lower temperatures and darker shades. (b-h) Individual samples.

The relative heights of the two main peaks in the quartz spectra vary, especially between bright blue and red luminescing quartz. Theoretically, this would make it possible to separate red and violet luminescing quartz from quartz with blue and brown CL colours. Since the absolute intensity of the CL signal depends not only on the CL properties of differently luminescing quartz grains, but also on excitation conditions, a direct comparison of the peak heights would be misleading. To overcome this problem, the peak heights are compared to the depth of the trough between the peaks in Figure 9. The grains are sorted according to their optically identified colours and, as in the wavelength diagram (Fig. 7), a large overlap between quartz grains of different CL colours is present. However, red and violet luminescing quartz is relatively well separated from blue and brown luminescing quartz (Fig. 9). As expected, a trend can be seen from bright blue, through blue and dark blue, to brown luminescing quartz.

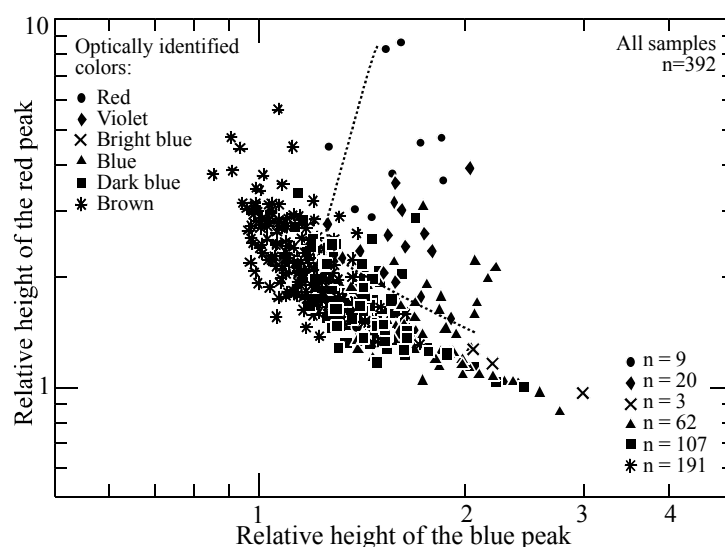


Fig. 9. Comparison of the relative peak heights for the total quartz grain population, calculated by dividing the counts at the peak position by the counts at the trough position. The symbols indicate optically detected colours. Note the logarithmic scale. Most of the quartz grains that were optically identified as red and violet luminescing grains plot to the right of the dotted line.

The trend seen in Figure 9 is even more obvious in Figure 10, where the quartz grains are sorted after spectral types. This diagram shows only minor overlap for the different spectral types. Comparison of the relative heights has the advantage over comparison of the peak positions, that it is possible to identify spectra typical of red and violet luminescing quartz (*cf.* Fig. 10). Despite this, some of those grains plot in areas dominated by dark blue and brown luminescing quartz. This occurs when the relative heights of the emission bands are comparatively low. For brown luminescing quartz, the blue emission band can have a very low relative height, sometimes below 1.0 (*i. e.*, the “trough” is higher than the blue peak). This is usually accompanied by a high relative height for the red emission band, and a blue peak so small, that it is almost unrecognizable (*cf.* Fig. 5).

To base interpretations on optically detected CL colours can give a false picture of the origin of the quartz grains. Particularly populations of quartz grains with dark CL colours tend to be overestimated. Interpretation based on the properties of the CL spectra gives a more objective view of the grain populations. Interpretations based on the classification into different spectral types give similar results to those based on the peak and trough positions

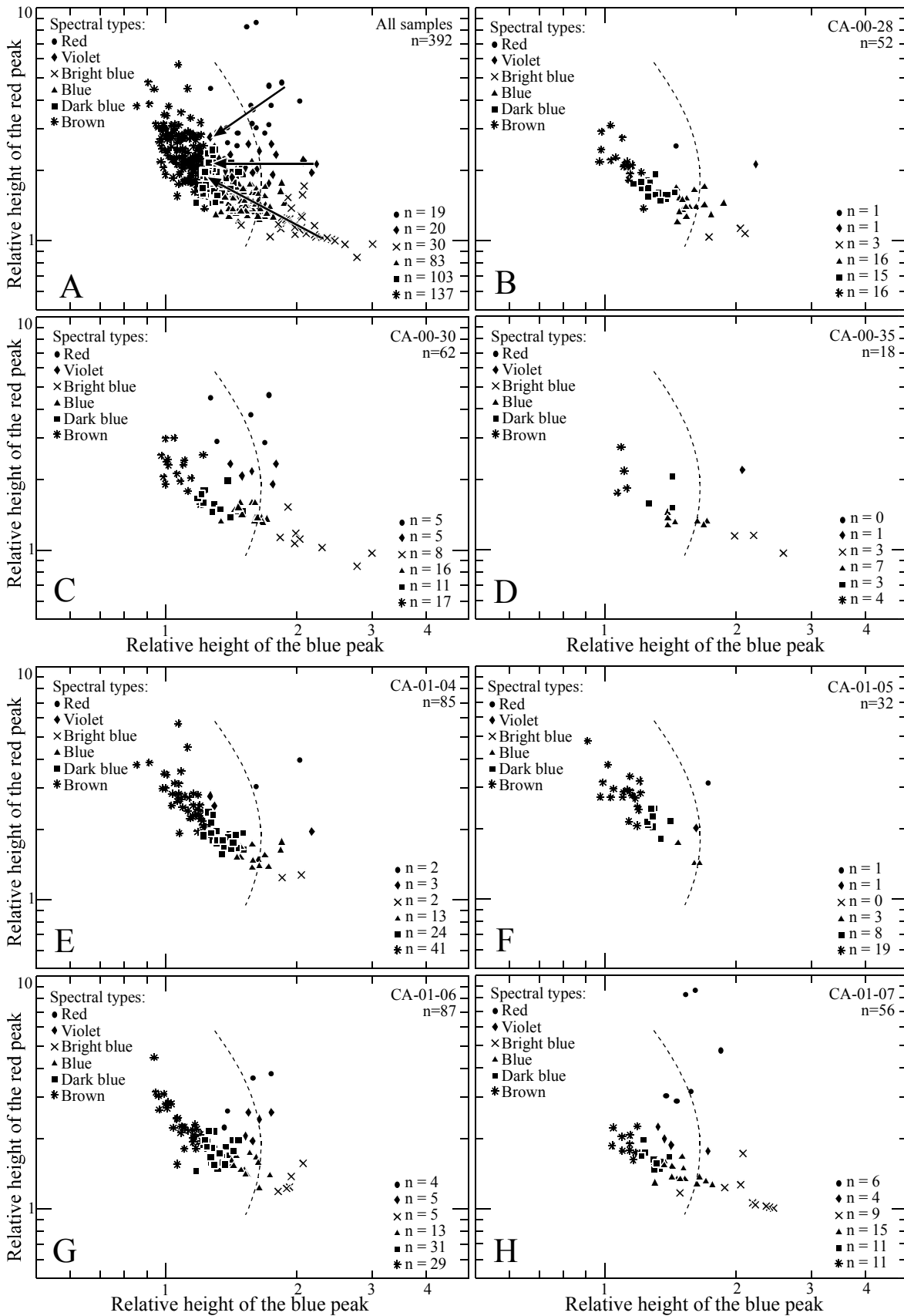


Fig. 10. Comparison of the relative peak heights, sorted by spectral types. The dotted line is an arbitrarily set dividing line between red and violet luminescing quartz grains with high and low relative peak heights. (a) The 392 randomly selected quartz grains from all seven samples. The arrows show the trends from red, violet and blue luminescing quartz grains affected by events at high temperatures towards lower temperatures and darker colours. (b-h) Individual samples.

and their heights, as illustrated by the good separation of quartz with different spectral types in Figures 8 and 10. Despite the demonstrated reliability of this new data evaluation method, it needs to be tested thoroughly with quartz of well-known origin to confirm its usefulness.

3.2.4. Cathodoluminescence of quartz: implications

Thirty five percent of the analysed quartz grains have CL spectra typical of brown luminescing quartz. According to Zinkernagel (1978), they should have a regional metamorphic origin, whereas the 26 % classified as spectra typical of dark blue luminescing quartz should have a plutonic origin. The grains with spectra typical of blue luminescing quartz constitute an intermediate group between dark blue luminescing grains, with a likely plutonic origin, and bright blue luminescing grains, with a probable volcanic origin. They comprise 21 % of the total grain population, for which either a volcanic or a plutonic origin is possible. The bright blue, violet and red luminescing quartz grains would, according to the type spectra of Zinkernagel (1978) be of volcanic origin. They constitute 18 % (8 % bright blue, 5 % violet, 5 % red) of the total population. For violet and red luminescing grains, the optically made discrimination gave similar results to the discrimination based on quartz spectra (Fig. 6a). This is most likely due to the large difference in relative height for the two main peaks for red, blue and brown luminescing quartz. In Figure 10, it is shown that the CL spectra of red and violet luminescing quartz can have very variable relative peak heights. Although the population is small ($n = 39$), a trend can be seen for these populations. By optical means, some grains with CL spectra typical of red or violet luminescing quartz and with low relative peak heights were classified as dark blue or brown, while others appeared dark red or dark violet. In Figure 10, these grains plot close to the fields dominated by spectra typical of dark blue and brown luminescing quartz. The variation in relative peak heights of red and violet luminescing quartz can probably be compared to the trend seen for blue luminescing quartz, where bright blue luminescing quartz is affected by events at higher temperatures and with faster cooling rates than for dark blue luminescing quartz. Zinkernagel (1978) and Walderhaug & Rykkje (2000) observed, without presenting corresponding spectra, that plutonic rocks sometimes also can contain red luminescing quartz grains. This would mean that the population of quartz grains with a volcanic origin might be overestimated if all spectra typical of red and violet luminescing quartz are ascribed to this origin. The dotted line in Figure 10 is an arbitrary dividing line for red and violet luminescing quartz, separating grains with high and low relative peak heights. If the red and violet luminescing quartz grains on the left side of this line are excluded, 50 % of the red and violet luminescing quartz grains fall outside the group with a probable volcanic origin, leaving only 13 % to this category (8 % bright blue and 5 % red or violet). It is more likely that the red and violet luminescing quartz grains with low relative peak heights have a plutonic or metamorphic origin.

Walderhaug & Rykkje (2000) observed variations in the CL colour of quartz, from violet to blue brown in plutonic rocks, and yellow brown to violet brown and violet in metamorphic rocks. According to these authors, this variation is caused by the orientation of the c-axis in the single quartz crystals. Spectra of the different shades were not presented. Violet luminescing quartz grains with high relative peak heights in metamorphic rocks could become a problem in provenance studies. On the other hand, if the violet luminescing quartz of metamorphic origin presented by Walderhaug & Rykkje (2000) has low relative peak

heights, this would confirm the suggestion that violet quartz with low relative peak heights is of plutonic or metamorphic origin. Although the relevance of such colour variations cannot be neglected in provenance studies, the shading differences presented by Walderhaug & Rykkje (2000) seem to be of minor importance for the classification of CL spectra in this study.

Some variations of quartz CL properties can be seen for the individual samples. The wavelength diagrams and the relative peak height diagrams (Fig. 8b-h & 10b-h) reveal a larger spread in CL colour shades for the samples from the Chilean Eastern Andean Metamorphic Complex (CA-00-28, -30, -35) than for the samples from the Argentinean Bahía de la Lancha Formation (CA-01-04, -05, -06, -07). This is confirmed by the classification of 28 % of the spectra from the quartz grain population of the Chilean samples as brown, and 22 % as dark blue, luminescing quartz, whereas for the Argentinean samples 38 % and 28 %, respectively, have these spectral patterns (*cf.* Fig. 6b). This is balanced by a higher percentage of blue and bright blue luminescing quartz grains for the Chilean samples (30 % blue, 11 % bright blue) than for the Argentinean ones (17 % blue, 6 % bright blue). The populations of red and violet luminescing quartz grains are small (5 % red and 5 % violet for both areas). 50 % of these spectra have such low relative peak heights that they plot on the left side of the arbitrary dividing line in Figure 10.

A few grains with red radiation damage have been found, all from the Bahía de la Lancha Formation. Quartz with radiation damage caused by alpha radiation from radioactive elements may luminesce red to yellow in damaged parts of the grains (Owen, 1988; Meunier *et al.*, 1990; Götze *et al.*, 2001). The cores of the damaged grains in this study are brown to blue luminescing and unzoned. Also volcanic quartz phenocrysts may have reddish rims, but the core is commonly zoned, and the reddish colour of the rim can often also be seen in cracks in the crystals (*cf.* Matter & Ramseyer, 1985; Götze *et al.*, 2001). Quartz with radiation rims can appear in leached sediments with former contents of radiogenic minerals, or where the source of radiation was present in a circulating fluid (Meunier *et al.*, 1990). The grains found in the Argentinean sediments show signs of post-radiation abrasion. Thus, the damage is assumed to be of pre-depositional nature, and the grains, irrelevant of the core colour, were probably derived from older sediments.

Some grains from the Bahía de la Lancha Formation show very dark-luminescing diagenetic overgrowths. These, as well as radiation rims, have formed in older sediments. This stresses the fact that recycled quartz from rocks not metamorphosed or heated to above *ca.* 300°C, can inherit the CL colour from older events (Zinkernagel, 1978). Thus, the CL characteristics do not always indicate the last environment for the quartz grains, before incorporation into the sediments.

3.3. Heavy minerals

Ideally, the heavy mineral assemblage in sediments reflects their source rocks. However, due to differences in hydraulic behaviour of different heavy minerals, heavy mineral grains of a uniform size will be deposited in sediments with different grain sizes (*e. g.*, Morton & Hallsworth, 1999). Thus, sediments of varying grain size with a common source might have considerable differences in their heavy mineral suites (*e. g.*, Morton & Hallsworth, 1999). Therefore, a small grain size interval usually is chosen for conventional heavy mineral studies. Zircon, tourmaline and rutile are considered among the most stable heavy minerals,

both mechanically and chemically (*e. g.*, Morton & Hallsworth, 1999). They concentrate in sand-size sediments through sorting processes. However, the dominance of these stable heavy minerals in many sediments can be an artefact, produced by intense chemical weathering in the source area, burial diagenesis and / or metamorphism (*e. g.*, Morton & Hallsworth, 1999). Thus, studies of total heavy mineral suites should be interpreted carefully. For a more reliable interpretation of the heavy mineral content, this approach can be combined with varietal studies of a number of detrital heavy minerals (Götze, 1996, and references therein). In this study, the analysis of the total heavy mineral suites is combined with a varietal study of tourmaline.

3.3.1. Heavy minerals: methods

Twelve sandstone samples were quantitatively analysed for their heavy mineral content (Tab. 1). The 100-125 μm heavy mineral fraction was separated with sodium polytungstate (2.95 g/cm^3). Preferably > 100 transparent heavy mineral grains were counted in each sample.

A total of 94 points in 85 tourmaline grains from 11 samples of the Cochrane unit and the Bahía de la Lancha Formation were analysed with a JEOL Superprobe JXA-8600 MX for their chemistry (Tab. 2). The microprobe investigations were carried out with carbon coated polished thin sections. The system was operated at 15 kV and 15 nA. The analyses were carried out with a focused beam hitting an area of 1-2 μm in diameter. Measuring times were 10 s.

3.3.2. Heavy minerals: content

The heavy mineral content of seven greywackes of the Cochrane unit, four arenites of the Bahía de la Lancha Formation and one greywacke of the southern Chilean archipelago part of the Eastern Andean Metamorphic Complex are presented in Table 1. Most of the analysed sediments have a large proportion of opaque minerals, mainly Fe-oxides and pyrite, and many are rich in leucoxen. In the samples containing titanite, the leucoxen is present in an assemblage of remnants of titanite, calcite and quartz. This was not observed in other samples. Considering the possible origin of leucoxen from titanite and several Fe-, Ti-oxides (Morad & Aldahan, 1985; Klein & Hurlbut, 1993), the leucoxen in titanite-free samples is not treated together with the provenance indicative primary minerals in Table 1. However, the leucoxen in titanite-bearing samples is presented together with titanite. Secondary chlorite was found to varying degrees in all but one sample (CA-00-09). The assemblage zircon, tourmaline, rutile and apatite is present in all but one sample (FA-01). Apart from that, the dominant heavy minerals rather vary from sample to sample than between different units. The heavy mineral assemblage of the samples CA-00-17, CA-00-30, CA-01-04 and CA-01-06 are dominated by the stable minerals zircon, tourmaline and rutile. CA-00-09, CA-00-15, CA-00-23 and CA-00-42 have high contents of titanite and / or epidote group minerals. In CA-00-32 and CA-01-07, garnet is the most common heavy mineral. The heavy mineral suite of FA-01 is totally dominated by secondary biotite. Among the primary heavy mineral phases, zircon and apatite are most common. For all samples, metamorphic heavy minerals and the ultra-stable minerals zircon, tourmaline and rutile are dominating over magmatically formed heavy minerals (Fig. 11).

A sorting index for sandstones, the ZTR-index, was developed by Hubert (1962). In

Table 2. *Tourmaline chemistry*

Sample colour†	SiO ₂ (wt%)	TiO ₂ (wt%)	Al ₂ O ₃ (wt%)	FeO (wt%)	MnO (wt%)	MgO (wt%)	CaO (wt%)	Na ₂ O (wt%)	K ₂ O (wt%)	Sum (wt%)	Formula‡	Filled sites‡
Cochrane unit												
CA-00-09:												
09.01	35.78	0.41	31.81	12.53	0.14	3.05	0.40	2.30	0.05	86.47	(Na _{0.75} Ca _{0.05} K _{0.01})(Fe _{1.70} Mg _{0.76} Al _{0.22} Ti _{0.05} Mn _{0.02})(Al _{6.00})(Si _{1.99} Al _{1.01})(BO ₃) ₃ (OH) ₄	X _{0.83} Y _{2.88} Z _{6.00} T _{6.00} O ₁₈ (BO ₃) ₃ (W) ₄
09.03	36.11	0.31	34.82	11.20	0.09	2.19	0.07	1.41	0.02	86.21	(Na _{0.45} Ca _{0.05} K _{0.01})(Fe _{1.55} Mg _{0.54} Al _{0.74} Ti _{0.04} Mn _{0.01})(Al _{6.00})(Si _{1.96} Al _{0.04})(BO ₃) ₃ (OH) ₄	X _{0.47} Y _{2.87} Z _{6.00} T _{6.00} O ₁₈ (BO ₃) ₃ (W) ₄
09.04	36.27	0.84	33.81	9.75	0.02	3.83	0.19	1.98	0.03	86.72	(Na _{0.35} Ca _{0.05} K _{0.01})(Fe _{1.34} Mg _{0.95} Al _{0.74} Ti _{0.10} Mn _{0.01})(Al _{6.00})(Si _{1.94} Al _{0.06})(BO ₃) ₃ (OH) ₄	X _{0.67} Y _{2.89} Z _{6.00} T _{6.00} O ₁₈ (BO ₃) ₃ (W) ₄
09.05	36.96	0.28	34.69	10.86	0.06	2.08	0.07	1.52	0.04	86.55	(Na _{0.48} Ca _{0.05} K _{0.01})(Fe _{1.49} Mg _{0.51} Al _{0.75} Ti _{0.03} Mn _{0.01})(Al _{6.00})(Si _{1.96} Al _{0.04})(BO ₃) ₃ (OH) ₄	X _{0.50} Y _{2.74} Z _{6.00} T _{6.00} O ₁₈ (BO ₃) ₃ (W) ₄
09.06	35.20	0.54	34.42	12.53	0.09	0.73	0.14	1.78	0.03	85.45	(Na _{0.38} Ca _{0.02} K _{0.01})(Fe _{1.70} Mg _{0.18} Al _{0.75} Ti _{0.07} Mn _{0.01})(Al _{6.00})(Si _{1.92} Al _{0.08})(BO ₃) ₃ (OH) ₄	X _{0.61} Y _{2.78} Z _{6.00} T _{6.00} O ₁₈ (BO ₃) ₃ (W) ₄
09.07	36.58	0.65	34.48	9.50	0.08	3.75	0.11	1.79	0.02	86.96	(Na _{0.36} Ca _{0.02} K _{0.01})(Fe _{1.29} Mg _{0.91} Al _{0.56} Ti _{0.08} Mn _{0.01})(Al _{6.00})(Si _{1.95} Al _{0.05})(BO ₃) ₃ (OH) ₄	X _{0.59} Y _{2.88} Z _{6.00} T _{6.00} O ₁₈ (BO ₃) ₃ (W) ₄
CA-00-15:												
15.01c	36.69	0.64	34.58	8.26	0.02	4.04	0.19	1.78	0.05	86.23	(Na _{0.36} Ca _{0.05} K _{0.01})(Fe _{1.13} Mg _{0.98} Al _{0.62} Ti _{0.08} Mn _{0.01})(Al _{6.00})(Si _{1.98} Al _{0.02})(BO ₃) ₃ (OH) ₄	X _{0.60} Y _{2.89} Z _{6.00} T _{6.00} O ₁₈ (BO ₃) ₃ (W) ₄
15.02	36.83	1.20	31.13	8.11	0.05	5.07	0.20	2.03	0.02	84.63	(Na _{0.05} Ca _{0.03} K _{0.01})(Fe _{1.13} Mg _{1.26} Al _{0.11} Ti _{0.13} Mn _{0.01})(Al _{6.00})(Si _{1.64})(BO ₃) ₃ (OH) ₄	X _{0.69} Y _{2.65} Z _{6.00} T _{6.00} O ₁₈ (BO ₃) ₃ (W) ₄
15.03	36.29	0.64	33.27	6.36	0.04	6.04	0.91	1.80	0.05	85.40	(Na _{0.37} Ca _{0.16} K _{0.01})(Fe _{0.87} Mg _{1.46} Al _{0.38} Ti _{0.08} Mn _{0.01})(Al _{6.00})(Si _{1.95} Al _{0.05})(BO ₃) ₃ (OH) ₄	X _{0.74} Y _{2.81} Z _{6.00} T _{6.00} O ₁₈ (BO ₃) ₃ (W) ₄
CA-00-17:												
17.01	36.13	1.24	33.65	7.47	0.03	4.65	0.83	1.77	0.04	85.79	(Na _{0.36} Ca _{0.14} K _{0.01})(Fe _{1.02} Mg _{1.14} Al _{0.42} Ti _{0.15} Mn _{0.01})(Al _{6.00})(Si _{1.92} Al _{0.08})(BO ₃) ₃ (OH) ₄	X _{0.72} Y _{2.74} Z _{6.00} T _{6.00} O ₁₈ (BO ₃) ₃ (W) ₄
17.02	36.86	0.84	33.64	8.17	<0.01	4.37	0.36	1.89	0.04	86.16	(Na _{0.40} Ca _{0.05} K _{0.01})(Fe _{1.06} Mg _{1.06} Al _{0.47} Ti _{0.10} Mn _{0.01})(Al _{6.00})(Si _{1.92} Al _{0.08})(BO ₃) ₃ (OH) ₄	X _{0.67} Y _{2.74} Z _{6.00} T _{6.00} O ₁₈ (BO ₃) ₃ (W) ₄
17.03	35.89	0.97	33.15	9.63	0.07	3.86	0.46	1.83	0.04	85.90	(Na _{0.39} Ca _{0.08} K _{0.01})(Fe _{1.33} Mg _{0.95} Al _{0.41} Ti _{0.12} Mn _{0.01})(Al _{6.00})(Si _{1.94} Al _{0.06})(BO ₃) ₃ (OH) ₄	X _{0.68} Y _{2.88} Z _{6.00} T _{6.00} O ₁₈ (BO ₃) ₃ (W) ₄
17.04	36.54	0.49	33.62	9.02	<0.01	3.75	0.16	1.80	0.02	85.40	(Na _{0.38} Ca _{0.05} K _{0.01})(Fe _{1.25} Mg _{0.92} Al _{0.55} Ti _{0.06} Mn _{0.01})(Al _{6.00})(Si _{1.96} Al _{0.04})(BO ₃) ₃ (OH) ₄	X _{0.61} Y _{2.77} Z _{6.00} T _{6.00} O ₁₈ (BO ₃) ₃ (W) ₄
CA-00-23:												
23.01r	38.02	0.67	33.95	5.90	0.03	5.70	0.37	1.67	0.01	86.30	(Na _{0.32} Ca _{0.06} K _{0.01})(Fe _{0.79} Mg _{1.37} Al _{0.43} Ti _{0.08} Mn _{0.01})(Al _{6.00})(Si _{1.61})(BO ₃) ₃ (OH) ₄	X _{0.38} Y _{2.67} Z _{6.00} T _{6.00} O ₁₈ (BO ₃) ₃ (W) ₄
23.01c	36.15	1.29	33.34	7.98	0.04	5.17	0.98	1.76	0.04	86.75	(Na _{0.36} Ca _{0.17} K _{0.01})(Fe _{1.09} Mg _{1.26} Al _{0.29} Ti _{0.16} Mn _{0.01})(Al _{6.00})(Si _{1.90} Al _{0.10})(BO ₃) ₃ (OH) ₄	X _{0.73} Y _{2.89} Z _{6.00} T _{6.00} O ₁₈ (BO ₃) ₃ (W) ₄
23.02	36.67	0.26	33.99	11.44	0.15	2.65	0.15	1.84	0.04	87.17	(Na _{0.39} Ca _{0.03} K _{0.01})(Fe _{1.57} Mg _{0.50} Al _{0.57} Ti _{0.03} Mn _{0.02})(Al _{6.00})(Si _{1.60})(BO ₃) ₃ (OH) ₄	X _{0.62} Y _{2.84} Z _{6.00} T _{6.00} O ₁₈ (BO ₃) ₃ (W) ₄
23.03	37.27	0.76	33.43	6.40	<0.01	6.07	0.43	2.11	0.03	86.51	(Na _{0.06} Ca _{0.05} K _{0.01})(Fe _{0.88} Mg _{1.46} Al _{0.37} Ti _{0.09} Mn _{0.01})(Al _{6.00})(Si _{1.62})(BO ₃) ₃ (OH) ₄	X _{0.74} Y _{2.74} Z _{6.00} T _{6.00} O ₁₈ (BO ₃) ₃ (W) ₄
23.04	37.07	1.01	30.28	6.82	<0.01	7.62	0.78	2.45	0.02	86.05	(Na _{0.78} Ca _{0.14} K _{0.01})(Fe _{0.78} Mg _{1.86} Ti _{0.12} Mn _{0.01})(Al _{6.00})(Si _{1.63})(BO ₃) ₃ (OH) ₄	X _{0.92} Y _{2.77} Z _{6.00} T _{6.00} O ₁₈ (BO ₃) ₃ (W) ₄
23.05r	36.80	1.00	31.21	9.90	0.06	5.10	0.09	2.21	0.02	86.39	(Fe _{1.37} Mg _{1.25} Al _{0.07} Ti _{0.12} Mn _{0.01})(Al _{6.00})(Si _{1.60})(BO ₃) ₃ (OH) ₄	X _{0.73} Y _{2.88} Z _{6.00} T _{6.00} O ₁₈ (BO ₃) ₃ (W) ₄
23.05c	37.43	1.05	30.27	4.23	0.03	8.72	0.19	2.60	0.10	84.60	(Na _{0.43} Ca _{0.02} K _{0.01})(Fe _{0.43} Mg _{2.13} Ti _{0.13} Mn _{0.01})(Al _{6.00})(Si _{1.64})(BO ₃) ₃ (OH) ₄	X _{0.88} Y _{2.70} Z _{6.00} T _{6.00} O ₁₈ (BO ₃) ₃ (W) ₄
23.06	37.39	0.84	30.79	6.89	0.06	7.55	0.24	2.72	<0.01	86.47	(Na _{0.36} Ca _{0.04} K _{0.01})(Fe _{0.85} Mg _{1.83} Ti _{0.10} Mn _{0.01})(Al _{6.00})(Si _{1.60})(BO ₃) ₃ (OH) ₄	X _{0.90} Y _{2.79} Z _{6.00} T _{6.00} O ₁₈ (BO ₃) ₃ (W) ₄
23.07	36.96	0.82	32.42	7.03	0.07	6.34	0.71	2.13	0.03	86.51	(Na _{0.07} Ca _{0.12} K _{0.01})(Fe _{0.98} Mg _{1.54} Al _{0.21} Ti _{0.10} Mn _{0.01})(Al _{6.00})(Si _{1.60})(BO ₃) ₃ (OH) ₄	X _{0.80} Y _{2.81} Z _{6.00} T _{6.00} O ₁₈ (BO ₃) ₃ (W) ₄
CA-00-30:												
30.01	35.98	0.78	34.12	7.05	0.02	5.40	0.64	1.78	0.02	85.78	(Na _{0.36} Ca _{0.11} K _{0.01})(Fe _{0.96} Mg _{1.32} Al _{0.45} Ti _{0.10} Mn _{0.01})(Al _{6.00})(Si _{1.86} Al _{0.14})(BO ₃) ₃ (OH) ₄	X _{0.68} Y _{2.89} Z _{6.00} T _{6.00} O ₁₈ (BO ₃) ₃ (W) ₄
30.02	35.55	1.19	25.05	12.86	<0.01	7.89	3.21	1.12	0.06	86.93	(Na _{0.37} Ca _{0.58} K _{0.01})(Fe _{0.88} Mg _{2.00} Ti _{0.15} Mn _{0.01})(Al _{6.00})(Si _{1.60})(BO ₃) ₃ (OH) ₄	X _{0.97} Y _{2.99} Z _{6.00} T _{6.00} O ₁₈ (BO ₃) ₃ (W) ₄
30.04	36.09	1.00	31.31	8.45	<0.01	6.11	1.20	1.77	<0.01	85.93	(Na _{0.37} Ca _{0.21} K _{0.01})(Fe _{1.17} Mg _{1.07} Al _{0.27} Ti _{0.12} Mn _{0.01})(Al _{6.00})(Si _{1.97} Al _{0.03})(BO ₃) ₃ (OH) ₄	X _{0.78} Y _{2.86} Z _{6.00} T _{6.00} O ₁₈ (BO ₃) ₃ (W) ₄
30.06r	36.47	0.89	32.77	7.14	0.10	6.20	0.64	2.04	<0.01	86.25	(Na _{0.44} Ca _{0.11} K _{0.01})(Fe _{0.97} Mg _{1.51} Al _{0.25} Ti _{0.11} Mn _{0.01})(Al _{6.00})(Si _{1.95} Al _{0.05})(BO ₃) ₃ (OH) ₄	X _{0.76} Y _{2.86} Z _{6.00} T _{6.00} O ₁₈ (BO ₃) ₃ (W) ₄
30.06c	36.91	1.01	33.36	7.01	0.21	6.02	0.59	1.87	0.03	87.00	(Na _{0.38} Ca _{0.10} K _{0.01})(Fe _{0.95} Mg _{1.45} Al _{0.31} Ti _{0.12} Mn _{0.01})(Al _{6.00})(Si _{1.96} Al _{0.04})(BO ₃) ₃ (OH) ₄	X _{0.69} Y _{2.88} Z _{6.00} T _{6.00} O ₁₈ (BO ₃) ₃ (W) ₄
30.06c	36.80	1.02	32.53	7.76	0.08	5.83	0.74	1.93	0.02	86.71	(Na _{0.01} Ca _{0.13} K _{0.01})(Fe _{0.96} Mg _{1.41} Al _{0.23} Ti _{0.12} Mn _{0.01})(Al _{6.00})(Si _{1.99} Al _{0.01})(BO ₃) ₃ (OH) ₄	X _{0.74} Y _{2.85} Z _{6.00} T _{6.00} O ₁₈ (BO ₃) ₃ (W) ₄
30.07	37.52	0.44	32.48	7.39	<0.01	6.54	0.36	2.34	<0.01	87.07	(Na _{0.73} Ca _{0.06} K _{0.01})(Fe _{1.00} Mg _{1.58} Al _{0.18} Ti _{0.03} Mn _{0.01})(Al _{6.00})(Si _{1.60})(BO ₃) ₃ (OH) ₄	X _{0.80} Y _{2.81} Z _{6.00} T _{6.00} O ₁₈ (BO ₃) ₃ (W) ₄
30.08	37.10	0.38	34.78	9.18	0.06	3.55	0.16	1.81	0.01	87.04	(Na _{0.37} Ca _{0.03} K _{0.01})(Fe _{1.24} Mg _{0.86} Al _{0.64} Ti _{0.05} Mn _{0.01})(Al _{6.00})(Si _{1.60})(BO ₃) ₃ (OH) ₄	X _{0.60} Y _{2.80} Z _{6.00} T _{6.00} O ₁₈ (BO ₃) ₃ (W) ₄
30.09	37.26	0.67	34.05	6.64	0.06	6.27	0.15	2.22	0.03	87.34	(Na _{0.09} Ca _{0.01} K _{0.01})(Fe _{0.80} Mg _{1.50} Al _{0.40} Ti _{0.08} Mn _{0.01})(Al _{6.00})(Si _{1.97} Al _{0.03})(BO ₃) ₃ (OH) ₄	X _{0.70} Y _{2.87} Z _{6.00} T _{6.00} O ₁₈ (BO ₃) ₃ (W) ₄
30.10	36.12	0.55	33.86	8.92	0.07	4.05	0.13	2.02	0.04	85.75	(Na _{0.65} Ca _{0.02} K _{0.01})(Fe _{1.23} Mg _{1.00} Al _{0.53} Ti _{0.07} Mn _{0.01})(Al _{6.00})(Si _{1.95} Al _{0.05})(BO ₃) ₃ (OH) ₄	X _{0.68} Y _{2.84} Z _{6.00} T _{6.00} O ₁₈ (BO ₃) ₃ (W) ₄
30.11	36.68	0.50	33.76	6.82	0.04	6.33	0.83	1.92	0.05	86.92	(Na _{0.40} Ca _{0.05} K _{0.01})(Fe _{0.92} Mg _{1.52} Al _{0.10} Ti _{0.06} Mn _{0.01})(Al _{6.00})(Si _{1.92} Al _{0.08})(BO ₃) ₃ (OH) ₄	X _{0.75} Y _{2.86} Z _{6.00} T _{6.00} O ₁₈ (BO ₃) ₃ (W) ₄
30.12	35.95	0.70	31.62	11.90	0.14	4.38	0.58	2.28	0.09	87.63	(Na _{0.73} Ca _{0.10} K _{0.01})(Fe _{1.02} Mg _{1.10} Ti _{0.09} Mn _{0.02})(Al _{6.00})(Si _{1.94} Al _{0.06})(BO ₃) ₃ (OH) ₄	X _{0.85} Y _{2.92} Z _{6.00} T _{6.00} O ₁₈ (BO ₃) ₃ (W) ₄
30.13	36.80	0.46	34.13	6.46	<0.01	6.15	0.70	1.90	0.04	86.64	(Na _{0.60} Ca _{0.12} K _{0.01})(Fe _{0.87} Mg _{1.46} Al _{0.31} Ti _{0.06} Mn _{0.01})(

Continuation of Table 2

Sample colour†	Formula‡											Filled sites‡	
	SiO ₂	TiO ₂	Al ₂ O ₃	FeO	MnO	MgO	CaO	Na ₂ O	K ₂ O	Sum	Sum		
.grain*	(wt%)	(wt%)	(wt%)	(wt%)	(wt%)	(wt%)	(wt%)	(wt%)	(wt%)	(wt%)	(wt%)	(wt%)	
continuation CA-00-30:													
30.15	green	35.90	0.77	34.13	11.00	0.03	3.62	1.91	0.04	88.05	(Na _{0.09} Ca _{0.11} K _{0.01})(Fe _{1.50} Mg _{0.88} Al _{0.40} Ti _{0.09} Mn _{0.07} (Al _{6.00} (Si _{15.35} Al _{0.13} (BO ₃) ₃ (OH) ₄	X _{0.73} Y _{2.85} Z _{6.00} T _{6.00} O ₁₈ (BO ₃) ₃ (W) ₄	
30.16	yellow	36.25	1.13	32.30	7.00	0.04	6.44	1.83	0.09	86.25	(Na _{0.38} Ca _{0.20} K _{0.02})(Fe _{1.99} Mg _{1.37} Al _{0.15} Ti _{0.14} Mn _{0.01} (Al _{6.00} (Si _{9.95} Al _{0.07} (BO ₃) ₃ (OH) ₄	X _{0.80} Y _{2.85} Z _{6.00} T _{6.00} O ₁₈ (BO ₃) ₃ (W) ₄	
30.18	green	37.74	0.45	33.75	6.79	0.01	6.24	2.04	0.02	87.55	(Na _{0.63} Ca _{0.09} K _{0.03})(Fe _{0.91} Mg _{0.49} Al _{0.33} Ti _{0.05} Mn _{0.01} (Al _{6.00} (Si _{6.03} (BO ₃) ₃ (OH) ₄	X _{0.72} Y _{2.89} Z _{6.00} T _{6.00} O ₁₈ (BO ₃) ₃ (W) ₄	
30.20	green	37.30	0.46	33.70	8.31	<0.01	6.02	2.29	0.03	88.28	(Na _{0.71} Ca _{0.09} K _{0.01})(Fe _{1.11} Mg _{1.44} Al _{0.31} Ti _{0.06} Mn _{0.01} (Al _{6.00} (Si _{5.96} Al _{0.04} (BO ₃) ₃ (OH) ₄	X _{0.75} Y _{2.95} Z _{6.00} T _{6.00} O ₁₈ (BO ₃) ₃ (W) ₄	
30.21r	yellow	37.17	1.01	33.65	7.81	0.04	5.76	2.21	0.01	87.93	(Na _{0.69} Ca _{0.04} K _{0.01})(Fe _{1.05} Mg _{1.38} Al _{0.30} Ti _{0.12} Mn _{0.01} (Al _{6.00} (Si _{5.95} Al _{0.05} (BO ₃) ₃ (OH) ₄	X _{0.73} Y _{2.88} Z _{6.00} T _{6.00} O ₁₈ (BO ₃) ₃ (W) ₄	
30.21c	yellow	35.99	1.11	33.23	9.85	0.13	4.40	1.95	0.05	87.32	(Na _{0.62} Ca _{0.11} K _{0.01})(Fe _{1.35} Mg _{1.07} Al _{0.22} Ti _{0.14} Mn _{0.02} (Al _{6.00} (Si _{8.89} Al _{0.12} (BO ₃) ₃ (OH) ₄	X _{0.73} Y _{2.88} Z _{6.00} T _{6.00} O ₁₈ (BO ₃) ₃ (W) ₄	
30.22	green	36.39	0.48	35.48	7.54	0.10	4.37	1.96	0.03	86.67	(Na _{0.61} Ca _{0.06} K _{0.01})(Fe _{1.02} Mg _{1.05} Al _{0.66} Ti _{0.06} Mn _{0.01} (Al _{6.00} (Si _{5.86} Al _{0.11} (BO ₃) ₃ (OH) ₄	X _{0.68} Y _{2.89} Z _{6.00} T _{6.00} O ₁₈ (BO ₃) ₃ (W) ₄	
30.23	yellow	37.46	0.35	35.48	7.49	0.05	4.27	1.81	0.03	87.12	(Na _{0.56} Ca _{0.03} K _{0.01})(Fe _{1.00} Mg _{1.02} Al _{0.70} Ti _{0.04} Mn _{0.01} (Al _{6.00} (Si _{6.00} (BO ₃) ₃ (OH) ₄	X _{0.60} Y _{2.77} Z _{6.00} T _{6.00} O ₁₈ (BO ₃) ₃ (W) ₄	
30.24	green	36.16	0.48	32.73	8.59	<0.01	5.92	1.94	0.03	86.45	(Na _{0.42} Ca _{0.11} K _{0.01})(Fe _{1.18} Mg _{1.45} Al _{0.25} Ti _{0.06} Mn _{0.01} (Al _{6.00} (Si _{5.93} Al _{0.07} (BO ₃) ₃ (OH) ₄	X _{0.73} Y _{2.95} Z _{6.00} T _{6.00} O ₁₈ (BO ₃) ₃ (W) ₄	
30.26	blue	36.50	0.33	33.74	13.02	0.29	1.50	1.67	0.04	87.18	(Na _{0.53} Ca _{0.02} K _{0.01})(Fe _{1.80} Mg _{0.37} Al _{0.57} Ti _{0.04} Mn _{0.04} (Al _{6.00} (Si _{6.03} (OH) ₄	X _{0.56} Y _{2.85} Z _{6.00} T _{6.00} O ₁₈ (BO ₃) ₃ (W) ₄	
30.27	yellow	35.77	0.87	34.06	10.55	0.21	3.27	2.07	0.06	87.17	(Na _{0.66} Ca _{0.08} K _{0.01})(Fe _{1.45} Mg _{0.89} Al _{0.46} Ti _{0.11} Mn _{0.03} (Al _{6.00} (Si _{5.87} Al _{0.13} (BO ₃) ₃ (OH) ₄	X _{0.73} Y _{2.84} Z _{6.00} T _{6.00} O ₁₈ (BO ₃) ₃ (W) ₄	
CA-00-32:													
32.01	yellow	36.72	1.03	32.66	7.46	0.09	5.56	2.28	0.04	86.14	(Na _{0.72} Ca _{0.05} K _{0.01})(Fe _{1.02} Mg _{1.36} Al _{0.29} Ti _{0.13} Mn _{0.01} (Al _{6.00} (Si _{6.00} (BO ₃) ₃ (OH) ₄	X _{0.78} Y _{2.82} Z _{6.00} T _{6.00} O ₁₈ (BO ₃) ₃ (W) ₄	
32.02	green	35.99	0.15	31.68	8.90	0.06	6.18	2.14	0.08	85.68	(Na _{0.69} Ca _{0.09} K _{0.02})(Fe _{1.20} Mg _{1.35} Al _{0.17} Ti _{0.02} Mn _{0.01} (Al _{6.00} (Si _{5.97} Al _{0.03} (BO ₃) ₃ (OH) ₄	X _{0.80} Y _{2.91} Z _{6.00} T _{6.00} O ₁₈ (BO ₃) ₃ (W) ₄	
32.03	green	35.90	0.51	32.05	11.82	<0.01	4.47	1.93	0.06	87.68	(Na _{0.62} Ca _{0.16} K _{0.01})(Fe _{1.63} Mg _{1.10} Al _{0.14} Ti _{0.06} Mn _{0.01} (Al _{6.00} (Si _{5.92} Al _{0.08} (BO ₃) ₃ (OH) ₄	X _{0.79} Y _{2.92} Z _{6.00} T _{6.00} O ₁₈ (BO ₃) ₃ (W) ₄	
32.04	green	34.51	0.43	31.33	14.89	0.05	3.13	2.08	0.22	87.62	(Na _{0.32} Ca _{0.38} K _{0.05})(Fe _{2.10} Mg _{0.78} Al _{0.05} Mn _{0.01} (Al _{6.00} (Si _{5.81} Al _{0.19} (BO ₃) ₃ (OH) ₄	X _{0.74} Y _{2.97} Z _{6.00} T _{6.00} O ₁₈ (BO ₃) ₃ (W) ₄	
32.05	yellow	36.78	0.44	34.16	6.88	<0.01	5.02	1.81	0.06	85.66	(Na _{0.57} Ca _{0.09} K _{0.01})(Fe _{0.94} Mg _{1.22} Al _{0.57} Ti _{0.05} Mn _{0.01} (Al _{6.00} (Si _{6.00} (BO ₃) ₃ (OH) ₄	X _{0.68} Y _{2.78} Z _{6.00} T _{6.00} O ₁₈ (BO ₃) ₃ (W) ₄	
32.06	green	36.78	0.55	33.19	6.80	<0.01	5.87	1.96	0.06	85.80	(Na _{0.62} Ca _{0.10} K _{0.01})(Fe _{0.95} Mg _{1.45} Al _{0.39} Ti _{0.07} Mn _{0.01} (Al _{6.00} (Si _{6.00} (BO ₃) ₃ (OH) ₄	X _{0.74} Y _{2.88} Z _{6.00} T _{6.00} O ₁₈ (BO ₃) ₃ (W) ₄	
32.07r	green	37.65	0.42	31.87	3.37	0.07	8.23	1.80	0.02	85.07	(Na _{0.64} Ca _{0.14} K _{0.01})(Fe _{0.46} Mg _{2.13} Al _{0.09} Ti _{0.05} Mn _{0.01} (Al _{6.00} (Si _{6.00} (BO ₃) ₃ (OH) ₄	X _{0.68} Y _{2.78} Z _{6.00} T _{6.00} O ₁₈ (BO ₃) ₃ (W) ₄	
32.07c	green	36.79	0.95	30.83	5.93	0.01	7.23	1.71	0.03	84.84	(Na _{0.55} Ca _{0.24} K _{0.01})(Fe _{0.82} Mg _{1.17} Al _{0.12} Mn _{0.01} (Al _{6.00} (Si _{6.07} (BO ₃) ₃ (OH) ₄	X _{0.79} Y _{2.72} Z _{6.00} T _{6.00} O ₁₈ (BO ₃) ₃ (W) ₄	
32.08r	green	36.94	0.53	31.81	7.10	0.13	6.50	1.15	0.04	85.65	(Na _{0.78} Ca _{0.03} K _{0.01})(Fe _{0.99} Mg _{1.59} Al _{0.16} Ti _{0.07} Mn _{0.02} (Al _{6.00} (Si _{6.00} (BO ₃) ₃ (OH) ₄	X _{0.82} Y _{2.81} Z _{6.00} T _{6.00} O ₁₈ (BO ₃) ₃ (W) ₄	
32.08c	green	36.95	0.62	31.24	8.93	0.20	5.63	1.14	0.03	86.08	(Na _{0.75} Ca _{0.03} K _{0.01})(Fe _{1.23} Mg _{1.39} Al _{0.07} Ti _{0.08} Mn _{0.03} (Al _{6.00} (Si _{6.09} (BO ₃) ₃ (OH) ₄	X _{0.78} Y _{2.89} Z _{6.00} T _{6.00} O ₁₈ (BO ₃) ₃ (W) ₄	
32.09	green	36.78	0.38	33.07	7.93	0.08	5.06	2.00	0.03	85.73	(Na _{0.64} Ca _{0.09} K _{0.01})(Fe _{1.00} Mg _{1.24} Al _{0.46} Ti _{0.05} Mn _{0.01} (Al _{6.00} (Si _{6.03} (OH) ₄	X _{0.71} Y _{2.78} Z _{6.00} T _{6.00} O ₁₈ (BO ₃) ₃ (W) ₄	
32.11	brown	34.67	1.58	35.67	9.85	0.06	3.27	1.96	0.08	88.01	(Na _{0.62} Ca _{0.15} K _{0.01})(Fe _{1.34} Mg _{0.79} Al _{0.46} Ti _{0.19} Mn _{0.01} (Al _{6.00} (Si _{5.65} Al _{0.37} (BO ₃) ₃ (OH) ₄	X _{0.78} Y _{2.79} Z _{6.00} T _{6.00} O ₁₈ (BO ₃) ₃ (W) ₄	
CA-00-42:													
42-01	green	37.00	0.22	29.82	7.57	0.13	7.81	2.16	0.02	85.64	(Na _{0.69} Ca _{0.16} K _{0.01})(Fe _{0.86} Mg _{1.92} Ti _{0.03} Mn _{0.02} (Al _{15.81} Fe _{0.19} (Si _{6.12} (BO ₃) ₃ (OH) ₄	X _{0.86} Y _{2.82} Z _{6.00} T _{6.12} O ₁₈ (BO ₃) ₃ (W) ₄	
Bahia de la Lancha Formation													
CA-01-04:													
04-02r	green	37.19	0.73	30.93	8.21	0.06	6.21	1.10	1.74	0.04	86.20	(Na _{0.55} Ca _{0.19} K _{0.01})(Fe _{1.12} Mg _{1.52} Ti _{0.09} Mn _{0.01} (Al _{5.99} Fe _{0.01} (Si _{6.11} (BO ₃) ₃ (OH) ₄	X _{0.75} Y _{2.88} Z _{6.00} T _{6.11} O ₁₈ (BO ₃) ₃ (W) ₄
04-02c	green	36.59	0.75	27.12	13.41	0.05	6.01	2.36	1.55	0.05	87.89	(Na _{0.30} Ca _{0.42} K _{0.01})(Fe _{1.22} Mg _{1.30} Ti _{0.09} Mn _{0.01} (Al _{5.34} Fe _{0.66} (Si _{6.12} (BO ₃) ₃ (OH) ₄	X _{0.93} Y _{2.85} Z _{6.00} T _{6.12} O ₁₈ (BO ₃) ₃ (W) ₄
04-04	green	36.94	0.42	33.76	6.96	<0.01	6.07	0.96	1.88	0.04	87.04	(Na _{0.59} Ca _{0.17} K _{0.01})(Fe _{0.94} Mg _{1.46} Al _{0.38} Ti _{0.05} Mn _{0.01} (Al _{6.00} (Si _{5.96} Al _{0.04} (BO ₃) ₃ (OH) ₄	X _{0.76} Y _{2.85} Z _{6.00} T _{6.00} O ₁₈ (BO ₃) ₃ (W) ₄
04-06	green	37.72	0.66	31.86	6.00	<0.01	7.18	2.03	0.03	86.21	(Na _{0.64} Ca _{0.13} K _{0.01})(Fe _{0.81} Mg _{1.73} Al _{0.08} Mn _{0.01} (Al _{6.00} (Si _{6.11} (BO ₃) ₃ (OH) ₄	X _{0.77} Y _{2.71} Z _{6.00} T _{6.11} O ₁₈ (BO ₃) ₃ (W) ₄	
04-08	green	37.09	0.68	33.07	7.73	0.06	5.76	0.40	2.11	0.08	86.98	(Na _{0.66} Ca _{0.07} K _{0.02})(Fe _{1.05} Mg _{1.39} Al _{0.31} Ti _{0.08} Mn _{0.01} (Al _{6.00} (Si _{6.01} (BO ₃) ₃ (OH) ₄	X _{0.75} Y _{2.89} Z _{6.00} T _{6.00} O ₁₈ (BO ₃) ₃ (W) ₄
04-09	brown	37.47	0.38	34.28	7.65	0.01	5.04	1.16	1.83	0.02	86.82	(Na _{0.57} Ca _{0.03} K _{0.01})(Fe _{0.93} Mg _{1.21} Al _{0.51} Ti _{0.05} Mn _{0.01} (Al _{6.00} (Si _{6.04} (BO ₃) ₃ (OH) ₄	X _{0.60} Y _{2.89} Z _{6.00} T _{6.04} O ₁₈ (BO ₃) ₃ (W) ₄
04-10	green	37.05	0.64	34.30	6.10	0.11	6.37	0.90	1.76	0.07	87.30	(Na _{0.55} Ca _{0.15} K _{0.01})(Fe _{0.82} Mg _{1.52} Al _{0.40} Ti _{0.08} Mn _{0.01} (Al _{6.00} (Si _{5.95} Al _{0.07} (BO ₃) ₃ (OH) ₄	X _{0.71} Y _{2.85} Z _{6.00} T _{6.00} O ₁₈ (BO ₃) ₃ (W) ₄
CA-01-05:													
05-01	green	36.46	0.56	34.43	7.92	0.06	4.30	2.20	1.95	0.02	85.91	(Na _{0.62} Ca _{0.14} K _{0.01})(Fe _{0.98} Mg _{1.05} Al _{0.60} Ti _{0.07} Mn _{0.01} (Al _{6.00} (Si _{5.96} Al _{0.04} (BO ₃) ₃ (OH) ₄	X _{0.66} Y _{2.81} Z _{6.00} T _{6.00} O ₁₈ (BO ₃) ₃ (W) ₄
05-02	blue	35.89	0.25	33.78	11.83	0.22	2.44	0.08	1.95	0.05	86.49	(Na _{0.63} Ca _{0.09} K _{0.01})(Fe _{1.61} Mg _{0.60} Al _{0.57} Ti _{0.05} Mn _{0.01} (Al _{6.00} (Si _{5.96} Al _{0.04} (BO ₃) ₃ (OH) ₄	X _{0.65} Y _{2.85} Z _{6.00} T _{6.00} O ₁₈ (BO ₃) ₃ (W) ₄
05-03	yellow	36.63	0.54	34.32	6.14	<0.01	5.75	0.65	1.73	0.04	85.79	(Na _{0.54} Ca _{0.11} K _{0.01})(Fe _{0.83} Mg _{1.39} Al _{0.52} Ti _{0.07} Mn _{0.01} (Al _{6.00} (Si _{5.95} Al _{0.03} (BO ₃) ₃ (OH) ₄	X _{0.67} Y _{2.81} Z _{6.00} T _{6.00} O ₁₈ (BO ₃) ₃ (W) ₄
05-04	green	36.76	0.27	35.16	6.87	0.04	5.00	0.37	1.34	0.02	85.84	(Na _{0.42} Ca _{0.09} K _{0.01})(Fe _{0.93} Mg _{1.21} Al _{0.68} Ti _{0.05} Mn _{0.01} (Al _{6.00} (Si _{5.96}	

Continuation of Table 2

Sample colour	SiO ₂ (wt%)	TiO ₂ (wt%)	Al ₂ O ₃ (wt%)	FeO (wt%)	MnO (wt%)	MgO (wt%)	CaO (wt%)	Na ₂ O (wt%)	K ₂ O (wt%)	Sum (wt%)	Formula†	Filled sites‡
05.06 yellow	36,65	0,67	34,30	7,40	0,03	5,16	0,24	1,86	0,02	86,32	(Na _{0,59} Ca _{0,04} K _{0,01})(Fe _{1,25} Mg _{1,25} Al _{0,51} Ti _{0,08} Mn _{0,01})(Al _{6,00})(Si _{5,95} Al _{0,05})(BO ₃) ₃ (OH) ₄	X _{0,63} Y _{2,88} Z _{6,00} T _{6,00} O ₁₈ (BO ₃) ₃ (W) ₄
05.07 yellow	35,99	0,86	33,91	9,09	0,02	4,38	0,31	1,94	0,02	86,50	(Na _{0,61} Ca _{0,05} K _{0,01})(Fe _{1,34} Mg _{1,07} Al _{0,44} Ti _{0,11} Mn _{0,01})(Al _{6,00})(Si _{5,89} Al _{0,11})(BO ₃) ₃ (OH) ₄	X _{0,67} Y _{2,88} Z _{6,00} T _{6,00} O ₁₈ (BO ₃) ₃ (W) ₄
05.08r green	36,61	0,10	29,82	7,42	0,05	7,70	0,16	2,65	0,08	84,60	(Na _{0,86} Ca _{0,03} K _{0,02})(Fe _{0,91} Mg _{1,92} Ti _{0,01} Mn _{0,01})(Al _{5,87} Fe _{0,13})(BO ₃) ₃ (OH) ₄	X _{0,91} Y _{2,88} Z _{6,00} T _{6,12} O ₁₈ (BO ₃) ₃ (W) ₄
05.08c green	35,15	0,45	29,06	16,19	0,10	3,24	0,17	2,43	0,04	86,84	(Na _{0,80} Ca _{0,03} K _{0,01})(Fe _{2,10} Mg _{0,83} Ti _{0,06} Mn _{0,01})(Al _{5,85} Fe _{0,15})(BO ₃) ₃ (OH) ₄	X _{0,84} Y _{3,02} Z _{6,00} T _{6,01} O ₁₈ (BO ₃) ₃ (W) ₄
05.09 yellow	35,43	0,79	32,55	7,24	0,10	6,00	1,01	1,68	0,06	84,86	(Na _{0,54} Ca _{0,18} K _{0,01})(Fe _{1,01} Mg _{1,49} Al _{0,27} Ti _{0,10} Mn _{0,01})(Al _{6,00})(Si _{5,89} Al _{0,11})(BO ₃) ₃ (OH) ₄	X _{0,73} Y _{2,87} Z _{6,00} T _{6,00} O ₁₈ (BO ₃) ₃ (W) ₄
05.10 green	36,42	0,54	33,59	9,60	0,03	3,88	0,21	1,91	0,04	86,22	(Na _{0,61} Ca _{0,04} K _{0,01})(Fe _{1,32} Mg _{1,95} Al _{0,50} Ti _{0,07} Mn _{0,01})(Al _{6,00})(Si _{5,99} Al _{0,01})(BO ₃) ₃ (OH) ₄	X _{0,65} Y _{2,88} Z _{6,00} T _{6,00} O ₁₈ (BO ₃) ₃ (W) ₄
CA-01-06:												
06.01 green	35,71	0,38	32,89	8,78	0,02	5,78	0,97	1,94	0,08	86,55	(Na _{0,62} Ca _{0,17} K _{0,02})(Fe _{1,21} Mg _{1,42} Al _{0,24} Ti _{0,05} Mn _{0,01})(Al _{6,00})(Si _{5,87} Al _{0,13})(BO ₃) ₃ (OH) ₄	X _{0,80} Y _{2,91} Z _{6,00} T _{6,00} O ₁₈ (BO ₃) ₃ (W) ₄
06.02 green	34,97	0,87	29,38	10,48	0,19	5,93	2,06	1,68	0,09	85,64	(Na _{0,55} Ca _{0,37} K _{0,02})(Fe _{1,26} Mg _{1,49} Ti _{0,11} Mn _{0,03})(Al _{5,78} Fe _{0,22})(Si _{5,92} Al _{0,08})(BO ₃) ₃ (OH) ₄	X _{0,94} Y _{2,95} Z _{6,00} T _{6,00} O ₁₈ (BO ₃) ₃ (W) ₄
06.06 yellow	37,11	0,60	33,39	6,21	0,02	5,26	0,22	2,01	0,03	84,83	(Na _{0,54} Ca _{0,04} K _{0,01})(Fe _{0,88} Mg _{1,29} Al _{0,45} Ti _{0,07} Mn _{0,01})(Al _{6,00})(Si _{6,09})(BO ₃) ₃ (OH) ₄	X _{0,68} Y _{2,66} Z _{6,00} T _{6,09} O ₁₈ (BO ₃) ₃ (W) ₄
06.08 green	37,25	0,29	32,82	5,64	0,08	6,60	0,54	1,95	0,02	85,19	(Na _{0,62} Ca _{0,09} K _{0,01})(Fe _{0,77} Mg _{1,61} Al _{0,32} Ti _{0,04} Mn _{0,01})(Al _{6,00})(Si _{6,08})(BO ₃) ₃ (OH) ₄	X _{0,72} Y _{2,74} Z _{6,00} T _{6,08} O ₁₈ (BO ₃) ₃ (W) ₄
06.09 green	35,72	0,36	31,97	8,10	0,03	6,39	1,52	1,62	0,06	85,78	(Na _{0,57} Ca _{0,27} K _{0,01})(Fe _{1,12} Mg _{1,88} Al _{0,14} Ti _{0,04} Mn _{0,01})(Al _{6,00})(Si _{5,91} Al _{0,09})(BO ₃) ₃ (OH) ₄	X _{0,80} Y _{2,88} Z _{6,00} T _{6,00} O ₁₈ (BO ₃) ₃ (W) ₄
06.10 green	36,89	0,48	32,05	7,58	0,03	6,07	0,57	2,16	0,02	85,85	(Na _{0,69} Ca _{0,10} K _{0,01})(Fe _{0,95} Mg _{1,08} Al _{0,20} Ti _{0,06} Mn _{0,01})(Al _{6,00})(Si _{6,05})(BO ₃) ₃ (OH) ₄	X _{0,79} Y _{2,79} Z _{6,00} T _{6,05} O ₁₈ (BO ₃) ₃ (W) ₄
06.11 green	35,96	0,74	28,93	9,03	0,11	7,35	2,43	1,48	0,06	86,07	(Na _{0,48} Ca _{0,35} K _{0,01})(Fe _{0,95} Mg _{1,03} Ti _{0,08} Mn _{0,02})(Al _{6,00})(Si _{6,09})(BO ₃) ₃ (OH) ₄	X _{0,93} Y _{2,88} Z _{6,00} T _{6,00} O ₁₈ (BO ₃) ₃ (W) ₄
06.12 green	36,57	0,32	32,91	9,05	0,13	4,94	0,39	2,13	0,06	86,50	(Na _{0,68} Ca _{0,07} K _{0,01})(Fe _{1,24} Mg _{1,21} Al _{0,36} Ti _{0,04} Mn _{0,02})(Al _{6,00})(Si _{6,00})(BO ₃) ₃ (OH) ₄	X _{0,76} Y _{2,87} Z _{6,00} T _{6,04} O ₁₈ (BO ₃) ₃ (W) ₄
06.13 yellow	37,32	0,13	34,17	9,54	0,07	4,16	0,12	1,80	0,01	87,31	(Na _{0,56} Ca _{0,02} K _{0,01})(Fe _{1,29} Mg _{1,00} Al _{0,52} Ti _{0,02} Mn _{0,01})(Al _{6,00})(Si _{6,04})(BO ₃) ₃ (OH) ₄	X _{0,59} Y _{2,84} Z _{6,00} T _{6,04} O ₁₈ (BO ₃) ₃ (W) ₄
06.14 yellow	37,13	0,67	34,20	5,89	0,02	5,36	0,29	1,73	0,01	85,30	(Na _{0,55} Ca _{0,05} K _{0,01})(Fe _{0,80} Mg _{1,30} Al _{0,55} Ti _{0,08} Mn _{0,01})(Al _{6,00})(Si _{6,04})(BO ₃) ₃ (OH) ₄	X _{0,60} Y _{2,74} Z _{6,00} T _{6,04} O ₁₈ (BO ₃) ₃ (W) ₄
06.15 yellow	35,37	0,51	33,79	13,39	0,21	0,94	0,16	1,91	0,05	86,32	(Na _{0,62} Ca _{0,03} K _{0,01})(Fe _{1,88} Mg _{0,23} Al _{0,61} Ti _{0,06} Mn _{0,03})(Al _{6,00})(Si _{5,95} Al _{0,07})(BO ₃) ₃ (OH) ₄	X _{0,66} Y _{2,88} Z _{6,00} T _{6,00} O ₁₈ (BO ₃) ₃ (W) ₄
06.16 green	36,21	0,55	32,23	8,48	< 0,01	5,78	0,68	2,10	0,05	86,07	(Na _{0,67} Ca _{0,03} K _{0,01})(Fe _{1,17} Mg _{1,42} Al _{0,22} Ti _{0,07} Mn _{0,01})(Al _{6,00})(Si _{5,97} Al _{0,03})(BO ₃) ₃ (OH) ₄	X _{0,80} Y _{2,88} Z _{6,00} T _{6,00} O ₁₈ (BO ₃) ₃ (W) ₄
06.17 yellow	35,43	0,66	33,98	14,32	0,17	1,06	0,16	1,97	0,04	87,79	(Na _{0,63} Ca _{0,03} K _{0,01})(Fe _{1,99} Mg _{0,26} Al _{0,52} Ti _{0,08} Mn _{0,02})(Al _{6,00})(Si _{5,88} Al _{0,12})(BO ₃) ₃ (OH) ₄	X _{0,67} Y _{2,87} Z _{6,00} T _{6,00} O ₁₈ (BO ₃) ₃ (W) ₄
06.18 brown	36,41	1,09	28,50	10,21	< 0,01	7,21	1,52	2,11	< 0,01	87,05	(Na _{0,68} Ca _{0,27} K _{0,01})(Fe _{0,98} Mg _{1,78} Ti _{0,14} Mn _{0,01})(Al _{5,57} Fe _{0,43})(BO ₃) ₃ (OH) ₄	X _{0,95} Y _{2,99} Z _{6,00} T _{6,04} O ₁₈ (BO ₃) ₃ (W) ₄
06.19 green	36,02	0,58	33,69	9,56	0,04	3,72	0,25	1,94	0,04	85,84	(Na _{0,62} Ca _{0,04} K _{0,01})(Fe _{1,32} Mg _{0,92} Al _{0,51} Ti _{0,07} Mn _{0,01})(Al _{6,00})(Si _{5,95} Al _{0,05})(BO ₃) ₃ (OH) ₄	X _{0,67} Y _{2,87} Z _{6,00} T _{6,00} O ₁₈ (BO ₃) ₃ (W) ₄
CA-01-07:												
07.01 yellow	36,85	0,63	33,36	5,25	0,04	6,92	1,29	1,68	0,11	86,13	(Na _{0,53} Ca _{0,22} K _{0,02})(Fe _{0,72} Mg _{1,62} Al _{0,32} Ti _{0,08} Mn _{0,01})(Al _{6,00})(Si _{5,96} Al _{0,04})(BO ₃) ₃ (OH) ₄	X _{0,77} Y _{2,76} Z _{6,00} T _{6,00} O ₁₈ (BO ₃) ₃ (W) ₄

*c, rc, and r denotes analysis in the core, inner rim and outer rim, respectively. †Formula calculated assuming filled Z and T sites, 3 apfu for B, and W sites filled with OH. Normalization was made on the basis of 29 oxygens. ‡Maximum absorption colour.

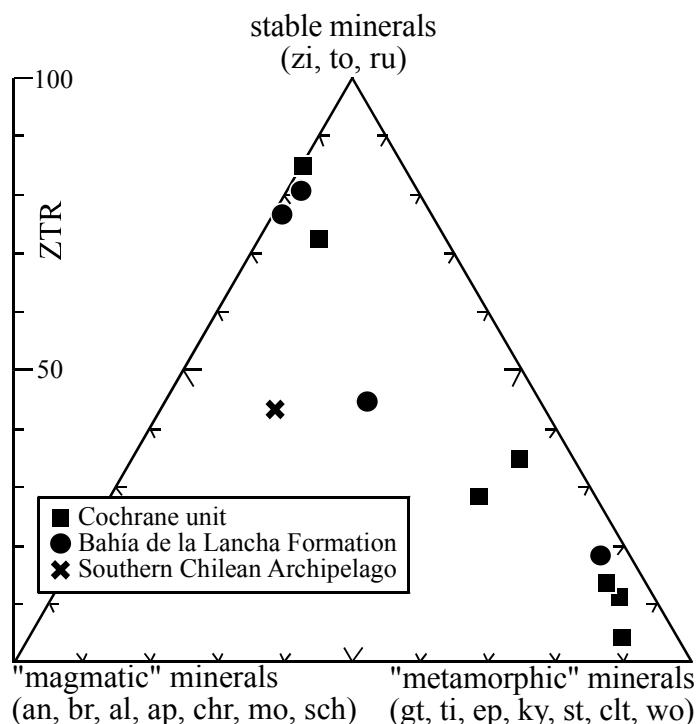


Fig. 11. Heavy mineral content. Al = allanite, an = anatase, ap = apatite, br = brookite, chr = chromite, clt = cloritoid, ep = epidote, zoisite and clinozoisite, gt = garnet, ky = kyanite, mo = monazite, ru = rutile, sch = scheelite, st = staurolite, ti = titanite, tu = tourmaline, wo = wollastonite, zi = zircon.

this, the percentage of the highly stable minerals zircon, tourmaline and rutile is divided by the total content of the transparent detrital heavy minerals, with the exclusion of micas. The heavy mineral samples dominated by zircon, tourmaline and rutile have ZTR values of 70-90 (Tab. 1, Fig. 11). The samples with high contents of titanite, epidote group minerals and garnet have ZTR of 4-44 (Tab. 1, Fig. 11).

Implications. The large quantities of detrital epidote-group minerals, garnet and titanite in some of the samples indicate a major contribution from metamorphic sources. However, in other samples these minerals are absent. This large variation in heavy mineral content probably is the result of influences from different sources for the different sediments. The variation could be produced by fluvial systems which change tracks through time, or that the sediments were fed by partly different fluvial systems. Further, it might mirror tectonic activity in the source regions. However, it can not be excluded that the heavy mineral content is partly an artefact due to break-down of unstable minerals during post-depositional diagenesis and metamorphism for those heavy mineral separates rich in the ultra-stable minerals zircon, tourmaline and rutile.

The sediments with high ZTR values can be expected to have different main heavy mineral sources to those with low ZTR values and high contents of metamorphic heavy minerals. The high stability of zircon, tourmaline and rutile makes it possible that most of the heavy mineral grains, at least in the samples with high ZTR values, have had long transportation paths, or have undergone sedimentary recycling processes before becoming part of the studied sediments (*cf.* Section 3.2.4. & 3.3.3.).

3.3.3. Heavy minerals: chemical composition of tourmaline

Tourmaline is a common accessory mineral in sediments and it is resistant to both chemical

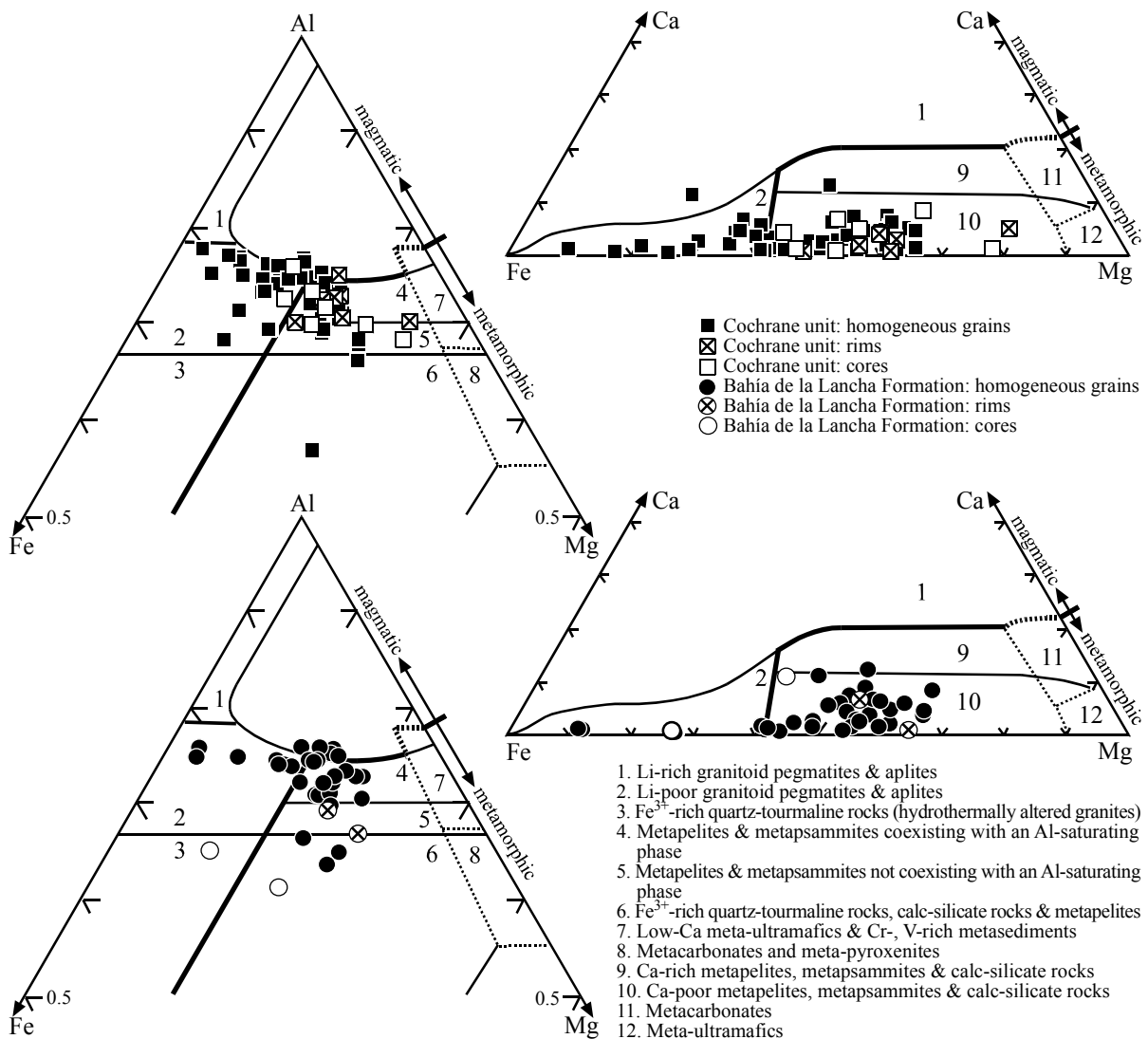


Fig. 12. Chemistry of tourmaline (molecular percentages). Discrimination fields from Henry & Guidotti (1985). and mechanical weathering (Morton & Hallsworth, 1999, and references therein). The composition of tourmaline reflects the composition of the rock in which it formed, or is affected by circulating fluids (Henry & Guidotti, 1985; Henry & Dutrow, 1996). It has been shown that the major element composition of tourmaline can be useful as a provenance tool (Henry & Guidotti, 1985; Willner, 1987).

The analysed tourmaline grains are mainly subrounded to rounded. Only a few grains are euhedral. They have maximum absorption colours of green, yellow, blue and brown shades (Tab. 2). The grains have compositions between burgerite, schorl and dravite. Thus, they have high Fe and Mg contents and low Ca contents (Tab. 2).

The ternary discrimination diagrams of Henry & Guidotti (1985), encompassing Al, Fe, Mg and Ca in molecular percentages, give indications of the protolith of the tourmalines. Of the 60 analysed spots in 53 tourmaline grains from the Cochrane unit, 60 % indicate metasedimentary protoliths in both diagrams (Fig. 12). 28 % have a chemistry typical for tourmaline grown in granitoids, whereas the remaining 12 % indicate metasedimentary origin in one of the diagrams and granitoid origin in the other. Seven grains show discontinuous compositional zoning. In them, both the cores and the rims generally have compositions indicating metasedimentary formation environments (Fig. 12). No geographical trends were

observed for the Cochrane unit.

Of the 34 analysed spots in detrital tourmalines of the Argentinean Bahía de la Lancha Formation, the majority (73 %) has compositions typical for metasedimentary formation environments (Fig. 12). 15 % have compositions indicating granitoid protoliths, whereas the remaining 12 % indicate a metasedimentary origin in one of diagrams of Henry & Guidotti (1985) and a granitoid origin in the other. A large discrepancy between the composition of the cores and the rims in the two heterogeneous grains indicates different formation environments for the different growth phases, although tourmaline grains formed in one single growth stage can show some chemical heterogeneity. Furthermore, some chemical heterogeneity for tourmalines from the same source can appear due to chemical polar asymmetry (Willner, 1987; Henry & Dutrow, 1992, 1996).

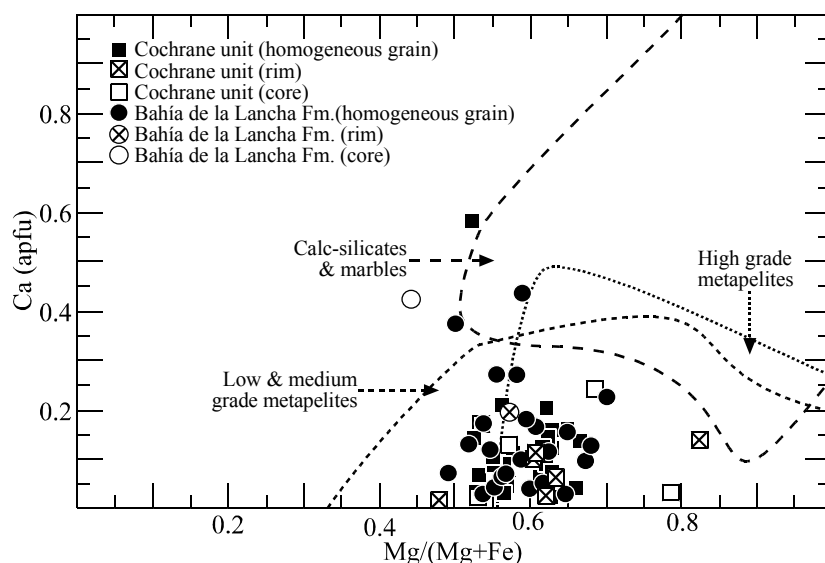


Fig. 13. Mg/(Mg+Fe) vs. Ca calculated in atoms per formula unit (apfu). Fields sketched for composition of tourmaline in metapelites and calcareous metasediments. The data used to construct the compositional fields were assembled from several publications by Henry & Dutrow (1996). Only grains with indications of a metasedimentary origin in *both* of the ternary diagrams of Figure 12 are plotted.

Based on the chemistry of tourmaline grains formed in metasediments, discrimination into different types of metasediments and metasediments affected by different metamorphic grades can be done. Most of the grains that indicate metasedimentary protoliths in the two ternary diagrams of Figure 12 have Mg/(Mg+Fe) ratios (in molar proportions) between 0.5 and 0.7 (Fig. 13). The calculated Ca content at the X-site is mostly < 0.2 atoms per formula unit (apfu; Tab. 2, Fig. 13). This is similar to tourmalines grown in metapelites of varying metamorphic grade presented by Henry & Dutrow (1996; Fig. 13). Most of the analysed tourmalines have Mg/(Mg+Fe) values and Ca contents similar to tourmalines formed in metapelites of low to medium metamorphic grade (*cf.* Henry & Dutrow, 1996). Some variation in tourmaline chemistry exists between Al-poor and Al-rich metapelites. The major element compositional variation is larger for Al-rich metapelites, which enables a grouping of such tourmalines of different metamorphic grades (Fig. 14; *cf.* Henry & Dutrow, 1996). Tourmaline grown in low to medium grade Al-rich metapelites often have more X-site vacancies than grains in both Al-poor and high grade Al-rich metapelites, although an overlap occur around 0.2-0.3 vacancies (*cf.* Fig. 14; Henry & Dutrow, 1996). The majority of the tourmalines with a probable metasedimentary origin are estimated to have 0.2-0.4 X-site

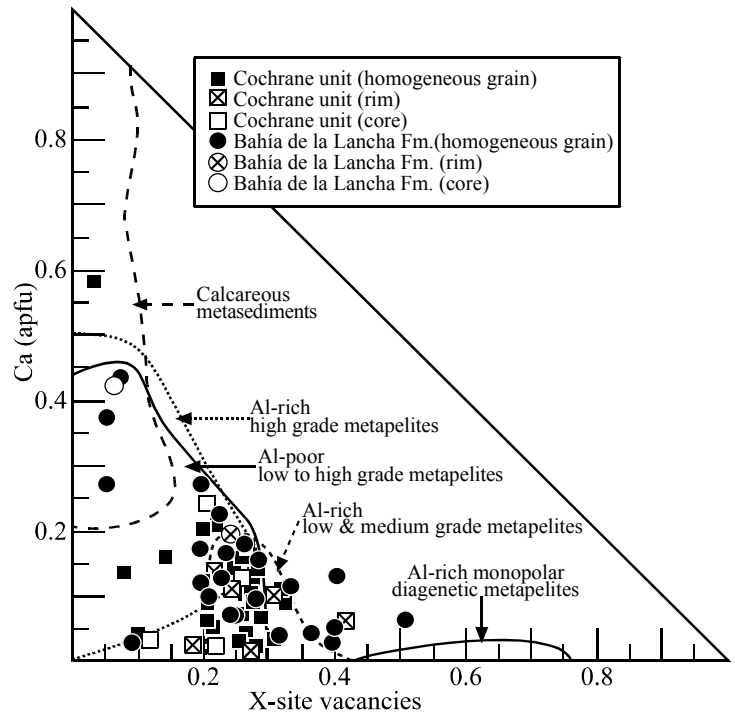


Fig. 14. X-site vacancies vs. Ca calculated (in atoms) per formula unit. Fields are sketched for composition of tourmaline formed in different metapelites and in calcareous metasediments. The data used to construct the compositional fields were assembled from several publications by Henry & Dutrow (1996). Only grains with indications of a metasedimentary origin in *both* of the ternary diagrams of Figure 12 are plotted.

vacancies, an amount which occurs in tourmalines from several types of metapelites (Tab. 2, Fig. 14). However, the amount of X-site vacancies in combination with the Ca content, shows that most of the analysed tourmalines are similar to those presented by Henry & Dutrow (1996) for Al-rich metapelites of low to medium metamorphic grade (Fig. 14). In Fig. 13 and 14, no difference in chemistry of the likely metasedimentary tourmalines can be seen between the Cochrane unit and the Bahía de la Lancha Formation, or geographically within the two geological units.

Attempts have been made to use the tourmaline colours as provenance indicators

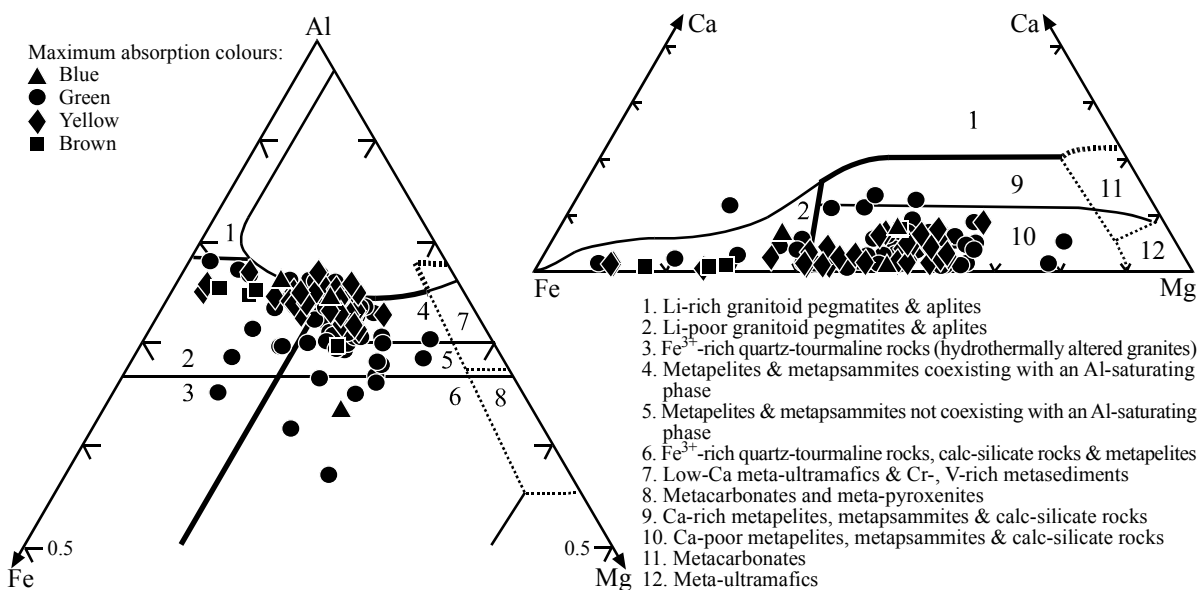


Fig. 15. Chemistry of tourmaline (molecular percentages) with different maximum absorption colours. Discrimination fields from Henry & Guidotti (1985).

(e. g., Krynine, 1946; Lihou & Mange-Rajetzky, 1996). However, Henry & Dutrow (1992) showed that optical analysis of them can produce misleading results for provenance studies. This is emphasised by the analysed detrital tourmalines in this study. In Figure 15, it is shown that tourmaline grains with varying maximum absorption colours have overlapping chemistry. *Implications.* The likely metasedimentary origin of a majority of the tourmaline grains, indicates sedimentary recycling. The possible metasedimentary formation environment for both the cores and the rims of most chemically heterogeneous tourmalines indicates that they might have been affected by several generations of recycling. However, it must be kept in mind that tourmalines from the same growth stage and source can show chemical heterogeneity (Willner, 1987; Henry & Dutrow, 1992, 1996). The partly different chemistry of the tourmaline grains of the Cochrane unit compared to those of the Bahía de la Lancha Formation reveals that the sediments partly were fed by different sources or with different amounts of detritus from the different sources. The chemistry of the tourmaline grains indicating a metasedimentary origin is similar for both units. Most grains have a chemical composition similar to Al-rich low and medium grade metapelites of Henry & Dutrow (1996), which makes this a possible dominant metasedimentary source rock type for the tourmalines of metasedimentary origin. However, it is not possible to exclude that parts of the grain population originate from Al-poor and / or high grade Al-rich metapelites.

3.4. Petrography: discussion

To provide information about the provenance from the petrography of sediments, post-depositional changes have to be considered. The petrography of the studied sediments shows indications of post-depositional recrystallisation and metamorphism. (1) In many cases, the matrix is composed of a mixture of secondary fine-grained quartz and layers of mica. (2) The generally high matrix content is at least partly the result of post-depositional break-down of unstable mineral phases. A direct indication of this is the heavy mineral content, with the occurrence of leucoxen in an assembly of titanite, calcite and quartz. (3) The sediments that proved unsuitable for the study of the CL properties of quartz in a provenance perspective have a homogeneous brown CL colour of metamorphic origin, or a homogeneous authigenic blue CL colour, which turns brown after less than a minute of electron bombardment. The post-depositional metamorphic effect, which is smallest in the southern part of the mainland sampling area, is accentuated by the samples used for the CL study of quartz; all sampled south of 48°S.

As indicated by (1) the chemistry of tourmaline and (2) the CL characteristics of quartz, the sediments (exclusively of the Cochrane unit and the Bahía de la Lancha Formation) had a large input from regional metamorphic, and, less from, plutonic sources. This is supported by (3) a large content of metamorphic heavy minerals in some of the sediment samples. The input from volcanic sources was probably minor, as indicated from the CL study.

The metamorphic sources might have been of low- to medium-grade as supported by (1) the CL study, where the brown CL colour of quartz is typical for low-grade metamorphic quartz. Furthermore, (2) the chemistry of tourmaline grains with a probable metasedimentary origin are similar to tourmalines grown in low- to medium-grade metamorphic metasediments. However, as mentioned in Section 3.3.3., it is not possible to exclude that a

part of the grain population originates from higher-grade metasediments.

There are several petrographic signs of pre-depositional sedimentary recycling in the studied sediments. (1) All identified lithic fragments in the breccia of the Cochrane unit and in the greywackes are of sedimentary origin. (2) The tourmaline chemistry indicates that a large part of the analysed grain population has a metasedimentary origin, and that some of them might have survived several recycling phases. (3) In the CL study of quartz, radiation rims and diagenetic overgrowths, that were formed prior to deposition, were observed. Furthermore, (4) a large amount of quartz grains obtained their CL characteristics in regional metamorphic environments. This indirectly supports the idea that a considerable proportion of the sedimentary detritus derived from older sediments. The recycling implies that the source characteristics indicated by the chemistry of tourmalines and the CL properties of quartz are not obviously related to the last environment of the detrital grains, that predates the deposition of the studied sediments.

No obvious differences between the geological units were observed by the light- and heavy-mineral content. The varietal studies of quartz and tourmaline were performed only with sediments from the Cochrane unit and the Bahía de la Lancha Formation, because these samples were most suitable for the techniques. The CL study shows that the Bahía de la Lancha Formation samples have a larger proportion of quartz with a possible regional metamorphic origin than the Cochrane unit samples (Fig. 6). Quartz grains in the Bahía de la Lancha Formation with radiation damage and diagenetic overgrowths further point to possible differences in source areas. Furthermore, the tourmaline chemistry indicates a larger influence of sedimentary and metamorphic sources for the Bahía de la Lancha Formation than for the Cochrane unit (Fig. 12). Despite these differences, the variations in dominant source rocks seem to be larger between individual samples than between the different geological units. This is concealed in the framework mineralogy, but revealed by the heavy mineral content and the CL results.

A sedimentary petrography like the one in this study can be expected from active tectonic margins lacking volcanism, or from passive margins. At non-volcanic convergent margins, the detritus might originate from older crustal rocks in adjacent areas, or from unroofed rocks, produced as a consequence of subduction (Schwab, 1986). Sediments deposited along passive continental margins can be expected to be dominated by quartz grains of plutonic, metamorphic and recycled affinities, although it is possible for sediments to be transported across tectonic setting boundaries (Potter, 1994). Depositional basins at passive margins are often fed by sources from the interior of continents, the rocks of which were produced at ancient active plate margins.

Varietal studies (*e. g.*, chemistry of tourmaline and CL of quartz) made within a stratigraphic sequence would probably better discriminate subduction-related sediments without volcanic affinity from passive margin sediments. The similarity in expected proportions of differently luminescing quartz grains and compositionally different tourmaline grains associated with such different tectonic environments usually makes it necessary to combine these techniques with other provenance-indicative techniques. This is also emphasised by the possible overlap in CL colour for quartz grains of different origins and the possibility for recycled quartz and tourmaline grains to inherit the CL characteristics and chemistry, respectively, of older events.

4. Whole-rock chemistry¹

The chemistry of sediments, including radiogenic isotopes, is a useful tool for characterizing the provenance of sediments when combined with petrographic methods (*e. g.*, Bhatia & Crook, 1986; Roser & Korsch, 1988; McLennan *et al.*, 1989, 1990; von Eynatten *et al.*, 2003; Zimmermann & Bahlburg, 2003). However, processes such as weathering, sorting, diagenesis and metamorphism all affect and potentially modify the chemical and isotopic signatures of sediments (McLennan *et al.*, 1993; Mildowski & Zalasiewicz, 1991; Condie *et al.*, 1995; Roser & Nathan, 1997). Even the Nd isotope system, which is in common use in provenance studies, since it is generally unaffected by metamorphism, can be disturbed during weathering, diagenesis and metamorphism under certain circumstances (Zhao *et al.*, 1992; McDaniel *et al.*, 1994). Here, the whole-rock element chemistry is combined with Sm-Nd and Rb-Sr isotopes for a number of samples (Tab. 3-6). They are used to complement to the petrography to track their main source rocks.

4.1. Whole-rock major and trace element chemistry

4.1.1. Whole-rock major and trace element chemistry: methods

Thirty greywackes and 7 pelites from the Eastern Andean Metamorphic Complex, Río Lácteo Formation and Bahía de la Lancha Formation were analysed for their whole-rock major and trace element composition (Tab. 3). The samples were powdered in an agate mill and the analyses were performed by ACME lab in Vancouver, Canada. Major elements, Ba, Ni and Sc were measured by ICP-ES, and other trace elements by ICP-MS.

$C_{\text{carbonate}}$ was measured on a CS-MAT 5500 at the Geologisch-Paläontologisches Institut, Münster, Germany. This is performed by quantifying the CO_2 , that is evolved by addition of hot HCl to the sample, with an infrared detector. The CaCO_3 standard ($\geq 99\%$ CaCO_3) has a relative error of 1 %.

4.1.2. Whole-rock major and trace element chemistry: results and chemical weathering

For the study of whole-rock chemistry, the greywacke parts of the turbidite deposits were analysed preferentially, although pelites were considered as well. Major and trace elements are presented in Table 3. The greywackes have SiO_2 contents of 70-88%, whereas the pelites range from 53 to 78%, with the exception of one calcite rich sample. The wide $\text{CaO}_{\text{total}}$ range of 0.1-15% is due to the $\text{CaO}_{\text{carbonate}}$ content of the samples (Tab. 3).

Weathering. The molecular proportions of Al_2O_3 , $\text{CaO}_{\text{silicate}}$, Na_2O and K_2O can be used to calculate the chemical index of alteration (CIA; Nesbitt & Young, 1982). This is a measure of the alteration of feldspars to clay minerals. For the eleven carbonate free sandstone samples, the values range from 57 to 66, whereas the four carbonate free pelite samples have values of 64-72. Calculations with a carbonate phase content of 100 % calcite for the remaining samples give maximum CIA values of 55-66 and 63-72 for all 30 sandstones and all seven pelites, respectively (Tab. 3, Fig. 16). These values indicate a moderate degree of alteration. The K_2O content of up to 5 % can be explained by K-metasomatism (Fedó *et al.*, 1995). McLennan *et al.* (1990) used the K/Cs ratio as weathering indicator. Although both elements

¹Parts of the whole-rock element results and the Sm-Nd isotope in Section 4 are published in Augustsson & Bahlburg (2003a).

Table 3. Major and trace elements

	Lago General Carrera unit			Cochrane unit									
	CA-00 -03-S	CA-00 -03-S*	CA-00 -02-M	CA-00 -04-S	CA-00 -09-S	CA-00 -10-S	CA-00 -12-S	CA-00 -13-S	CA-00 -15-S	CA-00 -17-S	CA-00 -21-S	CA-00 -22-S	CA-00 -23-S
SiO ₂	73.41	72.96	67.89	73.92	79.92	74.28	75.38	76.31	73.00	74.63	80.96	73.24	81.48
Al ₂ O ₃	12.60	13.01	15.13	12.66	9.90	12.35	11.96	11.31	12.19	12.06	9.56	12.35	8.45
Fe ₂ O ₃	3.36	3.55	6.18	3.71	2.56	4.08	3.28	2.90	3.49	3.19	2.22	4.28	2.59
MgO	1.26	1.35	1.76	1.28	0.94	1.53	1.10	0.89	1.52	1.14	0.64	1.44	0.90
CaO	0.90	0.89	0.19	0.17	0.46	0.91	0.72	0.59	1.53	0.75	0.16	0.38	0.54
Na ₂ O	3.78	3.81	2.39	3.29	1.72	0.77	2.49	2.91	3.35	3.49	2.85	1.97	1.84
K ₂ O	1.99	1.94	2.44	1.84	2.27	3.30	2.35	2.07	1.59	1.68	1.18	2.76	1.60
TiO ₂	0.57	0.55	0.77	0.68	0.52	0.68	0.63	0.52	0.59	0.63	0.49	0.79	0.48
P ₂ O ₅	0.07	0.09	0.14	0.12	0.06	0.12	0.12	0.10	0.06	0.08	0.09	0.11	0.09
MnO	0.04	0.04	0.05	0.05	0.03	0.04	0.05	0.05	0.06	0.05	0.03	0.04	0.04
Cr ₂ O ₃	0.009	0.006	0.008	0.003	0.007	0.007	0.008	0.005	0.011	0.005	0.008	0.008	0.008
LOI	1.9	1.7	2.8	2.2	1.5	1.8	1.8	2.2	2.4	2.2	1.6	2.5	1.9
Sum	99.93	99.91	99.81	99.97	99.93	99.94	99.96	99.92	99.83	99.94	99.82	99.93	99.95
S	< 0.01	0.01	< 0.01	< 0.01	0.02	0.06	0.02	0.02	0.06	0.12	0.02	0.07	0.04
C	0.08	0.09	0.24	0.12	0.07	0.13	0.11	0.16	0.26	0.27	0.05	0.23	0.18
C†	0.03		< 0.01	< 0.01	< 0.01	< 0.01	< 0.01	0.05	0.20	0.08	< 0.01	0.03	0.07
CaO‡	0.14		-	-	-	-	-	0.23	0.93	0.37	-	0.14	0.33
CIA§	56.4		68.6	62.1	61.8	65.5	60.1	59.6	59.4	59.4	60.4	65.0	62.1
Ba	344	353	502	369	411	590	601	548	350	329	286	548	316
Sc	10	10	13	10	7	11	8	7	11	10	6	11	6
Co	7.9	8.9	11.3	6.0	5.3	8.1	4.6	7.2	8.7	7.3	3.9	11.2	5.6
Cs	4.6	5.0	6.9	3.6	5.4	6.3	4.1	3.9	3.6	4.2	2.8	7.9	3.8
Ga	14.6	15.0	18.7	14.3	10.6	15.2	14.3	13.5	13.7	13.8	9.6	15.7	9.6
Hf	5.9	5.5	6.9	5.9	8.4	5.9	8.4	6.3	5.4	8.1	8.6	6.2	8.4
Nb	7.4	7.3	12.2	10.2	7.6	10.5	11.4	10.1	8.6	9.3	6.4	13.1	6.8
Rb	90.6	87.4	121.6	92.0	102.3	136.4	104.4	91.0	70.5	90.0	56.5	123.7	70.3
Sr	162.1	166.1	73.3	38.8	52.1	93.5	131.0	119.8	136.8	88.1	67.7	60.3	70.2
Ta	0.9	0.7	1.1	1.2	0.9	1.2	1.2	1.1	1.1	1.2	0.8	1.4	0.9
Th	7.8	7.8	14.6	9.9	7.6	9.2	12.1	10.9	6.4	8.7	8.8	11.3	7.3
Tl	1.4	0.5	0.3	1.2	1.1	1.2	1.1	0.8	0.9	0.7	1.1	0.9	0.7
U	2.2	2.1	3.3	2.8	2.5	2.4	3.3	3.0	1.9	2.3	2.4	3.0	2.0
V	60	62	105	74	50	74	47	39	59	61	35	74	42
Zr	187.1	192.5	268.8	188.5	278.1	191.2	272.6	211.8	178.7	264.7	278.3	197.9	275.1
Y	23.2	23.3	28.4	21.8	22.8	25.1	31.5	26.8	22.6	24.1	22.9	30.9	20.5
La	26.1	25.8	26.8	27.6	29.3	30.9	37.2	32.0	25.8	30.1	29.8	33.2	27.1
Ce	54.2	53.1	62.4	58.8	59.3	63.7	77.2	66.5	51.4	61.4	60.1	69.8	55.2
Pr	6.70	6.28	6.89	6.96	7.19	7.49	8.96	7.82	6.37	7.34	7.06	8.28	6.51
Nd	26.6	25.8	26.7	27.8	28.2	30.2	35.1	31.1	26.0	28.4	27.8	32.6	25.2
Sm	5.0	5.1	5.5	5.2	5.1	6.0	6.7	5.8	5.0	5.5	5.0	6.4	4.6
Eu	1.43	1.23	1.12	1.13	1.17	1.22	1.56	1.20	1.39	1.27	0.98	1.34	1.03
Gd	4.74	4.63	5.11	4.71	4.52	5.01	6.23	5.42	4.47	4.94	4.45	5.86	4.32
Tb	0.63	0.67	0.78	0.64	0.66	0.70	0.82	0.73	0.65	0.69	0.66	0.88	0.61
Dy	4.47	4.20	5.14	4.25	4.31	4.89	5.87	5.03	4.13	4.55	4.33	5.88	4.16
Ho	0.92	0.87	1.17	0.82	0.87	0.96	1.16	1.00	0.87	0.91	0.81	1.18	0.78
Er	2.50	2.56	3.46	2.26	2.44	2.69	3.40	2.83	2.33	2.74	2.46	3.33	2.33
Tm	0.37	0.36	0.45	0.33	0.35	0.39	0.47	0.41	0.37	0.39	0.35	0.47	0.33
Yb	2.63	2.50	3.37	2.19	2.56	2.74	3.13	2.78	2.37	2.73	2.40	3.28	2.36
Lu	0.38	0.38	0.49	0.29	0.36	0.36	0.43	0.36	0.35	0.37	0.32	0.48	0.33
Cu	5	8	18	9	6	< 1	3	8	3	4	5	18	7
Pb	15	15	7	11	15	4	13	19	14	12	7	16	13
Zn	50	45	62	50	36	66	31	49	45	39	17	69	28
Ni	10	10	30	13	13	22	10	11	17	12	10	21	12
As	5	4	6	2	7	8	2	3	2	5	< 2	7	4

Oxides, C and S in %, other elements in ppm. S and M denotes greywackes and pelites respective. n. m. = not measured. *Mean values of 5 (CA-00-03-S) and 3 (CA-00-32-S) measurements. For S, means are calculated with 4 and 2 values, respectively. †C in carbonates.

‡Maximum CaO in carbonates calculated from the measured C in carbonates. §CIA = $Al_2O_3 / (Al_2O_3 + Ca_{silicate} + Na_2O + K_2O) \cdot 100$ calculated from the molecular ratios. ||Data from Dobrzinski (2001), measured by XRF.

tend to be adsorbed on clay minerals during weathering, the K/Cs ratio decreases with increasing degree of weathering. The narrow range for the ratios between values for the upper continental crust (McLennan, 2001) and Post-Archean average Australian shale (Taylor & McLennan, 1985) is in agreement with the medium-high CIA values and a minor to moderate K-metasomatic effect (Fig. 16; cf. McLennan *et al.*, 1990; Fedo *et al.*, 1995). Note that the greywackes (but not the pelite) of the southern sampling area in the southern Chilean

Continuation of Table 3

	Cochrane unit											
	CA-00 -26-S	CA-00 -28-S	CA-00 -30-S	CA-00 -32-S	CA-00 -32-S*	CA-00 -33-S	CA-00 -37-S	CA-00 -42-S	CA-00 -14-M	CA-00 -19-M	CA-00 -25-M	CA-00 -27-M
SiO ₂	75.42	80.36	79.68	79.83	80.00	74.94	74.28	71.61	64.96	68.73	53.61	43.33
Al ₂ O ₃	12.02	9.48	9.60	7.86	7.78	11.00	12.46	9.43	16.38	14.40	22.28	12.51
Fe ₂ O ₃	3.62	2.58	3.08	2.32	2.39	3.94	2.03	2.62	6.16	5.76	8.47	6.20
MgO	1.28	0.85	1.09	0.74	0.73	1.51	0.90	1.14	2.11	1.89	2.70	2.04
CaO	0.29	0.36	0.21	2.27	2.32	0.78	1.67	5.24	0.24	0.49	0.25	15.11
Na ₂ O	2.57	2.12	2.19	2.13	2.11	2.64	4.06	2.49	2.03	2.06	1.91	2.35
K ₂ O	1.83	1.58	1.38	1.24	1.19	1.66	1.35	1.35	4.02	2.67	4.84	1.79
TiO ₂	0.65	0.57	0.63	0.50	0.45	0.65	0.36	0.41	0.82	0.81	1.02	0.64
P ₂ O ₅	0.10	0.07	0.11	0.13	0.10	0.14	0.08	0.04	0.13	0.14	0.14	0.38
MnO	0.04	0.03	0.03	0.05	0.04	0.05	0.05	0.08	0.10	0.04	0.11	0.40
Cr ₂ O ₃	0.008	0.009	0.010	0.009	0.008	0.009	0.002	0.006	0.010	0.010	0.019	0.007
LOI	2.1	1.9	1.9	2.7	2.7	2.6	2.7	5.5	2.9	2.9	4.3	14.6
Sum	99.97	99.94	99.94	99.81	99.90	99.96	99.97	99.95	99.98	99.96	99.75	99.40
S	0.03	0.06	0.08	< 0.01	0.01	0.04	0.04	< 0.01	< 0.01	0.10	0.55	0.03
C	0.15	0.14	0.08	0.53	0.52	0.21	0.39	1.17	0.29	0.36	0.44	3.74
C†	0.02	0.04	< 0.01	0.43		0.11	0.28	1.05	< 0.01	0.05	< 0.01	3.36
CaO‡	0.09	0.19	-	2.01		0.51	1.31	4.90	-	0.23	-	15.11
CIA§	64.7	63.2	63.7	59.6		62.4	58.6	60.4	66.8	68.1	71.6	68.3
Ba	336	284	254	215	214	334	244	285	1058	475	852	329
Sc	10	7	8	6	7	9	6	6	16	13	22	12
Co	9.0	5.4	7.1	4.8	5.4	8.0	3.7	4.9	14.2	17.3	17.7	12.9
Cs	5.0	3.1	3.4	2.7	2.9	4.4	2.5	3.2	8.8	7.2	14.6	4.3
Ga	14.9	10.6	11.0	7.6	8.0	12.8	14.4	10.3	25.3	18.4	29.9	16.0
Hf	7.9	8.9	8.9	10.3	10.6	6.0	5.0	5.0	4.8	6.2	4.3	3.4
Nb	10.7	8.0	9.3	6.2	6.5	9.4	7.0	6.2	15.1	13.6	17.7	11.1
Rb	99.2	75.4	72.3	48.8	52.8	74.3	66.9	66.3	186.0	135.9	218.0	89.3
Sr	47.8	73.5	55.4	122.7	132.9	93.6	142.4	272.4	72.1	70.1	37.7	575.2
Ta	1.2	0.9	1.1	0.7	0.6	1.1	0.9	0.7	1.4	1.3	1.7	1.1
Th	9.8	6.9	8.2	7.8	8.2	7.3	11.1	5.7	18.3	12.8	18.4	11.0
Tl	0.7	0.6	0.7	0.1	0.1	0.2	0.1	0.1	0.7	0.8	0.4	0.4
U	2.8	2.1	2.3	2.0	2.2	2.0	2.2	1.6	5.4	3.4	3.9	2.5
V	75	45	53	33	32	62	36	43	119	117	195	95
Zr	249.4	284.9	302.9	349.3	376.7	190.8	158.2	160.8	169.3	212.9	139.9	118.2
Y	27.1	22.4	22.6	19.7	21.5	26.4	19.9	18.6	35.9	31.9	34.8	29.4
La	32.9	27.6	29.9	27.9	29.3	29.1	34.2	22.5	44.3	37.2	50.3	33.3
Ce	67.3	55.3	59.4	56.2	57.4	59.7	66.9	43.8	96.1	80.1	104.2	68.5
Pr	8.14	6.67	7.01	6.28	6.35	7.26	7.82	5.13	11.30	9.23	12.15	7.77
Nd	32.0	25.7	27.3	25.3	25.3	29.1	28.8	19.9	44.5	37.5	47.0	31.3
Sm	5.9	5.1	5.1	4.5	4.6	5.6	4.9	4.0	8.8	7.4	9.8	6.2
Eu	1.31	1.15	1.18	1.02	0.94	1.42	1.02	1.02	1.53	1.47	1.69	1.25
Gd	5.20	4.71	4.34	3.77	4.05	5.43	4.00	3.45	7.16	6.38	6.65	5.61
Tb	0.76	0.59	0.65	0.54	0.61	0.80	0.56	0.48	1.05	0.93	1.08	0.75
Dy	5.03	4.19	4.14	3.68	3.59	4.88	3.58	3.18	6.62	6.01	6.74	4.66
Ho	1.07	0.82	0.84	0.73	0.74	1.01	0.73	0.66	1.39	1.33	1.35	1.08
Er	2.90	2.51	2.51	2.13	2.20	2.77	1.94	2.07	4.22	3.75	4.00	3.12
Tm	0.45	0.36	0.33	0.32	0.35	0.40	0.28	0.28	0.53	0.44	0.58	0.36
Yb	2.94	2.45	2.65	2.16	2.23	2.81	2.02	1.98	3.91	3.51	3.70	2.95
Lu	0.40	0.33	0.37	0.31	0.35	0.38	0.27	0.30	0.58	0.50	0.59	0.44
Cu	15	9	10	4	4	12	1	1	20	13	36	20
Pb	12	12	12	14	16	13	6	13	23	6	28	14
Zn	51	26	27	19	21	38	13	27	73	45	134	69
Ni	17	10	14	7	8	14	5	9	28	32	34	21
As	3	4	3	3	3	2	2	< 2	5	11	19	< 2

Oxides, C and S in %, other elements in ppm. S and M denotes greywackes and pelites respective. n. m. = not measured. *Mean values of 5 (CA-00-03-S) and 3 (CA-00-32-S) measurements. For S, means are calculated with 4 and 2 values, respectively. †C in carbonates.

‡Maximum CaO in carbonates calculated from the measured C in carbonates. §CIA = $Al_2O_3 / (Al_2O_3 + Ca_{silicate} + Na_2O + K_2O) \cdot 100$ calculated from the molecular ratios. ||Data from Dobrzinski (2001), measured by XRF.

archipelago (FA-; Fig. 1c) have lower CIA values and higher K/Cs than those from the northern sampling area (FF-; Fig. 1c).

Concentrations of provenance indicative trace elements. Provenance indicative elements such as Ti, Nb, Th, La, Co and Sc have values close to upper continental crust and Post-Archean average Australian Shale (Tab. 3, Fig. 17). Among these elements, Co is the only one that does not exceed the value for the upper continental crust in any sample. For the part of the

Continuation of Table 3

	Río Lácteo Formation			Bahía de la Lancha Formation				Southern Chilean archipelago						
	CA-01-02-S	CA-01-03-S	CA-01-01-M	CA-01-04-S	CA-01-05-S	CA-01-06-S	CA-01-07-S	FF-01-S	FF-04-S	FF-06-S	FA-01-S	FA-02-S	FA-11-S	FA-10-M
SiO ₂	79.44	75.88	77.61	79.64	78.50	80.87	86.96	81.45	87.59	75.63	70.06	65.84	66.35	56.10
Al ₂ O ₃	9.56	11.28	11.24	9.91	9.35	8.72	6.46	8.52	5.26	11.85	15.43	16.13	14.81	20.55
Fe ₂ O ₃	3.53	3.89	3.26	2.48	3.04	2.54	1.09	3.09	2.61	3.61	4.19	5.15	4.67	7.46
MgO	1.08	0.85	0.93	0.84	0.99	1.00	0.37	0.78	0.69	1.12	1.57	1.84	1.68	2.62
CaO	0.31	0.38	0.17	0.76	1.22	1.09	0.15	0.48	0.38	0.47	1.38	1.88	6.00	1.23
Na ₂ O	2.98	3.55	2.57	2.17	2.12	1.83	1.99	2.22	1.35	1.57	3.68	1.72	1.67	0.98
K ₂ O	1.09	1.27	1.77	1.66	1.52	1.44	1.22	1.04	0.47	2.44	1.68	4.40	1.44	5.37
TiO ₂	0.53	0.57	0.48	0.51	0.63	0.45	0.35	0.40	0.30	0.56	0.65	0.70	0.58	0.96
P ₂ O ₅	0.10	0.11	0.09	0.08	0.14	0.10	0.07	0.06	0.04	0.08	0.09	0.13	0.18	0.16
MnO	0.04	0.05	0.04	0.04	0.05	0.05	0.02	0.03	0.02	0.03	0.06	0.06	0.10	0.07
Cr ₂ O ₃	0.009	0.009	0.009	0.012	0.006	0.013	0.008	0.005	0.007	0.008	0.007	0.010	0.008	0.016
LOI	1.1	1.9	1.6	1.7	2.2	1.7	1.1	1.8	1.1	2.4	1.2	2.0	1.6	3.8
Sum	99.80	99.77	99.81	99.85	99.79	99.84	99.82	99.90	99.83	99.83	99.95	99.84	99.03	99.28
S	0.01	0.04	< 0.01	< 0.01	< 0.01	0.01	0.20	0.07	0.08	0.04	< 0.01	0.05	0.01	0.12
C	0.09	0.10	0.08	0.18	0.29	0.26	0.01	0.29	0.11	0.43	n. m.	n. m.	n. m.	n. m.
C†	0.02	0.03	< 0.01	0.11	0.19	0.17	< 0.01	0.02	< 0.01	< 0.01	< 0.01	< 0.01	0.37	0.02
CaO‡	0.09	0.14	-	0.51	0.89	0.79	-	0.11	-	-	-	-	1.75	0.08
CIA§	59.6	59.6	63.5	63.0	62.0	63.1	57.0	61.0	60.6	66.1	59.7	59.4	55.2	68.3
Ba	196	237	353	333	234	221	226	204	92	520	758	762	388	1039
Sc	7	9	8	7	8	7	5	7	4	9	12	14	11	18
Co	7.4	9.0	6.9	7.0	7.0	7.3	3.1	7.1	7.0	6.6	9.8	11.9	8.3	15.3
Cs	2.4	2.7	3.8	3.3	4.1	3.0	2.7	3.9	1.6	5.7	2.7	6.9	3.2	5.8
Ga	9.4	11.1	12.1	11.2	10.3	9.5	6.9	10.3	5.8	15.4	19.4	20.4	20.4	30.7
Hf	7.3	5.8	5.0	7.3	7.6	7.8	8.4	6.8	11.5	8.3	6.0	5.2	4.7	4.5
Nb	6.8	7.7	6.9	6.9	9.4	7.8	6.0	8.1	5.0	9.9	10.6	11.6	9.7	16.0
Rb	44.3	50.6	73.5	67.3	56.3	63.3	45.8	53.9	27.6	113.8	79.4	165.3	100.7	244.5
Sr	86.3	108	44.6	48.5	84.2	73.4	79.5	91.1	73.2	76.3	228.5	130.7	178.6	114.4
Ta	0.6	0.8	0.7	0.7	1.0	0.7	0.6	0.8	0.5	0.8	1.5	1.2	0.9	1.5
Th	7.6	8.1	7.8	8.2	7.8	8.1	7.9	6.1	4.1	8.6	12.4	11.5	10.8	17.5
Tl	0.3	0.1	0.3	0.2	0.1	< 0.1	< 0.1	0.4	0.3	0.2	0.5	0.9	0.1	0.6
U	2.0	1.9	2.2	2.4	2.0	2.1	1.8	1.5	1.7	2.3	2.5	2.9	2.8	3.6
V	46	55	47	42	44	40	27	46	23	67	76	95	67	148
Zr	254.9	233.9	201.1	281.1	296.6	269.5	337.0	279.8	478.9	340.0	231.9	182.9	167.5	151.8
Y	17.5	19.8	20.5	17.8	22.0	19.0	17.1	17.2	14.6	22.3	20.9	24.6	20.4	32.1
La	21.5	26.2	24.0	25.6	26.7	25.5	23.1	23.7	11.9	26.5	35.6	33.7	18.1	41.6
Ce	48.8	56.1	50.3	54.4	54.4	53.6	47.6	46.0	25.5	54.3	74.7	70.1	42.6	90.6
Pr	5.45	6.52	5.93	6.27	6.84	6.08	5.36	5.17	2.84	6.07	8.60	8.05	5.09	10.20
Nd	21.9	25.9	22.3	24.2	28.8	23.4	21.3	19.6	11.8	22.5	33.2	33.2	21.7	41.5
Sm	4.5	5.6	4.5	4.8	5.7	5.5	3.7	4.0	2.6	4.3	6.1	6.3	4.4	7.8
Eu	0.94	1.19	0.98	0.97	1.27	1.05	0.69	0.67	0.47	0.80	1.25	1.29	1.04	1.59
Gd	3.60	4.20	3.69	3.69	4.89	3.86	3.23	3.71	2.74	3.67	4.67	5.22	4.03	6.32
Tb	0.57	0.68	0.64	0.52	0.74	0.62	0.52	0.52	0.36	0.56	0.61	0.76	0.55	1.01
Dy	3.23	3.87	3.56	3.12	4.62	3.80	3.33	2.94	2.21	3.80	3.96	4.57	3.29	6.10
Ho	0.63	0.72	0.73	0.67	0.79	0.69	0.61	0.57	0.48	0.77	0.79	0.97	0.75	1.30
Er	1.98	2.09	2.34	1.96	2.47	2.15	1.92	1.74	1.49	2.48	2.36	2.82	2.29	3.79
Tm	0.34	0.31	0.34	0.30	0.38	0.31	0.28	0.28	0.21	0.38	0.29	0.35	0.26	0.46
Yb	1.90	2.01	2.02	2.14	2.33	1.89	1.81	1.82	1.54	2.61	2.25	2.65	2.18	3.62
Lu	0.32	0.33	0.34	0.33	0.41	0.31	0.31	0.27	0.27	0.41	0.31	0.38	0.33	0.51
Cu	8	9	6	9	6	9	8	11	13	11	< 1	17	35	14
Pb	9	4	12	10	< 3	12	8	9	25	7	< 3	< 3	5	< 3
Zn	40	32	43	22	36	14	11	37	36	37	36	51	50	80
Ni	13	12	11	9	12	11	6	13	13	13	13	18	14	28
As	5	5	4	7	< 2	5	66	6	6	6	< 2	2	2	3

Oxides, C and S in %, other elements in ppm. S and M denotes greywackes and pelites respective. n. m. = not measured. *Mean values of 5 (CA-00-03-S) and 3 (CA-00-32-S) measurements. For S, means are calculated with 4 and 2 values, respectively. †C in carbonates.

‡Maximum CaO in carbonates calculated from the measured C in carbonates. §CIA = Al₂O₃/(Al₂O₃+Ca_{silicate}+Na₂O+K₂O)·100 calculated from the molecular ratios. ||Data from Dobrzinski (2001), measured by XRF.

Eastern Andean Metamorphic Complex cropping out in the southern Chilean archipelago, the element concentrations for the greywacke samples of the southern sampling area (FA-) are higher than those from the northern sampling area (FF-), except for the zircon-dominating Hf and Zr, where the opposite is true (Tab. 3). Except for Zr and Hf, the trace element concentrations of the pelites are higher than for sandstones, but with similar patterns

Table 4. *Selected element ratios*

	K/Cs	Zr/Sc	Hf/Sc	Th/Sc	Th/Co	La/Sc	Ti/Nb	Sm/Nd	La _N /Yb _N	Eu/Eu*	Ce/Ce*
Lago General Carrera unit:											
CA-00-03-S	3591	18.7†	0.59	0.78	0.99	2.61	462	0.19	6.71	0.90	0.96
CA-00-02-M	2936	20.7	0.53	1.12	1.29	2.06	378	0.21	5.37	0.65	1.08
Cochrane unit:											
CA-00-04-S	4243	18.9†	0.59	0.99	1.65	2.76	400	0.19	8.52	0.70	0.99
CA-00-09-S	3490	39.7†	1.20	1.09	1.43	4.19	410	0.18	7.73	0.74	0.96
CA-00-10-S	4348	17.4†	0.54	0.84	1.14	2.81	388	0.20	7.62	0.68	0.98
CA-00-12-S	4758	34.1†	1.05	1.51	2.63	4.65	331	0.19	8.03	0.74	0.99
CA-00-13-S	4406	30.3†	0.90	1.56	1.51	4.57	309	0.19	7.78	0.65	0.98
CA-00-15-S	3666	16.2†	0.49	0.58	0.74	2.35	411	0.19	7.36	0.90	0.94
CA-00-17-S	3321	26.5†	0.81	0.87	1.19	3.01	406	0.19	7.45	0.74	0.97
CA-00-21-S	3498	46.4†	1.43	1.47	2.26	4.97	459	0.18	8.39	0.63	0.97
CA-00-22-S	2900	18.0†	0.56	1.03	1.01	3.02	362	0.20	6.84	0.67	0.99
CA-00-23-S	3495	45.9†	1.40	1.22	1.30	4.52	423	0.18	7.76	0.71	0.97
CA-00-26-S	3038	24.9†	0.79	0.98	1.09	3.29	364	0.18	7.56	0.72	0.96
CA-00-28-S	4231	40.7†	1.27	0.99	1.28	3.94	427	0.20	7.61	0.72	0.95
CA-00-30-S	3369	37.9†	1.11	1.03	1.15	3.74	406	0.19	7.62	0.77	0.96
CA-00-32-S	3813	58.2†	1.72	1.30	1.63	4.65	483	0.18	8.73	0.76	0.99
CA-00-33-S	3132	21.2†	0.67	0.81	0.91	3.23	415	0.19	7.00	0.79	0.96
CA-00-37-S	4483	26.4†	0.83	1.85	3.00	5.70	308	0.17	11.44	0.70	0.96
CA-00-42-S	3502	26.8†	0.83	0.95	1.16	3.75	396	0.20	7.68	0.84	0.96
CA-00-14-M	3792	10.6	0.30	1.14	1.29	2.77	326	0.20	7.66	0.59	1.01
CA-00-19-M	3078	16.4	0.48	0.98	0.74	2.86	357	0.20	7.16	0.65	1.01
CA-00-25-M	2752	6.4	0.20	0.84	1.04	2.29	345	0.21	9.19	0.64	0.99
CA-00-27-M	3456	9.9	0.28	0.92	0.85	2.78	346	0.20	7.63	0.65	1.00
Río Lácteo Formation:											
CA-01-02-S	3770	36.4	1.04	1.09	1.03	3.07	467	0.21	7.65	0.71	1.06
CA-01-03-S	3905	26.0	0.64	0.90	0.90	2.91	444	0.22	8.81	0.75	1.01
CA-01-01-M	3867	25.1	0.63	0.98	1.13	3.00	417	0.20	8.03	0.73	0.99
Bahía de la Lancha Formation:											
CA-01-04-S	4176	40.2	1.04	1.17	1.17	3.66	443	0.20	8.08	0.70	1.01
CA-01-05-S	3078	37.1	0.95	0.98	1.11	3.34	402	0.20	7.74	0.74	0.94
CA-01-06-S	3985	38.5	1.11	1.16	1.11	3.64	346	0.24	9.12	0.70	1.01
CA-01-07-S	3751	67.4	1.68	1.58	2.55	4.62	350	0.17	8.62	0.61	1.00
Southern Chilean Archipelago:											
FF-01-S	2214	40.0	0.97	0.87	0.86	3.39	296	0.20	8.80	0.53	0.97
FF-04-S	2439	119.7	2.88	1.03	0.59	2.98	360	0.22	5.22	0.54	1.03
FF-06-S	3554	37.8	0.92	0.96	1.30	2.94	339	0.19	6.86	0.62	1.00
FA-01-S	5181	19.9	0.52	1.07	1.27	3.06	368	0.18	10.69	0.72	1.00
FA-02-S	5294	13.1	0.37	0.82	0.97	2.42	364	0.19	8.59	0.69	1.00
FA-11-S	3745	14.7	0.41	0.95	1.30	1.59	356	0.20	5.61	0.75	1.04
FA-10-M	7688	8.3	0.25	0.95	1.14	2.27	360	0.19	7.77	0.69	1.03

S and M denotes greywackes and pelites respective. $Eu/Eu^* = Eu_N/(Sm_N \cdot Gd_N)^{1/2}$ and $Ce/Ce^* = Ce_N/(La_N \cdot Pr_N)^{1/2}$. †The values reported in Augustsson & Bahlburg (2003a) are incorrect for these samples.

(Fig. 17). This points to a quartz dilution effect in the sandstones (*cf.* McLennan *et al.*, 1990). The Río Lácteo Formation is the only unit, where the trace element concentrations generally are similar for greywackes and shales (Tab. 3, Fig. 17). Element ratios of the incompatible elements La and Th *vs.* the compatible Sc and Co are for all geological units slightly above those for the upper continental crust (Fig. 18).

Zr & Hf and recycling. Only Zr and Hf of the elements treated here have generally higher concentrations in the greywackes than in the pelites (Tab. 3). The Zr and Hf concentrations show scatter, but most greywacke samples have concentrations higher than the values for the upper continental crust at 190 ppm and 5.8 ppm, respectively (Tab. 3, Fig. 17). Zr and Hf concentrations are indicators of the maturity of the sediments, since zircon, the most important mineral for Zr and Hf, is neither sensitive to chemical nor to mechanical weathering and is concentrated in sandstones during sorting processes (*e. g.*, Morton & Hallsworth, 1999). Zr/Sc and Hf/Sc are also values of sorting and recycling (*e. g.*, McLennan *et al.*, 1993). All of the analysed greywackes, except for one greywacke sample from the Southern Chilean archipelago, have concentrations above the values for the upper continental crust at 14.0 and 0.43 ppm (Tab. 4). The two samples of the Lago General Carrera unit differ from the others

Table 5. *Samarium-neodymium isotope data*

	$^{147}\text{Sm}/^{144}\text{Nd}$	$f^{\text{Sm}/\text{Nd}}$	$^{143}\text{Nd}/^{144}\text{Nd}$ (today)	2σ ($\cdot 10^{-6}$)	ϵ_{Nd} (today)	Estimated age (Ma)	$^{143}\text{Nd}/^{144}\text{Nd}$ (T_s)	ϵ_{Nd} (T_s)	T_{DM} (Ma)	T_{DM}^* (Ma)
Lago General Carrera unit:										
CA-00-03-S	0.12583	-0.360	0.512360	10	-5.4	350	0.512071	-2.3 ± 0.2	1320	1177
Cochrane unit:										
CA-00-09-S	0.12051	-0.387	0.512171	14	-9.1	350	0.511895	-5.7 ± 0.3	1543	1426
CA-00-10-S	0.11799	-0.400	0.512173	10	-9.1	350	0.511902	-5.6 ± 0.2	1502	1416
CA-00-13-S	0.12055	-0.387	0.512215	8	-8.2	350	0.511939	-4.8 ± 0.2	1475	1364
CA-00-15-S	0.12665	-0.356	0.512165	14	-9.2	350	0.511874	-6.1 ± 0.3	1659	1456
CA-00-17-S	0.12004	-0.390	0.512225	9	-8.0	350	0.511950	-4.6 ± 0.2	1451	1348
CA-00-21-S	0.11410	-0.420	0.512170	12	-9.1	350	0.511908	-5.4 ± 0.3	1450	1408
CA-00-23-S	0.11595	-0.411	0.512143	17	-9.7	350	0.511877	-6.1 ± 0.4	1517	1452
CA-00-28-S	0.11600	-0.410	0.512140	12	-9.7	350	0.511874	-6.1 ± 0.3	1521	1456
CA-00-30-S	0.11514	-0.415	0.512115	14	-10.2	350	0.511851	-6.6 ± 0.3	1545	1488
CA-00-32-S	0.11706	-0.405	0.512132	8	-9.9	350	0.511864	-6.3 ± 0.2	1550	1471
CA-00-33-S	0.12382	-0.371	0.512205	10	-8.5	350	0.511921	-5.2 ± 0.2	1543	1390
CA-00-37-S†	0.11222	-0.429	0.512300	70	-6.6	350	0.512043	-2.8 ± 1.4	1235	1217
CA-00-37-S‡	0.10889	-0.446	0.512273	11	-7.1	350	0.512024	-3.2 ± 0.2	1235	1244
CA-00-42-S	0.12041	-0.388	0.512131	30	-9.9	350	0.511855	-6.5 ± 0.6	1605	1483
16-2-2-S§	0.11372	-0.422	0.512211	15	-8.3	350	0.511950	-4.6 ± 0.3	1384	1348
18-2-1-M§	0.12166	-0.382	0.512139	14	-9.7	350	0.511861	-6.4 ± 0.3	1612	1475
Río Lácteo Formation:										
CA-01-02-S	0.12243	-0.378	0.512201	11	-8.5	350	0.511921	-5.2 ± 0.2	1526	1390
Bahía de la Lancha Formation:										
CA-01-04-S	0.11431	-0.419	0.512162	17	-9.3	320	0.511922	-5.9 ± 0.3	1465	1419
CA-01-05-S	0.12374	-0.371	0.512100	20	-10.5	320	0.511841	-7.5 ± 0.4	1711	1533
CA-01-06-S	0.11865	-0.397	0.512129	12	-9.9	320	0.511881	-6.7 ± 0.3	1578	1477
CA-01-07-S	0.10795	-0.451	0.512087	11	-10.7	320	0.511861	-7.1 ± 0.2	1483	1505
Southern Chilean Archipelago:										
FF-01-S	0.11534	-0.414	0.512212	10	-8.3	350	0.511948	-4.7 ± 0.2	1404	1351
FA-01-S	0.10611	-0.461	0.512249	10	-7.6	280	0.512054	-4.4 ± 0.2	1238	1273
FA-02-S	0.10951	-0.443	0.512227	11	-8.0	280	0.512026	-4.9 ± 0.2	1308	1312

$T_{\text{DM}} = \ln\left(\frac{^{143}\text{Nd}/^{144}\text{Nd}_{\text{sample, today}} - ^{143}\text{Nd}/^{144}\text{Nd}_{\text{DM, today}}}{(^{147}\text{Sm}/^{144}\text{Nd}_{\text{sample, today}} - ^{147}\text{Sm}/^{144}\text{Nd}_{\text{DM, today}}) + 1}\right) / \lambda$ and $T_{\text{DM}}^* = \ln\left(\frac{^{143}\text{Nd}/^{144}\text{Nd}_{\text{sample, } T_s} - ^{143}\text{Nd}/^{144}\text{Nd}_{\text{DM, } T_s}}{(^{147}\text{Sm}/^{144}\text{Nd}_{\text{sample, } T_s} - ^{147}\text{Sm}/^{144}\text{Nd}_{\text{DM, } T_s}) + 1}\right) / \lambda + T_s$, where T_s is the estimated stratigraphic age. $^{147}\text{Sm}/^{144}\text{Nd}_{\text{crust, } T_s}$ was calculated assuming $^{147}\text{Sm}/^{144}\text{Nd}_{\text{crust, today}} = 0.11$ (Albarède & Brouxel, 1987). †Not included in figures and discussion ‡Multiple analysis. §Geochemistry published in Faúndez *et al.* (2002). For sampling locations, see Figure 1b.

by having higher Zr and Hf concentrations in the pelite sample than in the greywacke sample (Tab. 3). The overall high values indicate that the sediments are relatively well recycled. *Rare earth elements.* The rare earth element (REE) patterns are similar to Post-Archean average Australian Shale and the upper continental crust (Fig. 19). The chondrite-normalized La_N/Yb_N is only slightly lower than the value for the upper continental crust at 9.2 (Tab. 4). Ce can occur as Ce^{4+} , and Eu as Eu^{2+} , as well as the normal REE +3 state. Eu^{2+} readily replaces Ca^{2+} in plagioclase, thus the Eu anomaly (Eu/Eu^*) reflects the plagioclase fractionation. Felsic rocks and sediments usually have negative anomalies due to lithospheric or intracrustal feldspar fractionation, or breakdown of feldspars during weathering processes (Condie *et al.*, 1995). According to the study of McLennan *et al.* (1990), active margin sediments, in contrast to passive margin sediments, often show lower Eu/Eu^* values for shales than for greywackes. The studied rocks have negative anomalies with slightly lower values for pelites than for greywackes (Tab. 4, Fig. 19). Ce anomaly (Ce/Ce^*) can indicate REE redistribution during weathering, resulting in possible fractionation also for Sm and Nd isotopes (McDaniel *et al.*, 1994). The Ce/Ce^* ratios are close to 1, and the small difference in Ce/Ce^* for the studied rocks are within the uncertainties of the measurements. Thus no anomalous Ce/Ce^* can be deduced (Tab. 4, Fig. 19).

In similarity to other trace elements, the greywackes from the southern sampling area of the southern Chilean archipelago (FA-) show higher REE concentrations than those from the northern area (FF-; Tab. 3). Furthermore, they have less negative Eu anomalies than the samples from the northern area (Fig. 19).

Table 6. Rubidium-strontium isotope data

	Rb/Sr	$^{87}\text{Rb}/^{86}\text{Sr}^*$	$f^{\text{Rb/Sr}}$	$^{87}\text{Sr}/^{86}\text{Sr}$ (today)	2σ ($\cdot 10^{-6}$)	ϵ_{Sr} (today)	$^{87}\text{Sr}/^{86}\text{Sr}$ (T = 250 Ma)
Lago General Carrera unit:							
CA-00-03-S	0.559	1.566	17.93 ± 0.19	0.714854	13	147.0 ± 0.2	0.709286
Cochrane unit:							
CA-00-09-S	1.964	5.407	64.38 ± 0.65	0.734899	11	431.5 ± 0.2	0.715671
CA-00-10-S	1.459	4.157	49.26 ± 0.50	0.728526	11	341.0 ± 0.2	0.713744
CA-00-13-S	0.760	2.261	26.34 ± 0.27	0.721584	13	242.5 ± 0.2	0.713543
CA-00-15-S	0.515	1.564	17.91 ± 0.19	0.717419	12	183.4 ± 0.2	0.711858
CA-00-17-S	1.022	3.022	35.54 ± 0.37	0.723385	10	268.1 ± 0.2	0.712637
CA-00-21-S	0.835	1.707	19.65 ± 0.21	0.721925	11	247.3 ± 0.2	0.715853
CA-00-23-S	1.001	2.787	32.70 ± 0.34	0.724473	11	283.5 ± 0.2	0.714563
CA-00-28-S	1.026	2.856	33.54 ± 0.35	0.725711	14	301.1 ± 0.2	0.715554
CA-00-30-S	1.305	3.308	39.00 ± 0.40	0.729113	13	349.4 ± 0.2	0.717349
CA-00-32-S	0.397	1.153	12.95 ± 0.14	0.720420	10	226.0 ± 0.2	0.716318
CA-00-33-S	0.794	2.347	27.38 ± 0.28	0.723799	13	273.9 ± 0.2	0.715452
CA-00-37-S†	0.470	1.343	15.24 ± 0.16	0.716350	14	168.2 ± 0.2	0.711574
CA-00-37-S‡	0.470	1.291	14.61 ± 0.16	0.716321	18	167.8 ± 0.3	0.711731
CA-00-42-S	0.243	0.6995	7.46 ± 0.08	0.715874	12	161.5 ± 0.2	0.713387
16-2-2-S§	0.187	0.5407	5.54 ± 0.07	0.717920	12	190.5 ± 0.2	0.715997
18-2-1-M§	1.585	4.597	54.59 ± 0.56	0.731594	10	384.6 ± 0.2	0.715246
Río Lácteo Formation:							
CA-01-02-S	0.513	1.419	16.16 ± 0.17	0.717509	12	184.7 ± 0.2	0.712463
Bahía de la Lancha Formation:							
CA-01-04-S	1.388	4.050	47.97 ± 0.49	0.728220	13	336.7 ± 0.2	0.713817
CA-01-05-S	0.669	1.911	22.11 ± 0.23	0.721053	11	235.0 ± 0.2	0.714256
CA-01-06-S	0.862	2.635	30.86 ± 0.32	0.724892	14	289.5 ± 0.2	0.715523
CA-01-07-S	0.576	1.726	19.87 ± 0.21	0.722284	10	252.4 ± 0.2	0.716145
Southern Chilean Archipelago:							
FF-01-S	0.592	1.522	17.40 ± 0.18	0.715238	12	152.4 ± 0.2	0.709825
FA-01-S	0.347	1.002	11.12 ± 0.12	0.713065	13	121.6 ± 0.2	0.709500
FA-02-S	1.265	3.781	44.72 ± 0.46	0.718665	14	201.1 ± 0.2	0.705219

* $2\sigma = 1\%$. †Not included in discussion and figures. ‡Multiple analysis. §Geochemistry published in Faúndez *et al.* (2002). ||Measured with TIMS in Münster. Other Rb/Sr ratios are from analyses made by ACME lab, Vancouver.

4.1.3. Whole-rock major and trace element chemistry: implications

Several attempts have been made to use major elements as provenance indicators (*e. g.*, Roser & Korsch, 1986, 1988; Bhatia, 1983), although the major elements are prone to changes in

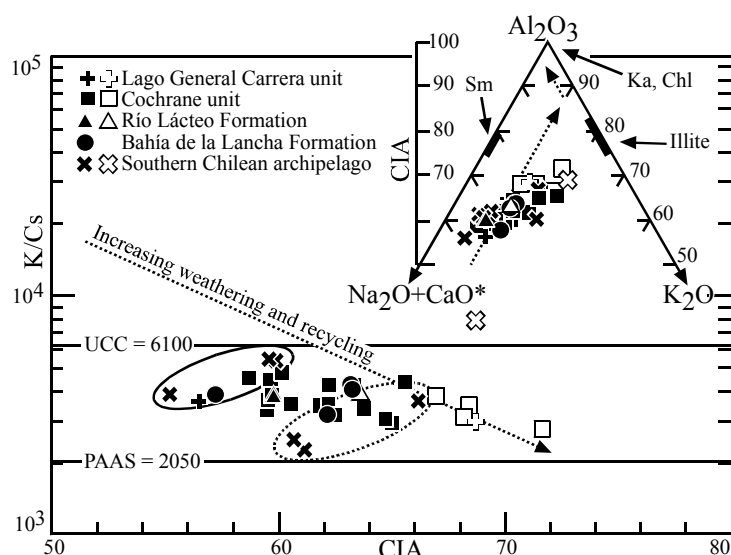


Fig. 16. Weathering condition of the sediments (oxides in molecular proportions). CaO^* is CaO in silicates. $\text{CaO}^* = \text{CaO}_{\text{total}} - \text{CaO}_{\text{max. in carbonates}}$ gives maximum CIA values. The arrows in the inset indicate ideal weathering from an approximate granodioritic composition. The observed trend towards illite composition is in concordance with a K-metasomatic effect. Filled symbols = greywackes, unfilled symbols = pelites, Chl = chlorite, Ka = kaolinite, Sm = smectite. Main diagram after McLennan *et al.* (1990), inset after Fedo *et al.* (1995). The solid line encircles FA-greywackes (southern area in the southern Chilean archipelago), the dotted line encircles FF-greywackes (northern sampling area in the archipelago).

concentrations and ratios during weathering, sorting, diagenesis and metamorphism. However, the discrimination procedure of Roser & Korsch (1988), which, irrespective of grain size, takes into account Al, Fe, Mg, Ti, K, Na and Ca_{silicate} , has been demonstrated to indicate source rock types for sediments. In their discrimination scheme, the major element compositions of the greywacke samples indicate felsic source rocks (Fig. 20). The greywacke sample points concentrate across the dividing-line between the fields for recycled source rocks and primary felsic source rocks, with a majority in the field indicative of recycled source rocks. The pelite samples have a larger spread, due to some chemical differences between the different grain sizes, and possibly as a result of larger sampling areas for finer grained sediments. The large scatter for the greywackes of the southern Chilean archipelago indicates different chemistry for the two sampling areas. The samples of the Lago General Carrera unit and the southern sampling area in the southern Chilean archipelago (FA-) have indications of a dominance of sedimentary detritus from primary source rocks with a felsic or

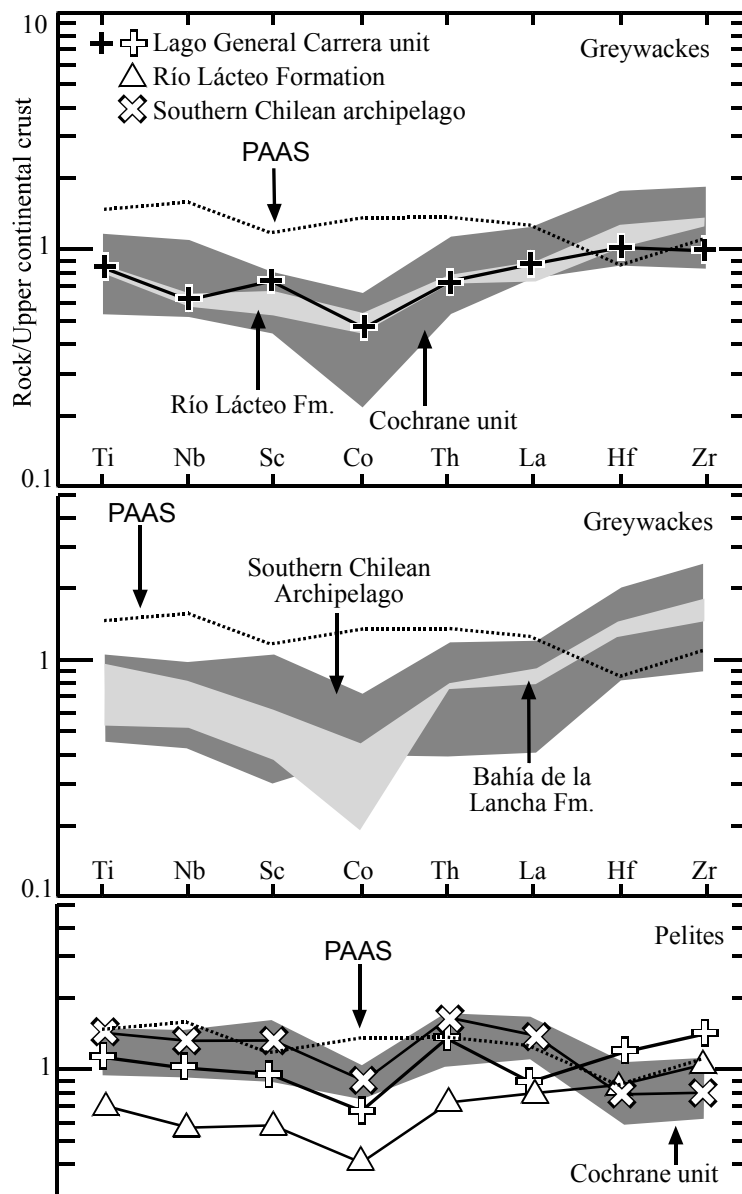


Fig. 17. Selected element ratios normalized to the upper continental crust (McLennan, 2001). PAAS = post-Archaean average Australian Shale (Taylor & McLennan, 1985).

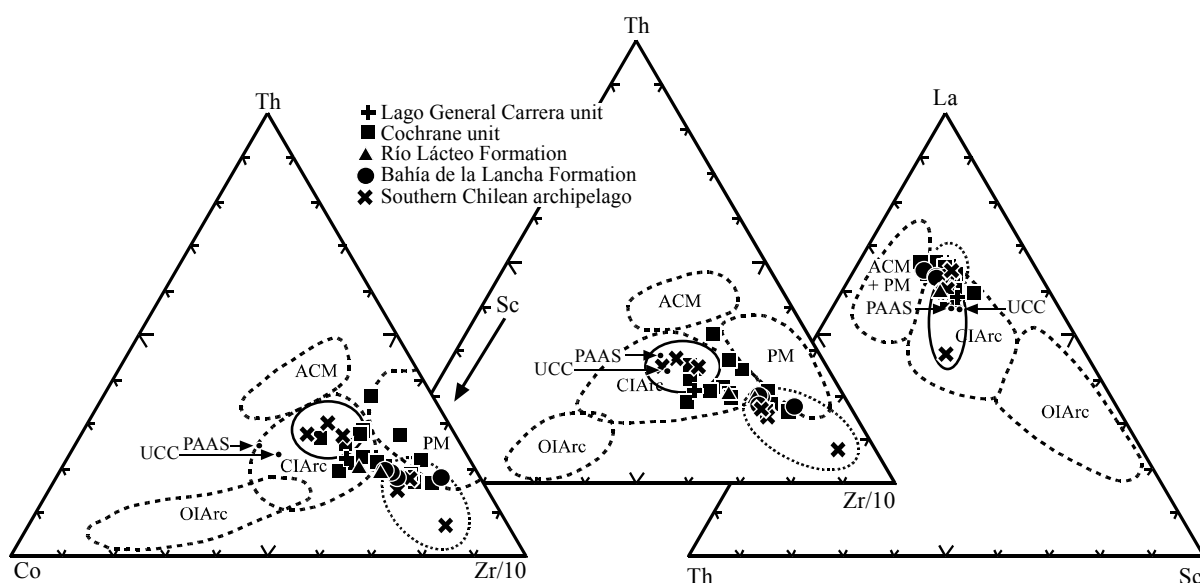


Fig. 18. Trace element diagrams with discrimination fields for greywackes from Bhatia & Crook (1986). ACM = active continental margin, CIArc = continental island arc, OIArc = oceanic island arc, PM = passive margin, PAAS = post-Archaean average Australian Shale (Taylor & McLennan, 1985), UCC = upper continental crust (McLennan, 2001). The solid line encircles FA-samples (southern sampling area in the southern Chilean archipelago), the dotted line encircles FF-samples (northern sampling area in the archipelago).

intermediate mafic - felsic composition (Fig. 20). The sediments from the northern area (FF-) indicate that most of the sedimentary material derives from recycled sources.

Bhatia & Crook (1986) showed that comparisons of the incompatible elements Th and La with the compatible elements Co and Sc can be powerful discriminators in provenance studies for greywackes, provided that mantle fractionation processes dominate the elemental signatures. This assumes that all four elements are relatively immobile during weathering and diagenesis. The small range in La/Sc, Th/Sc and Th/Co values (Tab. 4, Fig. 18) indicates that most of the greywacke samples could have a similar history. The high values point to felsic source rocks with a continental origin. However, taking the sorting and recycling dependent element Zr into account a larger spread can be seen. In Figure 18, a continental island arc setting is indicated for the main source rocks for a large part of the samples. Continental island arc environments are classified by Bhatia & Crook (1986) as island arcs at convergent plate margins resting on a well developed or thin continental crust. However, the relatively low Th/Zr, Co/Zr and Sc/Zr for many samples are typical of sediments deposited in a passive margin environment (which includes extensional regimes with rifting; Bhatia & Crook, 1986). The dominant sources of such sediments often have a long history of weathering, sorting, recycling *etc.*, which allows for enrichment of zircon and Zr. Of the samples from the southern Chilean archipelago, the sediments from the southern part (FA-) have Th/Zr, Co/Zr and Sc/Zr ratios in a range indicating main sources of continental island arc origin, whereas the values are lower for the northern samples (FF-) and typical for passive margin sediments (Fig. 18, Tab. 4).

The element ratio Ti/Zr was used by Bhatia & Crook (1986) as a provenance proxy for greywackes, although Zr is highly dependent on the zircon content. Ti is usually moderately incompatible and concentrated in minerals typical of mafic rocks (Van Baalen, 1993). It is immobile during weathering and diagenesis, but large concentrations of rutile, titanite and ilmenite in sediments will affect the concentration (Van Baalen, 1993) and can

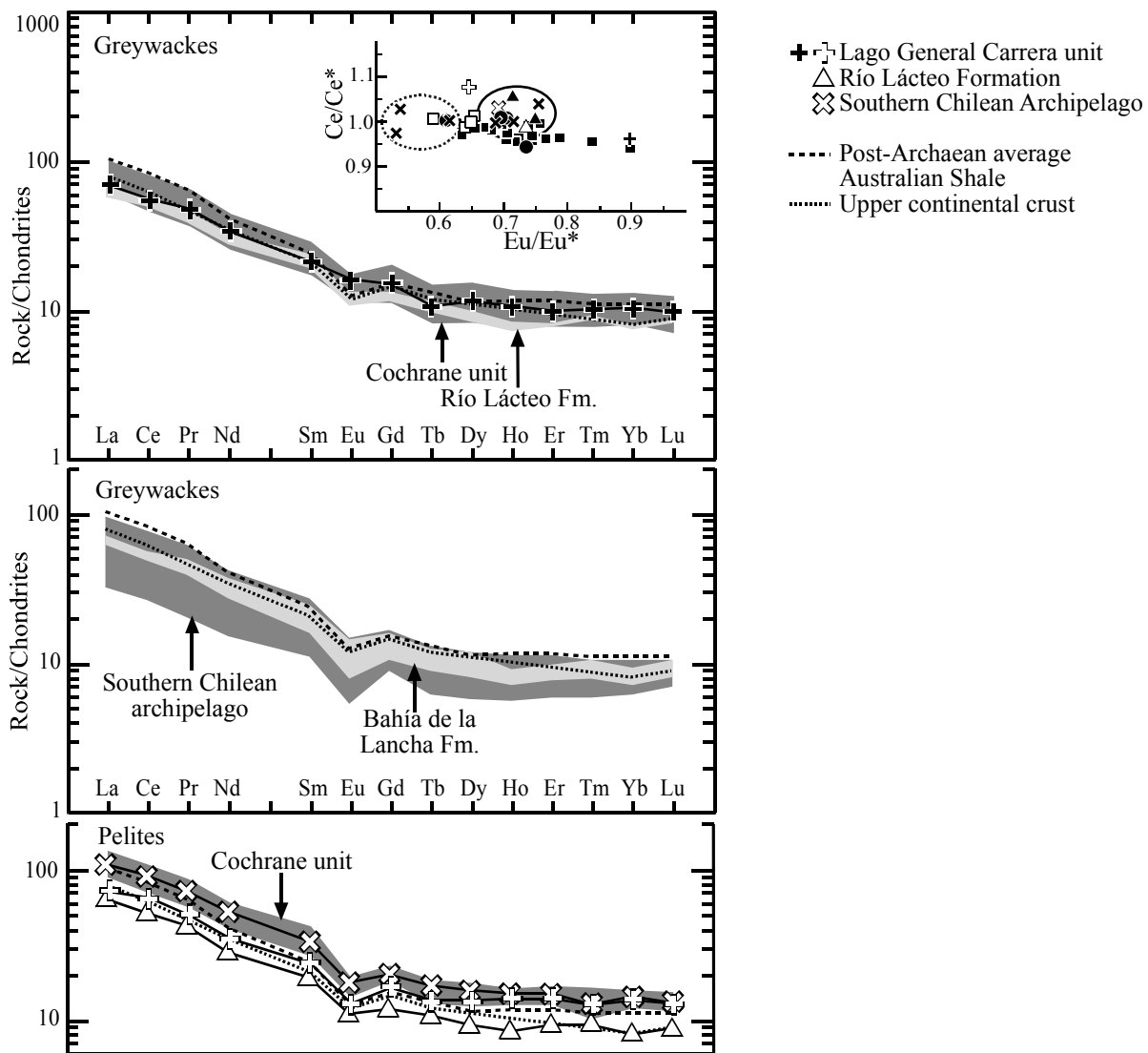


Fig. 19. REE pattern and Eu/Eu^* vs. Ce/Ce^* . Filled symbols = greywackes, unfilled symbols = pelites. The solid line in the inset encircles FA-samples, the dotted line encircles FF-samples.

disturb the provenance results. However, the analysed samples from the Eastern Andean Metamorphic Complex have no anomalous rutile or ilmenite concentrations. Furthermore, the sediments rich in titanite (CA-00-15, CA-00-23 and CA-00-42; Tab. 1) do not have anomalously high TiO_2 concentrations (Tab. 3). Ti/Zr , being dependent on the maturity of the sediments, have values of < 25 (Fig. 21). This is in a range common for sediments, that are dominated by continental sources. The combination with the provenance indicative ratio La/Sc provides a useful chemical tool. As plotted in the discrimination diagram of Bhatia & Crook (1986; Fig. 21), the values for Ti/Zr are too high, and the La/Sc values too low, to indicate a passive margin setting for the source rocks (Fig. 21). They rather indicate a main derivation from sources with an active continental margin or a continental island arc origin. Active continental margins are described by Bhatia & Crook (1986) as continental margins of Andean type or strike-slip continental margins. Of the samples from the southern Chilean archipelago, the sediments from the southern part have higher Ti/Zr and slightly lower La/Sc than those from the northern part (Fig. 21).

Ti/Nb can give some indications of the provenance for sedimentary rocks (*e.g.*, Bonjour & Dabard, 1991; Jenchen, 2001; see also the opposite view of *e.g.*, Condie *et al.*,

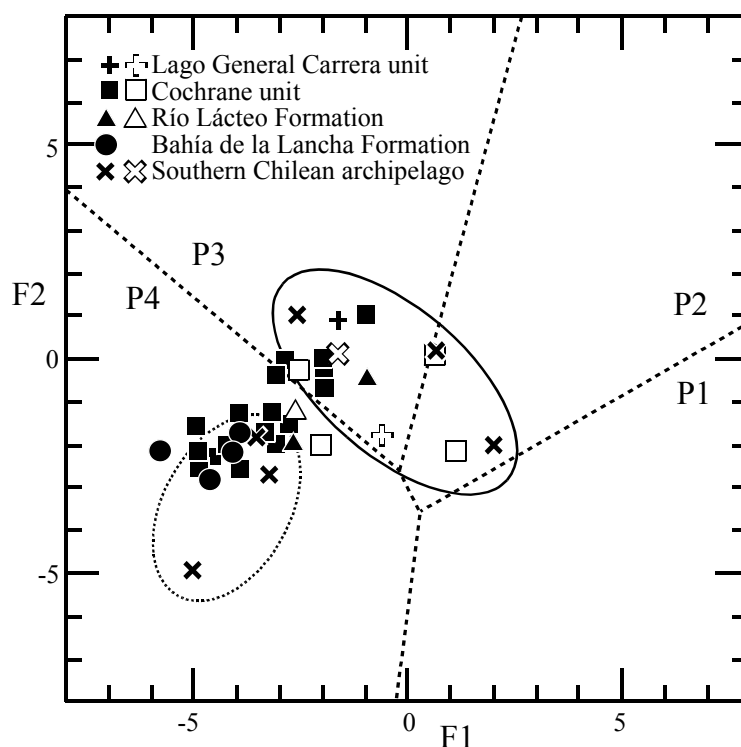


Fig. 20. Discrimination scheme for major elements. P1 = primary mafic sources, P2 = primary intermediate mafic - felsic sources, P3 = primary felsic sources, P4 = recycled sources, filled symbols = greywackes, unfilled symbols = pelites. The solid line encircles FA-samples, the dotted line encircles FF-samples. Diagram after Roser & Korsch (1988).

1995). The highly incompatible Nb is considered immobile, as well as the moderately incompatible Ti, and it often appears in the same heavy minerals as Ti (Bonjour & Dabard, 1991). Due to the higher incompatibility of Nb, Ti/Nb tend to decrease with an increasing amount of felsic components and textural maturity. The low Ti/Nb range of *ca.* 300-500

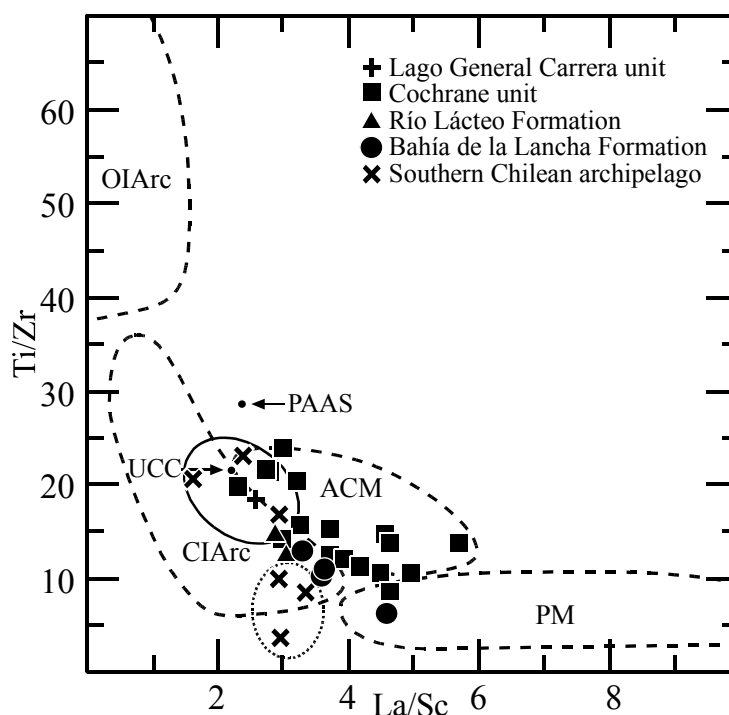


Fig. 21. La/Sc vs. Ti/Zr with discriminating fields for greywackes after Bhatia & Crook (1986). Abbreviations and symbols as in Figure 18. The solid line encircles FA-samples, the dotted line encircles FF-samples.

(Tab. 4) for the studied sediments indicates a dominance of felsic source rocks. For this ratio, no separation can be made between the southern and the northern sampling area of the southern Chilean archipelago (Tab. 4). The narrow range emphasises the chemical homogeneity across the sampling areas (*cf.* Jenchen, 2001).

The most commonly used provenance discrimination schemes for trace elements (Bhatia & Crook, 1986; Floyd & Leveridge, 1987; McLennan *et al.*, 1993) discriminate felsic active margin source rocks from passive margin rocks partly based on the Zr or Hf concentrations in the sediments, since the zircon content increases with increasing maturity of the sediments and recycling. Sand sized sediments contain more zircons, *i. e.*, more Zr and Hf, than finer grained sediments. They usually have higher incompatible *vs.* compatible element ratios than accompanying mudstones, which often tend to average larger sampling areas. Hence, care must be employed when comparing sediment samples of different grain sizes. Furthermore, erosional debris can be transported across tectonic margins with their inherited petrographic and chemical signatures still preserved (McLennan *et al.*, 1990; Potter, 1994). Thus, although being an effective discriminative method in relation to the analytical effort needed (von Eynatten *et al.*, 2003), provenance analysis involving the whole-rock major and trace element composition of sediments needs to be combined with other analytical results to be convincing. Furthermore, interpretations need to be done with consideration of the regional geology.

4.2. Sm-Nd and Rb-Sr isotopes

4.2.1. Sm-Nd and Rb-Sr isotopes: methods

For 22 greywacke samples, which also were analysed for their whole-rock major and trace elements, as well as one greywacke and one pelite with their compositions presented in Faúndez *et al.* (2002), Rb-Sr and Sm-Nd isotopes were measured at the Zentrallaboratorium für Geochronologie, Münster, and the standard methods for this laboratory were used. 100 mg powder of each sample were spiked with a mixed $^{87}\text{Rb}/^{84}\text{Sr}$ and $^{150}\text{Nd}/^{149}\text{Sm}$ tracer. The dissolution procedure included a first step with HF in Teflon® bombs at 175 °C for 2 days and a second step with HClO_4 to ensure complete dissolution of all minerals, including zircon. Rb, Sr, Sm and Nd were separated on cation exchange columns with HCl solutions. Rb measurements were performed on a single collector thermal ion mass spectrometer (Teledyn NBS style 12-inch MS), and Sm concentrations and Sr and Nd isotopes were measured on a VG Sector 54 mass spectrometer (MS-TIMS). Normalizations were made to $^{86}\text{Sr}/^{88}\text{Sr} = 0.1194$ (Steiger & Jäger, 1977) and $^{146}\text{Nd}/^{144}\text{Nd} = 0.7219$ (O’Nions *et al.*, 1977).

The mean laboratory $^{87}\text{Sr}/^{86}\text{Sr}$ value for the NBS 987 standard was 0.710294 ± 0.000014 (2σ , $n = 40$) during the measuring period. Laboratory Rb and Sr blanks of < 30 pg and < 150 pg, respectively, are negligible for the samples discussed here. $\text{Sr}_{\text{sample}}/\text{Sr}_{\text{blank}}$ ratios were always $> 1,000,000$. For the calculations, the following values were used: $\lambda = 1.42 \cdot 10^{-11} \text{a}^{-1}$ (Steiger & Jäger, 1977), $^{87}\text{Rb}/^{86}\text{Sr}_{\text{UR}} = 0.0827$ and $^{87}\text{Sr}/^{86}\text{Sr}_{\text{UR}} = 0.7045$ (Shaw & Wasserburg, 1982).

The mean laboratory $^{143}\text{Nd}/^{144}\text{Nd}$ value for La Jolla standard was 0.511860 ± 0.000011 (2σ , $n = 50$) during the measuring period. Laboratory Sm and Nd blanks of < 200 pg are not considered to affect the calculations. $\text{Nd}_{\text{sample}}/\text{Nd}_{\text{blank}}$ ratios were always $> 10,000$. The model of Goldstein *et al.* (1984), with $\lambda = 6.54 \cdot 10^{-12} \text{a}^{-1}$, $^{143}\text{Nd}/^{144}\text{Nd}_{\text{DM, today}} = 0.51315$,

$^{147}\text{Sm}/^{144}\text{Nd}_{\text{DM, today}} = 0.217$, $^{143}\text{Nd}/^{144}\text{Nd}_{\text{CHUR, today}} = 0.512638$ and $^{147}\text{Sm}/^{144}\text{Nd}_{\text{CHUR, today}} = 0.1967$, was used.

4.2.2. Sm-Nd isotopes: results and implications

The sediment samples analysed for their Sm-Nd isotope systematics have $^{147}\text{Sm}/^{144}\text{Nd}$ between 0.106 and 0.127 and $^{143}\text{Nd}/^{144}\text{Nd}$ of 0.5120-0.5124 (Tab. 5). Initial $^{143}\text{Nd}/^{144}\text{Nd}$ values range from 0.5118 to 0.5121 ($T = 280\text{-}350$ Ma). To allow for different depositional ages in the sedimentary basement, the depositional ages were approximated to 280-350 Ma (Tab. 5). This is based on U-Pb ages and chemical differences (see Section 1.3. above and 4.3. & 5.1. below) of sediments in different geographical areas.

McLennan *et al.* (1989) noticed that Nd isotope compositions can vary with grain size due to the concentration of components from different sources during transport and sorting. This can result in differences in isotopic signatures for sediments of different grain size, reflecting differences in the concentration of mafic and felsic source components. The sandstones of the studied geological units have whole-rock REE patterns parallel to the pelites, and the sandstones and pelites have similar Sm/Nd ratios (Fig. 19, Tab. 4), which is interpreted to be due to the dilution with quartz in the greywackes (*cf.* McLennan *et al.*, 1990). Hence, the Sm-Nd isotope systematics of the sandstones in the whole-rock isotope study should be representative also for the pelites.

Due to the higher incompatibility of Nd compared to Sm and the decay of ^{147}Sm to ^{143}Nd , mafic mantle rocks will evolve towards higher $^{143}\text{Nd}/^{144}\text{Nd}$ faster than felsic crustal rocks. The comparison of $^{143}\text{Nd}/^{144}\text{Nd}$ of a measured sample to $^{143}\text{Nd}/^{144}\text{Nd}$ of chondrites (CHUR, chondritic uniform reservoir), taken as an estimate of the bulk earth composition, makes it possible to compare Nd-isotope data from different laboratories that use different mass fractionation corrections. The value is often expressed as ϵ_{Nd} , which can be defined as

$$\epsilon_{\text{Nd}} = \left(\frac{^{143}\text{Nd}/^{144}\text{Nd}_{\text{sample}} - ^{143}\text{Nd}/^{144}\text{Nd}_{\text{CHUR}}}{^{143}\text{Nd}/^{144}\text{Nd}_{\text{CHUR}}} \right) \cdot 10^4. \quad [1]$$

Thus $\epsilon_{\text{CHUR}} \equiv 0$. With time the depleted mantle evolves towards more positive values, whereas material that separates from the depleted mantle to become a part of the crust will evolve from the ϵ_{Nd} value of the depleted mantle towards lower and negative ϵ_{Nd} . The calculation of $\epsilon_{\text{Nd}}(T)$, where T is the depositional age of a given sediment and $^{143}\text{Nd}/^{144}\text{Nd}(T)$ are used in the calculation, can provide information about the nature of the source rocks. Sediments with their isotopic signature dominated by components from old crustal rocks tend to have negative ϵ -values, whereas components from juvenile mantle rocks lead to an increase in the ϵ -values. For the analysed samples, $\epsilon_{\text{Nd}}(T)$ is negative (-8 to -2; Tab. 5, Fig. 22). The values are in agreement with the felsic signature of the samples based on the trace element composition. The highest value (-2.3) is from the sample of the Lago General Carrera unit (CA-00-03) and the three lowest ones are from the Bahía de la Lancha Formation (-7.5 to -6.7; Tab. 5). The values are common for both passive and active margin greywackes (McLennan & Hemming, 1992). For active margin sediments, this can be explained by mixing of an important component of old continental sources, and a smaller influence from younger mantle derived sources (*cf.* McLennan & Hemming, 1992). The diagram of $\epsilon_{\text{Nd}}(T)$ vs. time (Fig. 22) shows the relationship of a possible influence of both old continental crust and more juvenile material in the isotopic signature of the sediments.

One-stage Nd model ages (T_{DM}) can give estimates of the mean crustal residence time

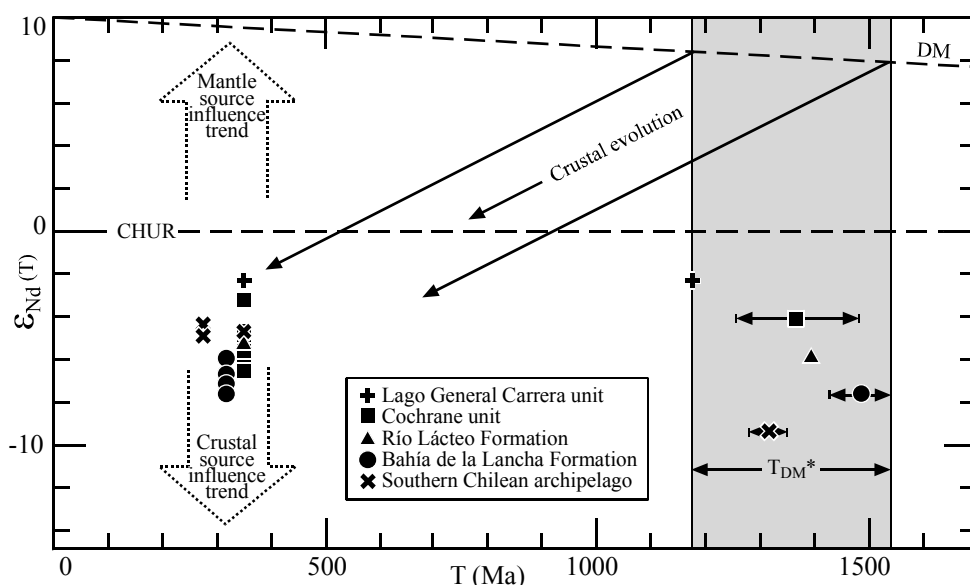


Fig. 22. Time vs. $\epsilon_{Nd}(T)$ as indicator of source rock type. Dotted arrows show the effect of syndepositional mixing of old crustal and juvenile mantle rocks. CHUR = Chondritic uniform reservoir, DM = depleted mantle.

of the sedimentary source rocks, assuming a depleted mantle source (DePaolo, 1981). However, with respect to the $^{147}\text{Sm}/^{144}\text{Nd}$ evolution of the crust, Frost & Winston (1987) and DePaolo *et al.* (1991) suggested a revision of the model age calculation to allow for disturbance of the isotope signature at a post-crustal formation stage. By the calculation of such two-stage model ages (T_{DM}^*) for sediments, the isotopic composition of the sedimentary constituents is assumed to have followed the estimated crustal evolution path from the time when the sedimentary source material became incorporated into the crust to the time when deposition took place (*cf.* Fig. 22). Syn-depositional isotopic fractionation makes it possible for the isotopic signature of the sediment to deviate from the estimated crustal evolution after the deposition. Nd model ages have been calculated here for comparative purposes both in the conventional way (Nd T_{DM}), and with the considerations made by Frost & Winston (1987) and DePaolo *et al.* (1991; Nd T_{DM}^*).

The youngest Nd T_{DM}^* (1177 Ma) is the one from the Lago General Carrera unit and the oldest ones are from the Bahía de la Lancha Formation (1505 and 1533 Ma; Tab. 5). Overall, Nd T_{DM}^* are in the range 1170-1540 Ma, which is a difference of up to *ca.* 200 Ma from corresponding (one-stage) Nd T_{DM} (Tab. 5). This difference in Nd T_{DM} and Nd T_{DM}^* indicates that minor post-crustal formation fractionation of Sm and Nd may have occurred, probably at a near syn-depositional stage. This can be expected for sediments, due to processes such as weathering and diagenesis. Furthermore, it must be kept in mind that whole-rock Nd model ages for sediments indicate the *mean* crust formation age of the source components. Thus, with the Nd T_{DM}^* range of 1170-1540 Ma the oldest crustal components in the sediments must have even longer crustal residence times.

4.2.3. Rb-Sr isotopes: results and implications

The sediment samples analysed for their Sr isotopes have $^{87}\text{Rb}/^{86}\text{Sr}$ between 1.00 and 5.41 and $^{87}\text{Sr}/^{86}\text{Sr}$ of 0.713-0.735 (Tab. 6). Similar to whole-rock Nd isotopes signatures of sediments, the Sr isotopes of sediments can be used to obtain information about the source rocks. Rb is more incompatible than Sr, which leads to a faster accumulation of the daughter isotope ^{87}Sr

in the crust compared to the mantle. Thus, $^{87}\text{Sr}/^{86}\text{Sr}$ will be higher for crustal rocks than for mantle rocks (*cf.* Fig. 23). However, the Sr isotope signature is the result of a number of pre- and post-depositional processes, which can have modified the original Sr isotope signature of sediments.

The chemical breakdown during weathering of unstable Rb- and Sr-rich minerals such as feldspars and biotite, and the formation of secondary clay minerals leads to a net decrease both in Rb and Sr. This decrease results in an increase in the Rb/Sr of the residue (Stille & Shields, 1997). Due to the decay of ^{87}Rb to ^{87}Sr , the $^{87}\text{Sr}/^{86}\text{Sr}$ of Rb rich secondary clay minerals increases faster than for sedimentary constituent containing less Rb. As a result of the different mineral constituents of weathering products and the fine grained suspended load in rivers, the $^{87}\text{Sr}/^{86}\text{Sr}$ ratios can vary with grain size (Aubert *et al.*, 2001; Douglas *et al.*, 1995). Interaction with fluid phases can have an effect on the Sr isotope signature both by *in-situ* weathering, transport and deposition, and by diagenetic and metamorphic processes.

The sea-water residence times for Rb and Sr are longer than the ocean water mixing time (McLennan, 1989). Due to this, oceanic water tend to have a homogeneous Sr isotope signature. This isotopic signature can lead to the modification of the Sr isotope signatures of marine sediments by the interaction with sea-water. Further modifications by mineral phase changes take place during diagenesis. Sr commonly replaces Ca in mineral structures. Thus, in open systems the formation of secondary carbonates can increase the Sr concentration in the sediments and affect the Sr isotope signature. This will generally result in lower $^{87}\text{Sr}/^{86}\text{Sr}$ ratios.

It has been assumed that metamorphism can reset the radiogenic Rb-Sr “clock”. This has been the base for the earlier common whole-rock Rb-Sr dating of metamorphic rocks. However, in a closed system only the constituent minerals will change their Rb-Sr systematics, whereas the isotopic signature remains constant in the total system. Thus, the

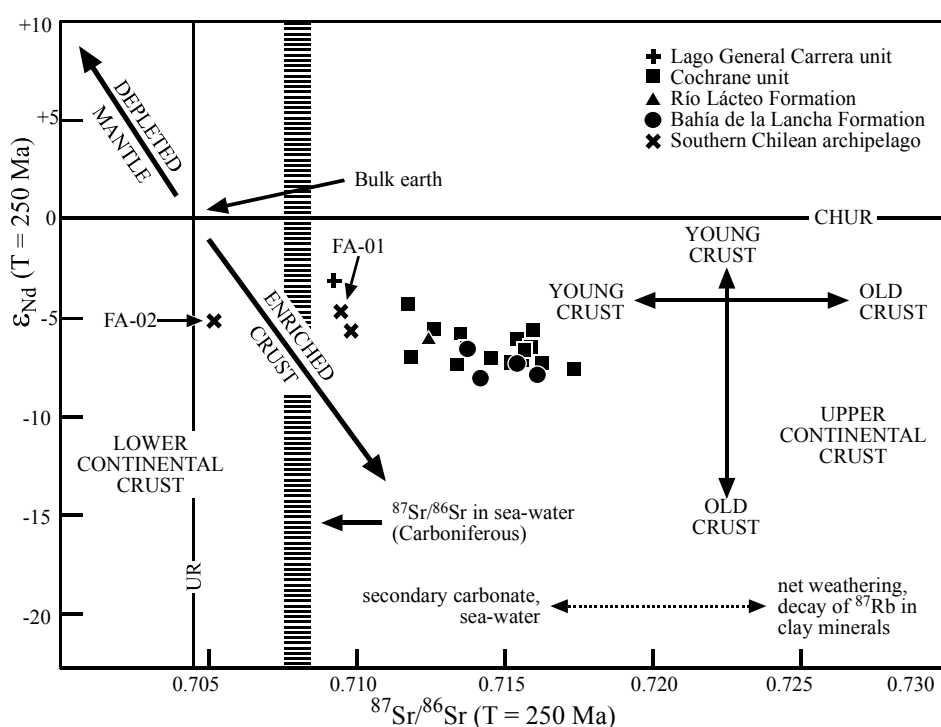


Fig. 23. $^{87}\text{Sr}/^{86}\text{Sr}_{\text{today}}$ vs. $\epsilon_{\text{Nd}}(T = 250 \text{ Ma})$. Sea-water composition from Burke *et al.* (1982). CHUR = Chondritic uniform reservoir, UR = uniform reservoir.

whole-rock Rb-Sr isotopic signature of sediments will be a mixture of the isotope signature of minerals of the source rocks and the isotopic signature of secondary minerals, *e. g.*, illite. A summary of the affecting factors is given in Figure 23.

In Figure 23, $^{87}\text{Sr}/^{86}\text{Sr}(\text{T})$ is plotted against $\epsilon_{\text{Nd}}(\text{T})$, where T equals 250 Ma. This age most likely post-dates the deposition of the studied sediments and approximates the metamorphic age of a majority of the sediments (*cf.* Fig. 3). The high $^{87}\text{Sr}/^{86}\text{Sr}$ (*i. e.*, high ϵ_{Sr}) and negative ϵ_{Nd} are indicative of a continental origin (Fig. 23). The sediments from the Lago General Carrera unit and the southern Chilean archipelago have lower $^{87}\text{Sr}/^{86}\text{Sr}(\text{T})$ than the rest of the sample population (Fig. 23). Partly, this is most likely an effect of the processes depicted above, but it also indicates that these samples might be dominated by material from more juvenile source rocks than the others. Particularly, FA-02 from the southern sampling area of the southern Chilean archipelago is different from the others (Fig. 23).

4.3. Whole-rock chemistry: discussion

To deduce the provenance from whole-rock chemistry of sediments, also pre-, syn- and post-depositional chemical changes, that are not related to the source rocks, must be considered. The studied sediments show obvious signs of post-depositional petrographic alterations (see Section 3.4.). However, they show only moderate chemical alteration effects, as indicated by the whole-rock element compositions (Fig. 16).

A general dominance of felsic source rocks is indicated by both the major and the minor elements, with high ratios of incompatible *vs.* compatible elements (*e. g.*, Fig. 18). The similarity to the estimated trace element compositions of the UCC and PAAS points to a large influence of continental sources. Additionally, the Nd- and Sr-isotope signatures, with low and high $\epsilon(\text{T})$, respectively, are typical for crustal, felsic rocks as the main sources. The whole-rock Nd T_{DM}^* , with estimates of crustal residence times between 1170 and 1540 Ma, indicate that a major part of the detritus contributing to the isotopic signature might have undergone recycling in the crust. Furthermore, the major element indications of a large dominance of recycled material for most sediments (*cf.* Fig. 20) is in agreement with the petrographic features that indicate a large influence from recycled, metasedimentary and metamorphic sources. Also the high Zr and Hf contents, reflecting the zircon contents, point to well recycled sediments.

The Lago General Carrera unit greywacke differs slightly from the other greywackes. The CIA values are among the lowest, the Eu-anomaly among the highest, and its isotopic signatures indicate slightly younger source rocks, than for the adjacent Cochrane unit, with a larger part of the signature originating from mantle derived mafic sources. Due to the absence of further greywacke analyses from this unit, this difference may be purely accidental.

The petrographic differences between the Cochrane unit and the Bahía de la Lancha Formation (see Section 3.4.) are not obvious in the whole-rock element compositions. However, the low $\epsilon_{\text{Nd}}(\text{T})$ for the Bahía de la Lancha Formation (Fig. 22) is in agreement with the higher content of recycled detrital quartz and tourmaline grains in this Formation compared to the Cochrane unit.

Most of the chemical provenance proxies show differences between the two study areas in the southern Chilean archipelago. However, this is not the case for the ratios La/Sc, Th/Sc and Th/Co (Fig. 18). Although the chemical similarity implies a dominance of felsic

source rocks for both areas, the differences in other proxies show that the sources are at least partly different. The isotope data indicate that the sediments from the northern sampling area are slightly more dominated by crustal rocks than those from the southern area (Fig. 22 & 23). Furthermore, the whole-rock Nd model ages for the sediments of the southern area (FA-) are somewhat lower than for FF-01 from the northern area. In accordance with this, the high Zr/Sc and low Ti/Zr (Fig. 21) indicates that the sediments from the northern area are more recycled than those from the southern area.

The general dominance of felsic, crustal source rocks and recycling of the sediments are typical for sediments deposited adjacent to continental margins. However, the provenance indicative element ratios cannot be used unambiguously to discriminate an active from a passive margin origin for the total sample population. The element ratios give general indications of an active margin origin, but ratios for individual samples are similar to those typical of sediments in passive margin settings. The isotopic signatures indicate a dominance of old continental felsic source rocks with a possible minor contribution from younger mantle derived mafic rocks. Thus, generally an active margin setting would seem plausible.

As stated above (Sections 3.4. and 4.1.3.), sedimentary debris can be transported across tectonic margins with their inherited signal preserved (McLennan *et al.*, 1990; Potter, 1994). Thus, in a narrow sense, the presented results are not proof of the tectonic setting of the depositional basin, but rather an indication of the tectonic setting of the source rocks. Two different options in the interpretation of the Eastern Andean Metamorphic Complex, the Río Lácteo and Bahía de la Lancha formations are possible, both of which are consistent with the petrography of the sediments. (1) The sediments could have been deposited in a basin adjacent to an active margin, but with its main contribution deriving from more mature sources. This would explain the Sr and Nd isotopic signatures, including the old whole-rock Nd model ages, as well as the chemical active margin indications. (2) Alternatively, most of the sediments were deposited in a sedimentary basin at a passive margin with its chemical and isotopic signatures inherited from source rocks formed at an active margin. In this case, the erosional debris was transported across a tectonic margin.

The probably youngest sediments, from the southern sampling area of the southern Chilean archipelago, (see Section 1.3. and Fig. 3) are, as mentioned above, chemically different from at least the northern sampling area of the southern Chilean archipelago. The chemical parameters stressed in this study show that these sediments are among the least felsic and least recycled. Furthermore, the whole-rock Nd $T_{DM}^*(T)$ are among the youngest. The greywacke of the Lago General Carrera unit is in many cases similar, however, due to the small sample population (one greywacke and one pelite) this may be a coincidence.

Based on the regional geology, petrography and whole-rock chemistry, it is suggested here that (*maybe* the Lago General Carrera unit,) the Cochrane unit (or at least parts of it; see Section 1.3.), the Eastern Andean Metamorphic Complex of the northern sampling area in the southern Chilean archipelago, and the two Argentinean formations were deposited at a passive margin. This was followed by development of a subduction zone and the deposition of the Eastern Andean Metamorphic Complex that crops out in the southern sampling area of the southern Chilean archipelago.

A passive margin setting for the main part of the studied sediments would not only account for the Sr and Nd isotopic signatures and the chemical felsic signatures. It would also

account for the regional geological features, including the absence of coeval magmatism; the oldest dated plutonism being *ca.* 310 m. y. old (R. de la Cruz, pers. comm.; Fig. 3). Limestones in the northern part of the Lago General Carrera unit are interpreted to be deposited in a platform environment (Hasegawa *et al.*, 1971; Hervé *et al.*, 2000). On Peninsula Florida at Lago O'Higgins (Fig. 1b), continental pillow basalts are interbedded in the sedimentary pile of the Cochrane unit (Hervé *et al.*, 1999). Hervé *et al.* (1999) suggested a transform fault zone as the setting of the subaqueous volcanism. Thus, at the time of deposition, at least a thin continental crust was present in the area. An Early Cambrian granodiorite from a borehole on Tierra del Fuego (Fig. 2; Söllner *et al.*, 2000; Pankhurst *et al.*, 2003b) probably formed part of this continental crust. Furthermore, the first indications of subduction are of Late Carboniferous age.

It is important to note that whole-rock chemical provenance analysis does not give any time constraints. Input from active margin type magmatic source rocks does not necessarily indicate magmatism coeval with sedimentation. The source rocks may have been produced during older active margin stages, and later included into a tectonically inactive area. Thus, sediments can have chemical signatures inherited from an active tectonic margin, although no such margin existed at the time of sedimentary deposition. The Nd isotopic signature gives indications of mixing between old crustal rocks and younger mantle rocks. However, as stated above, the younger rocks do not have to be formed coeval with the sedimentary deposition.

Deposition for the major part of the studied sediments at a passive margin would imply post-depositional incorporation into the backstop of the Late Palaeozoic to Early Mesozoic sedimentary wedge at the southwestern Pacific margin of Gondwana (present coordinates). However, it is important to be aware that the chemical differences observed, particularly between the two sampling areas in the southern Chilean archipelago, could be due to different weathering and diagenetic conditions. Therefore, further analysis was needed to be able to test the above depicted hypothesis.

5. Zircon U-Pb ages and Hf isotopes

Studies on the variability of detrital zircon can give important insights into the pre-depositional history of sediments. The study of U-Pb ages, Hf isotope compositions, zircon zoning and trace element chemistry can all aid in provenance studies (*e. g.*, Williams & Claesson, 1987; Stevenson & Patchett, 1990; Ireland, 1992; Geslin *et al.*, 1999; Rubatto & Gebauer, 2000; Belousova *et al.*, 2002). The value of studies of individual detrital zircons is that they give information about their source (*e. g.*, age and chemical composition). This is different from whole-rock chemistry data, which is the product of a mixture of detritus from several sources. In this section, U-Pb ages of detrital zircons and the Hf isotope composition of selected dated zircon grains are used as provenance indicators of the sediments of the Eastern Andean Metamorphic Complex and the Bahía de la Lancha Formation. Additionally, the zircon zoning and trace element chemistry have been considered in the interpretations.

5.1. U-Pb ages

Sensitive high-resolution ion micro-probe (SHRIMP) U-Pb dating allows for the dating of individual growth phases in complex zircons. Several regions with different crystallisation ages can be dated. This makes it possible to track the pre-depositional history of single zircons back in time to their original source with age information about single growth stages (*e. g.*, Black *et al.*, 1986; Collins & Williams, 1995). For provenance studies, it is common practice to date the youngest pre-depositional growth phase of a large number of zircons to get an indication of the last protolith in which the zircons grew (*e. g.*, Froude *et al.*, 1983; Williams & Claesson, 1987; Pell *et al.*, 1997). The age spectra of such data are often typical for specific source areas. Thus, by comparison of ages of detrital zircons with ages of potential source rocks, the sedimentary sources in which the zircons were deposited can be identified (*e. g.*, Ireland, 1992; Pell *et al.*, 1997; Geslin *et al.*, 1999). Here, the SHRIMP U-Pb technique was used to track the sources of the studied south Patagonian sediments. Furthermore, the youngest dated grain in each zircon separate gives a maximum depositional age of the sediment. Thus, depositional ages for the Chilean Eastern Andean Metamorphic Complex and the Argentinean Bahía de la Lancha Formation have been improved by the U-Pb dating (see Section 1.3.).

5.1.1. U-Pb ages: methods

Zircons from five sediments were dated by the U-Th-Pb method at the Research School of Earth Sciences, Australian National University, Canberra, Australia. After sieving, the heavy mineral fraction of the < 250 μm fraction was separated using diiodinemethane. A random selection of the total zircon fraction was mounted in epoxy together with the FC1 (see Paces & Miller, 1993) and SL13 (see Claoué-Long *et al.*, 1995) reference zircons and polished to expose the centres of the grains. To minimise bias in the age spectra results, morphology and size were ignored when selecting grains for analysis. Zircon regions suitable for analysis were identified from cathodoluminescence images.

From each sample 60-70 single detrital zircons were analysed following the method described in Williams (1998, and references therein). U-Th-Pb analyses were made using the sensitive high-resolution ion micro-probes SHRIMP-RG and SHRIMP I at the Research School of Earth Sciences, Canberra. The rims of the grains were preferentially analysed. The

spot size was < 30 μm . The isotope data consist of 4 scans through the mass spectrum. They were reduced using a procedure similar to that described by Williams (1998, and references therein) using the SQUID/Ex Macro of Ludwig (2001a). The Pb/U ratios were normalized relative to $^{206}\text{Pb}/^{238}\text{U} = 0.1859$ of the FC1 reference zircons, equivalent to an age of 1099 Ma (see Paces & Miller, 1993). For zircons older than approximately 800 Ma, $^{207}\text{Pb}/^{206}\text{Pb}$ ratios were used for age calculation. Due to the small variability of $^{207}\text{Pb}/^{206}\text{Pb}$ between Phanerozoic ages, $^{206}\text{Pb}/^{238}\text{U}$ ages were generally obtained for younger zircons. The $^{207}\text{Pb}/^{206}\text{Pb}$ ages were corrected for common Pb based on ^{204}Pb , whereas $^{206}\text{Pb}/^{238}\text{U}$ ages were corrected based on ^{207}Pb as outlined in Williams (1998). Age calculations and statistical treatment were made using Isoplot/Ex (Ludwig, 2001b), where ages were calculated using $\lambda(^{238}\text{U}) = 1.551 \cdot 10^{-10} \text{a}^{-1}$ and $\lambda(^{235}\text{U}) = 9.849 \cdot 10^{-10} \text{a}^{-1}$ (Steiger & Jäger, 1977).

5.1.2. U-Pb ages: results

The zircon U-Pb isotope results of three sandstone samples from the Cochrane unit of the Eastern Andean Metamorphic Complex (CA-00-15, CA-00-23, CA-00-30), one of the Bahía de la Lancha Formation (CA-01-06) and one from the part of the Eastern Andean Metamorphic Complex that is located in the southern Chilean archipelago (FA-01) are presented in Tables 7-11. The results are graphically presented in the Tera-Wasserburg plots and probability curves in Figure 24 and 25. In these Figures, analysed zircon regions with multiple growth phases have been discarded (*cf.* Tab. 7-11). Furthermore, some of the grains with large uncertainties have been ignored in the following interpretation (see Fig. 24).

Cathodoluminescence images of the 300 analysed zircon spots interpreted to have only one single growth phase reveal that 186 (62 %) have oscillatory zoning, or, in some cases, sector zoning (*cf.* Fig. 26a-b). These zoning patterns are interpreted to be of magmatic origin (*cf.* Hanchar & Miller, 1993; Rubatto & Gebauer, 2000). One hundred fourteen analysed spots (38 %) are homogeneous or have rounded concentric or irregular zoning (*cf.* Fig. 26c-e). These growth zones are interpreted to be of metamorphic origin (*cf.* Hanchar & Miller, 1993; Rubatto & Gebauer, 2000).

In the five analysed zircon separates, there is an overall predominance of zircons with concordant ages at 400-700 Ma, with additional peaks at 1000-1500 Ma and sparse zircons of Archaean age (Fig. 27a). The comparison of age spectra for zircons with a presumed metamorphic and a presumed magmatic origin points to large similarities in age spectra, especially for grains with U-Pb ages above 700 Ma. However, among the younger zircons some differences occur. The spectra for the metamorphically and the magmatically zoned zircons show age populations at similar ages, but metamorphically zoned zircons have a larger dominance in the age interval 500-700 Ma. Only one of the dated zircon from FA-01 has an age between 500 and 700 Ma. This zircon is interpreted to be of metamorphic origin (Fig. 28). Overall, magmatically zoned zircons have a dominance of zircons < 500 Ma (Fig. 28). In the latter age interval, particularly the age peak at 421 Ma (Fig. 27) is totally dominated by magmatic zircons. The peaks at *ca.* 300 Ma originate from zircons of sample FA-01 alone (Fig. 27 & 28).

The zircons typically contain 10-1000 ppm Th and 50-1000 ppm U, and they mostly have Th/U ratios of 0.1-1.0. These ratios are common for both zircons of igneous and metamorphic origin (Rubatto & Gebauer, 2000; Rubatto, 2002; Belousova *et al.*, 2002). These

Table 7. SHRIMP U-Pb zircon results for sample CA-00-15

Grain #/ spot ~c	Measured ratios						Radiogenic ratios [‡]						Age (Ma)		Disc.		
	U (ppm)	Th (ppm)	Th/U	Pb* (ppm)	²⁰⁴ Pb/ ²⁰⁶ Pb	f ₂₀₆ [†] (%)	²⁰⁶ Pb/ ²³⁸ U	²⁰⁷ Pb/ 1σ	²⁰⁷ Pb/ ²³⁸ U	1σ	²⁰⁶ Pb/ 1σ	²⁰⁶ Pb/ 1σ	²⁰⁷ Pb/ 1σ	(%)§			
01.1 #	812	279	0.34	45.7	0.000027	0.05	0.0655	0.0007				409	4				
02.1 ~	1436	24	0.02	170.4	0.000030	0.05	0.1380	0.0014	1.425	0.017	0.0749	0.0004	833	8	1065¶	11	28
03.1 ~	559	168	0.30	31.8	0.000087	0.15	0.0661	0.0008				412	5				
04.1 ~	321	156	0.49	72.9	0.000031	0.05	0.2640	0.0032	3.376	0.049	0.0927	0.0007	1510	16	1483¶	15	-2
05.1 #	720	83	0.12	46.1	0.000158	0.27	0.0743	0.0009				462	5				
06.1 #	402	82	0.20	25.3	<0.000001	<0.01	0.0733	0.0009				456	5				
07.1¶	446	318	0.71	48.3	0.000113	0.19	0.1259	0.0015	1.146	0.019	0.0660	0.0008	764¶	9	807	24	6
08.1 #	350	97	0.28	20.2	0.000099	0.17	0.0670	0.0008				418	5				
09.1 ~	854	7	0.01	151.5	0.000040	0.07	0.2065	0.0022	2.279	0.028	0.0800	0.0005	1210	12	1198¶	12	-1
10.1 #	576	142	0.25	34.1	0.000036	0.06	0.0688	0.0008				429	5				
11.1 ~	195	99	0.51	93.1	<0.000001	<0.01	0.5564	0.0064	15.861	0.196	0.2068	0.0009	2852	27	2880¶	7	1
12.1 ~	1351	194	0.14	234.3	0.000011	0.02	0.2018	0.0021	2.130	0.024	0.0765	0.0003	1185	11	1109¶	9	-6
13.1 #	610	130	0.21	34.6	0.000139	0.24	0.0659	0.0007				411	4				
14.1 #	402	64	0.16	73.8	0.000076	0.13	0.2135	0.0024	2.378	0.034	0.0808	0.0007	1247	13	1216¶	17	-2
15.1 #	244	107	0.44	14.2	0.000110	0.19	0.0675	0.0009				421	5				
16.1 ~	228	159	0.70	57.9	0.000038	0.06	0.2955	0.0034	4.390	0.060	0.1078	0.0008	1669	17	1762¶	13	6
17.1 ~	167	81	0.48	15.4	0.000004	0.01	0.1077	0.0021	0.910	0.024	0.0613	0.0011	659¶	12	651	37	-1
18.1 ~	185	13	0.07	29.8	0.000767	1.30	0.1852	0.0023	2.107	0.073	0.0825	0.0027	1095	13	1258¶	64	15
19.1 #	163	66	0.41	32.3	0.000094	0.16	0.2306	0.0029	2.681	0.052	0.0843	0.0012	1338	15	1300¶	29	-3
20.1 #	224	127	0.57	16.8	<0.000001	<0.01	0.0876	0.0011				541	7				
21.1 ~	629	50	0.08	113.2	0.000018	0.03	0.2095	0.0023	2.311	0.029	0.0800	0.0005	1226	12	1197	12	-2
22.1 #	440	174	0.40	25.8	0.000373	0.63	0.0676	0.0008				422	5				
23.1 ~	574	16	0.03	34.7	0.000125	0.21	0.0702	0.0008				437	5				
24.1 #	315	124	0.39	18.6	0.000168	0.28	0.0686	0.0009				428	5				
25.1 #	3106	604	0.19	180.6	0.000190	0.32	0.0675	0.0007				421	4				
26.1 #	148	54	0.36	8.8	0.000252	0.43	0.0693	0.0010				432	6				
27.1 ~	78	20	0.26	10.0	0.000213	0.36	0.1486	0.0023	1.460	0.041	0.0713	0.0017	893¶	13	965	48	8
28.1 #	475	257	0.54	25.4	0.000159	0.27	0.0622	0.0008				389	5				
29.1 ~c	208	69	0.33	45.3	<0.000001	<0.01	0.2532	0.0031	3.184	0.049	0.0912	0.0009	1455	16	1451¶	18	0
30.1 #	330	174	0.53	53.6	<0.000001	<0.01	0.1895	0.0022	2.048	0.031	0.0784	0.0008	1119	12	1156¶	20	3
31.1¶	152	130	0.86	26.7	0.000165	0.28	0.2046	0.0027	2.178	0.050	0.0772	0.0015	1200	15	1127¶	38	-6
31.2 ¹ ~c	81	83	1.03	14.6	0.000461	0.79	0.2113	0.0034	2.389	0.058	0.0820	0.0015	1236	21	1245¶	36	1
32.1¶	509	43	0.08	96.4	0.000032	0.05	0.2205	0.0024	2.555	0.032	0.0840	0.0005	1285	13	1294¶	12	1
33.1 ~	400	110	0.27	23.3	<0.000001	<0.01	0.0678	0.0008				423	5				
34.1 #	894	308	0.34	53.1	0.000063	0.11	0.0691	0.0008				431	5				
35.1 #	299	115	0.38	17.9	<0.000001	<0.01	0.0698	0.0009				435	5				
36.1 ~	218	88	0.40	13.2	0.000094	0.16	0.0703	0.0010				438	6				
37.1¶	151	77	0.51	26.9	0.000053	0.09	0.2064	0.0029	2.245	0.049	0.0789	0.0013	1210	15	1168¶	33	-3
38.1¶	509	56	0.11	34.3	<0.000001	<0.01	0.0784	0.0009				487	5				
39.1¶	714	226	0.32	44.5	0.000224	0.38	0.0723	0.0008				450	5				
40.1 ~	250	11	0.05	20.5	<0.000001	<0.01	0.0957	0.0012				589	7				
41.1¶	403	78	0.19	24.1	0.000012	0.02	0.0696	0.0008				434	5				
42.1 #	236	61	0.26	13.1	<0.000001	<0.01	0.0643	0.0008				402	5				
43.1 ~	141	85	0.60	10.6	0.000233	0.39	0.0875	0.0012				541	7				
44.1 #	938	131	0.14	54.5	0.000140	0.24	0.0674	0.0008				421	5				
45.1 ~c	202	54	0.27	11.2	<0.000001	<0.01	0.0648	0.0009				405	5				
46.1 #	339	115	0.34	17.3	<0.000001	<0.01	0.0595	0.0008				373	5				
46.2 ¹ #c	301	99	0.33	18.9	<0.000001	<0.01	0.0731	0.0011				455	7				
47.1 #c	310	102	0.33	17.9	0.000134	0.23	0.0673	0.0008				420	5				
48.1 #	370	240	0.65	60.4	<0.000001	<0.01	0.1902	0.0021	1.988	0.028	0.0758	0.0006	1122	12	1090¶	17	-3
49.1 #	286	191	0.67	13.7	0.000080	0.13	0.0556	0.0007				349	4				
50.1 #	208	49	0.24	14.2	0.000084	0.14	0.0795	0.0010				493	6				
51.1 #	523	107	0.20	105.7	<0.000001	<0.01	0.2352	0.0026	3.006	0.037	0.0927	0.0005	1361	14	1482¶	11	9
52.1¶	173	71	0.41	10.2	0.000287	0.49	0.0680	0.0010				424	6				
53.1 #	400	150	0.37	23.2	<0.000001	<0.01	0.0676	0.0008				422	5				
54.1¶	434	26	0.06	27.7	0.000043	0.07	0.0743	0.0009				462	5				
58.2¶ ¹	219	53	0.24	12.3	<0.000001	<0.01	0.0656	0.0009				409	6				
59.2 ¹ #	156	148	0.95	43.9	0.000142	0.22	0.3260	0.0044	5.009	0.097	0.1114	0.0015	1819	21	1823¶	25	0
60.2 ¹ #	610	368	0.60	33.3	0.000152	0.28	0.0633	0.0008				396	5				
61.1 ¹ ~	1060	378	0.36	80.6	0.000031	0.06	0.0885	0.0010				547	6				
62.1 ¹ ~	138	67	0.48	8.8	0.000066	0.12	0.0739	0.0012				459	7				
63.1 ¹ #c	98	119	1.21	16.9	<0.000001	<0.01	0.2006	0.0035	2.560	0.182	0.0926	0.0064	1179¶	19	1479	130	25
64.1 ¹ #	222	99	0.44	12.1	0.000809	1.50	0.0623	0.0012				390	7				
65.1 ¹ ~	118	52	0.44	21.8	<0.000001	<0.01	0.2171	0.0033	2.575	0.086	0.0860	0.0026	1267	18	1338¶	58	6
66.1 ¹ #	412	141	0.34	23.3	0.000068	0.12	0.0658	0.0009				411	5				
67.1 ¹ #c	731	218	0.30	42.2	0.000038	0.07	0.0671	0.0008				419	5				
68.1 ¹ ~	225	1	0.01	40.0	<0.000001	<0.01	0.2069	0.0027	2.381	0.049	0.0834	0.0013	1212	15	1280¶	31	6
69.1 ¹ #	609	236	0.39	33.7	<0.000001	<0.01	0.0645	0.0008				403	5				
70.1 ¹ #	1404	355	0.25	98.8	<0.000001	<0.01	0.0820	0.0009				508	6				
71.1 ¹ #	356	153	0.43	31.1	<0.000001	<0.01	0.1017	0.0013				624	8				

Pb* = radiogenic Pb. †f₂₀₆ = percentage of ²⁰⁶Pb that is common Pb. ‡Correction for common Pb made using the measured ²⁰⁴Pb/²⁰⁶Pb ratio.

§0 % denotes a concordant analysis. ¶More than one crystallization phase analysed - corresponding ages were not used for the statistics.

¶Preferred ages. # = Zoning interpreted to be of magmatic origin. ~ = Zoning & homogeneous areas estimated to be of metamorphic origin.

c = core / inner zoning. ¹Dated with SHRIMP I, all other points were dated with SHRIMP-RG.

Table 8. SHRIMP U-Pb zircon results for sample CA-00-23

Grain #/ spot	U ~c	Th (ppm)	Measured ratios				Radiogenic ratios [‡]				Age (Ma)				Disc.			
			Th/U	Pb* (ppm)	²⁰⁴ Pb/ ²⁰⁶ Pb	f ₂₀₆ [†] (%)	²⁰⁶ Pb/ ²³⁸ U	²⁰⁷ Pb/ 1σ	²⁰⁷ Pb/ ²³⁵ U	1σ	²⁰⁶ Pb/ 1σ	²⁰⁶ Pb/ ²³⁸ U	1σ	²⁰⁶ Pb/ 1σ		(%)§		
02.2 ¹	~	218	51	0.24	25.6	<0.000001	<0.01	0.1363	0.0017	1.230	0.026	0.0654	0.0011	824 [¶]	10	789	34	-4
03.2 ¹	#c	313	196	0.62	25.8	0.000190	0.32	0.0956	0.0013					589	7			
04.2 ¹		283	111	0.39	24.8	<0.000001	<0.01	0.1019	0.0013					626	8			
05.2 ¹		413	48	0.12	28.4	<0.000001	<0.01	0.0800	0.0010					496	6			
06.2 ¹	~	424	324	0.76	32.1	<0.000001	<0.01	0.0880	0.0011					544	6			
08.2 ¹	#	652	336	0.52	35.4	0.000106	0.18	0.0632	0.0008					395	5			
25.1		200	97	0.49	55.1	0.000040	0.07	0.3200	0.0040	6.351	0.091	0.1440	0.0010	1790	20	2275 [¶]	12	27
26.1	~	216	60	0.28	13.3	0.000477	0.81	0.0708	0.0009					441	6			
27.1	#	496	296	0.60	33.9	0.000011	0.02	0.0796	0.0009					494	5			
28.1	#	83	69	0.83	14.4	0.000081	0.14	0.2018	0.0029	2.350	0.060	0.0844	0.0018	1185	15	1303 [¶]	42	10
29.1	~	1110	194	0.18	106.4	0.000033	0.06	0.1114	0.0012					681	7			
30.1		399	166	0.42	31.1	<0.000001	<0.01	0.0909	0.0011					561	6			
31.1	~	233	112	0.48	18.8	0.000346	0.58	0.0937	0.0013					577	7			
32.1	~	200	38	0.19	19.5	0.000092	0.16	0.1135	0.0015					693	9			
33.1	~	1228	77	0.06	177.1	0.000006	0.01	0.1678	0.0018	1.747	0.021	0.0755	0.0004	1000	10	1083 [¶]	11	8
34.1	#	1310	293	0.22	89.5	0.000028	0.05	0.0795	0.0008					493	5			
35.1	#	330	37	0.11	24.9	0.000775	1.31	0.0866	0.0013					536	8			
36.1		87	80	0.93	6.7	0.000226	0.38	0.0894	0.0014					552	8			
37.1	#	1004	436	0.43	159.4	0.000038	0.06	0.1846	0.0020	1.962	0.024	0.0771	0.0004	1092	11	1123 [¶]	11	3
38.1	#	274	157	0.57	19.2	0.000139	0.24	0.0811	0.0010					503	6			
39.1		1503	281	0.19	102.1	0.000014	0.02	0.0790	0.0008					490	5			
40.1	~	191	77	0.40	21.4	0.000239	0.40	0.1298	0.0029	1.184	0.042	0.0661	0.0018	787 [¶]	16	811	58	3
41.1	#	311	100	0.32	19.1	0.000132	0.22	0.0713	0.0009					444	5			
42.1		333	34	0.10	44.2	0.000061	0.10	0.1544	0.0021	1.574	0.047	0.0739	0.0020	926	12	1040 [¶]	54	12
43.1	~	186	136	0.73	16.1	0.000106	0.18	0.1006	0.0013					618	8			
44.1	~	124	88	0.71	10.1	<0.000001	<0.01	0.0951	0.0016					586	9			
45.1	~	204	104	0.51	15.2	0.000139	0.24	0.0865	0.0012					535	7			
46.1	#	128	50	0.39	14.6	0.000212	0.36	0.1316	0.0018					797	10			
47.1	~	556	2	<0.01	39.4	0.000030	0.05	0.0823	0.0009					510	5			
48.1	#	609	351	0.58	45.9	0.000063	0.11	0.0877	0.0010					542	6			
49.1	#	90	51	0.56	5.9	0.000436	0.74	0.0758	0.0012					471	7			
50.1	#	1316	610	0.46	69.3	0.000027	0.05	0.0612	0.0007					383	4			
51.1	#	490	241	0.49	31.6	<0.000001	<0.01	0.0751	0.0009					467	5			
52.1	~	186	40	0.22	78.5	0.000020	0.03	0.4916	0.0066	11.482	0.169	0.1694	0.0010	2577	28	2552 [¶]	10	-1
53.1	#	1406	850	0.61	173.7	0.000014	0.02	0.1439	0.0015	1.431	0.018	0.0721	0.0004	866 [¶]	9	990	13	14
54.1	~	210	55	0.26	16.0	0.000239	0.40	0.0883	0.0012					545	7			
55.1	~	288	201	0.70	20.5	0.000066	0.11	0.0829	0.0010					513	6			
56.1	#	268	93	0.35	77.0	<0.000001	<0.01	0.3348	0.0040	5.309	0.072	0.1150	0.0008	1862	19	1880 [¶]	12	1
57.1	~	615	320	0.52	45.2	0.000067	0.11	0.0854	0.0009					528	6			
58.1	~	210	42	0.20	15.5	<0.000001	<0.01	0.0860	0.0011					532	6			
59.1	#	492	160	0.32	67.8	0.000039	0.07	0.1604	0.0018	1.597	0.024	0.0722	0.0007	959 [¶]	10	992	20	3
60.1	~	424	65	0.15	66.4	0.000050	0.08	0.1824	0.0022	1.881	0.029	0.0748	0.0007	1080 [¶]	12	1063	20	-2
61.1	~	996	877	0.88	85.0	0.000025	0.04	0.0993	0.0011					610	6			
62.1	~	245	29	0.12	17.0	0.000102	0.17	0.0808	0.0010					501	6			
63.1	~	1214	550	0.45	164.8	<0.000001	<0.01	0.1580	0.0017	1.564	0.019	0.0718	0.0004	946 [¶]	9	979	11	4
64.1	#	227	144	0.63	39.6	<0.000001	<0.01	0.2027	0.0026	2.219	0.046	0.0794	0.0013	1190 [¶]	14	1182	32	-1
65.1	~	171	145	0.85	13.7	0.000096	0.16	0.0929	0.0014					573	9			
66.1	#	317	110	0.35	40.2	<0.000001	<0.01	0.1479	0.0020	1.543	0.031	0.0757	0.0011	889 [¶]	11	1086	30	22
67.1	~	139	71	0.52	9.7	<0.000001	<0.01	0.0815	0.0012					505	7			
68.1	#	437	168	0.39	30.4	<0.000001	<0.01	0.0810	0.0010					502	6			
69.1	#	378	135	0.36	22.3	<0.000001	<0.01	0.0686	0.0009					428	5			
70.1	~	183	459	2.51	25.5	<0.000001	<0.01	0.1619	0.0023	1.668	0.036	0.0747	0.0012	967 [¶]	13	1061	33	10
71.2 ¹	~	14	3	0.19	1.3	<0.000001	<0.01	0.1026	0.0032					629	19			
72.2 ¹	#	320	83	0.26	34.6	0.003265	5.52	0.1190	0.0027					725	15			
73.1	#	223	95	0.42	91.0	0.000043	0.07	0.4739	0.0055	11.921	0.157	0.1825	0.0011	2500	24	2675 [¶]	10	7
74.1	#c	348	115	0.33	46.4	0.000063	0.11	0.1551	0.0020	1.418	0.043	0.0663	0.0018	930 [¶]	11	815	57	-12
75.1		408	186	0.46	63.2	<0.000001	<0.01	0.1804	0.0021	1.919	0.029	0.0772	0.0007	1069	12	1126 [¶]	18	5
76.1	#c	262	275	1.05	20.6	0.000032	0.05	0.0913	0.0012					563	7			
77.1	#	865	94	0.11	46.4	0.000074	0.13	0.0624	0.0007					390	4			
78.1	~	39	21	0.54	5.6	0.000700	1.18	0.1650	0.0037	1.587	0.137	0.0697	0.0058	985 [¶]	20	920	172	-7
79.1	#	513	172	0.34	66.5	<0.000001	<0.01	0.1509	0.0018	1.536	0.025	0.0738	0.0008	906 [¶]	10	1037	21	14
80.1	#	387	187	0.48	22.3	0.000124	0.21	0.0670	0.0010					418	6			
81.1	#c	520	130	0.25	60.2	<0.000001	<0.01	0.1347	0.0018	1.347	0.028	0.0726	0.0012	815 [¶]	10	1001	32	23
82.1 ¹	#	379	173	0.45	25.9	0.000188	0.32	0.0792	0.0011					491	6			

Pb* = radiogenic Pb. †f₂₀₆ = percentage of ²⁰⁶Pb that is common Pb. ‡Correction for common Pb made using the measured ²⁰⁴Pb/²⁰⁶Pb ratio.
 §0 % denotes a concordant analysis. ||More than one crystallization phase analysed - corresponding ages have not been used for the statistics.
 ¶Preferred ages. # = Zoning interpreted to be of magmatic origin. ~ = Zoning & homogeneous areas estimated to be of metamorphic origin.
 c = core / inner zoning. ¹Dated with SHRIMP I, all other points were dated with SHRIMP-RG.

Table 9. SHRIMP U-Pb zircon results for sample CA-00-30

Grain #/ spot	U ~c (ppm)	Th (ppm)	Measured ratios				Radiogenic ratios‡						Age (Ma)					
			Th/U	Pb*	²⁰⁴ Pb/ ²⁰⁶ Pb	f_{206}^{\dagger} (%)	²⁰⁶ Pb/ ²³⁸ U	1σ	²⁰⁷ Pb/ ²³⁵ U	1σ	²⁰⁷ Pb/ ²⁰⁶ Pb	1σ	²⁰⁶ Pb/ ²³⁸ U	1σ	²⁰⁷ Pb/ ²⁰⁶ Pb	1σ	Disc.	
01.1	~	74	33	0.45	15.0	0.000279	0.47	0.2348	0.0036	2.872	0.089	0.0887	0.0024	1360	19	1398¶	51	3
02.1	#	814	489	0.60	124.6	<0.000001	<0.01	0.1782	0.0019	1.858	0.023	0.0756	0.0005	1057	10	1085¶	13	3
03.1	~	62	297	4.79	3.9	0.000493	0.83	0.0736	0.0012					458	7			
04.1	#	244	141	0.58	29.1	0.000057	0.10	0.1388	0.0017	1.310	0.023	0.0684	0.0009	838¶	10	882	26	5
05.1	~	420	109	0.26	37.5	0.000132	0.22	0.1036	0.0012					636	7			
06.1	~	1256	96	0.08	510.9	0.000008	0.01	0.4733	0.0050	11.004	0.119	0.1686	0.0004	2498	22	2544¶	4	2
07.1	#c	217	71	0.33	17.3	0.000186	0.31	0.0926	0.0012					571	7			
08.1	#	371	96	0.26	31.5	0.000153	0.26	0.0985	0.0012					606	7			
09.1	~c	200	58	0.29	22.6	0.000046	0.08	0.1315	0.0017	1.193	0.025	0.0658	0.0011	796¶	10	801	36	1
10.1	#	280	115	0.41	14.4	<0.000001	<0.01	0.0601	0.0008					376	5			
11.1	#	442	58	0.13	24.8	<0.000001	<0.01	0.0652	0.0008					407	5			
12.1	~	155	59	0.38	34.7	0.000073	0.12	0.2608	0.0034	3.435	0.063	0.0955	0.0012	1494	18	1538¶	24	3
13.1	~	439	98	0.22	33.5	0.000082	0.14	0.0888	0.0011					548	6			
14.1	~	123	25	0.20	18.1	0.000001	<0.01	0.1716	0.0023	1.766	0.040	0.0746	0.0013	1021¶	13	1059	36	4
15.1		565	4	0.01	40.5	<0.000001	<0.01	0.0835	0.0009					517	6			
16.1	#	251	91	0.36	14.2	0.000198	0.33	0.0657	0.0008					410	5			
17.1	#	234	42	0.18	18.8	0.000075	0.13	0.0930	0.0012					573	7			
18.1	#	293	115	0.39	17.4	0.000116	0.20	0.0689	0.0008					429	5			
19.1	#c	98	37	0.38	15.2	0.000267	0.45	0.1797	0.0032	1.775	0.060	0.0716	0.0021	1065¶	17	976	59	-8
20.1	~	108	47	0.43	6.0	0.002190	3.70	0.0621	0.0020					388	12			
21.1	#c	300	84	0.28	34.2	0.000050	0.08	0.1324	0.0019	1.333	0.030	0.0730	0.0012	802¶	11	1015	35	27
22.1	~	278	91	0.33	20.3	<0.000001	<0.01	0.0851	0.0016					527	10			
23.1	~	723	172	0.24	62.4	0.000036	0.06	0.1004	0.0011					617	7			
24.1	#	702	254	0.36	389.9	<0.000001	<0.01	0.6462	0.0070	27.155	0.301	0.3048	0.0006	3213	28	3495¶	3	9
25.1	#	900	360	0.40	63.8	0.000032	0.05	0.0825	0.0009					511	5			
26.1	~	612	268	0.44	98.0	<0.000001	<0.01	0.1864	0.0021	1.910	0.025	0.0743	0.0006	1102¶	11	1050	15	-5
27.1	~c	140	165	1.18	38.0	0.000019	0.03	0.3157	0.0044	4.865	0.089	0.1118	0.0013	1769	22	1828¶	21	3
28.1	#	250	69	0.28	39.3	0.000105	0.18	0.1828	0.0023	1.846	0.038	0.0733	0.0012	1082¶	13	1021	32	-6
29.1	~	113	108	0.96	17.2	0.000058	0.10	0.1781	0.0025	1.874	0.043	0.0763	0.0014	1056¶	14	1104	36	4
30.1	~	72	58	0.80	13.7	0.000089	0.15	0.2207	0.0035	2.737	0.075	0.0900	0.0020	1285	18	1425¶	43	11
31.1	~	1321	44	0.03	547.3	0.000016	0.03	0.4821	0.0051	12.104	0.130	0.1821	0.0004	2537	22	2672¶	4	5
32.1	#	436	104	0.24	29.3	0.000013	0.02	0.0780	0.0009					484	5			
33.1	#	311	124	0.40	123.7	0.000034	0.06	0.4621	0.0054	11.137	0.139	0.1748	0.0008	2449	24	2604¶	7	6
34.1	~	148	144	0.97	10.6	<0.000001	<0.01	0.0832	0.0011					515	7			
35.1	#	920	54	0.06	60.0	0.000064	0.11	0.0758	0.0009					471	5			
36.1	~	244	71	0.29	91.7	0.000009	0.02	0.4378	0.0052	9.565	0.123	0.1585	0.0008	2341	23	2439¶	8	4
37.1	#	282	68	0.24	18.9	0.000189	0.32	0.0779	0.0010					484	6			
38.1	~	228	79	0.35	23.9	0.000077	0.13	0.1221	0.0016					743	9			
39.1	#	145	45	0.31	62.7	0.000041	0.07	0.5026	0.0074	12.064	0.198	0.1741	0.0012	2625	32	2597¶	12	-1
40.1	~	934	72	0.08	85.5	0.000022	0.04	0.1066	0.0011					653	7			
41.1	#	268	104	0.39	15.6	<0.000001	<0.01	0.0678	0.0009					423	5			
42.1	#	379	44	0.12	67.4	0.000018	0.03	0.2066	0.0030	2.201	0.040	0.0772	0.0008	1211¶	16	1127	22	-7
43.1	#	122	36	0.29	13.6	<0.000001	<0.01	0.1291	0.0020					783	11			
44.1	~	97	50	0.52	18.0	0.000134	0.23	0.2150	0.0035	2.614	0.076	0.0882	0.0021	1255	19	1386¶	47	10
45.1	#	594	32	0.05	37.3	0.000053	0.09	0.0730	0.0008					454	5			
46.1	~	291	137	0.47	44.6	0.000050	0.09	0.1784	0.0022	1.804	0.030	0.0733	0.0009	1058¶	12	1023	24	-3
47.1	~	103	16	0.15	11.0	0.000127	0.21	0.1243	0.0019					755	11			
48.1	~	694	35	0.05	78.1	0.007269	12.28	0.1149	0.0048					701	28			
49.1	~	43	67	1.57	7.9	0.000083	0.14	0.2131	0.0041	2.270	0.098	0.0773	0.0030	1245¶	22	1128	77	-9
50.1	#	1350	535	0.40	68.7	0.000034	0.06	0.0592	0.0006					371	4			
50.2 ¹	#	908	252	0.28	45.1	0.000070	0.12	0.0578	0.0008					362	5			
51.1	~	40	32	0.80	7.2	0.000531	0.90	0.2098	0.0040	2.091	0.115	0.0723	0.0037	1227¶	21	994	105	-19
52.1		586	98	0.17	57.9	0.000068	0.12	0.1149	0.0013					701	7			
53.1	~	89	81	0.91	22.4	<0.000001	<0.01	0.2945	0.0041	4.072	0.079	0.1003	0.0014	1664	20	1630¶	25	-2
54.1	~	55	34	0.62	9.7	0.000043	0.07	0.2062	0.0036	2.255	0.064	0.0793	0.0018	1209¶	19	1180	44	-2
55.1	#	160	71	0.44	66.7	0.000020	0.03	0.4860	0.0060	12.516	0.171	0.1868	0.0011	2553	26	2714¶	9	6
56.1	#	162	96	0.59	23.1	0.000108	0.18	0.1658	0.0023	1.632	0.038	0.0714	0.0013	989¶	13	968	39	-2
57.1	~	496	82	0.16	39.3	0.000002	<0.01	0.0923	0.0011					569	6			
58.1	~	251	143	0.57	20.9	<0.000001	<0.01	0.0968	0.0012					596	7			
59.1	#	209	70	0.33	11.1	<0.000001	<0.01	0.0621	0.0008					389	5			
60.1	~	46	65	1.43	3.5	<0.000001	<0.01	0.0912	0.0021					563	12			
61.1 ¹	#	481	47	0.10	82.9	0.000059	0.10	0.2005	0.0026	2.239	0.036	0.0810	0.0008	1178	14	1221¶	19	4
62.1 ¹	#	107	53	0.49	45.4	0.000012	0.02	0.4940	0.0074	12.471	0.207	0.1831	0.0013	2588	32	2681¶	12	4
63.1 ¹	#	135	44	0.33	8.4	0.000181	0.31	0.0725	0.0011					451	7			
64.1 ¹	#	169	70	0.42	13.7	0.000277	0.47	0.0937	0.0014					578	9			
65.1 ¹	~	5	<1	<0.01	0.5	0.016647	28.12	0.0806	0.0172					500	102			
66.1 ¹	#	970	32	0.03	265.2	<0.000001	<0.01	0.3183	0.0035	4.582	0.053	0.1044	0.0004	1781	17	1704¶	7	-4
67.1 ¹	#	748	188	0.25	58.5	0.000060	0.10	0.0909	0.0010					561	6			
68.1 ¹	~	55	66	1.19	4.7	0.001049	1.77	0.0971	0.0023					597	14			

Pb* = radiogenic Pb. † f_{206} = percentage of ²⁰⁶Pb that is common Pb. ‡Correction for common Pb made using the measured ²⁰⁴Pb/²⁰⁶Pb ratio.

§0 % denotes a concordant analysis. ||More than one crystallization phase analysed - corresponding ages have not been used for the statistics.

¶Preferred ages. # = Zoning interpreted to be of magmatic origin. ~ = Zoning & homogeneous areas estimated to be of metamorphic origin.

c = core / inner zoning. ¹Dated with SHRIMP I, all other points were dated with SHRIMP-RG.

Table 10. SHRIMP U-Pb zircon results for sample CA-01-06

Grain #/spot	~c	Measured ratios						Radiogenic ratios [‡]						Age (Ma)			Disc.	
		U (ppm)	Th (ppm)	Th/U	Pb* (ppm)	²⁰⁴ Pb/ ²⁰⁶ Pb	f ₂₀₆ [†] (%)	²⁰⁶ Pb/ ²³⁸ U	1σ	²⁰⁷ Pb/ ²³⁵ U	1σ	²⁰⁷ Pb/ ²⁰⁶ Pb	1σ	²⁰⁶ Pb/ ²³⁸ U	1σ	²⁰⁷ Pb/ ²⁰⁶ Pb		1σ
01.1	~	44	37	0.83	3.3	0.002423	4.09	0.0824	0.0019					511	11			
02.1		924	73	0.08	122.4	0.000127	0.21	0.1538	0.0016	1.521	0.021	0.0717	0.0007	922¶	9	978	19	6
03.1	~	306	70	0.23	26.4	0.000053	0.09	0.1002	0.0012					616	7			
04.1	#	483	37	0.08	44.5	0.000080	0.14	0.1071	0.0012					656	7			
05.1	~	220	121	0.55	65.1	<0.000001	<0.01	0.3439	0.0051	7.510	0.120	0.1584	0.0009	1905	25	2439¶	9	28
06.1	#	481	137	0.28	29.6	0.000154	0.26	0.0713	0.0008					444	5			
07.1	#	584	236	0.40	47.1	0.000072	0.12	0.0938	0.0011					578	6			
08.1	#	518	226	0.44	27.2	0.000140	0.24	0.0611	0.0007					382	4			
09.1	~	103	69	0.67	10.7	<0.000001	<0.01	0.1213	0.0019					738	11			
10.1	~	76	88	1.16	25.1	<0.000001	<0.01	0.3860	0.0059	9.315	0.164	0.1750	0.0015	2104	28	2606¶	14	24
11.1	~	107	46	0.43	7.8	0.000474	0.80	0.0842	0.0012					521	7			
12.1	~	467	22	0.05	34.5	0.000177	0.30	0.0857	0.0009					530	6			
13.1	~	373	90	0.24	33.0	0.000082	0.14	0.1029	0.0012					631	7			
14.1	~	188	21	0.11	15.1	0.000012	0.02	0.0935	0.0012					576	7			
15.1	~	507	353	0.70	27.1	0.000251	0.42	0.0621	0.0007					388	4			
16.1	#	330	136	0.41	17.6	0.000499	0.84	0.0615	0.0008					384	5			
17.1	~	124	93	0.75	8.7	<0.000001	<0.01	0.0812	0.0011					503	7			
18.1	#	404	230	0.57	35.2	0.000156	0.26	0.1012	0.0012					621	7			
19.1	#	469	203	0.43	23.9	0.001299	2.19	0.0580	0.0007					363	4			
20.1	#	382	211	0.55	21.8	<0.000001	<0.01	0.0663	0.0008					414	5			
21.1	#	91	54	0.59	6.5	<0.000001	<0.01	0.0829	0.0013					514	8			
22.1	#	295	177	0.60	48.0	0.000177	0.30	0.1885	0.0023	1.988	0.041	0.0765	0.0013	1113¶	13	1108	34	0
23.1	~	308	45	0.15	23.6	0.000213	0.36	0.0886	0.0010					547	6			
24.1	#	369	93	0.25	49.7	0.000082	0.14	0.1563	0.0018	1.623	0.027	0.0753	0.0009	936	10	1077¶	23	15
25.1	~	308	167	0.54	27.1	<0.000001	<0.01	0.1024	0.0012					629	7			
26.1	#	345	48	0.14	38.5	0.000084	0.14	0.1296	0.0015					786	9			
27.1		543	124	0.23	48.5	0.000252	0.43	0.1037	0.0016					636	10			
28.1	~	212	41	0.19	37.2	0.000216	0.37	0.2036	0.0030	2.118	0.058	0.0755	0.0017	1194	16	1081¶	46	-10
29.1	#	316	40	0.13	21.1	0.000056	0.09	0.0776	0.0009					482	6			
30.1	~	684	14	0.02	87.6	0.000097	0.16	0.1488	0.0016	1.390	0.022	0.0677	0.0008	894¶	9	861	25	-4
31.1	#	605	214	0.35	27.7	0.000186	0.31	0.0532	0.0007					334	4			
31.2 ¹	#	382	164	0.43	18.0	<0.000001	<0.01	0.0549	0.0010					345	6			
32.1	#	70	71	1.01	10.7	0.000019	0.03	0.1780	0.0076	1.779	0.104	0.0725	0.0029	1056¶	42	1000	80	-5
33.1	~	387	210	0.54	27.0	0.000842	1.42	0.0801	0.0009					497	6			
34.1	~	406	749	1.85	35.0	0.000088	0.15	0.1002	0.0011					616	7			
35.1	~	227	67	0.29	32.0	0.000244	0.41	0.1631	0.0023	1.619	0.044	0.0720	0.0017	974¶	13	987	48	1
36.1	#	1667	761	0.46	109.0	0.001278	2.16	0.0745	0.0008					463	5			
37.1	#	179	140	0.79	47.4	0.000059	0.10	0.3085	0.0037	4.799	0.070	0.1128	0.0009	1733	18	1846¶	15	6
38.1	#	337	144	0.43	24.0	0.000100	0.17	0.0827	0.0010					512	6			
39.1	~	258	44	0.17	22.8	0.000034	0.06	0.1029	0.0012					631	7			
40.1	#c	621	440	0.71	59.7	0.000006	0.01	0.1120	0.0014					684	8			
41.1	~	476	96	0.20	56.6	0.000432	0.73	0.1375	0.0017	1.405	0.035	0.0741	0.0016	830¶	10	1045	44	26
42.1	#	839	72	0.09	48.2	0.000048	0.08	0.0669	0.0007					417	4			
43.1	#	236	148	0.63	12.9	0.000224	0.38	0.0635	0.0009					397	6			
44.1		463	146	0.31	54.3	0.000028	0.05	0.1365	0.0020	1.410	0.026	0.0749	0.0008	825¶	11	1066	21	29
45.1		1907	1392	0.73	76.3	0.000396	0.67	0.0463	0.0005					292	3			
45.2 ¹	#	689	348	0.51	30.4	<0.000001	<0.01	0.0514	0.0008					323	5			
46.1	~	228	100	0.44	95.4	0.000033	0.05	0.4874	0.0061	11.755	0.328	0.1749	0.0044	2560	26	2605¶	41	2
47.1	#	230	53	0.23	20.7	0.000152	0.26	0.1047	0.0012					642	7			
48.1	#	254	56	0.22	15.7	0.000048	0.08	0.0716	0.0008					446	5			
49.1	#	354	151	0.43	21.6	0.000719	1.21	0.0703	0.0009					438	5			
50.1	#	827	197	0.24	39.1	0.000037	0.06	0.0550	0.0006					3454				
51.1	~	503	192	0.38	96.2	0.000018	0.03	0.2226	0.0024	2.716	0.033	0.0885	0.0005	1296	13	1393¶	11	8
52.1	~c	671	154	0.23	48.3	0.000046	0.08	0.0837	0.0009					518	6			
53.1		789	848	1.07	201.1	0.000013	0.02	0.2965	0.0032	4.530	0.054	0.1108	0.0005	1674	16	1813¶	9	8
54.1	~	1054	435	0.41	62.3	0.000251	0.42	0.0685	0.0007					427	4			
55.1	#	732	309	0.42	49.0	0.000361	0.61	0.0775	0.0009					481	5			
56.1	#	288	95	0.33	20.2	0.000097	0.16	0.0815	0.0009					505	5			
57.1	~	49	1	0.03	3.5	0.000659	1.11	0.0823	0.0014					510	8			
58.1	~	375	69	0.18	50.7	0.000023	0.04	0.1573	0.0017	1.564	0.021	0.0721	0.0006	941¶	10	990	17	5
59.1	~	99	63	0.63	28.8	<0.000001	<0.01	0.3374	0.0043	5.145	0.080	0.1106	0.0010	1874	21	1809¶	16	-3
60.1	#	546	99	0.18	57.1	0.000037	0.06	0.1217	0.0014	1.078	0.017	0.0643	0.0007	740¶	8	751	24	1
61.1 ¹	#	271	2	0.01	49.5	0.000019	0.03	0.2122	0.0028	2.440	0.044	0.0834	0.0010	1241	15	1278¶	24	3
62.1 ¹	#	765	363	0.47	101.7	0.000058	0.10	0.1546	0.0042	1.486	0.043	0.0697	0.0007	927¶	23	919	20	-1
63.1 ¹	#	276	402	1.46	27.7	0.000030	0.05	0.1166	0.0017					711	10			
64.1 ¹	#	200	124	0.62	14.2	0.000054	0.09	0.0828	0.0012					513	7			
65.1 ¹	#c	163	149	0.92	94.3	<0.000001	<0.01	0.6750	0.0087	26.503	0.362	0.2848	0.0012	3325	34	3389¶	7	2
66.1 ¹	#	79	38	0.48	13.5	0.000599	1.01	0.2008	0.0032	2.277	0.056	0.0823	0.0015	1165	17	1252¶	37	7

Pb* = radiogenic Pb. †f₂₀₆ = percentage of ²⁰⁶Pb that is common Pb. ‡Correction for common Pb made using the measured ²⁰⁴Pb/²⁰⁶Pb ratio. §0 % denotes a concordant analysis. ||More than one crystallization phase analysed - corresponding ages have not been used for the statistics. ¶Preferred ages. # = Zoning interpreted to be of magmatic origin. ~ = Zoning & homogeneous areas estimated to be of metamorphic origin. c = core / inner zoning. ¹Dated with SHRIMP I, all other points were dated with SHRIMP-RG.

Table 11. SHRIMP U-Pb zircon results for sample FA-01

Grain #/ spot	Measured ratios						Radiogenic ratios [‡]						Age (Ma)			Disc. (%)§	
	U c (ppm)	Th (ppm)	Th/U	Pb* (ppm)	²⁰⁴ Pb/ ²⁰⁶ Pb	f ₂₀₆ [†] (%)	²⁰⁶ Pb/ ²³⁸ U	²⁰⁷ Pb/ 1σ	²⁰⁷ Pb/ ²³⁵ U	1σ	²⁰⁶ Pb/ 1σ	²⁰⁷ Pb/ 1σ	²⁰⁶ Pb/ 1σ	²⁰⁷ Pb/ 1σ			
01.1 #	434	172	0.40	17.1	0.000089	0.15	0.0459	0.0006				289	4				
01.2 ¹ #	247	118	0.48	9.5	<0.000001	<0.01	0.0447	0.0006				282	4				
02.1 #	1360	652	0.48	73.7	0.000067	0.11	0.0630	0.0007				394	4				
03.1	256	53	0.21	37.8	0.000041	0.07	0.1716	0.0022	1.706	0.052	0.0721	0.0020	1021¶	12	989	56	-3
04.1	203	155	0.77	8.8	0.000250	0.42	0.0501	0.0007				315	4				
05.1 #	347	70	0.20	14.6	0.000060	0.10	0.0491	0.0006				309	4				
06.1 #	332	161	0.49	13.9	<0.000001	<0.01	0.0489	0.0006				308	4				
07.1 #	437	128	0.29	25.5	0.000050	0.09	0.0679	0.0008				423	5				
08.1 #	357	47	0.13	82.9	0.000020	0.03	0.2703	0.0032	3.823	0.083	0.1026	0.0018	1542	16	1671¶	33	8
09.1 #	186	113	0.61	7.7	<0.000001	<0.01	0.0485	0.0007				306	4				
10.1 ~	98	38	0.39	13.6	<0.000001	<0.01	0.1614	0.0021	1.727	0.046	0.0776	0.0018	965	12	1136¶	47	18
11.1 ~	578	10	0.02	26.0	0.000371	0.63	0.0520	0.0006				327	4				
12.1 ~	444	109	0.24	24.1	0.000099	0.17	0.0632	0.0007				395	4				
13.1 #	1215	144	0.12	65.1	0.000018	0.03	0.0624	0.0007				390	4				
14.1 ~c	93	49	0.52	16.5	0.000218	0.37	0.2055	0.0028	2.348	0.059	0.0829	0.0018	1205	15	1266¶	42	5
15.1 #	342	117	0.34	14.6	0.000082	0.14	0.0495	0.0006				312	4				
16.1 #	194	117	0.61	10.6	0.000182	0.31	0.0637	0.0008				398	5				
17.1 #	268	86	0.32	14.5	0.000088	0.15	0.0628	0.0008				393	5				
18.1 ~c	47	24	0.52	14.7	0.000333	0.56	0.3618	0.0060	6.859	0.173	0.1375	0.0026	1991	28	2196¶	33	10
19.1 ~	167	60	0.36	8.2	0.000136	0.23	0.0565	0.0008				355	5				
20.1 #	115	48	0.42	4.7	0.000762	1.29	0.0467	0.0007				294	4				
21.1 #	2296	146	0.06	146.1	0.000045	0.08	0.0740	0.0008				460	5				
22.1 #	1335	1111	0.83	59.7	0.000013	0.02	0.0520	0.0006				327	3				
23.1 #	5399	1204	0.22	229.9	0.000001	<0.01	0.0496	0.0005				312	3				
24.1 #	142	69	0.49	6.8	<0.000001	<0.01	0.0559	0.0008				351	5				
25.1 #	436	145	0.33	24.4	<0.000001	<0.01	0.0652	0.0008				407	5				
26.1 #	556	205	0.37	32.4	0.000084	0.14	0.0678	0.0007				423	5				
27.1 #	161	95	0.59	6.4	0.000338	0.57	0.0460	0.0006				290	4				
28.1 #	905	251	0.28	48.7	0.000065	0.11	0.0625	0.0007				391	4				
29.1 #	549	86	0.16	28.8	0.000093	0.16	0.0610	0.0007				382	4				
30.1 #	859	398	0.46	48.1	0.000010	0.02	0.0652	0.0007				407	4				
31.1 #	163	105	0.65	6.5	0.000464	0.78	0.0463	0.0007				291	5				
32.1 #	455	208	0.46	18.8	0.000074	0.12	0.0481	0.0006				303	4				
33.1 #	273	141	0.52	10.9	0.000041	0.07	0.0463	0.0006				292	4				
34.1 ~	119	17	0.14	9.5	0.000256	0.43	0.0932	0.0019				574	11				
35.1 #	153	59	0.39	6.9	0.000954	1.61	0.0516	0.0008				324	5				
36.1 ~	116	42	0.36	17.2	0.000227	0.38	0.1718	0.0023	1.770	0.055	0.0747	0.0021	1022	13	1061¶	56	4
37.1 #	2381	566	0.24	132.6	0.000002	0.00	0.0648	0.0007				405	4				
38.1	538	234	0.44	23.6	0.000226	0.38	0.0510	0.0006				320	4				
39.1 #	407	70	0.17	17.0	0.000172	0.29	0.0486	0.0006				306	4				
40.1 #	295	101	0.34	94.6	0.000070	0.12	0.3733	0.0044	6.316	0.084	0.1227	0.0008	2045	21	1996¶	11	-2
41.1 #	191	125	0.65	8.5	0.000273	0.46	0.0517	0.0007				325	4				
42.1 #	176	91	0.52	8.6	0.000305	0.51	0.0569	0.0008				357	5				
43.1 #	1525	204	0.13	65.8	0.000036	0.06	0.0502	0.0005				316	3				
44.1 ~	55	26	0.47	2.4	0.001711	2.89	0.0488	0.0012				307	8				
45.1	1374	172	0.13	81.1	0.000089	0.15	0.0686	0.0007				428	4				
46.1 #	1938	200	0.10	110.5	<0.000001	<0.01	0.0664	0.0007				414	4				
47.1 #	842	175	0.21	48.3	0.000134	0.23	0.0666	0.0008				415	5				
48.1 ~	142	121	0.85	31.6	0.000139	0.23	0.2574	0.0033	3.185	0.078	0.0897	0.0019	1476	17	1420¶	40	-4
49.1 #	303	140	0.46	64.6	0.000016	0.03	0.2479	0.0029	3.366	0.047	0.0985	0.0008	1428	15	1595¶	15	12
50.1 #	287	253	0.88	12.0	0.000169	0.29	0.0484	0.0006				305	4				
51.1 #	308	139	0.45	12.7	0.000122	0.21	0.0478	0.0006				301	4				
52.1 #	156	74	0.48	8.0	0.000077	0.13	0.0596	0.0009				373	6				
53.1 #	760	382	0.50	44.0	0.000038	0.06	0.0673	0.0007				420	4				
54.1 #	210	122	0.58	12.7	<0.000001	<0.01	0.0704	0.0009				439	6				
55.1 #	768	991	1.29	30.6	0.000000	0.00	0.0463	0.0005				292	3				
56.1 #	209	120	0.58	8.7	0.000200	0.34	0.0481	0.0007				303	4				
57.1 #	623	196	0.31	32.3	0.000114	0.19	0.0603	0.0007				377	4				
58.1 #	263	86	0.33	42.1	0.000053	0.09	0.1865	0.0022	1.943	0.032	0.0756	0.0009	1102	12	1084¶	24	-2
59.1 #	213	172	0.81	8.9	0.000387	0.65	0.0484	0.0007				305	4				
60.1 #	413	166	0.40	17.2	0.000223	0.38	0.0483	0.0006				304	4				
61.1 #	83	47	0.56	3.4	<0.000001	<0.01	0.0473	0.0008				298	5				
62.1 #c	382	172	0.45	24.1	0.000189	0.32	0.0731	0.0009				455	5				
63.1 #	211	91	0.43	8.7	<0.000001	<0.01	0.0481	0.0007				303	4				
64.1 #c	585	224	0.38	28.5	0.000084	0.14	0.0566	0.0007				355	4				

Pb* = radiogenic Pb. †f₂₀₆ = percentage of ²⁰⁶Pb that is common Pb. ‡Correction for common Pb made using the measured ²⁰⁴Pb/²⁰⁶Pb ratio.

§0 % denotes a concordant analysis. ||More than one crystallization phase analysed - corresponding ages have not been used for the statistics.

¶Preferred ages. # = Zoning interpreted to be of magmatic origin. ~ = Zoning & homogeneous areas estimated to be of metamorphic origin.

c = core / inner zoning. ¹Dated with SHRIMP I, all other points were dated with SHRIMP-RG.

dominant values for the concentrations and ratios are independent from zonation type.

However, the lowest Th and U concentrations (< 80 and < 35, respectively) and the lowest Th/U ratios (< 0.05) are usually present in homogeneous areas or in areas with irregular or

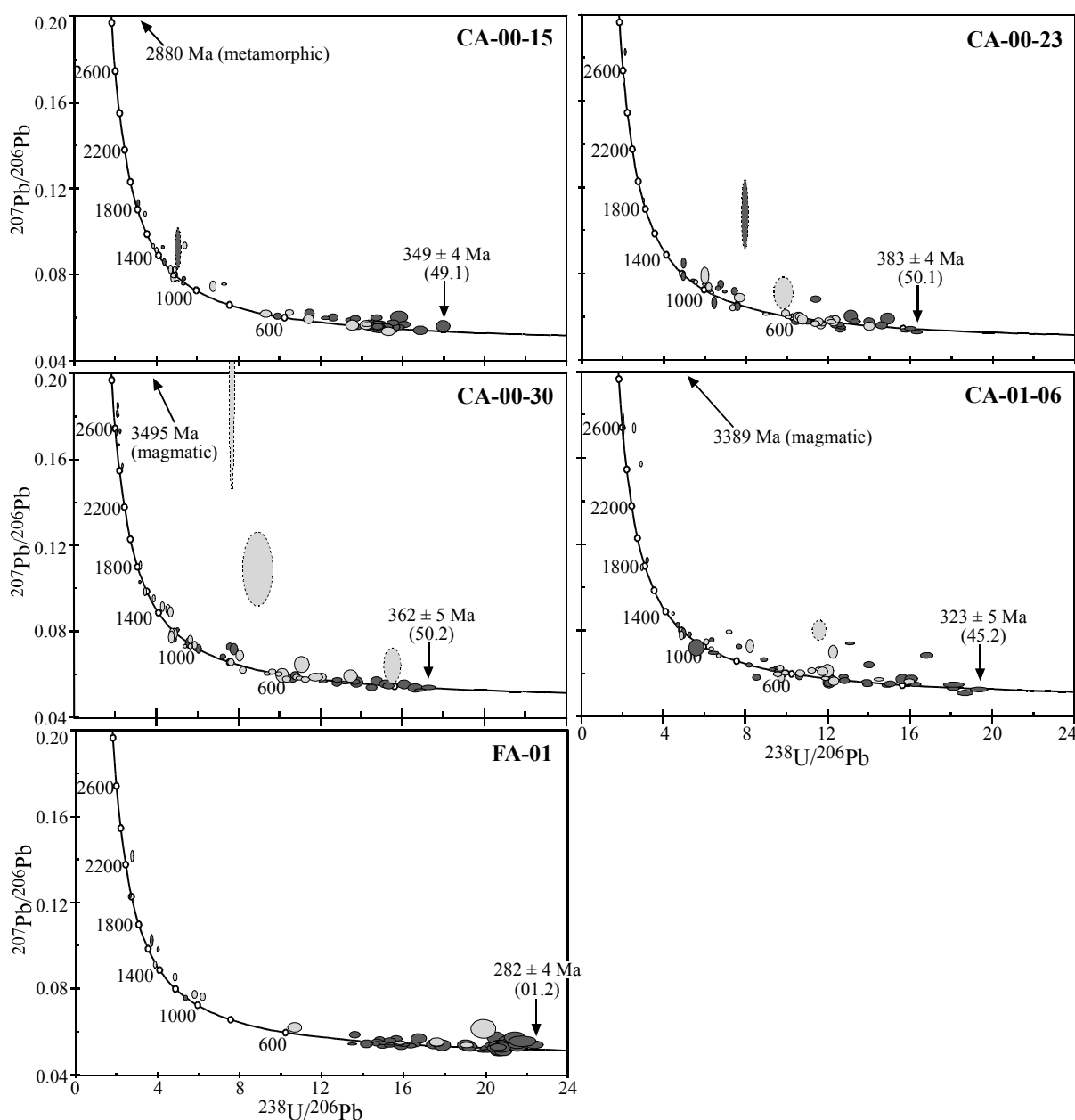


Fig. 24. Tera-Wasserburg plots of the SHRIMP U-Pb data. Individual analysis numbers are given for the youngest grain. Dark grey = analysis spots in magmatically zoned zircon areas, light grey = analysis spots in metamorphically zoned zircon area. Analyses with error ellipses with dotted rims have not been used in the interpretation and are not included in Figures 25, 27 and 28. The excluded analyses are CA-00-15:63.1, CA-00-23:71.2, -23:72.2, CA-00-30:20.1, -30:48.1, -30:65.1 and CA-01-06:01.1.

rounded concentric zoning, *i. e.*, metamorphic zircons. The highest U concentrations (> 1500 ppm) are present in areas with oscillatory or sector zoning (Tab. 7-11). Neither Th/U ratios nor Th or U concentrations correlate with the zircon ages in any of the samples.

The grains of the three zircon separates of the Cochrane unit (CA-00-15, -23, -30) are typically 50-150 μm long and sub-rounded to rounded. However, euhedral, elongated grains, usually with oscillatory zoning are also present. The zoning points to a mixture of metamorphic and magmatic sources for these zircons. Of the 177 zircon spots with a single growth phase, 159 (90 %) are younger than 1500 Ma (Tab. 7-9). The SHRIMP U-Pb age spectra of the Cochrane unit are dominated by a broad age peak in the interval 400-700 Ma (Fig. 25). The major smaller age peaks in this broad interval are around 420 Ma for sample

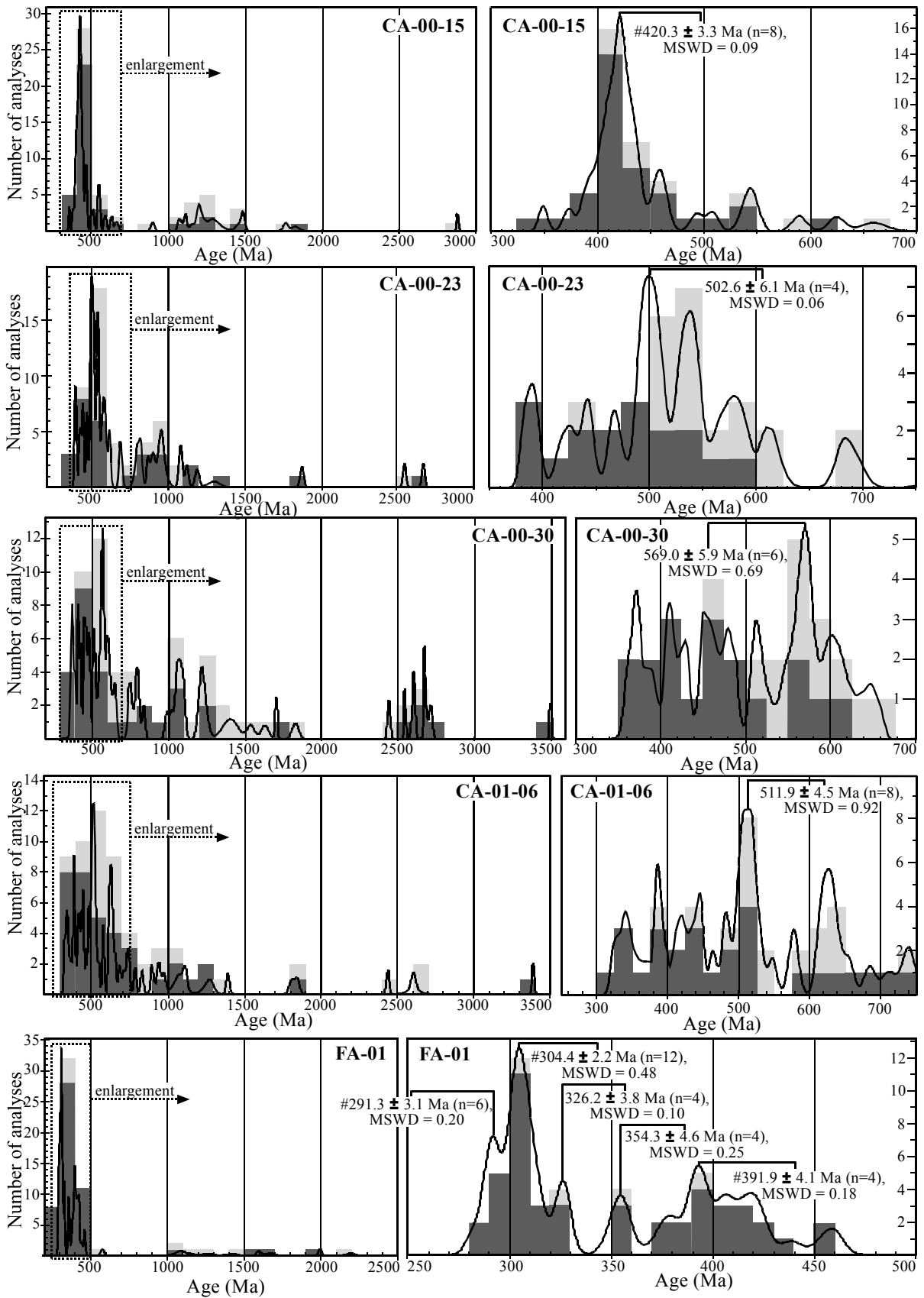


Fig. 25. SHRIMP U-Pb ages of the individual samples, including probability curves and weighted mean ages. Each histogram block spans 100 Ma in the left diagrams, and 25 Ma in the four upper diagrams on the right-hand side. The histogram blocks in the lowestmost diagram to the right span 10 Ma. \pm -values = 2σ -errors. # = ages calculated only with zircons interpreted to be of magmatic origin. For each of them, one metamorphic zircon was discarded from the population. Dark grey = analysis spots in magmatically zoned zircon areas, light grey = analysis spots in metamorphically zoned zircon area.

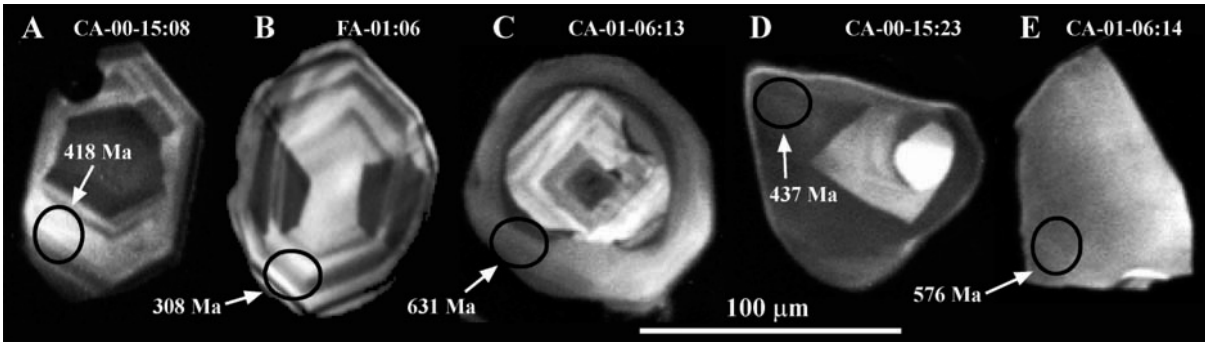


Fig. 26. Examples of differently zoned zircons. (a) Oscillatory zoning. (b) Oscillatory and sector zoning. (c) Overgrowth with rounded concentric zoning. (d) Irregular zoning. (e) Unzoned / homogeneous zircon.

CA-00-15 (dominated by magmatic zircons), at *ca.* 500 Ma for CA-00-23, and at *ca.* 570 Ma for CA-00-30 (Fig. 25). However, of the six zircons in the 570 Ma peak, the three youngest are interpreted to be of magmatic origin, whereas the three oldest appear to be metamorphic. Thus, this age peak is probably an effect of two different zircon formation phases of similar ages. A minor broad peak for the Cochrane unit samples is also apparent at 1000-1500 Ma. Ten (5 %) of the analysed zircon grains are of Archaean age, of which the oldest one is dated at 3.5 Ga (Tab. 9). The youngest grain in each sample have ages in the interval 340-390 Ma (Fig. 24). Considering the 1σ -errors, these grains point to maximum depositional ages of 353, 387 and 367 Ma for the three sediments, respectively (*cf.* Fig. 3).

The zircons of sample CA-01-06 from the Bahía de la Lancha Formation are typically 50-100 µm long and have similar morphology and zoning to those of the Cochrane unit. The

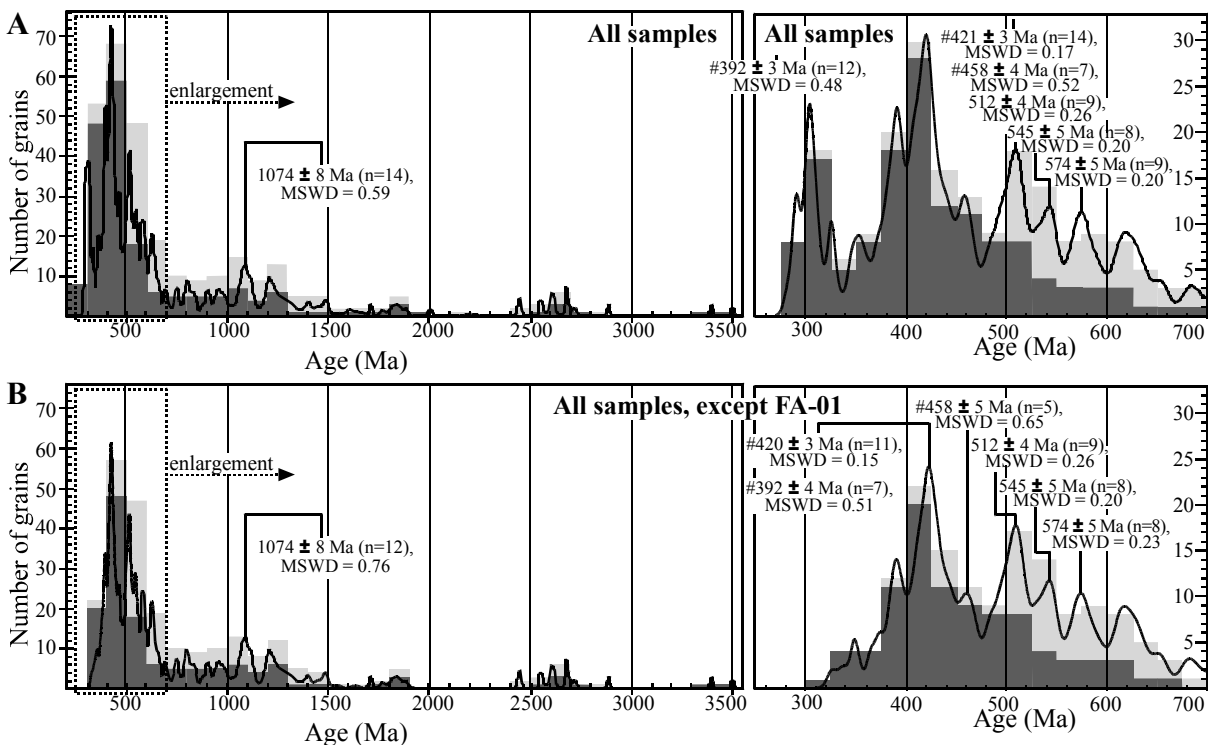


Fig. 27. SHRIMP U-Pb ages with probability curves and weighted mean ages. Dark grey = analysis spots in magmatically zoned zircon areas, light grey = analysis spots in metamorphically zoned zircon area. Each histogram block spans 100 Ma in the left diagrams, and 25 Ma in the diagrams on the right-hand side. \pm -values = 2σ -errors. # = ages calculated only with zircons interpreted to be of magmatic origin. (a) All samples. From the 392 Ma peak, two metamorphic zircons were discarded, one from the 421 Ma population and two from the 458 Ma population. (b) All samples except for FA-01. From the 392 Ma peak, one metamorphic zircon was discarded, one from the 420 Ma population and two from the 458 Ma population.

age spectrum is also similar to those of the Cochrane unit (Fig. 25). Of the 62 zircon areas with a single growth phase, 55 (89 %) are younger than 1500 Ma (Tab. 10). The age spectrum has a dominant peak at 350-700 Ma, and a minor one at 900-1400 Ma. In the broad 350-700 Ma age interval, the dominant narrow age peak is situated at *ca.* 510 Ma (Fig. 25). The sample contains three zircon grains (5 %) of Archaean age with the oldest one dated at 3.4 Ga (Tab. 10). A first measurement of the youngest analysed zircon grain gave a discordant age of 292 ± 3 Ma. However, CL imaging revealed that this age is the result of measurement in an inner magmatic, and an outer metamorphic rim (Fig. 29). A second measurement in the inner magmatic part gave a concordant age of 323 ± 5 Ma (Tab. 10; Fig. 24 & 29). This second age yields a maximum depositional age of 328 Ma for the sediment (*cf.* Fig. 3).

The SHRIMP U-Pb age spectra of the greywacke FA-01 from the part of the Eastern Andean Metamorphic Complex that crops out in the Chilean archipelago is distinctly different from the other four age spectra in this study (Fig. 25). The zircons are usually 100-200 μm long, and euhedral elongated grains with oscillatory zoning dominate. Of the 61 zircon spots with a single growth phase, 57 (93 %) are younger than 1500 Ma, 51 (84 %) are younger than

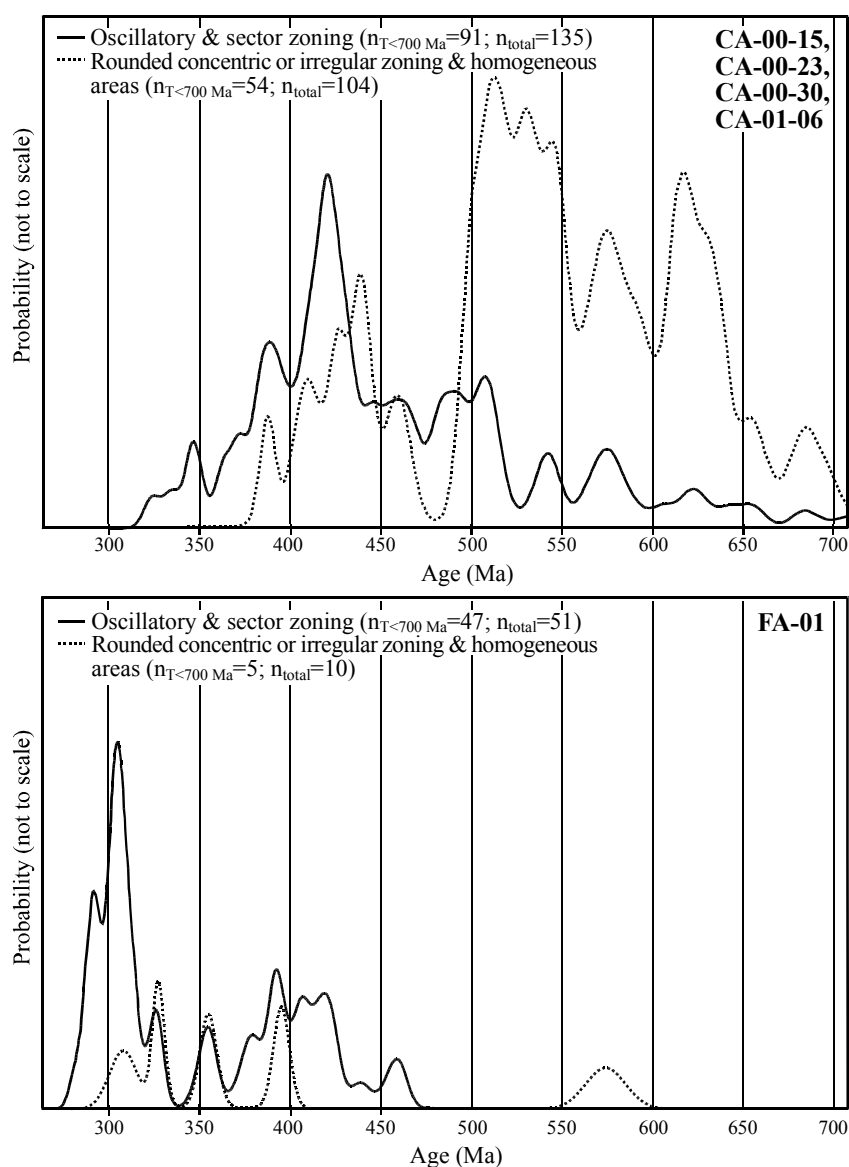


Fig. 28. Probability curves for the whole zircon population with U-Pb ages ≤ 700 Ma. Zircons with a presumed magmatic origin (solid lines) are separated from zircons with a presumed metamorphic origin (dotted lines).

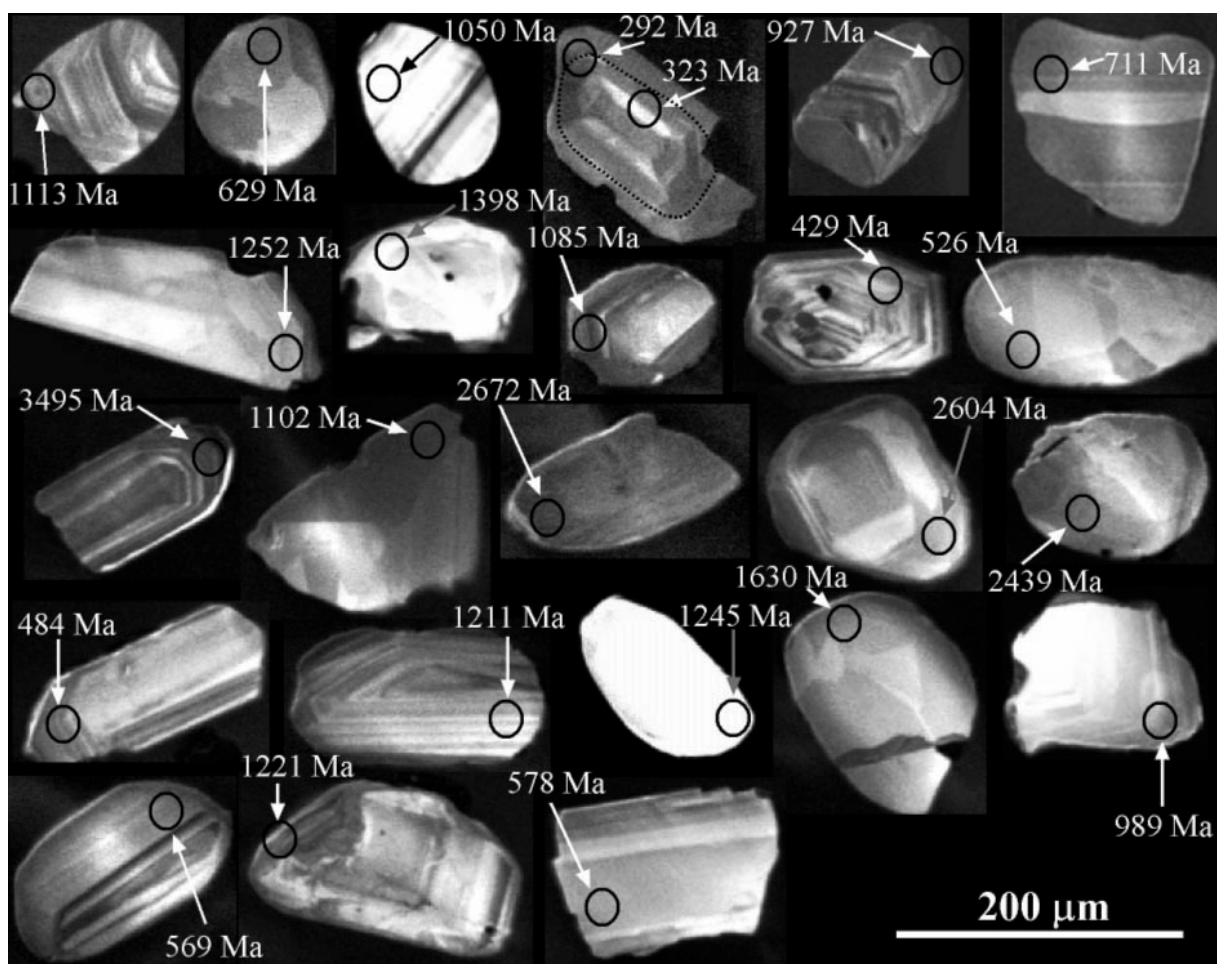


Fig. 29. Cathodoluminescence images and U-Pb ages of zircons used for the Hf isotope study. A dotted line separates the magmatic core from the metamorphic overgrowth of CA-01-06:45. CA-01-06:63 is shown in the upper right corner ($T = 711$ Ma).

500 Ma, and 27 (44 %) are still younger than 330 Ma (Tab. 11). The oldest zircon in this sample has an age of 2.2 Ga. The major distinct age peaks are at 291 ± 3 Ma and 305 ± 3 Ma (2σ ; Fig. 25). They are dominated by zircons with a probable magmatic origin. The youngest peak (291 ± 3 Ma) can be used as an estimate of the maximum depositional age of this sediment. However, if the youngest individual grain at 282 ± 4 Ma (1σ ; Fig. 24) can be considered concordant, this would constrain the depositional age of the sediment to a maximum of 286 Ma (*cf.* Fig. 3).

5.1.3. U-Pb ages: implications

The youngest analysed spots in each zircon sample give maximum depositional ages for the respective sediments. For the Cochrane unit, these are Middle to Late Devonian, but the true depositional ages are most likely even younger (Fig. 3 & 24). The mixture of magmatic and metamorphic zircons, and the broad age spectra of the individual samples of the Cochrane unit, imply a mixture of zircons from a vast number of source rocks of varying ages and origin.

The sandstone of the Bahía de la Lancha Formation has a maximum depositional age of 328 Ma. However, the presence of a younger overgrowth on the youngest dated zircon grain, and its discordant age of 292 ± 3 Ma, that is influenced by two growth phases, argues that this sediment is younger than Early Carboniferous, although Upper Devonian to Lower

Carboniferous fossils have been reported from the Bahía de la Lancha Formation (Riccardi, 1971). Although the general pattern of the SHRIMP U-Pb age spectrum is similar to those of the Cochrane unit, several grains are younger than the youngest grains from the Cochrane unit. This points to partly younger sources for this Formation. Either the Bahía de la Lancha Formation is different in age to the U-Pb analysed sediments of the Cochrane unit, or they are coeval, but were fed by detritus from partly different source areas. The latter is in concordance with both the petrography and the chemistry (see Sections 3.4. & 4.3.). This does however not exclude a difference in depositional age.

The difference in the pattern of the age spectrum of sediment FA-01 from the southern Chilean archipelago to the other four age spectra show fundamental differences in the dominant sources. The narrow and distinct age peaks among the youngest ages (290-350 Ma), imply a predominance of rocks of these ages in the source areas. The zoning of the zircons indicates that the main source rocks are of igneous origin. The greywacke with its maximum depositional age of 286 Ma is most likely younger than the sediments from both the Cochrane unit and the Bahía de la Lancha Formation.

The SHRIMP U-Pb age spectra in this study are similar to spectra published by Hervé *et al.* (2003a) from the Cochrane unit and the archipelago part of the Eastern Andean Metamorphic Complex. The general age patterns of the spectra are similarly changing from broad age peaks in the samples with the oldest maximum depositional ages to distinct narrow age peaks in samples with the youngest maximum depositional ages. By a combination of zircon SHRIMP U-Pb age data from this study and Hervé *et al.* (2003a) and zircon fission track data of Thomson & Hervé (2002) partly from the same samples also analysed for U-Pb ages by Hervé *et al.* (2003a), it becomes apparent that the depositional history of the Eastern Andean Metamorphic Complex and the Argentinean Río Lácteo and Bahía de la Lancha formations is more complex than previously known (see Section 1.3. for a discussion of the “new” stratigraphy of these and other geological units belonging to the basement of the Andes in southern Patagonia). The observed differences in zircon rounding, CL zoning and SHRIMP U-Pb age peaks for greywackes in geographically different parts of the Eastern Andean Metamorphic Complex and the Bahía de la Lancha Formation show that rocks of significantly different age and origin were to a different degree affected by abrasion, eroded and transported to the south Patagonian Late Palaeozoic Pacific margin of Gondwana (present coordinates).

The sampling of lithologically similar sediments (turbiditic greywackes) with a possible deposition in different tectonic environments indicates that the differences in SHRIMP U-Pb age spectra mirror the tectonic evolution of the Palaeozoic South Patagonian Pacific continental margin of Gondwana, and that the age spectra are less controlled by lithological variations in the sample population (*cf.* DeGraaff-Surpless *et al.*, 2003). A possible scenario (also depicted in Section 4.3.) for the continental margin would be the transformation from a passive into an active continental margin during the Late Palaeozoic. The large variety of source rocks with different ages and origin for the Bahía de la Lancha Formation and a large part of the Cochrane unit is consistent with sediment transport to a sedimentary basin in a passive margin environment (*e. g.*, McLennan & Taylor, 1991; Pell *et al.*, 1997). The U-Pb spectra with their distinct age peaks in sediments sampled in the southern Chilean Archipelago (Hervé *et al.*, 2003a; this study), the euhedral zircons usually

with oscillatory CL zoning, and the relatively young maximum depositional ages (Fig. 2 & 3) indicate that a change from a passive to an active margin might have occurred before the deposition of these sediments. Sediments deposited in an active margin basin are less severely affected by sedimentary recycling and can be expected to have a larger detrital supply from local sources, since an active tectonic regime often implies rapid new exposure of potential source rocks (Potter, 1978; Veizer & Jansen, 1985; McLennan & Taylor, 1991).

5.2. Hf isotopes

In combination with U-Pb dating of individual detrital zircons, the Hf isotope signature of the same zircon grains can serve as a powerful tool in provenance studies of sediments. This is particularly the case for provenance studies where several potential source areas with similar ages exist (*cf.* Jacobsen, 2002; Millar *et al.*, 2003). These source areas may be indistinguishable by U-Pb dating of zircon grains. Several studies have demonstrated the usefulness of Hf isotope measurements of single detrital zircons to issues related to crustal evolution and terrane studies (Amelin *et al.*, 1999; Knudsen *et al.*, 2001; Bodet & Schärer, 2000; Jacobsen, 2002; Millar *et al.*, 2003; Samson *et al.*, 2003). Furthermore, recent developments of chemical separation techniques and the multiple collector inductively coupled plasma source mass spectrometer (MC-ICP-MS) technique have facilitated the previously complicated preparation and measuring procedures and allow for analysis of the Hf isotope composition of single zircon grains down to *ca.* 50 μm (coarse silt) with high precision and accuracy (Münker *et al.*, 2001; Rehkämper *et al.*, 2001; Jacobsen, 2002). The possibility to analyse such small grains is of considerable importance in sedimentary provenance studies, since hydraulic differences between minerals result in the accumulation of heavy minerals of smaller grain sizes in light-mineral dominated sand size sediments (Morton & Hallsworth, 1999).

The Hf concentrations in zircons commonly exceeds 1 %, whereas Lu is present only in trace amounts. This means that the decay of ^{176}Lu to ^{176}Hf , with a half life of *ca.* 37 Ga (Scherer *et al.*, 2001), will lead to the production of a very small amount of ^{176}Hf in zircons even over the whole life time of the Earth. Thus, the measured $^{176}\text{Hf}/^{177}\text{Hf}_{\text{today}}$ is more or less a “frozen-in” signature of the Hf isotope composition of the whole-rock environment at the time the zircon crystallised (Fig. 30; *e. g.*, Patchett, 1983).

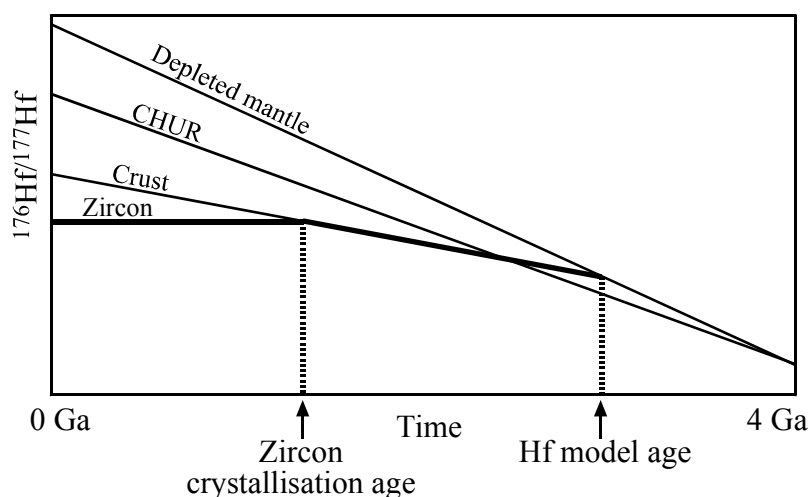


Fig. 30. The evolution through time of $^{176}\text{Hf}/^{177}\text{Hf}$ in zircons, crustal rocks, CHUR (chondritic uniform reservoir) and depleted mantle. Modified from Amelin *et al.* (2000).

An advantage of the use of Hf isotope compositions from zircons in provenance studies is the similarity between the ^{176}Lu - ^{176}Hf and the ^{147}Sm - ^{143}Nd decay systems. In both cases, the parent isotope (^{176}Lu , ^{147}Sm) is more compatible than the daughter isotope (^{176}Hf , ^{143}Nd). Thus, crust formation processes lead to an enrichment of Lu and Sm in the mantle, whereas Hf and Nd are enriched in the crust. Since the mantle is depleted in Hf and Nd, the decay of ^{176}Lu to ^{176}Hf and ^{147}Sm to ^{143}Nd will lead to that the mantle evolves towards higher $^{176}\text{Hf}/^{177}\text{Hf}$ and $^{143}\text{Nd}/^{144}\text{Nd}$ ratios than crustal rocks (*cf.* Fig. 30). Thus, ϵ , the expression for $^{176}\text{Hf}/^{177}\text{Hf}$ and $^{143}\text{Nd}/^{144}\text{Nd}$ compared to CHUR ($\epsilon_{\text{CHUR}} \equiv 0$), evolves towards positive values for the depleted mantle, whereas crustal rocks will evolve towards negative values through time. The similarities between the two isotope systems lead to a correlation between Nd and Hf isotope compositions (*e. g.* Patchett, 1983; Vervoort *et al.*, 1999). Thus, ϵ_{Hf} is strongly coupled to ϵ_{Nd} , although the absolute values are not the same. However, this coupling is useful in provenance studies. By the measurement of the Hf isotope composition of single detrital zircons, two-stage Hf model ages ($\text{Hf } T_{\text{DM}}^*$ = estimate of the crustal residence age of the protolith of the zircon) can be calculated in a similar manner as Nd T_{DM}^* (*cf.* Fig. 30 and Section 4.2.2.). To identify the source of the zircon using its Hf isotope composition, the $\text{Hf } T_{\text{DM}}^*$ has to agree with the Nd crustal residence age (Nd T_{DM}^*) of its source material. Thus, a direct comparison of zircon $\text{Hf } T_{\text{DM}}^*$ and whole-rock Nd T_{DM}^* of rocks with the same ages as the zircons can lead to an accurate identification of the source areas for detrital zircons and makes it possible to track the sedimentary transportation paths from the depositional basin back to the sources.

5.2.1. Hf isotopes: methods

Seventeen zircons from sample CA-00-30 and 7 zircons from CA-01-06 were analysed for their Lu and Hf concentrations and Hf isotope compositions at the Zentrallaboratorium für Geochronologie, Münster. After removal of the zircons from the epoxy they were embedded in for the U-Pb dating, they were spiked with a mixed $^{176}\text{Lu}/^{180}\text{Hf}$ tracer. The dissolution procedure included a first step with HF and HNO_3 in Teflon® bombs at 175°C for 4 days. For Lu-Hf separation, the element separation method of Jacobsen (2002) was used. This procedure includes separation of Lu and Hf in a single step using ion-exchange columns filled with Eichrom LN Spec resin with HCl and HF. Lu and Hf measurements were performed using a MC-ICP-MS (VG-Isoprobe, which is a mass spectrometer of the second generation). The operation conditions followed those described in Münker *et al.* (2001). Mean laboratory $^{176}\text{Hf}/^{177}\text{Hf}$ values for the Hf standard JMC 475 on the three days of measurement were 0.282151 ± 0.000050 , 0.282146 ± 0.000044 and 0.282146 ± 0.000037 (\pm -values = 2σ). Laboratory Lu and Hf blanks were < 1 pg and < 10 pg, respectively, and are negligible for Hf isotope ratio and concentration determinations. Blank corrections for Lu were always $< 5\%$. The mean external reproducibility is $\pm 0.5 \epsilon_{\text{Hf}}$ -units (2σ). All data are given relative to $^{176}\text{Hf}/^{177}\text{Hf} = 0.282160$ for JMC 475 (Blichert-Toft *et al.*, 1997). For the calculations, the following values were used: $\lambda(^{176}\text{Lu}) = 1.865 \cdot 10^{-11}$ (Scherer *et al.*, 2001), $^{176}\text{Lu}/^{177}\text{Hf}_{\text{CHUR, today}} = 0.0332$, $^{176}\text{Hf}/^{177}\text{Hf}_{\text{CHUR, today}} = 0.282772$ (Blichert-Toft & Albarède, 1997), $^{176}\text{Lu}/^{177}\text{Hf}_{\text{DM, today}} = 0.03813$, $^{176}\text{Hf}/^{177}\text{Hf}_{\text{DM, today}} = 0.283224$ (Vervoort *et al.*, 2000). The epoxy (from Epirez Construction Products, Australia), in which the zircons were embedded, was analysed for its Lu-Hf contents to ensure that epoxy residue did not affect the zircon analyses. Any

contributions of Lu and Hf to the samples from the epoxy are similar to the values for the blank sample.

5.2.2. Hf isotopes: results and implications

To be able to identify the main detrital source areas more accurately than possible with U-Pb dating alone, the Hf isotope composition of selected dated zircon grains were measured. Care was taken to select zircons with only one growth phase. The analytical results of 17 zircons from the zircon separate CA-00-30 (Cochrane unit) and 7 zircons of CA-01-06 (Bahía de la Lancha Formation) are presented in Table 12. Cathodoluminescence images of the analysed zircons are shown in Figure 29. Mainly zircons from the major U-Pb age peaks at 400-700 Ma and 900-1400 Ma were selected for the Hf isotope study. Additionally, some older grains were analysed, the oldest one having a SHRIMP U-Pb age of 3.5 Ga (Tab. 12). Excluding two zircons with multiple growth phases (CA-01-06:45 and CA-01-06:63, see Fig. 29), all zircons analysed for their Hf-isotopes have Lu and Hf contents of <340 ppm and > 1.1 %, respectively (Tab. 12). Their measured $^{176}\text{Lu}/^{177}\text{Hf}$ are < 0.002 and $^{176}\text{Hf}/^{177}\text{Hf}$ are 0.2810-0.2825. The results of grain CA-01-06:63 with multiple growth phases are not used in the interpretation below.

The initial $^{176}\text{Hf}/^{177}\text{Hf}$, expressed as $\epsilon_{\text{Hf}}(\text{T})$ in Figure 31, indicates the formation environment of the individual zircons and the crustal history of their respective sources prior to crystallisation of the zircons. For the different age groups, a large spread in $\epsilon_{\text{Hf}}(\text{T})$ is apparent (Fig. 31). However, in many cases the zircons younger than 700 Ma have lower $\epsilon_{\text{Hf}}(\text{T})$ values than those with ages of 900-1650 Ma. In the older group, two zircons of the Bahía de la Lancha Formation have $\epsilon_{\text{Hf}}(\text{T})$ values which coincide with the values for the

Table 12. *Lu-tetium-hafnium isotope data*

# /	Lu	Hf	$^{176}\text{Lu}/^{177}\text{Hf}$	$f^{\text{Lu/Hf}}$	$^{176}\text{Hf}/^{177}\text{Hf}$	2σ	ϵ_{Hf}	Age†	$^{176}\text{Hf}/^{177}\text{Hf}$	ϵ_{Hf}	T_{DM}	T_{DM}^*	
~	(ppm)	(ppm)			(today)	($\cdot 10^{-6}$)	(today)	(Ma)	(initial)	(initial)	(Ma)	(Ma)	
Cochrane unit:													
CA-00-30:01	~	32	12343	0.00036	-0.989	0.282083	21	-24.4	1398	0.282073	6.3±0.7	1596	1658
CA-00-30:02	#	170	29246	0.00082	-0.975	0.282041	20	-25.9	1085	0.282024	-2.5±0.7	1674	1846
CA-00-30:18	#	274	38811	0.00100	-0.970	0.282482	23	-10.3	429	0.282474	-1.1±0.8	1061	1241
CA-00-30:22	~	9	55224	0.00002	-0.999	0.282223	14	-19.4	526	0.282222	-7.9±0.5	1391	1666
CA-00-30:24	#	160	20399	0.00112	-0.966	0.280561	25	-78.2	3495	0.280486	-1.8±0.9	3725	3791
CA-00-30:26	~	221	34656	0.00091	-0.973	0.282337	19	-15.4	1102	0.282318	8.3±0.7	1263	1310
CA-00-30:31	~	217	44013	0.00070	-0.979	0.281190	17	-55.9	2672	0.281154	2.8±0.6	2838	2887
CA-00-30:33	#	112	42321	0.00038	-0.989	0.281082	21	-59.8	2604	0.281063	-2.0±0.7	2959	3069
CA-00-30:36	~	70	26441	0.00037	-0.989	0.281207	23	-55.3	2439	0.281190	-1.3±0.8	2791	2899
CA-00-30:37	#	263	23338	0.00160	-0.952	0.282416	18	-12.6	484	0.282401	-2.5±0.6	1173	1356
CA-00-30:42	#	238	48298	0.00070	-0.979	0.281943	18	-29.3	1211	0.281927	-3.1±0.6	1805	1981
CA-00-30:49	~	64	17093	0.00053	-0.984	0.281796	31	-34.5	1245	0.281784	-7.4±1.1	1998	2225
CA-00-30:53	~	86	17845	0.00068	-0.980	0.281975	20	-28.2	1630	0.281954	7.3±0.7	1759	1798
CA-00-30:56	#	205	29460	0.00099	-0.970	0.282334	14	-15.5	989	0.282315	5.7±0.5	1270	1351
CA-00-30:57	~	23	36125	0.00009	-0.997	0.282032	15	-26.2	569	0.282032	-13.7±0.5	1654	1996
CA-00-30:61	#	331	26239	0.00179	-0.946	0.282249	19	-18.5	1221	0.282208	7.1±0.7	1419	1471
CA-00-30:64	#	120	22777	0.00075	-0.977	0.282429	18	-12.1	578	0.282421	0.3±0.6	1129	1291
Bahía de la Lancha Formation:													
CA-01-06:22	#	40	11419	0.00051	-0.985	0.282059	21	-25.2	1113	0.282048	-1.0±0.7	1635	1794
CA-01-06:25	~	30	48806	0.00009	-0.997	0.282399	14	-13.2	629	0.282397	0.6±0.5	1151	1317
CA-01-06:32	#	53	13857	0.00054	-0.984	0.282461	26	-11.0	1056	0.282450	12.0±0.9	1078	1084
CA-01-06:45	mix	325	17603	0.00262	-0.921	0.282643	19	-4.5	323	0.282628	2.0±0.7	870	995
CA-01-06:62	#	130	17873	0.00104	-0.969	0.282232	20	-19.1	927	0.282214	0.7±0.7	1415	1554
CA-01-06:63	mix	22	13710	0.00023	-0.993	0.281519	17	-44.3	711	0.281516	-28.8±0.6	2360	2868
CA-01-06:66	#	103	17607	0.00083	-0.975	0.282335	19	-15.5	1252	0.282316	11.6±0.7	1263	1266

$T_{\text{DM}} = \ln\left[\frac{(^{176}\text{Hf}/^{177}\text{Hf})_{\text{sample, today}} - ^{176}\text{Hf}/^{177}\text{Hf}_{\text{DM, today}}}{(^{176}\text{Lu}/^{177}\text{Hf})_{\text{sample, today}} - ^{176}\text{Lu}/^{177}\text{Hf}_{\text{DM, today}}}\right] / \lambda$ and $T_{\text{DM}}^* = \ln\left[\frac{(^{176}\text{Hf}/^{177}\text{Hf})_{\text{sample, T}} - ^{176}\text{Hf}/^{177}\text{Hf}_{\text{DM, T}}}{(^{176}\text{Lu}/^{177}\text{Hf})_{\text{sample, T}} - ^{176}\text{Lu}/^{177}\text{Hf}_{\text{DM, T}}}\right] / \lambda + T$. $^{176}\text{Lu}/^{177}\text{Hf}_{\text{crust, T}}$ was calculated assuming $^{176}\text{Lu}/^{177}\text{Hf}_{\text{crust, today}} = 0.0093$ (Amelin *et al.*, 2000). †U-Pb zircon ages, see Tables 9-10. ‡Grain with several growth phases. # = Zoning interpreted to be of magmatic origin. ~ = Zoning interpreted to be of metamorphic origin.

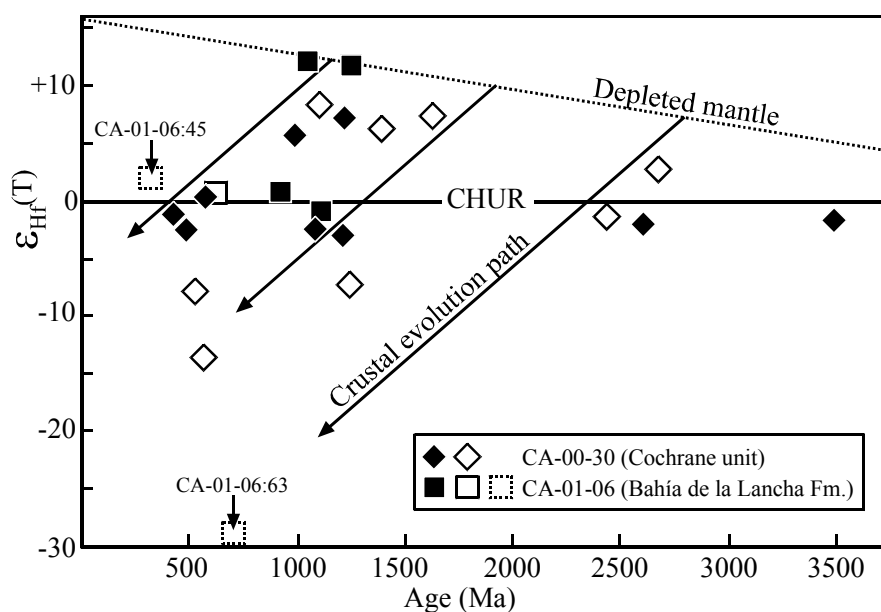


Fig. 31. Time vs. $\epsilon_{\text{Hf}}(T)$ of single detrital zircons. The arrows show typical crustal evolution paths. Filled symbols = zircons with oscillatory or sector zoning, open symbols with solid rim = homogeneous zircons or grains with rounded concentric or irregular zoning; symbols with dotted rim = zircons with multiple growth phases. The 2σ -errors (0.5-1.1 ϵ -units) are smaller than the symbol sizes for the individual zircons. CHUR = Chondritic uniform reservoir.

depleted mantle. The protoliths of these zircons were extracted from the mantle coeval with the zircon growth or shortly before. Thus, these zircons can be treated as juvenile. The negative $\epsilon_{\text{Hf}}(T)$ values of some other zircons indicate zircon crystallisation from recycled old crustal material.

By following the crustal evolution paths in Figure 31 back in time to the line for the depleted mantle, similar crustal residence ages ($\text{Hf } T_{\text{DM}}^*$) are calculated for the zircons < 700 Ma and for those with ages 900-1650 Ma (Fig. 31, Tab. 12). The two-stage Hf model ages ($\text{Hf } T_{\text{DM}}^*$; cf. single-stage Hf model ages, which also are listed in Tab. 12), which take into account fractionation of the isotopic composition at the zircon crystallisation age, are mainly between 1000 and 2000 Ma. The similarity in $\text{Hf } T_{\text{DM}}^*$ indicates that the source material for the youngest zircons was possibly partly recycled from the material of the 900-1650 m. y. old zircons. Only the four oldest zircons and CA-00-30:49 (U-Pb age = 1.2 Ga, $\text{Hf } T_{\text{DM}}^* = 2.2$ Ga) have older crustal residence ages (Tab. 12). Generally, there is no distinct difference in $\text{Hf } T_{\text{DM}}^*$ for zircons from the different samples.

The trace elements of single zircons can give further indications of their origin. Belousova *et al.* (2002) constructed a classification and regression tree (CART) for igneous zircons based on elements commonly reported by combined U-Pb and Hf isotope studies (U, Th, Y, Yb, Lu and Hf). A simplified version is shown in Figure 32. For the zircons with magmatic zoning, the Lu, Hf and U element concentrations indicate a chemistry typical for zircons from syenites, monzonites and other granitoids (Fig. 32, Tab. 12). Thus, a large portion of the zircons probably had felsic sources. Similar indications are given by the whole-rock chemistry of turbidites from both the Chilean Eastern Andean Metamorphic Complex and the two Argentinean formations (Río Lácteo and Bahía de la Lancha formations; see Section 4.3.).

The youngest dated grain of zircon separate CA-01-06 (grain 45) was analysed for its Hf isotope content, although it has multiple growth phases. The Hf isotope signature is the

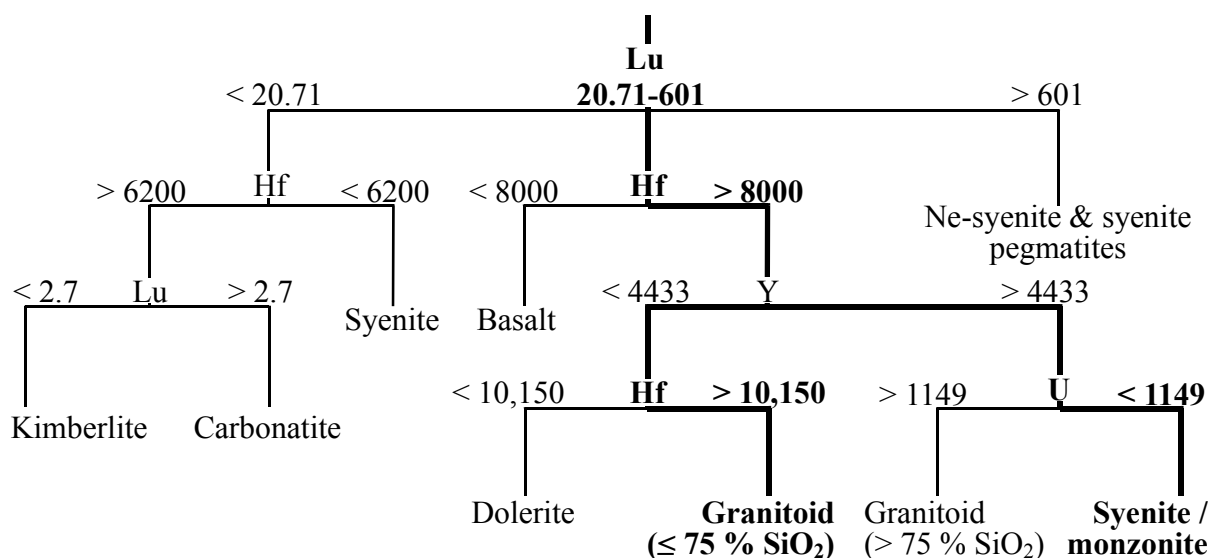


Fig. 32. Classification and regression tree for igneous zircons. Element concentrations are given in ppm. Simplified after Belousova *et al.* (2002).

result of a mixture of source material at the different growth stages. Thus, the slightly positive $\epsilon_{\text{Hf}}(T=323 \text{ Ma})$ and its zircon $\text{Hf } T_{\text{DM}}^*$ of *ca.* 1000 Ma (Fig. 31 & Tab. 12) are influenced by the two growth phases. If reworking of the host rock took place between the two growth stages, the two phases might have different protoliths. Assuming that the protoliths for these growth phases were similar, the Hf model age of zircon CA-01-06:45 can be treated as an estimate of the crustal residence age of the protolith. In this case, the source material of this zircon might have derived from the same source area as the juvenile zircons of “Grenville” age.

5.3. Zircon U-Pb and Hf isotope signatures: discussion

5.3.1. The Early to Late Carboniferous

The sources from which the individual zircons crystallised must have had the same Hf-isotope composition as the zircons themselves at the zircon formation age. Comparison of zircon age and Hf isotope signature with those of possible source rocks could therefore discriminate even between sources of similar ages (*e. g.*, Patchett, 1983). However, Hf isotope data are still scarce in the literature. As emphasised above, by using the similarity of the Sm-Nd and the Lu-Hf decay systems this problem can be overcome. For the studied sediments of southern Gondwana, Nd isotope data from a range of possible source areas are available in the literature. Thus, whole-rock Nd-isotope data of rocks from possible source areas in southern Gondwana (southern South America, Brazil, the Falkland Plateau, southern Africa and Antarctica) can be used to compare the corresponding Nd model ages of the rocks to the $\text{Hf } T_{\text{DM}}^*$ of the analysed zircons. References for the used Nd isotope data are listed in Table 13. From the literature raw data, whole-rock $\text{Nd } T_{\text{DM}}^*$ were recalculated using the Nd isotope reference values in Section 4.2.1. and Table 5. The recalculated whole-rock Nd model ages are plotted in Figure 33. Due to the coupling of the Sm-Nd and Lu-Hf isotopic systems, the whole-rock $\text{Nd } T_{\text{DM}}^*$ were directly compared to the Hf model ages of the individual detrital zircons in Figure 33. An overview of Gondwana areas with rocks with ages similar to those of the analysed zircons is given together with their whole-rock $\text{Nd } T_{\text{DM}}^*$ in Figure 34.

In this section, it will be argued that the main source areas for the zircons analysed for

Table 13. Comparing Nd and Hf isotope data from other studies

Argentinian Patagonia	NE Argentina - SE Brazil	Falkland Islands & Plateau	West Antarctica
Dalla Salda <i>et al.</i> (1991): Colohuincul Complex	Rapela <i>et al.</i> (2003): Sierra de la Ventana, Argentina	Thistlewood <i>et al.</i> (1997): Cape Meredith Complex (CMC)	Milne & Millar (1989): Target Hill
Pankhurst <i>et al.</i> (2003b): Deseado Massif	Teixeira <i>et al.</i> (2002): Río de la Plata craton, Argentina	Thomas <i>et al.</i> (1998): Cape Meredith Complex (CMC)	I. Millar (pers. comm.)*†:
	Babinski <i>et al.</i> (1996): São Gabriel Block, SE Brazil	Wareham <i>et al.</i> (1998): CMC & Maurice Ewing Bank	Storey <i>et al.</i> (1994): Haag Nunatak
	Babinski <i>et al.</i> (1997): Dom Feliciano Belt, SE Brazil		
N Chile, N & central Argentina	Central & E Brazil	Southern Africa	East Antarctica
Cingolani <i>et al.</i> (2003a & b): San Rafael Block, central Arg.	Teixeira <i>et al.</i> (1996): São Francisco craton (SFC)	Kröner <i>et al.</i> (1996): Barberton greenstone belt, S. Af.	Arndt <i>et al.</i> (1991): Dronning Maud Land
Sato <i>et al.</i> (2000): Las Matras Block, central Arg.	Brueckner <i>et al.</i> (2000): SFC, Araçuaí & Ribeira belts	Kröner <i>et al.</i> (1999): Limpopo belt, South Africa	Jacobs <i>et al.</i> (1998): Dronning Maud Land
Pankhurst <i>et al.</i> (1998b): Sierras Pampeanas, N Argentina	de Medeiros & Wiedemann (2001): Araçuaí-Ribeira belt	Wareham <i>et al.</i> (1998): Natal, South Africa	Paulsson & Austrheim (2003): Dronning Maud Land
Rapela <i>et al.</i> (1998): Sierras Pampeanas, N Argentina	Dantas <i>et al.</i> (2001) Goiás Massif	Jahn & Condie (1995): Kaapvaal craton, South Africa	Wareham <i>et al.</i> (1998): Dronning Maud Land
Bock <i>et al.</i> (2000): Puna, N Chile & NW Argentina	Junges <i>et al.</i> (2002): Goiás Massif	da Silva <i>et al.</i> (2000): Saldania Mobile belt, S. Africa	Storey <i>et al.</i> (1994): Coats Land
Lucassen <i>et al.</i> (2000): N Chile & NW Argentina	Pimentel <i>et al.</i> (1997): Goiás Massif	Condie <i>et al.</i> (1996): Mkhondo suite, Swaziland	Wareham <i>et al.</i> (2001): Transantarctic Mts
Höckenreiner <i>et al.</i> (2003): Las Termas Belt, NW Argentina	Moraes <i>et al.</i> (2003): Brasília belt	Mukasa <i>et al.</i> (1998): Great Dyke, Zimbabwe	Zhao <i>et al.</i> (1997): Prince Charles Mts
Kay <i>et al.</i> (1996)*: Precordillera xenoliths & Pie de Palo Block, N Argentina	Piuzana <i>et al.</i> (2003): Brasília belt	Oberthür <i>et al.</i> (2002): Great Dyke, Zimbabwe	Young <i>et al.</i> (1997): Mawson Coast
	de Assis Janasi (2002): Socorro-Guaxupé nappe	Singleton <i>et al.</i> (2003): Kalahara Desert, Botswana	
	Geraldes <i>et al.</i> (2001): Amazonian craton		
	Payolla <i>et al.</i> (2002): Amazonian craton		
	Pimentel <i>et al.</i> (2003): Amazonian craton		

*Isotope values used as published. †Hf-isotope data. All other data are Nd-isotope data.

their Hf isotope compositions are located in Patagonia, Sierra de la Ventana north of Patagonia, and the area which encompasses East Antarctica, the Falkland Plateau and southern Africa in the interior of Gondwana (Fig. 34 & 35). However, in order to explain the total zircon population analysed for their Hf isotope compositions, some additional sources might be required, such as central and eastern Brazil and the former Pacific Gondwana margin to the present day north of Patagonia (northern Chile and Argentina), and to the present day south (West Antarctica). This points to a general sedimentary transport from the part of the interior of Gondwana situated to the east of the study areas, as suggested in Figure 35.

Patagonia. Only a few outcrops with pre-Permian rocks exist in Patagonia, but the whole-rock Nd T_{DM}^* of these rocks indicate that this region is a suitable source area at least for zircons in the age interval 400-600 Ma (Fig. 33b). A *ca.* 425 Ma age of a granite in the Deseado Massif in southern Argentinean Patagonia south of Comodoro Rivadavia (Fig. 2; Pankhurst *et al.*, 2003b) is in agreement with a high age peak for the magmatically zoned U-Pb dated detrital zircons. Furthermore, a granodiorite from a borehole in Tierra del Fuego

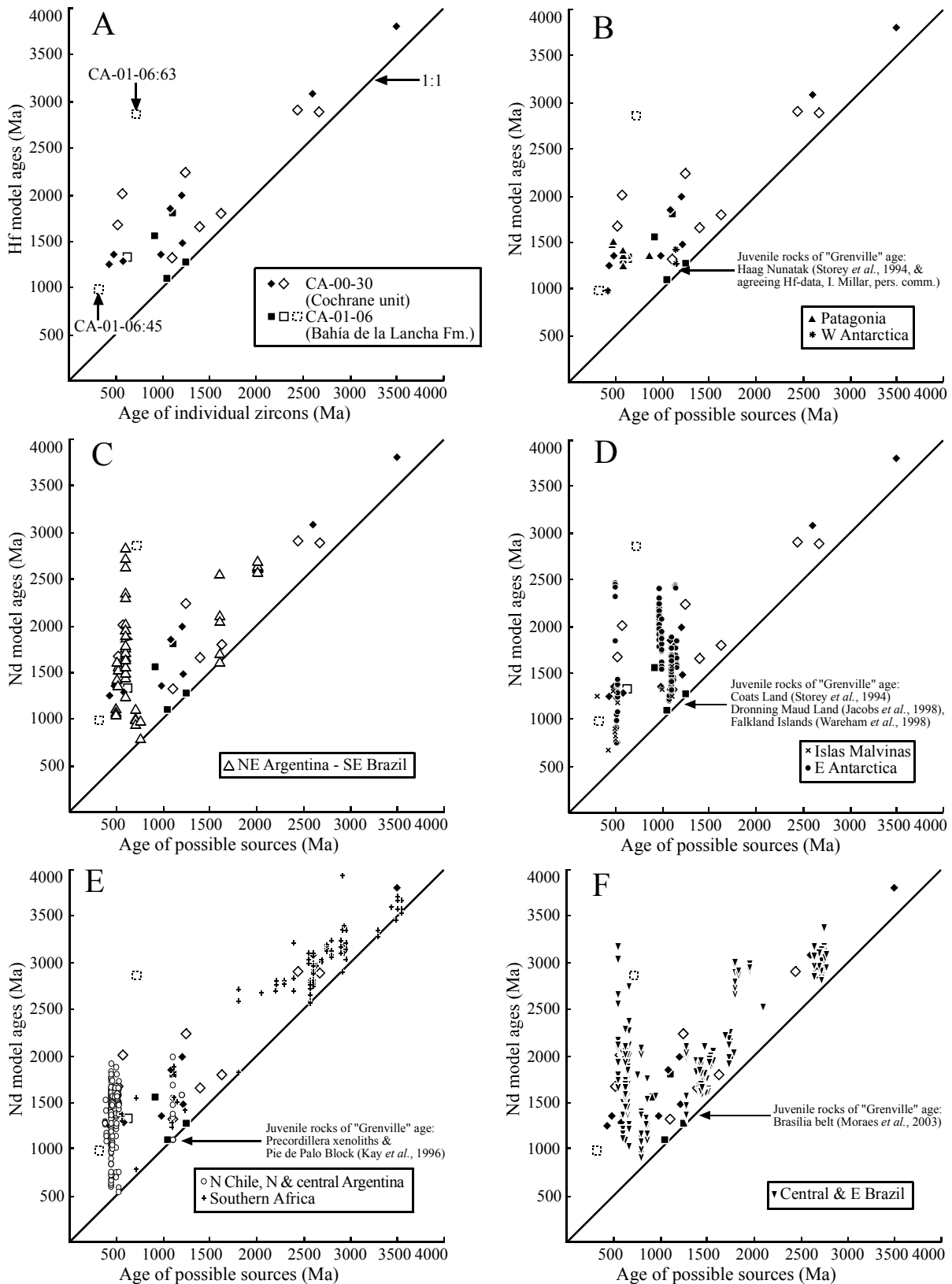


Fig. 33. Ages vs. model ages. Note that each symbol represents one single analysis. Thus, a large number of points for rocks of similar ages does not necessarily indicate a dominance of rocks of that age in the area. (a) SHRIMP U-Pb ages of individual zircons vs. zircon Hf T_{DM}^* . Filled symbols = zircons with oscillatory or sector zoning, unfilled symbols with solid rim = homogeneous zircons or grains with rounded concentric or irregular zoning; symbols with dotted rim = zircons with multiple growth phases. (b-f) Ages of rocks in possible sedimentary source areas of southern Gondwana vs. their whole-rock Nd T_{DM}^* . For comparative reasons, the zircons ages and their Hf-model ages are plotted in all diagrams. See Table 13 for references.

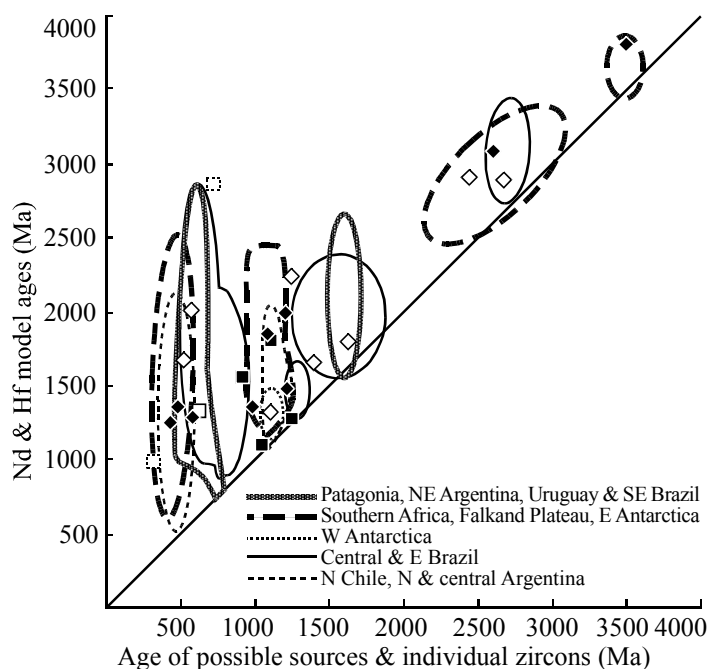


Fig. 34. Overview over the rock ages in different regions of southern Gondwana, and their corresponding whole-rock $Nd T_{DM}^*$. Additionally, the zircons ages and their $Hf T_{DM}^*$ are plotted (with symbols as in Figures 32 and 33). For references, see Table 13.

south of Patagonia was U-Pb dated at *ca.* 525 Ma (Fig. 2; Söllner *et al.*, 2000; Pankhurst *et al.*, 2003b). This locality is beyond Patagonia and the age has not been recorded for rocks in Patagonia. However, the 525 Ma granodiorite from Tierra del Fuego is similar in age to granite and rhyolite production at Sierra de la Ventana north of Patagonia (Rapela *et al.*, 2003). The occurrence of magmatic rocks *ca.* 525 m. y. old both south and north of Patagonia makes it plausible that this magmatism extended into Patagonia as well, as suggested by Pankhurst *et al.* (2003b). However, the zircons from this study that display similar ages (*ca.* 525 Ma) are interpreted to be of metamorphic origin (Fig. 28). For the zircon protoliths to be of Patagonian origin, this makes it necessary that metamorphic processes were active in Patagonia contemporaneously with the magmatic activity at *ca.* 525 Ma.

Easternmost Argentina, Uruguay and southeasternmost Brazil. In extra-Andean Argentina north of Patagonia, in Uruguay and southeasternmost Brazil, *ca.* 600 m. y. old rocks exist with a large variation of whole-rock $Nd T_{DM}^*$ (Fig. 33c). Those with whole-rock Nd model ages overlapping the Hf model ages of the detrital zircons are mainly situated in Argentinean Sierra de la Ventana slightly north of Patagonia (*ca.* 38°S; Rapela *et al.*, 2003). In Sierra de la Ventana, magmatic activity occurred in several intervals between *ca.* 600 and 500 Ma (Rapela *et al.*, 2003). However, most of the detrital zircons in this study and in the time interval *ca.* 600-500 Ma have been interpreted from their zoning to be of metamorphic origin. Thus, similar to the discussion above concerning the possible *ca.* 525 Ma magmatism in Patagonia, metamorphic processes must have been active in Sierra de la Ventana contemporaneously with the magmatic pulses between *ca.* 600 and 500 Ma if Sierra de la Ventana was a source area for the detrital zircons of that age.

In easternmost Argentina north of Sierra de la Ventana (Tandilia on the Río de la Plata craton), Uruguay and southernmost Brazil, the rocks dated at *ca.* 600 Ma have older whole-rock $Nd T_{DM}^*$ than those at Sierra de la Ventana. Furthermore, the area north of Sierra

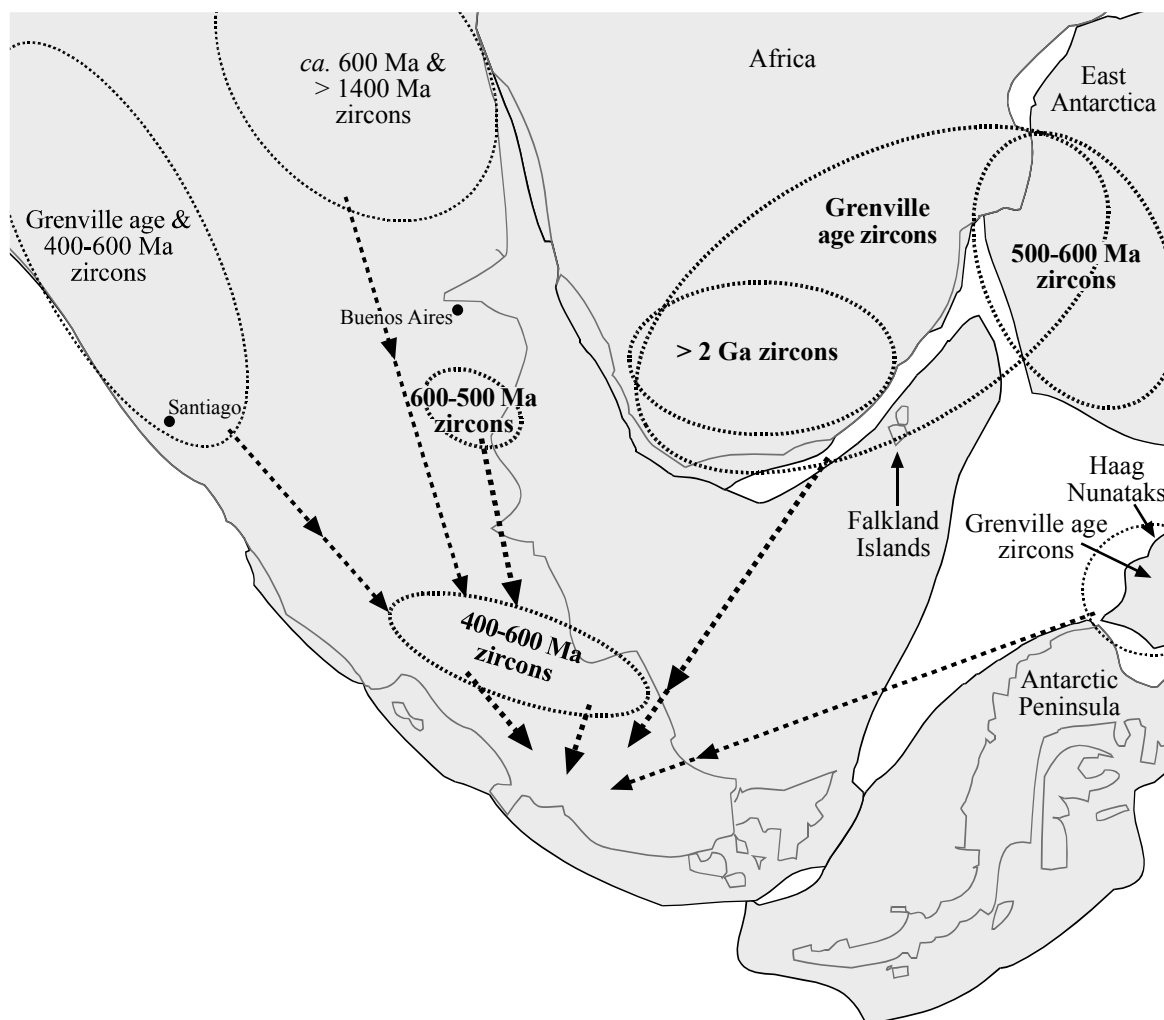


Fig. 35. Gondwana reconstruction after Lawver & Scotese (1987). Position of the Falkland Islands (Islas Malvinas) from Taylor & Shaw (1989). Possible source areas for the zircons of CA-00-30 and CA-01-06 are marked. The suggested dominant source areas are in bold.

de la Ventana has occurrences of rocks with Transamazonian ages (*ca.* 2 Ga; Preciozzi *et al.*, 1999; Teixeira *et al.*, 2002; Pankhurst *et al.*, 2003a). The latter ages are totally lacking in the U-Pb age spectra of sample CA-00-30 and CA-01-06 and is underrepresented in the total zircon population (Fig. 25 & 27). With a notable sedimentary transport from the area north of Sierra de la Ventana (Tandilia, Uruguay and southernmost Brazil), zircons of Transamazonian age would also be expected to appear in the sediments. Thus, sedimentary transport from easternmost Argentina, Uruguay and southeasternmost Brazil was most likely concentrated on Sierra de la Ventana in easternmost Argentina.

West Antarctica. West Antarctica is mainly composed of rocks < 300 Ma. However, the occurrence of relatively juvenile orthogneisses of “Grenville” age on the Haag Nunatak in West Antarctica (Storey *et al.*, 1994) makes this a possible source area, particularly for the *ca.* 1050 Ma juvenile zircon CA-01-06:32 (Fig. 33b). Hf isotope data of I. Millar (pers. comm.) from these orthogneisses confirm the occurrence of juvenile rocks of “Grenville” age at the Haag Nunatak. The Haag Nunatak was located on the continent side of the West Antarctic tectonic margin of Gondwana, which makes transport of “Grenville” age zircons from the Haag Nunatak to the Late Palaeozoic depositional basin in Patagonia possible.

East Antarctica and the Falkland Plateau. In Late Palaeozoic times, East Antarctica was part

of the interior of Gondwana. The Islas Malvinas (Falkland Islands) on the Falkland Plateau were located southeast of present southern Africa between East Antarctica and Africa (*e. g.*, Taylor & Shaw, 1989). Both in East Antarctica and on the Falkland Plateau, rocks *ca.* 500-600 m. y. old with whole-rock Nd T_{DM}^* similar to those of the analysed zircons have been reported (Fig. 33d; *e. g.*, Arndt *et al.*, 1991; Jacobs *et al.*, 1998; Wareham *et al.*, 2001; for full reference list, see Tab. 13). Furthermore, orthogneisses and felsic plutonic rocks in East Antarctica and orthogneisses on the Islas Malvinas are suitable candidates for the *ca.* 1050 m. y. old juvenile zircon (CA-01-06:32; Storey *et al.*, 1994; Jacobs *et al.*, 1998; Wareham *et al.*, 1998). Thus, with East Antarctica, the Falkland Plateau, Patagonia and Sierra de la Ventana alone, it is possible to explain most of the zircon population in the main U-Pb age groups of these sediments (Fig. 33 & 34).

Southern Africa. Southern Africa, which has large occurrences of Proterozoic and Archaean rocks, was part of the interior of Gondwana in Late Palaeozoic times and was attached to southern South America. For the oldest zircons analysed for their Hf isotope composition (2.4-3.5 Ga), this is a possible source area, as deduced from the whole-rock Nd T_{DM}^* of rocks from southern Africa with similar ages (2.4-3.5 Ga; Fig. 33e). Furthermore, the Archaean Barberton Greenstone Belt contains rock suitable as protolith for the 3.5 Ga zircon (CA-00-30:24). Thus, for the Patagonian sediments southern Africa might have been the main source for detritus of Archaean age.

Central and eastern Brazil. Central and eastern Brazil has a large variety of rocks of different age and origin. This area might have contributed with detrital zircons *ca.* 600 m. y. old (Fig. 33f). Furthermore, it might be a complementary source area to southern Africa for Archaean and Palaeozoic zircons. However, the Hf T_{DM}^* of the detrital zircons dated at 900-1400 Ma do not fully agree with the whole-rock Nd T_{DM}^* of rocks from central and eastern Brazil (Fig. 33f). Thus other areas (*e. g.*, Islas Malvinas and East Antarctica) better fit the source area requirements for the 900-1400 Ma zircons. The *ca.* 1250 m. y. old juvenile igneous zircon (CA-01-06:66) could be explained by sedimentary transport from the Brasília belt of central Brazil (Moraes *et al.*, 2003). If central and eastern Brazil was one of the main source areas for the Late Palaeozoic Patagonian sediments, erosion and pick-up from this area mainly took place from rocks of specific ages, such as Archaean and Palaeozoic ones.

Northern Chile and (northern and central) westernmost Argentina. In northern Chile and the northern and central parts of westernmost Argentina, *ca.* 400-600 m. y. old rocks with large variations in whole-rock Nd T_{DM}^* occur (Fig. 33e; *e. g.*, Bock *et al.*, 2000, for full reference list, see Tab. 13). Furthermore, *ca.* 1100-1200 m. y. old rocks with whole-rock Nd T_{DM}^* overlapping the Hf T_{DM}^* of the analysed zircons of this age have been reported (Fig. 33e; Kay *et al.*, 1996; Sato *et al.*, 2000). In Argentina, felsic gneiss xenoliths of “Grenville” age and an amphibolite at Pie de Palo (*ca.* 31°S) have isotope compositions similar to the depleted mantle (Kay *et al.*, 1996). Thus, central western Argentina could be the source of the *ca.* 1050 Ma juvenile zircon. However, transportation from central western Argentina would imply long transportation paths along the coeval continental margin.

The above interpretation of the zircon data assumes that Patagonia was a part of Gondwana in Late Palaeozoic times. However, Ramos (1984) commented that a major part of Patagonia might be an allochthonous continent that collided with Gondwana in Carboniferous to Late Permian or Early Triassic times. Similar origins for Patagonia have been suggested by

others since then. *E. g.*, Dalziel & Grunow (1992) suggested collision between Gondwana and a Patagonian arc, and recently von Gosen (2002) argued for a detachment from Gondwana before the arc - continent collision in Permian times on the basis of structural data. On the other hand, Varela *et al.* (1991) noted that common features between the North Patagonian Massif in northern Argentinean Patagonia and rocks beyond Patagonia are incompatible with a pre-Devonian allochthonous Patagonia. Furthermore, palaeomagnetic data (Rapalini, 1998, and references therein) do not support movement of Patagonia with respect to Gondwana since Early Devonian times. This suggests that Patagonia was a part of Gondwana in Late Palaeozoic times. In addition to that, the sedimentary detritus of the Late Palaeozoic passive margin sediments of the basement of the southern Patagonian Andes is suggested to mainly have had long transportation paths from the interior of Gondwana. This is incompatible with the origin of Patagonia as an exotic terrane that collided with Gondwana in Permian times.

5.3.2. The Early Permian

The predominance of euhedral, magmatic zircon grains younger than 500 Ma in zircon separate FA-01 from the part of the Eastern Andean Metamorphic Complex that crops out in the southern Chilean archipelago indicates differences in sources and in the abrasion history of the grains compared to the other four samples dated by SHRIMP U-Pb. The main age peak at *ca.* 305 Ma is similar to the age of a granite intrusion in the area of Lago General Carrera (R. de la Cruz, pers. comm.; Fig. 3), and is also similar to a granite and granodiorites in the Chilean Los Lagos region (*ca.* 40°S; Martin *et al.*, 1999), as well as a granite on the Islas Malvinas (Falkland Islands; Thistlewood *et al.*, 1997). Two older age peaks of FA-01 at *ca.* 325 Ma and *ca.* 390 Ma are similar to intrusive ages of felsic rocks at the Antarctic Peninsula (Millar *et al.*, 2001). Furthermore, in northern Patagonia between Neuquén in Argentina and Valdivia in Chile (*ca.* 39°S) plutonism correlatable with metamorphism in the same area occurred in several intervals between 400 and *ca.* 300 Ma (Franzese, 1995, and references therein). Thus, possible source rocks for the predominantly magmatic detrital zircons of FA-01 are present in Patagonia, as well as on the Islas Malvinas and in West Antarctica. However, further investigations have to show if they are suitable as source rocks.

The *ca.* 310 m. y. old granite in the area of Lago General Carrera (R. de la Cruz, pers. comm.) could be the source of the zircons in the *ca.* 305 Ma age peak of FA-01. This would imply a short transport distance to the depositional basin. Thus, this one granite, although it cannot be the sole source of the < 350 Ma zircons, shows the potential of finding suitable source rocks in the geographical vicinity of the depositional basin of the Permian metasediments of both the Duque de York Metamorphic Complex (see Fig. 2 & 3) and parts of the Eastern Andean Metamorphic Complex cropping out in the southern Chilean archipelago.

6. Final remarks

Due to the complexity of the material presented in this thesis, the interpretations of the data were discussed in the three discussion sections above. The main regional implications and interpretations were discussed in Sections 4.3. and 5.3. Below follow some remarks, which concern different parts of the thesis.

(1) The Chilean Cochrane unit is separated from the Bahía de la Lancha and Río Lácteo formations by the political boundary between Chile and Argentina. As expected, the whole-rock chemical compositions of these three units are similar. However, differences between the geological units were revealed by the CL properties of quartz and the chemistry of tourmaline. Using the advantages of the study of single grains of specific mineral types (quartz, tourmaline, zircon), the observed differences can be ascribed to partly different sources for the sediments of the Cochrane unit and the Bahía de la Lancha Formation. Thus, the differences between the geological units are neither an effect of the lower matrix content (Tab. 1) nor of the possibly more original mineralogy of the Bahía de la Lancha Formation. However, the Río Lácteo and Bahía de la Lancha formations can still, at least partly, be correlated with the Cochrane unit, as suggested in Figure 3. Further studies have to show if the above differences mirror pure geographical differences, or if they are related to a change in catchment area of the river systems, that transported detritus to the depositional basin.

(2) The Late Palaeozoic glacial period, which mainly affected southern Gondwana, has been recorded in South America by three glaciations in Early Carboniferous to earliest Late Carboniferous times and one in the Early Permian. They are recorded both in the Precordillera of northwestern Argentina and in the vicinity of Esquel (*ca.* 43°S, 71°W) in west-central Patagonia (González, 1990, and references therein). The older glaciations are in time close to the estimated depositional ages of a part of the Eastern Andean Metamorphic Complex, as well as the Río Lácteo and Bahía de la Lancha formations (Fig. 3). The younger glaciation predates the estimated age of a part of the Eastern Andean Metamorphic Complex that crops out in the southern Chilean archipelago (Fig. 3). The similarity in age of the glaciations and the estimated depositional ages of the Patagonian sediments makes it possible that some of the detritus of the studied sediments were redeposited from glacial deposits. This is particularly likely for the supposed Permian turbiditic sediments in the southern Chilean archipelago, since the Carboniferous glaciations were dominated by Alpine type glaciers, whereas the Permian one developed an extensive continental ice sheet (González, 1990, and references therein). Thus, additionally to local sources as suggested here for the supposed Permian turbidites, a considerable part of the detritus can have had long transportation paths, controlled by ice flow directions and melt water discharge patterns.

(3) This thesis gives an insight into the Late Palaeozoic geology of southern South America. From the knowledge we have today, the evolution of the Palaeozoic basement of the southern Patagonian Andean seems to coincide with the Devonian to Early Carboniferous evolution of northern Chile and northwestern Argentina further north along this margin. Here, the absence of deformation, magmatism and prograde metamorphism defines a period of tectonic quiescence from the Early Silurian to the end of the Early Carboniferous (Bahlburg & Hervé, 1997; Lucassen *et al.*, 2000). Facies patterns of thick, conformable Devonian - Early Carboniferous shallow marine siliciclastic successions are interpreted as deposits formed in a passive margin, although the chemistry indicates an active margin origin for the

source rocks (Bahlburg & Hervé, 1997; Bock *et al.*, 2000).

6.1. Conclusions

A new evaluation method for CL colour spectra of quartz was developed. The positions of the two dominant peaks in the CL spectra of quartz and their relative heights give accurate colour information about quartz grains. For the use of the CL colours of quartz as a tool in provenance studies, this method is more efficient than the data evaluation methods that usually are used.

As demonstrated above, in provenance studies it is necessary to combine different analytical techniques to gain as much different information as possible about the sediments and their sources. The different analytical techniques used in this study give considerable information about the sediments and their sources. Important results are the new maximum depositional ages that are given from the SHRIMP U-Pb zircon data. As discussed in Section 1.3. and summarized below, this has implications, together with other age data, for the age of the different geological units of the Andean basement sediments of the southern Patagonian Andes.

(1) The Cochrane unit of the Chilean Eastern Andean Metamorphic Complex most likely has considerably different depositional ages in different geographical areas. In this study, Early Carboniferous and Permian depositional intervals are suggested from the new age data and ages taken from the literature.

(2) A similar scenario to that for the Cochrane unit is suggested for the part of the Eastern Andean Metamorphic Complex cropping out in the southern Chilean archipelago. Early Carboniferous and Permian depositional intervals are suggested here.

(3) For the Argentinean Bahía de la Lancha Formation, the maximum depositional age of 328 Ma and the Late Devonian to Early Carboniferous fossils (Riccardi, 1971) constrain deposition of this Formation to Early Carboniferous times. However, the U-Pb age of 292 Ma (which is influenced by two growth phases) of the youngest grain of zircon separate CA-01-06, makes it possible that this Formation has an even younger age.

In Early Carboniferous times, the major part of Patagonia was a part of Gondwana and the south Patagonian Pacific margin of Gondwana (present coordinates) was a passive continental margin. Magmatic activity was absent. To a large part, the depositional basin at the margin was fed by turbiditic sediments containing much older material. A large part of the detritus had undergone sedimentary recycling or metamorphism. Although the Cochrane unit and the Bahía de la Lancha Formation were fed from chemically similar sources, the combination of provenance techniques shows that the Bahía de la Lancha Formation had a larger dominance of metamorphic or recycled sources. The original source areas for the detrital grains are suggested to encompass present extra-Andean Patagonia, as well as the Argentinean Sierra de la Ventana slightly north of Patagonia (Fig. 35). Furthermore, southern Africa, East Antarctica and the Falkland Plateau, situated in the interior of Gondwana, probably were important source areas for the sediments. Thus, the general sedimentary transport was from the inner area of Gondwana.

In the Permian, a subduction zone was already developed at the south Patagonian Pacific margin of Gondwana (present coordinates). By this time the depositional basin was fed by relatively young turbiditic detritus mainly of magmatic origin. The main source areas

for the sediments are suggested to have been relatively local, possible Patagonian. Thus, this study supports an onset of subduction at the Late Palaeozoic Pacific margin of Gondwana (present coordinates) in Late Carboniferous times.

Acknowledgements

This work would not have been possible without the support of Deutsche Forschungs-Gemeinschaft (DFG; grants Ba 1011/17-1, -2 and -3 to Heinrich Bahlburg) and the collaboration with Francisco “Pancho” Hervé (Departamento de Geología, Universidad de Chile, Santiago de Chile). Additionally, partial support for attending meetings were given by DFG (AU 189/1-1), IGCP 636, EUG and Geologische Vereinigung. Furthermore, this work would not have been done by *me* if Heinrich Bahlburg (Geologisch-Paläontologisches Institut und Museum, GPI) had not believed, that I was a suitable candidate for the work. The field work and sampling was supplemented by samples donated by Heinrich Bahlburg (GPI) and Juan-Pablo Lacassie (Departamento de Geología, Universidad de Chile, Santiago). Some of the preparatory work was done by GPI students. Thank you Nicole Dobrzinski, Antje Teuwsen and Eva Westervoß. Most of the analysing work took place in other institutions than the GPI. Particularly, I want to thank Jasper Berndt (Institut für Mineralogie, IM), Andreas Kaus (Institut für Planetologie), Heidi Bayer, Klaus Mezger and Carsten Münker (Zentrallabor für Geochronologie at IM) and Mark Fanning (Research School of Earth Sciences, Canberra) for their help and support. The following persons at GPI and IM in Münster were kind enough to read parts of previous versions of this thesis: Heinrich Bahlburg, Nicole Dobrzinski, Klaus Mezger, Carsten Münker, Judith Nagel, Christina Reimann and Robert Weiß. All other persons with whom I have worked and exchanged ideas - you are not forgotten, but the list would be too long for all of you. THANK YOU!

References

- AGUIRRE, L., HERVÉ, F. & GODOY, E., 1972. Distribution of metamorphic facies in Chile - an outline. *Krystalinikum*, **9**, 7-19.
- ALBARÈDE, F. & BROUXEL, M., 1987. The Sm/Nd secular evolution of the continental crust and the depleted mantle. *Earth and Planetary Science Letters*, **82**, 25-35.
- AMELIN, Y., LEE, D.-C., HALLIDAY, A. N. & PIDGEON, R. T., 1999. Nature of the Earth's earliest crust from hafnium isotopes in single detrital grains. *Nature*, **399**, 252-255.
- AMELIN, Y., LEE, D.-C. & HALLIDAY, A. N., 2000. Early-middle Archaean crustal evolution deduced from Lu-Hf and U-Pb isotopic studies of single zircon grains. *Geochimica et Cosmochimica Acta*, **64**, 4205-4225.
- ARNDT, N. T., TODT, W., CHAUVEL, C., TAPFER, M. & WEBER, K., 1991. U-Pb zircon age and Nd isotopic composition of granitoids, charnockites and supracrustal rocks from Heimfrontfjella, Antarctica. *Geologische Rundschau*, **80**, 759-777.
- AUBERT, D., STILLE, P. & PROBST, A., 2001. REE fractionation during granite weathering and removal by waters and suspended loads: Sr and Nd isotopic evidence. *Geochimica et Cosmochimica Acta*, **65**, 387-406.
- AUGUSTSSON, C. & BAHLBURG, H., 2003a. Active or passive margin? Geochemical and Nd isotope constraints of metasediments in the backstop of a pre-Andean accretionary wedge in southernmost Chile (46°30'-48°30'S). In: MCCANN, T. & SAINTOT, A. (eds.), *Tracing Tectonic Deformation Using the Sedimentary Record*. Geological Society, London, Special Publications, 208, 253-268.
- AUGUSTSSON, C. & BAHLBURG, H., 2003b. Cathodoluminescence spectra of detrital quartz as provenance indicators for Paleozoic metasediments in southern Andean Patagonia. *Journal of South American Earth Sciences*, **16**, 15-26.
- BABINSKI, M., CHEMALE JR, F., HARTMANN, L. A., VAN SCHMUS, W. R. & DA SILVA, L. C., 1996. Juvenile accretion at 750-700 Ma in southern Brazil. *Geology*, **24**, 439-442.
- BABINSKI, M., CHEMALE JR, F., VAN SCHMUS, W. R., HARTMANN, L. A. & DA SILVA, L. C., 1997. U-Pb and Sm-Nd geochronology of the Neoproterozoic granitic-gneissic Dom Feliciano Belt, southern Brazil. *Journal of South American Earth Sciences*, **10**, 263-274.
- BAHLBURG, H. & HERVÉ, F., 1997. Paleozoic geodynamic evolution and tectonostratigraphic terranes of northwestern Argentina and northern Chile. *Geological Society of America Bulletin*, **109**, 869-884.
- BANDEL, K. & QUINZIO-SINN, L. A., 1999. Paleozoic trace fossil from the Cordillera Costal near Concepción, connected to a review of the Paleozoic history of cenral Chile. *Neues Jahrbuch für Geologie und Paläontologie - Abhandlungen*, **211**, 171-200.
- BELL, C. M. & SUÁREZ, M., 2000. The Río Lácteo Formation of southern Chile. Late Paleozoic orogeny in the Andes of southernmost South America. *Journal of South American Earth Sciences*, **13**, 133-145.
- BELOUSOVA, E. A., GRIFFIN, W. L., O'REILLY, S. Y. & FISHER, N. I., 2002. Igneous zircon: trace element composition as an indicator of source rock type. *Contributions to Mineralogy and Petrology*, **143**, 602-622.

- BHATIA, M. R., 1983. Plate tectonics and geochemical composition of sandstones. *Journal of Geology*, **91**, 611-627.
- BHATIA, M. R. & CROOK, K. A. W., 1986. Trace element characteristics of graywackes and tectonic setting discrimination of sedimentary basins. *Contributions to Mineralogy and Petrology*, **92**, 181-193.
- BLACK, L. P., WILLIAMS, I. S. & COMPSTON, W., 1986. Four zircons ages from one rock: the history of a 3930 Ma-old granulite from Mount Sones, Enderby Land, Antarctica. *Contributions to Mineralogy and Petrology*, **94**, 427-437.
- BLICHERT-TOFT, J. & ALBARÈDE, F., 1997. The Lu-Hf isotope geochemistry of chondrites and the evolution of the mantle-crust system. *Earth and Planetary Science Letters*, **148**, 243-258.
- BLICHERT-TOFT, J., CHAUVEL, C. & ALBARÈDE, F., 1997. Separation of Hf and Lu for high-precision isotope analysis of rock samples by magnetic sector-multiple collector ICP-MS. *Contributions to Mineralogy and Petrology*, **127**, 248-260.
- BOCK, B., BAHLBURG, H., WÖRNER, G. & ZIMMERMANN, U., 2000. Tracing crustal evolution in the southern central Andes from Late Precambrian to Permian with geochemical and Nd and Pb isotope data. *Journal of Geology*, **108**, 515-535.
- BODET, F. & SCHÄRER, U., 2000. Evolution of the SE-Asian continent from U-Pb and Hf isotopes in single grains of zircon and baddeleyite from large rivers. *Geochimica et Cosmochimica Acta*, **64**, 2067-2091.
- BOGGS JR, S., KWON, Y.-I., GOLES, G. G., RUSK, B. G., KRINSLEY, D. & SEYEDOLALI, A., 2002. Is quartz cathodoluminescence color a reliable provenance tool? A quantitative examination. *Journal of Sedimentary Research*, **72**, 408-415.
- BONJOUR, J.-L. & DABARD, M.-P., 1991. Ti/Nb ratios of clastic terrigenous sediments used as an indicator of provenance. *Chemical Geology*, **91**, 257-267.
- BRUCE, R. M., NELSON, E. P., WEAVER, S. G. & LUX, D. R., 1991. Temporal and spatial variations in the southern Patagonian batholith; constraints on magmatic arc development. In: HARMON, R. S. & RAPELA, C. W. (eds.), *Andean Magmatism and Its Tectonic Setting*. Geological Society of America Special Papers, 265, 1-12.
- BRUECKNER, H. K., CUNNINGHAM, D., ALKMIN, F. F. & MARSHAK, S., 2000. Tectonic implications of Precambrian Sm-Nd dates from the southern São Francisco craton and adjacent Araçuaí and Ribeira belts, Brazil. *Precambrian Research*, **99**, 255-269.
- BURKE, W. H., DENISON, R. E., HEATHERINGTON, E. A., KOEPNIK, R. B., NELSON, H. F. & OTTO, J. B., 1982. Variation of seawater $^{87}\text{Sr}/^{86}\text{Sr}$ throughout Phanerozoic time, *Geology*, **10**, 516-519.
- CAMINOS, R. & GONZÁLEZ, P. D., 1996. *Mapa Geológico de la República Argentina*. Dirección Nacional del Servicio Geológico, 1:5,000,000.
- CINGOLANI, C. A., MANASSERO, M. & ABRE, P., 2003a. Composition, provenance, and tectonic setting of Ordovician siliciclastic rocks in the San Rafael block: Southern extension of the Precordillera crustal fragment, Argentina. *Journal of South American Earth Sciences*, **16**, 91-106.
- CINGOLANI, C. A., BASEI, M. A. S., LLAMBIÁS, E. J., VARELA, R., CHEMALE JR, F., SIGA JR, O. & ABRE, P., 2003b. The Rodeo Bordalesa Tonalite, San Rafael Block (Argentina): geochemical and isotopic age constraints. *10° Congreso Geológico Chileno, Concepción, Actas on CD-ROM*, 8 pp.
- CLAOUÉ-LONG, J. C., COMPSTON, W., ROBERTS, J. & FANNING, C. M., 1995. Two carboniferous age: a comparison of SHRIMP zircon dating with conventional zircon ages and $^{40}\text{Ar}/^{39}\text{Ar}$ analysis. In: BERGGREN, W. A., KENT, D. V., AUBRY, M.-P. & HARDENBOL, J. (eds.), *Geochronology, time scales and global stratigraphic correlation*. SEPM Special Publications, 54, 3-21.
- COLLINS, W. J. & WILLIAMS, I. S., 1995. SHRIMP ionprobe dating of short-lived Proterozoic tectonic cycles in the northern Arunta Inlier, central Australia. *Precambrian Research*, **71**, 69-89.
- CONDIE, K. C., DENGATE, J. & CULLERS, R. L., 1995. Behavior of rare earth elements in a paleoweathering profile on granodiorite in the Front Range, Colorado, USA. *Geochimica et Cosmochimica Acta*, **59**, 279-294.
- CONDIE, K. C., KRÖNER, A. & MILISENDA, C. C., 1996. Geochemistry and geochronology of the Mkhondo suite, Swaziland: evidence for passive-margin deposition and granulite facies metamorphism in the Late Archean of Southern Africa. *Journal of African Earth Sciences*, **21**, 483-506.
- DALLA SALDA, L., CINGOLANI, C. A. & VARELA, R., 1991. El basamento pre-andino igneo metamórfico de San Martín de los Andes, Neuquén. *Asociación Geológica Argentina Revista*, **46**, 223-234.
- DALZIEL, I. W. D. & GRUNOW, A. M., 1992. Late Gondwanide tectonic rotations within Gondwanaland.

- Tectonics*, **11**, 603-606.
- DANTAS, E. L., JOST, H., FUCK, R. A., PIMENTEL, M. M. & BROD, J. A., 2001. Provenance and depositional age of the Neoproterozoic volcano-metasedimentary sequence in the Santa Terezinha region, Goiás based on U-Pb single zircon and Sm-Nd isotope data. *III South American Symposium on Isotope Geology, Pucón, Chile, Extended Abstracts Volume*, 121-124.
- DA SILVA, L. C., GRESSE, P. G., SCHEEPERS, R., MCNAUGHTON, N. J., HARTMANN, L. A. & FLETCHER, I., 2000. U-Pb SHRIMP and Sm-Nd age constraints on the timing and sources of the Pan-African Cape Granite Suite, South Africa. *Journal of African Earth Sciences*, **30**, 795-815.
- DE ASSIS JANASI, V., 2002. Elemental and Sr-Nd isotope geochemistry of two Neoproterozoic mangerite suites in SE Brazil: Implications for the origin of the mangerite - charnockite - granite series. *Precambrian Research*, **119**, 301-327.
- DEGRAAFF-SURPLESS, K., MAHONEY, J. B., WOODEN, J. L. & MCWILLIAMS, M. O., 2003. Lithofacies control in detrital zircon provenance studies: Insights from the Cretaceous Methow basin, southern Canadian Cordillera. *GSA Bulletin*, **115**, 899-915.
- DE MEDEIROS, S. R. & WIEDEMANN, C. M., 2001. New Sm-Nd isotopic data from the southern Araçuaí-Ribera Belt: Paraíba do Sul Group and associated granitic intrusions. *III South American Symposium on Isotope Geology, Pucón, Chile, Extended Abstracts Volume*, 187-190.
- DEPAOLO, D. J., 1981. Neodymium isotopes in the Colorado Front Range and crust-mantle evolution in the Proterozoic. *Nature*, **291**, 193-196.
- DEPAOLO, D. J., LINN, A. M. & SCHUBERT, G., 1991. The continental age distribution: methods of determining mantle separation ages from Sm-Nd isotopic data and application to the southwestern United States. *Journal of Geophysical Research*, **96**, 2071-2088.
- DICKINSON, W. R., 1970. Interpreting detrital modes of graywacke and arkose. *Journal of Sedimentary Petrology*, **40**, 695-707.
- DICKINSON, W. R. & SUCZEK, C. A., 1979. Plate tectonics and sandstone compositions. *The American Association of Petroleum Geologists Bulletin*, **63**, 2164-2182.
- DOBZINSKI, N., 2001. Petrographie und Geochemie der paläozoischen Sedimente in S-Chile zwischen dem 48° und 51°S, Diploma Thesis, Westfälische Wilhelms-Universität Münster, 61 pp.
- DOUGLAS, G. B., GRAY, C. M., HART, B. T. & BECKETT, R., 1995. A strontium isotopic investigation of the origin of suspended particular matter (SPM) in the Murray-Darling River system, Australia. *Geochimica et Cosmochimica Acta*, **59**, 3799-3815.
- DUHART, P., McDONOUGH, M., MUÑOZ, J., MARTIN, M. & VILLENEUVE, M., 2001. El Complejo Metamórfico Bahía Mansa en la cordillera de la Costa del centro-sur de Chile (39°30'-42°00'): geocronología K-Ar, ⁴⁰Ar/³⁹Ar y U-Pb e implicancias en la evolución del margen sur-occidental de Gondwana. *Revista Geológica de Chile*, **28**, 179-208.
- ESCOBAR, F. (ed.), 1980. Mapa Geológico de Chile. Servicio Nacional de Geología y Minería, 1:1,000,000.
- FANG, Z., BOUCOT, A., COVACEVICH, V. & HERVÉ, F., 1998. Discovery of Late Triassic fossils in the Chonos Metamorphic Complex, Southern Chile. *Revista Geológica de Chile*, **25**, 165-174.
- FAÚNDEZ, V., HERVÉ, F. & LACASSIE, J. P., 2002. Provenance and depositional setting of pre-Late Jurassic turbidite complexes in Patagonia, Chile. *New Zealand Journal of Geology and Geophysics*, **45**, 411-425.
- FEDO, C. M., NESBITT, H. W. & YOUNG, G. M., 1995. Unraveling the effects of potassium metasomatism in sedimentary rocks and paleosols, with implications for paleoweathering conditions and provenance. *Geology*, **23**, 921-924.
- FLOYD, P. A. & LEVERIDGE, B. E., 1987. Tectonic environment of the Devonian Gramscatho basin, south Cornwall: framework mode and geochemical evidence from turbiditic sandstones. *Journal of the Geological Society, London*, **144**, 531-542.
- FORSYTHE, R., 1982. The late Palaeozoic to early Mesozoic evolution of southern South America: a plate tectonic interpretation. *Journal of the Geological Society, London*, **139**, 671-682.
- FORTEY, R., PANKHURST, R. J. & HERVÉ, F., 1992. Devonian Trilobites at Buill, Chiloé (42°S). *Revista Geológica de Chile*, **19**, 133-143.
- FRANZESE, J. R., 1995. El Complejo Piedra Santa (Neuquén, Argentina): parte de un cinturón metamórfico neopaleozoico del Gondwana suroccidental. *Revista Geológica de Chile*, **22**, 193-202.

- FROST, C. D. & WINSTON, D., 1987. Nd isotope systematics of coarse- and fine-grained sediments: examples from the Middle Proterozoic Belt-Purcell Supergroup. *Journal of Geology*, **95**, 309-327.
- FROUDE, D. O., IRELAND, T. R., KINNY, P. D., WILLIAMS, I. S., COMPSTON, W., WILLIAMS, I. R. & MYERS, J. R., 1983. Ion microprobe identification of 4,100-4,200 Myr-old terrestrial zircons. *Nature*, **304**, 616-618.
- GALLOWAY, W. E., 1974. Deposition and diagenetic alteration of sandstone in northeast Pacific arc-related basins: implications for graywacke genesis. *Geological Society of America Bulletin*, **85**, 379-390.
- GARCÍA, A., BECK, M. E., BURMEISTER, R. F., MUNIZAGA, F. & HERVÉ, F., 1988. Paleomagnetic reconnaissance of the Región de los Lagos, southern Chile, and its tectonic implications. *Revista Geológica de Chile*, **15**, 13-30.
- GERALDES, M. C., VAN SCHMUS, W. R., CONDIE, K. C., BELL, S., TEIXEIRA, W. & BABINSKI, M., 2001. Proterozoic geologic evolution of the SW part of the Amazonian Craton in Mato Grosso state, Brazil. *Precambrian Research*, **111**, 91-128.
- GESLIN, J. K., LINK, P. K. & FANNING, C. M., 1999. High-precision provenance determination using detrital-zircon ages and petrography of quaternary sands on the eastern Snake River Plain, Idaho. *Geology*, **27**, 295-298.
- GIACOSA, R. E., FRANCHI, M. & GENINI, A., 1999. *Carta Geológica de la República Argentina, Lago Posadas / Lago Belgrano, Hoja 4772-IV/III*. Subsecretaría de Minería de la Nación, Boletín N° 256, 1:250,000.
- GOLDSTEIN, S. L., O'NIONS, R. K. & HAMILTON, P. J., 1984. A Sm-Nd study of atmospheric dusts and particulates from major river systems. *Earth and Planetary Science Letters*, **70**, 221-236.
- GONZÁLEZ, C. R., 1990. Development of the Late Paleozoic glaciations of the South American Gondwana in western Argentina. *Palaeogeography, Palaeoclimatology, Palaeoecology*, **79**, 275-287.
- GONZÁLEZ-BONORINO, F. & AGUIRRE, L., 1970. Metamorphic facies series of the crystalline basement of Chile. *Geologische Rundschau*, **59**, 979-994.
- GÖTZE, J., 1996. Genetic information of accessory minerals in clastic sediments. *Zentralblatt für Geologie und Paläontologie, Teil I 1995, Heft 1/2*, 101-118.
- GÖTZE, J. & ZIMMERLE, W., 2000. Quartz and silica as guide to provenance in sediments and sedimentary rocks. *Contributions to Sedimentary Geology*, **21**, 91 pp.
- GÖTZE, J., PLÖTZE, M. & HABERMANN, D., 2001. Origin, spectral characteristics and practical applications of the cathodoluminescence (CL) of quartz - a review. *Mineralogy and Petrology*, **71**, 225-250.
- HANCHAR, J. M. & MILLER, C. F., 1993. Zircon zonation patterns as revealed by cathodoluminescence and backscattered electron images: Implications for interpretation of complex crustal histories. *Chemical Geology*, **111**, 1-13.
- HASEGAWA, K., MATSUSHITA, K., NISHIMURA, T., HERVÉ, F. & AKAGI, Y., 1971. Geological note at las Chivas District, Aysén Province, Chile. *Bulletin of the Geological Survey of Hokkaido, Sapporo*, **44**, 25-53.
- HENRY, D. J. & DUTROW, B. L., 1992. Tourmaline in a low grade clastic metasedimentary rock: an example of the petrogenetic potential of tourmaline. *Contributions to Mineralogy and Petrology*, **112**, 203-218.
- HENRY, D. J. & DUTROW, B. L., 1996. Metamorphic tourmaline and its petrologic applications. In: GREW, E. S. & ANOVITZ, L. M. (eds.), *Boron - Mineralogy, Petrology and Geochemistry*. Reviews in Mineralogy, **33**, 503-558.
- HENRY, D. J. & GUIDOTTI, C. V., 1985. Tourmaline as a petrogenetic indicator mineral: an example from the staurolite-grade metapelites of NW Maine. *American Mineralogist*, **70**, 1-15.
- HERVÉ, F., 1988. Late Paleozoic subduction and accretion in southern Chile. *Episodes*, **11**, 97-113.
- HERVÉ, F., 1993. Paleozoic metamorphic complexes in the Andes of Aysén, southern Chile (west of ?Occidentalía). *Proceedings of the First Circum-Pacific and Circum-Atlantic Terrane Conference*, Guanajuato, Mexico, 64-65.
- HERVÉ, F. & FANNING, M., 2001. Late Triassic detrital zircons in meta-turbidites of the Chonos Mesozoic Complex, southern Chile. *Revista Geológica de Chile*, **28**, 91-104.
- HERVÉ, F., MUNIZAGA, F., GODOY, E. & AGUIRRE, L., 1974. Late Paleozoic K/Ar ages of blueschists from Pichilemu, central Chile. *Earth and Planetary Science Letters*, **23**, 261-264.
- HERVÉ, F., KAWASHITA, K., MUNIZAGA, F. & BASSEI, M., 1984. Rb-Sr isotopic ages from late Palaeozoic metamorphic rocks of central Chile. *Journal of the Geological Society, London*, **141**, 877-884.
- HERVÉ, F., AGUIRRE, L., SEPÚLVEDA, V. & MORATA, D., 1999. Contrasting geochemistry and metamorphism of

- pillow basalts in metamorphic complexes from Aysén, S. Chile. *Journal of South American Earth Sciences*, **12**, 379-388.
- HERVÉ, F., DEMANT, A., RAMOS, V. A., PANKHURST, R. J. & SUÁREZ, M., 2000. The southern Andes. In: CORDANI, U. G., MILANI, E. J., THOMAZ FILHO A. & CAMPOS, D. A. (eds.), *Tectonic Evolution of South America*. 31st International Geological Congress, Rio de Janeiro, 605-634.
- HERVÉ, F., FANNING, C. M. & PANKHURST, R. J., 2003a. Detrital zircon age patterns and provenance of the metamorphic complexes of southern Chile. *Journal of South American Earth Sciences*, **16**, 107-123.
- HERVÉ, F., PANKHURST, R. J., TOUW, R. A. J., FANNING, C. M., DZOGOLYK, E., SOLARI, M. & SUÁREZ, M., 2003b. Geological observations at the western portion of the Scotia - South America plate boundary: results of the 'Penguin' 2003 cruise. *10° Congreso Geológico Chileno, Concepción, Actas on CD-ROM*, 8 pp.
- HÖCKENREINER, M., SÖLLNER, F. & MILLER, H., 2003. Dating the TIPA shear zone: an Early Devonian terrane boundary between the Famatinian and Pampean systems (NW Argentina). *Journal of South American Earth Sciences*, **16**, 45-66.
- HUBERT, J. F., 1962. A zircon-tourmaline-rutile maturity index and the interdependence of the composition of heavy mineral assemblages with the gross composition and texture of sandstones. *Journal of Sedimentary Petrography*, **32**, 440-450.
- IRELAND, T. R., 1992. Crustal evolution of New Zealand: Evidence from age distributions of detrital zircons in Western Province paragneisses and Torlesse greywackes. *Geochimica et Cosmochimica Acta*, **56**, 911-920.
- JACOBS, J., FANNING, C. M., HENJES-KUNST, F., OLESCH, M. & PAECH, H.-J., 1998. Contribution of the Mozambique Belt into East Antarctica: Grenville-age metamorphism and polyphase Pan-African high-grade events in Central Dronning Maud Land. *Journal of Geology*, **106**, 385-406.
- JACOBSEN, Y., 2002. *Geochemische Analysen detritischer Zirkone Neuzeelands - Hf Isotope als neuer Tracer für Provenanzanalysen*. Diploma thesis, Westfälische Wilhelms-Universität Münster, Germany, 66 pp.
- JAHN, B.-M. & CONDIE, K. C., 1995. Evolution of the Kaapvaal Craton as viewed from geochemical and Sm-Nd isotopic analyses of intracratonic pelites. *Geochimica et Cosmochimica Acta*, **59**, 2239-2258.
- JENCHEN, U., 2001. Fazies und Geochemie in kontinentalen Trias-Becken im westlichen Argentinien und in Patagonien (30°-50°S). *Münstersche Forschungen zur Geologie und Paläontologie, Münster*, 91 pp.
- JUNGES, S. L., PIMENTEL, M. M. & DE MORAES, R., 2002. Nd isotopic study of the Neoproterozoic Mara Rosa Arc, central Brazil: implications for the evolution of the Brasília Belt. *Precambrian Research*, **117**, 101-118.
- KAUS, A., 2002. *Kathodolumineszenz in der Planetologie: Methodik und Anwendung*. Dissertation, Westfälische Wilhelms-Universität Münster, 183 pp.
- KAY, S. M., ORRELL, S. & ABBRUZZI, J. M., 1996. Zircon and whole rock Nd-Pb isotopic evidence for a Grenville age and a Laurentian origin for the basement of the Precordillera in Argentina. *Journal of Geology*, **104**, 637-648.
- KLEIN, C. & HURLBUT JR, C. S., 1993. *Manual of Mineralogy, 21st edition*. John Wiley & sons Inc., New York, 683 pp.
- KNUDSEN, T.-L., GRIFFIN, W. L., HARTZ, E. H., ANDRESEN, A. & JACKSON, S. E., 2001. In-situ hafnium and lead isotope analyses of detrital zircons from the Devonian sedimentary basin of NE Greenland: a record of repeated crustal reworking. *Contributions to Mineralogy and Petrology*, **141**, 83-94.
- KRÖNER, A., HEGNER, E., WENDT, J. I. & BYERLY, G. R., 1996. The oldest part of the Barberton granitoid-greenstone terrain, South Africa: evidence for crust formation between 3.5 and 3.7 Ga. *Precambrian Research*, **78**, 105-124.
- KRÖNER, A., JAECKEL, P., BRANDL, G., NEMCHIN, A. A. & PIDGEON, R. T., 1999. Single zircon ages for granitoid gneisses in the Central Zone of the Limpopo Belt, Southern Africa and geodynamic significance. *Precambrian Research*, **93**, 299-337.
- KRYNINE, P. D., 1946. The tourmaline group in sediments, *Journal of Geology*, **54**, 65-87.
- LAGALLY, U., 1975. *Geologische Untersuchungen im Gebiet Lago General Carrera - Lago Cochrane, Prov. Aisén / Chile unter besonderer Berücksichtigung des Grundgebirges und seiner Tektonik*. Dissertation, Ludwig-Maximilians-Universität, München, 131 pp.
- LAWVER, L. A. & SCOTESE, C. R., 1987. A revised reconstruction of Gondwanaland. In: MCKENZIE, G. D. (ed.), *Gondwana Six: Structure, Tectonics and Geophysics*. Geophysical Monograph, 40, 17-23.
- LIHOU, J. C. & MANGE-RAJETZKY, M. A., 1996. Provenance of the Sardona Flysch, eastern Swiss Alps: example of high-resolution heavy mineral analysis applied to an ultrastable assemblage. *Sedimentary Geology*, **105**,

- 141-157.
- LING, H. Y. & FORSYTHE, R. D., 1987. Late Paleozoic pseudoalbaillellid radiolarians from southernmost Chile and their geological significance. *In: MCKENZIE, D. G. (ed.), Gondwana Six: Structure, Tectonics and Geophysics*. Geophysical Monograph, 40, 253-260.
- LING, H. Y., FORSYTHE, R. D. & DOUGLAS, R. C., 1985. Late Paleozoic microfaunas from southernmost Chile and their relation to Gondwanaland forearc development. *Geology*, **13**, 357-360.
- LUCASSEN, F., BECCHIO, R., WILKE, H.G., FRANZ, G., THIRLWALL, M.F., VIRAMONTE, J. & WEMMER, K.P., 2000. Proterozoic-Paleozoic development of the basement of the Central Andes (18-26°S) - a mobile belt of the South American craton. *Journal of South American Earth Sciences*, **13**, 697-715.
- LUDWIG, K. R., 2001a. SQUID 1.02, A User's Manual. *Berkeley Geochronology Centre Special Publications*, **2**, 22 pp.
- LUDWIG, K. R., 2001b. User's manual for Isoplot/Ex rev. 2.49, A Geochronological Toolkit for Microsoft Excel. *Berkeley Geochronology Centre Special Publications*, **1a**, 55 pp.
- MARSAGLIA, K. M. & INGERSOLL, R. V., 1992. Compositional trends in arc-related, deep-marine sand and sandstone: A reassessment of magmatic-arc provenance. *Geological Society of America Bulletin*, **104**, 1637-1649.
- MARTIN, M. W., KATO, T. T., RODRIGEZ, C., GODOY, E., DUHART, P., MCDONOUGH, M. & CAMPOS, A., 1999. Evolution of the late Paleozoic accretionary complex and overlying forearc - magmatic arc, south central Chile (38°-41°S): Constraints for the tectonic setting along the southwestern margin of Gondwana. *Tectonics*, **18**, 582-356.
- MATTER, A. & RAMSEYER, K., 1985. Cathodoluminescence microscopy as a tool for provenance studies of sandstones. *In: ZUFFA, G. G. (ed.), Provenance of Arenites*. NATO ASI Series, C:148, D. Reidel Publishing Company, Dordrecht, 191-211.
- MCDANIEL, D. K., HEMMING, S. R., MCLENNAN, S. M. & HANSON, G. N., 1994. Resetting of neodymium isotopes and redistribution of REEs during sedimentary processes: The Early Proterozoic Chelmsford Formation, Sudbury Basin, Ontario, Canada. *Geochimica et Cosmochimica Acta*, **58**, 931-941.
- MCLENNAN, S. M., 1989. Rare Earth Elements in Sedimentary Rocks: Influence of Provenance and Sedimentary Processes. *Reviews of Mineralogy*, **21**, 169-200.
- MCLENNAN, S. M., 2001. Relationships between the trace element composition of sedimentary rocks and upper continental crust. *Geochemistry, Geophysics, Geosystems (G³)*, **2**, <http://g-cubed.org/>, 24 pp.
- MCLENNAN, S. M. & HEMMING, S., 1992. Samarium / neodymium elemental and isotopic systematics in sedimentary rocks. *Geochimica et Cosmochimica Acta*, **56**, 887-898.
- MCLENNAN, S. M. & TAYLOR, S. R., 1991. Sedimentary rocks and crustal evolution: tectonic setting and secular trends. *Journal of Geology*, **99**, 1-21.
- MCLENNAN, S. M., MCCULLOCH, M. T., TAYLOR, S. R. & MAYNARD, J. B., 1989. Effects of sedimentary sorting on neodymium isotopes in deep-sea turbidites. *Nature*, **337**, 547-549.
- MCLENNAN, S. M., TAYLOR, S. R., MCCULLOCH, M. T. & MAYNARD, J. B., 1990. Geochemical and Nd-Sr isotopic composition of deep-sea turbidites: Crustal evolution and plate tectonic associations. *Geochimica et Cosmochimica Acta*, **54**, 2015-2050.
- MCLENNAN, S. M., HEMMING, S., MCDANIEL, D. K. & HANSON, G. N., 1993. Geochemical approaches to sedimentation, provenance and tectonics. *In: JOHNSSON, M. J. & BASU, A. (eds.), Processes Controlling the Composition of Clastic Sediments*. Geological Society of America, Special Papers, 284, 21-40.
- MEUNIER, J. D., SELIER, E. & PAGEL, M., 1990. Radiation-damage rims in quartz from uranium-bearing sandstones. *Journal of Sedimentary Petrology*, **60**, 53-58.
- MILDOWSKI, A. E. & ZALASIEWICZ, J. A., 1991. Redistribution of rare earth elements during diagenesis of turbidite / hemipelagite mudrock sequences of Llandovery age from central Wales. *In: MORTON, A. C., TODD, S. P. & HAUGHTON, P. D. W. (eds.), Developments in Sedimentary Provenance Studies*. Geological Society, London, Special Publications, 57, 101-124.
- MILLAR, I. L., WILLAN, R. C. R., WAREHAM, C. D. & BOYCE, A. J., 2001. The role of crustal and mantle sources in the genesis of granitoids of the Antarctic Peninsula and adjacent crustal blocks. *Journal of the Geological Society, London*, **158**, 855-867.
- MILLAR, I. L., FLOWERDEW, M. J. & VAUGHAN, A. P. M., 2003. Hf-isotopes in detrital zircon as a provenance tool in terrane studies. *Terrane Processes at the Pacific margin of Gondwana (TAPMOG)*, Cambridge,

Programme and Abstracts, 14-15.

- MILNE, A. J. & MILLAR, I. L., 1989. The significance of mid-Palaeozoic basement in Graham Land, Antarctic Peninsula. *Journal of the Geological Society, London*, **146**, 207-210.
- MORAD, S. & ALDAHAN, A. A., 1985. Leucoxen-calcite-quartz aggregates in sandstones and the relation to decomposition of sphene. *Neues Jahrbuch für Mineralogie, Monatsheft* **10**, 458-468.
- MORAES, R., FUCK, R. A., PIMENTEL, M. M., GIOIA, S. M. C. L. & GRACIANO FIGUEIREDO, A. M., 2003. Geochemistry and Sm-Nd isotopic characteristics of bimodal volcanic rocks of Juscelândia, Goiás, Brazil: Mesoproterozoic transition from continental rift to ocean basin. *Precambrian Research*, **125**, 317-336.
- MORTON, A. C. & HALLSWORTH, C. R., 1999. Processes controlling the composition of heavy mineral assemblages in sandstones. *Sedimentary Geology*, **124**, 3-29.
- MUKASA, S. B., WILSON, A. H. & CARLSON, R. W., 1998. A multielement geochronologic study of the Great Dyke, Zimbabwe: significance of the robust and reset ages. *Earth and Planetary Science Letters*, **164**, 353-369.
- MÜNKER, C., WEYER, S., SCHERER, E. & MEZGER, K., 2001. Separation of high field strength elements (Nb, Ta, Zr, Hf) and Lu from rock samples for MC-ICPMS measurements. *Geochemistry, Geophysics, Geosystems (G³)*, **2**, <http://g-cubed.org/>, 19 pp.
- MUTTI, E. & NORMARK, W. R., 1987. Comparing examples of modern and ancient turbidite systems: problems and concepts. In: LEGGETT, J. K. & ZUFFA, G. G. (eds.), *Marine Clastic Sedimentology*. Graham & Trotman, London, 1-38.
- NECHAEV, V. P. & ISPHORDING, W. C., 1993. Heavy-mineral assemblages of continental margins as indicators of plate-tectonic environments. *Journal of Sedimentary Petrology*, **63**, 1110-1117.
- NESBITT, H. W. & YOUNG, G. M., 1982. Early Proterozoic climates and plate motions inferred from major element chemistry of lutites. *Nature*, **299**, 715-717.
- NEUSER, R. D., RICHTER, D. K., VOLLBRECHT, A., 1989. Natural quartz with brown / violet cathodoluminescence - Genetic aspects evident from special analysis. *Zentralblatt für Geologie und Paläontologie, Teil I* **1988, Heft 7/8**, 919-930.
- NEUSER, R. D., BRUHN, F., GÖTZE, J., HABERMANN, D. & RICHTER, D. K., 1996. Kathodolumineszenz: Methodik und Anwendung. *Zentralblatt für Geologie und Paläontologie, Teil I* **1985, Heft 1/2**, 287-306.
- NULLO, F. E., PROSERPIO, C. & RAMOS, V. A., 1978. Estratigrafía y tectónica de la vertiente este del hielo continental patagónico, Argentina - Chile. *VII Congreso Geológico Argentino, Actas* **I**, 455-470.
- OBERTHÜR, T., DAVIS, D. W., BLENKINSOP, T. G. & HÖHNDORF, A., 2002. Precise U-Pb mineral ages, Rb-Sr and Sm-Nd systematics for the Great Dyke, Zimbabwe - constraints on late Archean events in the Zimbabwe craton and Limpopo belt. *Precambrian Research*, **113**, 293-305.
- OLIVARES, B., CEMBRANO, J., HERVÉ, F., LÓPEZ, G. & PRIOR, D., 2003. Geometría y cinemática de la Zona de Cizalle Seno Arcabuz, Andes patagónicas, Chile. *Revista Geológica de Chile*, **30**, 39-52.
- O'NIONS, R. K., HAMILTON, P. J. & EVENSEN, N. M., 1977. Variations in ¹⁴³Nd/¹⁴⁴Nd and ⁸⁷Sr/⁸⁶Sr ratios in oceanic basalts. *Earth and Planetary Science Letters*, **34**, 13-22.
- OWEN, M. R., 1988. Radiation-damage halos in quartz. *Geology*, **16**, 529-532.
- PACES, J. B. & MILLER JR, J. D., 1993. Precise U-Pb ages of Duluth Complex and related mafic intrusions, northeastern Minnesota: geochronological insights to physical, petrogenetic, paleomagnetic, and tectonomagmatic processes associated with the 1.1 Ga midcontinent rift system. *Journal of Geophysical Research*, **98B**, 13997-14013.
- PANKHURST, R. J., HERVÉ, F., ROJAS, L. & CEMBRANO, J., 1992. Magmatism and tectonics in continental Chiloé, Chile (42°-42°30'S). *Tectonophysics*, **205**, 283-294.
- PANKHURST, R. J., LEAT, P. T., SRUOGA, P., RAPELA, C. W., MÁRQUEZ, M., STOREY, B. C. & RILEY, T. R., 1998a. Chon Aike province of Patagonia and related rocks in West Antarctica: A silicic large igneous province. *Journal of Volcanology and Geothermal Research*, **81**, 113-136.
- PANKHURST, R. J., RAPELA, C. W., SAAVEDRA, J., BALDO, E., DAHLQUIST, J., PASCUA, I. & FANNING, C. M., 1998b. The Famatinian magmatic arc in the central Sierras Pampeanas: an Early to Mid-Ordovician continental arc on the Gondwana margin. In: PANKHURST, R. J. & RAPELA, C. W. (eds.), *The Proto-Andean Margin of Gondwana*, Geological Society, London, Special Publication, **142**, 343-367.
- PANKHURST, R. J., WEAVER, S. D., HERVÉ, F. & LARRONDO, P., 1999. Mesozoic-Cenozoic evolution of the North

- Patagonian Batholith in Aysén, southern Chile. *Journal of the Geological Society, London*, **156**, 673-694.
- PANKHURST, R. J., RAMOS, A. & LINARES, E., 2003a. Antiquity of the Río de la Plata craton in Tandilia, Buenos Aires province. *Journal of South American Earth Sciences*, **16**, 5-13.
- PANKHURST, R.J., RAPELA, C.W., LOSKE, W.P., MÁRQUEZ, M. & FANNING, C.M., 2003b. Chronological study of pre-Permian basement rocks of Southern Patagonia. *Journal of South American Earth Sciences*, **16**, 27-44.
- PATCHETT, P. J., 1983. Importance of the Lu-Hf isotopic system in studies of planetary chronology and chemical evolution. *Geochimica et Cosmochimica Acta*, **47**, 81-91.
- PAULSSON, O. & AUSTRHEIM, H., 2003. A geochronological and geochemical study of rocks from Gjelsvikfjella, Dronning Maud Land, Antarctica - implications for Mesoproterozoic correlations and assembly of Gondwana. *Precambrian Research*, **125**, 113-138.
- PAYOLLA, B. L., BETTENCOURT, J. S., KOZUCH, M., LEITE, W. B., FETTER, A. H. & VAN SCHMUS, W. R., 2002. Geological evolution of the basement rocks in the east-central part of the Rondônia Tin Province, SW Amazonian craton, Brazil: U-Pb and Sm-Nd isotopic constraints. *Precambrian Research*, **119**, 141-169.
- PELL, S. D., WILLIAMS, I. S. & CHIVAS, A. R., 1997. The use of protolith zircon-age fingerprints in determining the protosource areas for some Australian dune sands. *Sedimentary Geology*, **109**, 233-260.
- PIMENTEL, M. M., WHITEHOUSE, M. J., VIANA, M. G., FUCK, R. A. & MACHADO, N., 1997. The Mara Rosa Arc in the Tocantins Province: further evidence for Neoproterozoic crustal accretion in Central Brazil. *Precambrian Research*, **81**, 299-310.
- PIMENTEL, M. M., LINDENMAYER, Z. G., LAUX, J. H., ARMSTRONG, R. & ARAÚJO, J. C., 2003. Geochronology and Nd isotope geochemistry of the Gameleira Cu-Au deposit, Serra dos Carajás, Brazil: 1.8-1.7 Ga hydrothermal alteration and mineralization. *Journal of South American Earth Sciences*, **15**, 803-813.
- PIUZANA, D., PIMENTEL, M. M., FUCK, R. A. & ARMSTRONG, R., 2003. Neoproterozoic granulite facies metamorphism and coeval granitic magmatism in the Brasília Belt, central Brazil: regional implications of new SHRIMP U-Pb and Sm-Nd data. *Precambrian Research*, **125**, 245-273.
- POTTER, P. E., 1978. Significance and origin of big rivers. *Journal of Geology*, **86**, 13-33.
- POTTER, P. E., 1994. Modern sands of South America: composition, provenance and global significance. *Geologische Rundschau*, **83**, 212-232.
- PRECIOZZI, F., BASEI, M. A. S. & MASQUELIN, H., 1999. New geochronological data from the Piedra Alta Terrane (Río de la Plata Craton). *II South American Symposium on Isotope Geology, Córdoba, Argentina, Actas*, 341-353.
- RAMÍREZ, E. & SASSI, R., 2001. The baric character of the Patagonian basement as deduced from the muscovite $d_{060,33T}$ spacing: a first contribution from Eastern Andean Metamorphic Complex (Andes, Chile). *European Journal of Mineralogy*, **13**, 1119-1126.
- RAMÍREZ, E., HERVÉ, F. & SASSI, R., 2001. Utilización del geobarómetro b0 en micas blancas del Complejo Metamórfico Andino Oriental, Aysén, Chile. *XI Congreso Latinoamericano de Geología y III Congreso Uruguayo, Montevideo, Uruguay, Actas on CD-ROM*, Abstract 222, 6 pp.
- RAMOS, V. A., 1984. Patagonia: ¿un continente paleozoico a la deriva? *IX Congreso Geológico Argentino, Bariloche, Actas II*, 311-325.
- RAMOS, V. A., 1989. Andean foothills structures in northern Magellanes Basin, Argentina. *The American Association of Petroleum Geologists Bulletin*, **73**, 887-903.
- RAMSEYER, K., BAUMANN, J., MATTER, A. & MULLIS, J., 1988. Cathodoluminescence colours of α -quartz. *Mineralogical Magazine*, **52**, 669-677.
- RAPALINI, A. E., 1998. Syntectonic magnetization of the mid-Palaeozoic Sierra Grande Formation: further constraints on the tectonic evolution of Patagonia. *Journal of the Geological Society, London*, **155**, 105-114.
- RAPELA, C. W. & PANKHURST, R. J., 1992. The granites of northern Patagonia and the Gastre Fault System in relation to the break-up of Gondwana. In: STOREY, B. C., ALABASTER, T. & PANKHURST, R. J. (eds.), *Magmatism and the Causes of Continental Break-Up*. Geological Society, London, Special Publications, 68, 209-220.
- RAPELA, C. W., PANKHURST, R. J., CASQUET, C., BALDO, E., SAAVEDRA, J., GALINDO, C. & FANNING, C. M., 1998. The Pampean Orogeny of the southern proto-Andes: Cambrian continental collision in the Sierras de Córdoba. In: PANKHURST, R. J. & RAPELA, C. W. (eds.), *The Proto-Andean Margin of Gondwana*. Geological Society, London, Special Publication, 142, 181-217.

- RAPELA, C. W., PANKHURST, R. J., FANNING, C. M. & GRECCO, L. E., 2003. Basement evolution of the Sierra de la Ventana Fold Belt: new evidence for Cambrian continental rifting along the southern margin of Gondwana. *Journal of the Geological Society, London*, **160**, 613-628.
- REHKÄMPER, M., SCHÖNBÄCHLER, M. & STIRLING, C. H., 2001. Multiple Collector ICP-MS: Introduction to instrumentation, measurement techniques and analytical capabilities. *Geostandards Newsletter*, **25**, 23-40.
- REMANE, J., 2000. *International Stratigraphic Chart*. Commission on Stratigraphy.
- RICCARDI, A. C., 1971. Estratigrafía en el oriente de la Bahía de la Lancha, Lago San Marín, Santa Cruz, Argentina. *Revista del Museo de La Plata (nueva serie), Sección Geología*, **Tomo VII**, 245-318.
- RICCARDI, A. C. & ROLLERI, E. O., 1980. Cordillera patagónica austral. *2° Simposio de Geología Regional de Argentina, Actas II*, 1173-1306.
- ROSER, B. P. & KORSCH, R. J., 1986. Determination of tectonic setting of sandstone - mudstone suites using SiO₂ content and K₂O/Na₂O ratio. *Journal of Geology*, **94**, 635-650.
- ROSER, B. P. & KORSCH, R. J., 1988. Provenance signatures of sandstone - mudstone suites determined using discriminant function analysis of major-element data. *Chemical Geology*, **67**, 119-139.
- ROSER, B. P. & NATHAN, S., 1997. An evaluation of elemental mobility during metamorphism of a turbidite sequence (Greenland Group, New Zealand). *Geological Magazine*, **134**, 219-234.
- RUBATTO, D., 2002. Zircon trace element geochemistry: partitioning with garnet and the link between U-Pb ages and metamorphism. *Chemical Geology*, **184**, 123-138.
- RUBATTO, D. & GEBAUER, D., 2000. Use of cathodoluminescence for U-Pb zircon dating by ion microprobe: some examples from the western Alps, In: PAGEL, M., BARBIN, V., BLANC, P. & OHNENSTETTER, D. (eds.), *Cathodoluminescence in Geosciences*. Springer Verlag, Berlin, 373-400.
- SAMSON, S. D., D'LEMONS, R. S., Blichert-Toft, J. & VERVOORT, J., 2003. U-Pb geochronology and Hf-Nd isotope compositions of the oldest Neoproterozoic crust within the Cadomian orogen: new evidence for a unique juvenile crust. *Earth and Planetary Science Letters*, **208**, 165-180.
- SATO, A. M., TICKYJ, H., LLAMBÍAS, E. J. & SATO, K., 2000. The Las Matras tonalitic-trondhjemitic pluton, central Argentina: Grenvillian-age constraints, geochemical characteristics, and regional implications. *Journal of South American Earth Sciences*, **13**, 587-610.
- SCHERER, E., MÜNKER, C. & MEZGER, K., 2001. Calibration of the Lutetium-Hafnium clock. *Science*, **293**, 683-687.
- SCHWAB, F. L., 1986. Sedimentary 'signatures' of foreland basin assemblages: real or counterfeit? *Special Publication of the International Association of Sedimentologists*, **8**, 395-410.
- SHAW, H. F. & WASSERBURG, G. J., 1982. Age and provenance of the target materials for tectites and possible impactites as inferred from Sm-Nd and Rb-Sr systematics. *Earth and Planetary Science Letters*, **60**, 155-177.
- SINGLETARY, S. J., HANSON, R. E., MARTIN, M. W., CROWLEY, J. L., BOWRING, S. A., KEY, R. M., RAMOKATE, L. V., DIRENG, B. B. & KROL, M. A., 2003. Geochronology of basement rocks in the Kalahari Desert, Botswana, and implications for regional Proterozoic tectonics. *Precambrian Research*, **121**, 47-71.
- SÖLLNER, F., MILLER, H. & HERVÉ, M., 2000. An Early Cambrian granodiorite age from the pre-Andean basement of Tierra del Fuego (Chile): the missing link between South America and Antarctica? *Journal of South American Earth Sciences*, **13**, 163-177.
- STEIGER, R. H. & JÄGER, E., 1977. Submission on Geochronology: convention on the use of decay constants in geo- and cosmochronology. *Earth and Planetary Research Letters*, **36**, 359-362.
- STEVENSON, R. K. & PATCHETT, P. J., 1990. Implications for the evolution of continental crust from Hf isotope systematics of Archean detrital zircons. *Geochimica et Cosmochimica Acta*, **54**, 1683-1697.
- STILLE, P. & SHIELDS, G., 1997. Radiogenic Isotope Geochemistry of Sedimentary and Aquatic Systems. *Lecture Notes in Earth Sciences*, **68**, Springer, Berlin, 217 pp.
- STOREY, B. C., PANKHURST, R. J. & JOHNSON, A. C., 1994. The Grenville Province within Antarctica: a test of the SWEAT hypothesis. *Journal of the Geological Society, London*, **151**, 1-4.
- TAYLOR, G. K. & SHAW, J., 1989. The Falkland Islands: new palaeomagnetic data and their origin as a displaced terrane from southern Africa. In: HILLHOUSE, J. W. (ed.), *Deep Structure and Past Kinematics of Accreted Terranes*. Geophysical Monograph, 50, 59-72.
- TAYLOR, S. R. & McLENNAN, S. M., 1985. *The Continental Crust: its Composition and Evolution*. Blackwell, Oxford, 312 pp.

- TEIXEIRA, W., CARNEIRO, M. A., NOCE, C. M., MACHADO, N., SATO, K. & TAYLOR, P. N., 1996. Pb, Sr and Nd isotope constraints on the Archaean evolution of gneissic-granitoid complexes in the southern São Francisco Craton, Brazil. *Precambrian Research*, **78**, 151-164.
- TEIXEIRA, W., PINESE, J. P. P., IACUMIN, M., GIRARDI, V. A. V., PICCIRILLO, E. M., ECHEVESTE, H., RIBOT, A., FERNANDEZ, R., RENNE, P. R. & HEAMAN, L. M., 2002. Calc-alkaline and tholeiitic dyke swarms of Tandilia, Rio de la Plata craton, Argentina: U-Pb, Sm-Nd, and Rb-Sr $^{40}\text{Ar}/^{39}\text{Ar}$ data provide new clues for intraplate rifting shortly after the Trans-Amazonian orogeny. *Precambrian Research*, **119**, 329-353.
- THISTLEWOOD, L., LEAT, P. T., MILLAR, I. L., STOREY, B. C. & VAUGHAN, A. P. M., 1997. Basement geology and Palaeozoic-Mesozoic mafic dykes from the Cape Meredith Complex, Falkland Islands: a record of repeated intracontinental extension. *Geological Magazine*, **134**, 355-367.
- THOMAS, R. J., HENJES-KUNST, F. & JACOBS, J., 1998. Pre-lamporphyre mafic dykes of the Cape Meredith Complex, West Falkland, *Geological Magazine*, **135**, 495-500.
- THOMSON, S. N. & HERVÉ, F., 2002. New time constraints for the age of metamorphism at the ancestral Pacific Gondwana margin of southern Chile (42-52°S). *Revista Geológica de Chile*, **29**, 255-271.
- VAN BAALEN, M. R., 1993. Titanium mobility in metamorphic systems: a review. *Chemical Geology*, **110**, 233-249.
- VARELA, R., DALLA SALDA, L., CINGOLANI, C. & GOMEZ, V., 1991. Estructura, petrología y geocronología del basamento de la región del Limay, Provincias de Río Negro y Neuquén, Argentina. *Revista Geológica de Chile*, **18**, 147-163.
- VEIZER, J. & JANSEN, S. L., 1985. Basement and sedimentary recycling - 2: time dimension to global tectonics, *Journal of Geology*, **93**, 625-643.
- VERVOORT, J. D., PATCHETT, P. J., BLICHERT-TOFT, J. & ALBARÈDE, F., 1999. Relationships between Lu-Hf and Sm-Nd isotopic systems in the global sedimentary system. *Earth and Planetary Science Letters*, **168**, 79-99.
- VERVOORT, J. D., PATCHETT, P. J., ALBARÈDE, F., BLICHERT-TOFT, J., RUDNICK, R. & DOWNES, H., 2000. Hf-Nd isotopic evolution of the lower crust. *Earth and Planetary Science Letters*, **181**, 115-129.
- VON EYNATTEN, H. & GAUPP, R., 1999. Provenance of Cretaceous synorogenic sandstones in the Eastern Alps: constraints from framework petrography, heavy mineral analysis and mineral chemistry. *Sedimentary Geology*, **124**, 81-111.
- VON EYNATTEN, H., BARCELÓ-VIDAL, C. & PAWLOWSKI-GLAHN, V., 2003. Composition and discrimination of sandstones: a statistical evaluation of different analytical methods. *Journal of Sedimentary Research*, **73**, 47-57.
- VON GOSEN, W., 2002. Polyphase structural evolution in the northeastern segment of the North Patagonian Massif (southern Argentina). *Journal of South American Earth Sciences*, **15**, 591-623.
- WALDERHAUG, O. & RYKKJE, J., 2000. Some examples of the effect of crystallographic orientation of the cathodoluminescence colors of quartz. *Journal of Sedimentary Research*, **70**, 545-548.
- WAREHAM, C. D., PANKHURST, R. J., THOMAS, R. J., STOREY, B. C., GRANTHAM, G. H., GACOB, J. & EGLINGTON, B. M., 1998. Pb, Nd, and Sr isotope mapping of Grenville-age crustal provinces in Rodinia. *Journal of Geology*, **106**, 647-659.
- WAREHAM, C. D., STUMP, E., STOREY, B. C., MILLAR, I. L. & RILEY, T. R., 2001. Petrogenesis of the Cambrian Liv Group, a bimodal volcanic rock suite from the Ross orogen, Transantarctic Mountains. *Geological Society of America Bulletin*, **113**, 360-372.
- WILLIAMS, I. S., 1998. U-Th-Pb Geochronology by Ion Microprobe. In: MCKIBBEN, M. A., SHANKS III, W. C. & RIDLEY, W. I. (eds.), *Applications of microanalytical techniques to understanding mineralizing processes*. Reviews in Economic Geology, **7**, 1-35.
- WILLIAMS, I. S. & CLAEISSON, S., 1987. Isotopic evidence for the Precambrian provenance and Caledonian metamorphism of high grade paragneisses from the Seve Nappes, Scandinavian Caledonides. II. Ion microprobe zircon U-Th-Pb. *Contributions to Mineralogy and Petrology*, **97**, 205-217.
- WILLNER, A., 1987. Detrital tourmalines as indicators for the source rocks of Late Precambrian - Lower Cambrian Greywackes (Puncoviscana Formation) in NW Argentina. *Zentralblatt für Geologie und Paläontologie*, **Teil I 1987, Heft 7/8**, 885-891.
- WILLNER, A., HERVÉ, F. & MASSONNE, H.-J., 2000. Mineral chemistry and pressure-temperature evolution of two contrasting high-pressure - low-temperature belts in the Chonos Archipelago, southern Chile. *Journal of*

- Petrology*, **41**, 309-330.
- WOZAZEK, S. & KRAWINKEL, H., 2002. Development of the Côte d'Ivoire basin: reading provenance, sediment dispersal, and geodynamic implications from heavy minerals. *International Journal of Earth Sciences*, **91**, 906-921.
- YOSHIDA, K., 1981. *Estudio geológico del curso superior del río Baker, Aysén, Chile (47°05' a 47°42' Lat. S., 72°28' a 73°15' Long. W.)*. Dissertation, Universidad de Chile, Santiago, 341 pp.
- YOUNG, D. N., ZHAO, J.-X., ELLIS, D. J. & MCCULLOCH, M. T., 1997. Geochemical and Sr-Nd isotopic mapping of source provinces for the Mawson charnockites, East Antarctica: implications for Proterozoic tectonics and Gondwana reconstruction. *Precambrian Research*, **86**, 1-19.
- ZHAO, J. X., MCCULLOCH, M. T. & BENNETT, V. C., 1992. Sm-Nd and U-Pb zircon isotopic constraints on the provenance of sediments from the Amadeus Basin, central Australia: Evidence for REE fractionation. *Geochimica et Cosmochimica Acta*, **56**, 921-940.
- ZHAO, J.-X., ELLIS, D. J., KILPATRICK, J. A. & MCCULLOCH, M. T., 1997. Geochemical and Sr-Nd isotopic study of charnockites and related rocks in the northern Prince Charles Mountains, East Antarctica: implications for charnockite petrogenesis and Proterozoic crustal evolution. *Precambrian Research*, **81**, 37-66.
- ZIMMERMANN, U. & BAHLBURG, H., 2003. Provenance analysis and tectonic setting of the Ordovician clastic deposits in the southern Puna basin, NW Argentina. *Sedimentology*, **50**, 1079-1104.
- ZINKERNAGEL, U., 1978. Cathodoluminescence of quartz and its application to sandstone petrology. *Contributions to Sedimentology*, **8**, 69 pp.